

DEPLOYMENT-TIME RELIABILITY OF LEARNED ROBOT POLICIES

A DISSERTATION
SUBMITTED TO THE DEPARTMENT OF COMPUTER SCIENCE
AND THE COMMITTEE ON GRADUATE STUDIES
OF STANFORD UNIVERSITY
IN PARTIAL FULFILLMENT OF THE REQUIREMENTS
FOR THE DEGREE OF
DOCTOR OF PHILOSOPHY

Christopher Agia

March 2026

Abstract

Significant advances in learning-based robot manipulation have produced policies capable of executing complex, dexterous behaviors, raising the prospect of deploying robots in everyday human spaces. However, realizing this vision requires looking beyond demonstrated *capability* alone and toward *reliability*: during deployment, learned policies must contend with open-ended variability, distribution shift, and compounding errors that collectively undermine system performance.

This dissertation investigates how the reliability of learned robot policies can be improved at deployment time through mechanisms that operate around them. We develop three complementary classes of deployment-time mechanisms. First, we introduce runtime monitoring methods that detect impending failures by identifying inconsistencies in closed-loop policy behavior and deviations in task progress, without requiring failure data or task-specific supervision. Second, we propose a data-centric framework for policy interpretability that traces deployment-time successes and failures to influential training demonstrations using influence functions, enabling principled diagnosis and dataset curation. Third, we address reliable long-horizon task execution by formulating policy coordination as the problem of estimating and maximizing the success probability of behavior sequences, and we extend this formulation to open-ended, language-specified tasks through feasibility-aware task planning.

By centering on core challenges of deployment, these contributions advance practical foundations for the reliable, real-world use of learned robot policies. Continued progress on these foundations will be essential for enabling trustworthy and scalable robot autonomy in the future.

For Emily, Sandra, and Remon.

Acknowledgments

This PhD was a collective journey as much as a personal one, and I owe heartfelt thanks to many.

First and foremost, I would like to express my deepest gratitude to my advisors, Prof. Jeannette Bohg and Prof. Marco Pavone, whose dedication to my success and unwavering commitment to excellence shaped my entire PhD experience. From the very beginning, Jeannette generously devoted her time to strengthening my research foundations. She has taught me how to translate ambitious aspirations into steady, tangible research progress. She instilled in me the passion to pursue problems I believed were meaningful and worked tirelessly to create the conditions that made that pursuit possible—facilitating collaborations, securing resources and funding, and offering thoughtful guidance at every stage. When I first joined Stanford, many trusted colleagues encouraged me in no uncertain terms to consider working under Jeannette’s mentorship. Looking back, I am glad I did.

Marco’s guidance has likewise had a profound and lasting impact on my development—not only as a researcher, but as a technologist more broadly. Throughout my PhD, he continually challenged me to think with greater clarity, precision, and formal rigor, while also encouraging me to consider the broader impact of my work in a rapidly evolving field. He thoughtfully created leadership opportunities that fostered growth beyond my immediate projects. His insistence on searching for deeper insight and nuance in all things has fundamentally reshaped how I think and how I assign value to problems—and for that, I am especially grateful. I consider myself immensely fortunate to have had not one but two advisors who believed in my potential, supported the directions I chose to pursue, and helped me navigate the inevitable obstacles that ultimately make research so rewarding.

I would like to thank my thesis committee: Prof. Clark Barrett, Prof. Mykel Kochenderfer, and Prof. Iro Armeni. I appreciate Clark’s service on my reading committee; his work has broadened my understanding of the many dimensions in which safety must be addressed within robotics and AI. My interactions with Mykel throughout my PhD were always a genuine pleasure—his questions often revealed perspectives on my research that I had not previously considered. I am especially glad that Iro served as chair of my defense; it was through my undergraduate research building on her PhD work that I first found my way to Stanford. This has made for a unique and meaningful full circle.

I want to thank the wonderful staff in the Computer Science and Aeronautics and Astronautics departments—especially Jayanthi, Yaritza, Helen, Jimmy, Adele, Renee, Brian, Cassandra, Susan,

and Nelly. Their guidance and support greatly simplified the logistical complexities of my PhD, particularly as an international student navigating an unfamiliar system. I am especially grateful to Jayanthi for the countless questions she answered with patience and thoroughness. My thanks also go to the team at the Bechtel International Center for their continued support over the years.

I am deeply grateful to the colleagues, mentors, and friends I have found in Prof. Florian Shkurti, Prof. Hani Naguib, Prof. Jiajun Wu, Edward, Toki, Krishna, Rika, Manfred, and Ran. Their advice provided clarity and perspective at pivotal moments in my PhD. I feel especially fortunate to have had Toki and Edward as my first-year rotation mentors; the lessons I learned from them are reflected in nearly every project I have pursued since. I also want to acknowledge the steadfast encouragement that Florian, Krishna, and Hani have offered across many phases of my research journey.

I had the privilege of collaborating with an extraordinarily talented group of students at Stanford—Rohan, Jingyun, Amine, Joey, Jakob, Milan, Jacky, Kevin, Yixuan, Francesco, Guillem, Daniel, Alex, Jimmy, Matt, and Zi-ang. This work would not have been possible without them. In particular, I am grateful to Rohan and Jingyun for the many long nights they poured into our shared research; I am proud of what we accomplished together. I also want to thank Joey, who always kept an open door for long technical discussions. These shaped my research more than he would likely admit.

I am grateful to the industry scientists with whom I had the distinct pleasure of collaborating: Masha Itkina and Haruki Nishimura from the Toyota Research Institute, and Issa Nesnas and Saptarshi Bandyopadhyay from the NASA Jet Propulsion Laboratory. They welcomed me generously on a number of collaborations and guided me toward problems of greater practical significance. Working with them has broadened my perspective on what research can and should strive to achieve.

Teaching robotics was one of the most memorable, rewarding, and—at times—challenging parts of my PhD. I was incredibly fortunate to have shared this experience with such a dedicated team of course assistants: Alvin, Rohan, Aditya, Luis, Roger, and Suneel for Principles of Robot Autonomy; Jakob, Daniel, Luis, and Xilun for Test of AI & Emerging Technologies.

Of course, I was truly lucky to have had such smart, kind, and spirited labmates in Toki, Priya, Tyler, Jingyun, Marion, Carlota, Krishnan, Claire, Kevin, and Brandon from the IPRL, and Rohan, Amine, Jakob, Daniele, John, Hugo, Daniel, Luis, Matt, Milan, Jacky, Pranit, Somrita, Spencer, Thomas, Rachel, and Alvin from the ASL—along with many others who made these years so special. Because of them, Stanford felt like home in more ways than one.

Everything that made this PhD possible rests upon the unconditional love and support of my family. I am forever grateful to my parents, Sandra and Remon, for giving so selflessly of themselves so that I might have opportunities in life as meaningful as this one; and to my sister, Emily, for her vibrant spirit and for the wisdom beyond her years that carried me through every high and low.

Lastly, I thank my partner, Stephanie, for walking devotedly alongside me, for reminding me to see the color each day offers, and for showing me that the future is often closer than it seems. She has supported me in every imaginable way; none of this would have been possible without her.

Contents

Abstract	i
Acknowledgments	iii
1 Introduction	1
1.1 Background	1
1.2 Thesis Outline	3
1.2.1 Policy Monitoring and Interpretability (Part I)	3
1.2.2 Policy Coordination and Planning (Part II)	4
1.3 Publications	4
I Policy Monitoring and Interpretability	6
2 Monitoring Policies for Runtime Failure Detection	7
2.1 Introduction	7
2.2 Related Work	9
2.3 Problem Setup	10
2.4 Proposed Approach: Sentinel	11
2.4.1 STAC: Detecting Erratic Failures with Temporal Consistency	12
2.4.2 Detecting Task Progression Failures with VLMs	14
2.5 Experiments	15
2.6 Results	15
2.7 Conclusion	18
2.8 Limitations and Future Work	18
3 Understanding Policy Behavior through Training Data	20
3.1 Introduction	20
3.2 Related Work	22

3.3	Background: Data Attribution via Influence Functions	23
3.4	Problem Formulation	23
3.5	CUPID: Curating Performance-Influencing Demonstrations	25
3.5.1	Demonstration-Performance Influence	25
3.5.2	Data Curation with Performance Influence	27
3.5.3	Additional Quality Metrics	28
3.6	Experiments	28
3.6.1	Setting 1: Improving Policy Performance in Mixed-Quality Regimes	29
3.6.2	Setting 2: Identifying Robust Test-time Strategies from Policy Failures	31
3.6.3	Setting 3: Disentangling Spurious Correlations in Demonstration Data	32
3.7	Discussion and Ablations	33
3.7.1	How Is Curation Performance Affected by Properties of the Data and Task?	33
3.7.2	How Many Policy Rollouts Are Required for Effective Curation with CUPID?	33
3.7.3	Can Data Curated for Single-Task Policies Strengthen Generalist Policy Performance?	34
3.8	Conclusion	35
3.9	Limitations and Future Work	35

II Policy Coordination and Planning 37

4	Coordinating Policy Sequences for Long-Horizon Tasks	38
4.1	Introduction	38
4.2	Related Work	40
4.2.1	Robot Skill Learning	40
4.2.2	Long-Horizon Robot Planning	40
4.2.3	Task and Motion Planning	41
4.3	Problem Setup	41
4.3.1	Long-Horizon Planning	41
4.3.2	Task-Agnostic Policies	42
4.4	Sequencing Task-Agnostic Policies	43
4.4.1	Grounding Skill Sequences with Action Plans	43
4.4.2	Ensuring Action Plan Feasibility	44
4.5	Planning Action Sequences	45
4.6	Training Skills	46
4.6.1	Policies and Q-functions	46
4.6.2	Dynamics	46
4.6.3	Uncertainty Quantification	47

4.7	Experiments	47
4.7.1	Product of Q-Functions Approximates Task Success (H1)	48
4.7.2	STAP Skills Generalize to Long-Horizon Tasks (H2)	48
4.7.3	STAP Can be Extended for TAMP with UQ (H3)	50
4.7.4	Real-World Sequential Manipulation	51
4.8	Conclusion	51
4.8.1	Future Work	52
5	Searching for Feasible Policy Sequences from Language	53
5.1	Introduction	53
5.2	Related Work	55
5.2.1	Language for Robot Planning	55
5.2.2	Task and Motion Planning	56
5.3	Problem Setup	56
5.3.1	LLM and Skill Library	57
5.3.2	The Planning Objective	57
5.3.3	Geometric Feasibility Planning	58
5.4	Methods	58
5.4.1	Goal Prediction	59
5.4.2	Shooting-Based Planning	60
5.4.3	Search-Based Planning	61
5.4.4	Text2Motion	63
5.4.5	Out-of-Distribution Detection	64
5.5	Experiments	64
5.5.1	Baselines	65
5.5.2	Large Language Model	65
5.5.3	Prompt Engineering	65
5.5.4	Task Suite	67
5.5.5	Evaluation and Metrics	67
5.6	Results	68
5.6.1	Feasibility Planning Is Required to Solve Tasks with Geometric Dependencies (H1)	68
5.6.2	Search-Based Reasoning Is Required for PAP Tasks (H2)	69
5.6.3	Hybrid Planning Integrates the Strengths of Shooting-Based and Search-Based Methods (H3)	71
5.6.4	Plan Termination Is Made Reliable via Goal Prediction (H4)	72
5.7	Conclusion	73
5.8	Limitations and Future Work	73

6	Conclusion	75
6.1	Summary of Contributions and Findings	75
6.2	Directions for Future Work	76
6.3	Concluding Remarks	78
A	Additional Details: Sentinel	79
A.1	Method Details: Sentinel	79
A.1.1	Temporal Consistency Detection with STAC	80
A.1.2	Runtime Monitoring with Vision Language Models	82
A.2	Experiment Details	86
A.2.1	Environments	86
A.2.2	Diffusion Policies	88
A.2.3	Baselines	89
A.2.4	Evaluation Protocol	94
A.3	Additional Results	96
A.3.1	Ablation Experiments on STAC	96
A.3.2	Extended Results: VLM Runtime Monitor	97
A.4	Derivations	101
B	Additional Details: CUPID	104
B.1	Implementation Details	105
B.1.1	Influence Functions for Diffusion Policies	105
B.1.2	CUPID Hyperparameters	107
B.1.3	Combining Score Functions	107
B.2	Experimental Setup	108
B.2.1	Hardware Setup	108
B.2.2	Policy Architectures	108
B.2.3	Tasks and Datasets	109
B.2.4	Baseline Details	111
B.3	Additional Results and Analysis	112
B.3.1	Extended Discussion on RoboMimic Results (§3.7.1)	112
B.3.2	Ablation on Number of Policy Rollouts in RoboMimic (§3.7.2)	113
B.3.3	Additional Data Quality Results in RoboMimic	114
B.3.4	Data Filtering Curation Distributions in Franka Real-World	115
B.3.5	Data Selection Curation Distributions in Franka Real-World	116
B.3.6	Additional Results for Franka PI-0: Curated Dataset Transfer (§3.7.3)	117
B.4	Derivations	119
B.4.1	Proof of Proposition 2	119

B.4.2	Derivation of Performance Influence for Variable Length Trajectories	119
C	Additional Details: STAP	121
C.1	Discussion and Limitations	121
C.2	Manipulation Skill Library	124
C.2.1	Parameterized Manipulation Primitives	124
C.2.2	Training Manipulation Skills	124
D	Additional Details: Text2Motion	125
D.1	Implementation Details	125
D.1.1	Learning Robot Skills and Dynamics	126
D.1.2	Out-of-Distribution Detection	128
D.1.3	Task Planning with LLMs	129
D.1.4	Geometric Feasibility Planning	129
D.2	Experiment Details	130
D.2.1	Scene Descriptions as Symbolic States	130
D.2.2	In-Context Examples	131
D.3	Derivations	134
D.3.1	Skill Usefulness Derivation	134
D.3.2	Skill Feasibility Derivation	135
D.4	Real World Demonstration	135
D.4.1	Hardware Setup	135
D.4.2	Real-World Robot Demonstration	136

List of Tables

2.1	Failure detection results on simulated box closing diffusion policy (Sentinel)	17
2.2	Failure detection results on real-world chair tucking diffusion policy (Sentinel)	18
5.1	Ablation result on hybrid planner behavior for complex tasks (Text2Motion)	71
A.1	Hyperparameters for temporal consistency detection (Sentinel)	81
A.2	Ablation result on policy prediction horizon for failure detection (Sentinel)	97
A.3	Extended results on simulated box closing erratic failures (Sentinel)	98
A.4	Extended results on simulated object covering task-progress failures (Sentinel)	99
A.5	Extended results on simulated box closing task-progress failures (Sentinel)	100
B.1	Hyperparameters for PI-0 multi-task policy fine-tuning (CUPID)	109
D.1	Simulated TableEnv manipulation planning task suite details (Text2Motion)	130

List of Figures

2.1	Overview of Sentinel	8
2.2	Action chunk overlap during policy rollout (Sentinel)	11
2.3	System architecture for failure detection (Sentinel)	12
2.4	Detection threshold for temporal consistency score (Sentinel)	13
2.5	Failure detection results on simulated PushT diffusion policy (Sentinel)	16
2.6	Failure detection results on simulated object covering diffusion policy (Sentinel)	17
3.1	Overview of CUPID	21
3.2	System architecture for data curation (CUPID)	25
3.3	Data curation results on simulated RoboMimic diffusion policy (CUPID)	30
3.4	Data curation results on real-world diffusion policy (CUPID)	31
3.5	Curated dataset distributions for demo filtering on real-world tasks (CUPID)	32
3.6	Ablation result on the number of policy rollouts (CUPID)	34
3.7	Data curation results on real-world PI-0 multi-task policy (CUPID)	34
4.1	Overview of STAP	39
4.2	Coordinating policy behaviors in a 2D toy domain (STAP)	43
4.3	Policy training pipeline and policy sequence coordination tasks (STAP)	45
4.4	Ablation on sequence feasibility estimation and computation time (STAP)	49
4.5	Policy sequence coordination results in simulation (STAP)	50
4.6	Policy task and motion planning results in simulation (STAP)	51
5.1	Overview of Text2Motion	54
5.2	System architectures for shooting- and search-based policy planners (Text2Motion)	59
5.3	System architecture for proposed hybrid policy planner (Text2Motion)	63
5.4	Simulated TableEnv manipulation planning task suite (Text2Motion)	66
5.5	Policy planning results in the TableEnv simulated task suite (Text2Motion)	69
5.6	Ablation result on planning failure modes under partial observability (Text2Motion)	70
5.7	Ablation result on planning termination strategies (Text2Motion)	72

A.1	Simulated and real-world evaluation tasks for failure detection (Sentinel)	87
A.2	Ablation result on policy prediction and execution horizon for failure detection (Sentinel)	96
A.3	Ablation result on statistical distance function for failure detection (Sentinel)	97
B.1	Ablation result on number of policy rollouts in RoboMimic state (CUPID)	113
B.2	Ablation result on number of policy rollouts in RoboMimic image (CUPID)	114
B.3	Extended results on curated data quality in RoboMimic state (CUPID)	114
B.4	Extended results on curated data quality in RoboMimic image (CUPID)	114
B.5	Distributions of demos filtered on real-world tasks (CUPID)	115
B.6	Curated dataset distributions for demo selection on real-world tasks (CUPID)	116
B.7	Distributions of demos selected for real-world tasks (CUPID)	117
B.8	Extended results on real-world PI-0 multi-task policy performance (CUPID)	117

Chapter 1

Introduction

1.1 Background

Robotics is undergoing a period of consequential change. Systems once confined to repetitive automation in highly structured settings—such as factory assembly lines—are gradually shifting toward intelligent, autonomous operation in the unstructured and dynamic environments that characterize everyday human spaces, including homes, offices, and retail stores [6, 286, 298]. To operate effectively in these contexts, robots must possess more than just accurate perception of the structure and semantics of their environments, or the ability to plan sequences of actions toward a goal. They must also know how to physically interact with the world: how to execute planned actions safely, robustly, and reliably through closed-loop control. It is this capacity for reliable physical interaction that ultimately determines whether a robot can function autonomously outside carefully engineered environments.

While the robotics community has made rapid progress in general-purpose perception [71, 127] and planning [2, 68]—driven in large part by advances in computer vision, natural language processing, and foundation models [26]—comparable progress in generalist robot manipulation has lagged behind. To date, the most compelling results have emerged through large-scale learning from demonstration [19, 124, 262], where robot policies parameterized by deep neural networks are trained to map high-dimensional sensory observations to control targets via imitation of behaviors demonstrated by human operators across a diversity of manipulation tasks (e.g., folding clothes, making coffee, assembling objects). Yet current results remain limited in scope, as today’s most capable manipulation policies—those adapted from foundation models, termed Vision-Language-Action (VLA) models [309]—cover only a small fraction of the behaviors required for general-purpose deployment and fall well short of human-level reliability. For instance, VLA policies remain highly sensitive to variations in object geometry, pose, and appearance, to changes in lighting and scene context, to instruction phrasing, and to spurious environmental features—resulting in failure modes

which may be difficult or impossible for system designers to anticipate beforehand [91, 98, 104, 180]. As such, the development of generalist robot manipulation policies remains a central focus of contemporary robotics research, drawing substantial investment and attention across academia, industry, and the broader technology ecosystem.

At the research frontier, much of the field’s efforts have focused on expanding the *operational envelope* of generalist robot policies: The range of tasks and environments within which they can be expected to perform competently. This effort has taken multiple, complementary forms, including the development of hardware platforms that enable large-scale collection of dexterous manipulation data [41, 305], the transfer of internet-scale priors through foundation models such as Large Language Models (LLMs) and Vision-Language Models (VLMs) [146, 309], and the introduction of more sophisticated robot learning algorithms capable of training on increasingly diverse and heterogeneous data sources (e.g., teleoperated robot demonstrations [40], cross-embodiment datasets collected from different robotic platforms [47], data gathered during online deployment [123], and off-domain data such as human videos [160]).

While these efforts have broadened the scope of behaviors learned robot policies can exhibit in carefully controlled evaluation settings [85], real-world deployment presents a persistent and markedly more unforgiving set of challenges for which the benefits of e.g., increased data coverage and richer priors alone are insufficient. That is, the open-ended variability, complexity, and non-stationarity of everyday, real-world environments ensure that, regardless of the scale or diversity of a policy’s training data or the richness of its learned priors, deployed systems will eventually encounter situations that lead to erroneous or undesirable behavior [250]. This observation highlights a complementary line of inquiry: alongside continued efforts to advance learned policies toward deployment readiness, we must also consider how to maintain reliability at deployment time—where failures are costly, difficult to diagnose, and often irreversible. Herein, we consider three representative challenges that arise in the real-world deployment of robot policies:

1. **Failure Mitigation:** The black-box, task-agnostic nature of modern policies—particularly those initialized from large foundation models—obscures not only whether a deployed policy is nominally within the support of its training distribution, but whether it is operating in regions of that distribution where experience is sufficiently dense to support reliable behavior. As a result, even minor and seemingly indistinguishable shifts in the environment may push a policy outside the reliable support of its training data. This lack of visibility complicates the timely detection of failures and the ability to intervene before unsafe or irreversible outcomes occur.
2. **Model Interpretability:** The same opacity of modern policies makes it extremely difficult to understand why a policy succeeds or fails during closed-loop execution, hindering post-hoc diagnosis, systematic debugging, and principled dataset curation—processes that are essential for improving policy performance over time.

- 3. Long-Horizon Tasks:** Learning and executing an entire multi-step task with a single policy behavior is often unreliable due to compounding prediction errors, motivating approaches that instead chain together shorter, independent behaviors with higher per-step reliability. However, even when shorter behaviors are learned reliably, composing them to accomplish new multi-step tasks often fails due to unmodeled dependencies, which may compromise the feasibility of downstream behaviors. Achieving reliable outcomes therefore requires explicitly reasoning about the probability of success of behavior sequences and coordinating policy outputs accordingly.

Notably, addressing these challenges motivates a distinct class of methods that operate *around* learned policies, explicitly accounting for the closed-loop, real-time, and safety-critical constraints inherent to robotic deployment. We argue that developing such deployment-time mechanisms—alongside continued advances in policy learning—is essential for bringing generalist robot policies out of the lab and into reliable real-world use, and it is this perspective that motivates and unifies the contributions of this dissertation.

1.2 Thesis Outline

What it means for a learned robot policy to be reliable at deployment differs fundamentally from achieving strong performance during training or in controlled evaluation settings. Experience from adjacent domains, most notably autonomous driving, has demonstrated that reliability in the long tail of real-world deployment is not a property of any single model class (e.g., a VLA policy) nor a simple consequence of increased data scale, but rather emerges from the careful orchestration of reliability-promoting mechanisms spanning the autonomy stack and development lifecycle [92, 280]. As learned manipulation policies grow in capability and are increasingly deployed in open-ended, real-world environments, the need for such deployment-time considerations becomes both unavoidable and urgent. Accordingly, this dissertation investigates how the reliability of learned robot policies—and, by extension, systems and tasks composed of them—can be enhanced at deployment through three complementary lenses: (1) detecting when policies are likely to fail, (2) interpreting policy behavior through the data that shaped it, and (3) coordinating learned policy behaviors for reliable long-horizon task execution. **Part I** of the thesis addresses (1-2), while **Part II** is dedicated to (3).

1.2.1 Policy Monitoring and Interpretability (**Part I**)

Chapter 2 addresses the challenge of detecting when a learned robot policy is likely to fail during deployment, even when operating under seemingly nominal conditions. We present a runtime monitoring framework for closed-loop, generative manipulation policies that detects failures online without requiring failure data or task-specific supervision. Our framework judiciously integrates runtime monitors to capture both low-level, real-time inconsistencies in policy behavior and higher-level deviations in task progress. Through simulation and real-world experiments, this chapter

demonstrates that structuring runtime monitoring around a hierarchy of specialized detectors—aligned with different granularities of policy failure—enables earlier and more reliable intervention than any single monitoring approach alone. [Chapter 3](#) addresses a complementary challenge: while monitoring can prevent unsafe outcomes, it does not explain why a policy behaves as it does. This chapter introduces a data-centric perspective on policy interpretability, focusing on how individual training demonstrations influence closed-loop behavior at deployment. We propose a methodology based on influence functions that connects deployment-time performance metrics—such as task success or failure rates—to examples in the training dataset. By enabling counterfactual reasoning about data, this chapter shows how greater interpretability mechanisms can support principled dataset curation, diagnose spurious correlations, and systematically improve policy reliability under distribution shift.

1.2.2 Policy Coordination and Planning ([Part II](#))

[Chapter 4](#) examines a central limitation of behavior-centric policy learning: reliable execution of individual behaviors does not guarantee reliable outcomes when those behaviors are composed over time to accomplish real-world, long-horizon tasks. The key insight is that success in such settings depends on how individual behaviors interact when executed in sequence, which motivates the need for explicit coordination. We formalize behavior coordination as the problem of estimating and maximizing the joint success probability of a given sequence of learned policy behaviors using models produced during policy training. Building on this foundation, [Chapter 5](#) introduces a language-based task and motion planning framework. This framework extends our behavior coordination formulation to open-ended goals expressed in natural language, using LLMs to search for candidate behavior sequences and feasibility-aware estimates to guide their selection. Together, these approaches show that explicitly reasoning about the success probability of coordinated policy behaviors is critical for reliable operation in complex, real-world manipulation scenarios.

Collectively, these contributions advance the reliability of learned robot policies by addressing a complementary set of challenges inherent to deployment. While not exhaustive, these challenges lie on the critical path toward trustworthy and scalable robot autonomy. Looking ahead, several promising directions for future research remain, which we outline in [Chapter 6](#).

1.3 Publications

Parts of this dissertation are adapted from the following previously published works¹:

- [\[3\] Christopher Agia*](#), Toki Migimatsu*, Jiajun Wu, and Jeannette Bohg. *STAP: Sequencing Task-Agnostic Policies*. In IEEE International Conference on Robotics and Automation, 2023.

¹For papers with multiple authors, Christopher Agia led or co-led all aspects of the research, including conception, methodology, experiments, analysis, and writing. Co-first authorship is indicated with an asterisk (*).

© 2023 IEEE. Reprinted, with permission, from the above publication.

- [2] **Christopher Agia***, Kevin Lin*, Toki Migimatsu, Marco Pavone, and Jeannette Bohg. *Text2motion: From Natural Language Instructions to Feasible Plans*. Autonomous Robots, 2023. © 2023 Springer Nature. Reproduced with permission from Springer Nature.
- [5] **Christopher Agia**, Rohan Sinha, Jingyun Yang, Ziang Cao, Rika Antonova, Marco Pavone, and Jeannette Bohg. *Unpacking Failure Modes of Generative Policies: Runtime Monitoring of Consistency and Progress*. Proceedings of the 8th Conference on Robot Learning, 2024. © 2024 PMLR.
- [4] **Christopher Agia**, Rohan Sinha, Jingyun Yang, Rika Antonova, Marco Pavone, Haruki Nishimura, Masha Itkina, and Jeannette Bohg. *CUPID: Curating Data your Robot Loves with Influence Functions*. Proceedings of the 9th Conference on Robot Learning, 2025. © 2025 PMLR.

Part I

Policy Monitoring and Interpretability

Chapter 2

Monitoring Policies for Runtime Failure Detection

2.1 Introduction

The central objective of this thesis is to investigate how the reliability of learned robot policies can be improved during real-world deployment. As discussed in [Chapter 1](#), recent advances in robot learning—particularly the adaptation of generative, pretrained foundation models to large and heterogeneous robotics datasets—have enabled policies to exhibit increasingly rich and flexible behavior across a wider variety of tasks, environments [\[309\]](#), and embodiments [\[47\]](#).

This chapter focuses on a challenge that persists even as such capabilities improve: when robot policies are deployed in real-world settings—where conditions cannot be perfectly controlled—they will inevitably encounter *out-of-distribution* (OOD) scenarios in which their behavior becomes unreliable and difficult to predict [\[13\]](#). Moreover, as such environmental shifts may be subtle and their relation to the *in-distribution*, reliable regime of a policy’s experience is often unclear—particularly for policies initialized from internet-pretrained foundation models—failures may arise abruptly and without clear warning. Consequently, methods that monitor learned policies at deployment time and provide early indicators of failure are essential for enabling scalable and reliable real-world robotics deployment.

Identifying when a learned model behaves unreliably is typically framed as an OOD detection problem, for which a taxonomy of methods exist [\[250, 294\]](#). While these methods can signal distribution shift [\[220, 224\]](#) or quantify uncertainty [\[80, 154\]](#) *w.r.t.* individual input-output samples, they do not fully characterize closed-loop policy failures that arise from multiple, time-correlated prediction errors along a trajectory rollout. Action multimodality further complicates the failure detection problem: that is, actions sampled from multimodal generative policies can vary greatly from one timestep to the next, leading to complex runtime behaviors and, by extension, diverse

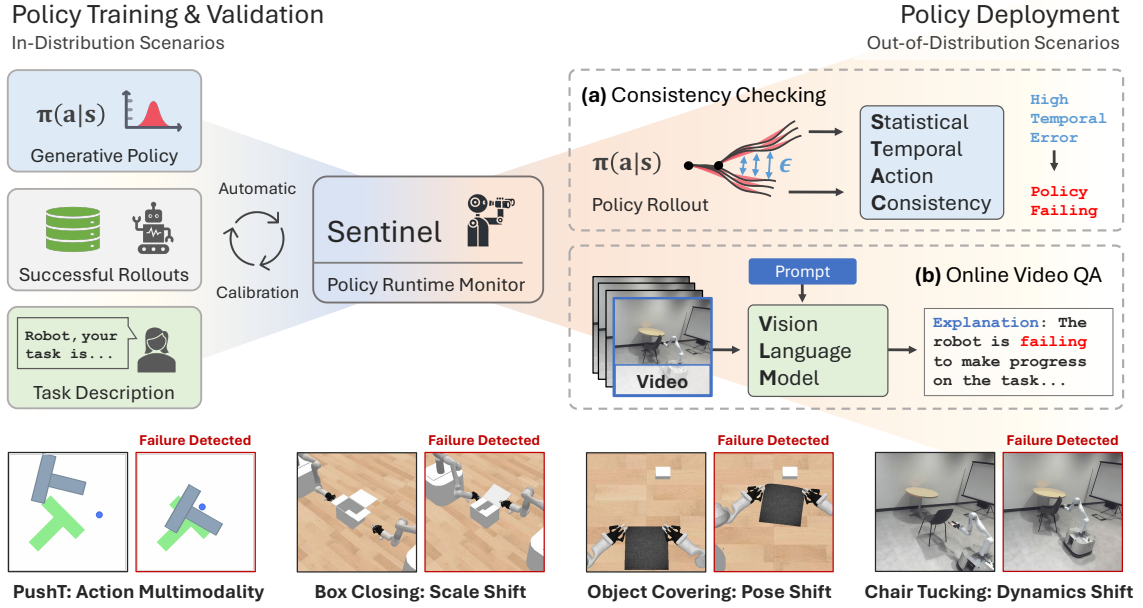


Figure 2.1: We present **Sentinel**, a runtime monitor that detects unknown failures of generative robot policies at deployment time. Constructing Sentinel requires only a set of successful policy rollouts and a description of the task, from which it detects diverse failures by monitoring (a) the temporal consistency of action-chunk distributions generated by the policy and (b) the task progress of the robot(s) through video QA with Vision-Language Models. More details can be found on the Sentinel website: <https://sites.google.com/stanford.edu/sentinel>.

failure modes compared to previous model-free policies [183, 304]. Therefore, the special case of generative robot policies necessitates the design of new failure detectors suited to their multimodal characteristics and closed-loop operational nature in deployment.

In this chapter, we present **Sentinel**, a runtime monitoring framework that splits the task of detecting generative policy failures into two complementary categories. The first is the detection of failures in which the policy exhibits erratic behavior as characterized by its temporal inconsistency. For example, the robot may collide with its surroundings if the policy’s action distributions contain conflicting action modes across time. To detect erratic failures, we propose to evaluate *how much* a generative policy’s action distributions are changing across time using Statistical measures of Temporal Action Consistency (STAC). The second category is the detection of failures in which the policy is temporally consistent but struggles to make progress on its task. For example, the robot can stall in place or drift astray if the policy produces constant outputs. We propose to detect task progression failures (undetectable by STAC) zero-shot with Vision-Language Models (VLMs), which can distinguish off-nominal behavior when prompted to reason about the robot’s progress in a video question answering setup. Notably, one would want to catch erratic failures (the first category) fast, whereas task progression failures (the second category) do not require immediate intervention.

Our contributions are three-fold: 1) A formulation of failure detection for generative policies that splits failures into two complementary categories, thus admitting the use of specialized detectors toward system-level performance increases (i.e., a *divide-and-conquer* strategy); 2) We propose STAC, a novel temporal consistency detector that tracks the statistical consistency of a generative policy’s action distributions to detect erratic failures; 3) We propose the use of VLMs to monitor the task progress of a policy over the duration of its rollout, and we offer practical insights for their use as failure detectors. Provided with only a set of successful policy rollouts and a natural language description of the task, **Sentinel** (which runs STAC and the VLM monitor in parallel) detects over 97% of unknown failures exhibited by diffusion policies [40] across simulated and real-world robotic mobile manipulation domains.

2.2 Related Work

Advances in **robot imitation learning** include new policy architectures [23, 40, 93, 297], hardware innovations for data collection [41, 78, 305], community-wide efforts to scale robot learning datasets [47, 143, 274], and training high-capacity behavior policies on these datasets [29, 146, 201, 309]. Of recent interest is the use of generative models [111, 156, 256, 270] to effectively learn from heterogeneous and multimodal datasets of human demonstrations [40, 47, 146, 201]. *Generative policies* thereby learn to represent highly multimodal distributions from which diverse robot actions can be sampled. While state-of-the-art generative policies demonstrate remarkable performance, their inherent multimodality results in more stochastic runtime behavior than that of previous model-free policies [77, 99, 183, 197, 214, 304]. In this chapter, we focus on characterizing the behavior of generative robot policies for failure detection.

Despite recent progress, it is well known that **learned policies may fail** beyond their training distribution [13, 250, 294], in part due to compounding prediction errors on states induced by the policy [221, 222]. As such, a recent work proposes to bound the performance of imitation learned policies prior to deployment [272]. Other works propose to retrain the policy on OOD states using corrective supervision from humans [18, 50, 113, 140, 182]. Notably, these methods apply *after* failures have occurred, maintaining the need for runtime monitors that detect policy failures and prevent their downstream consequences. Thus, our focus can be viewed as complementary to methods that learn post hoc from corrective feedback.

The existing literature on **out-of-distribution detectors** and **runtime monitoring** for learned models is highly diverse, spanning multiple categories of methods. Model-based methods (e.g., [169, 186]) are not directly applicable to the model-free policies we consider. Some methods only pursue failure modes that are known *a priori* [55, 74, 122, 212], whereas we seek to detect unknown failures at deployment time. Many OOD detection works detect dissimilarity from training data via reconstruction [220, 225] or embedding similarity [158, 224], however, observational differences may

not always result in policy failure. Other methods directly quantify epistemic uncertainty [80, 154, 170, 239], but come with considerable computational expense or may not be suitable for autoregressive, generative policy architectures, e.g., diffusion policies [40]. Several works monitor symbolic states to detect manipulation failures [107, 193], but assume access to multiple sensor modalities (e.g., vision, haptic, proprioception) for symbolic state estimation. Most related to our approach are algorithms that perform consistency checks across sensor modalities [159] and time [12]. Different from these, we directly monitor the consistency of a learned policy’s action distributions and its task progress to detect closed-loop failure.

There is a growing interest in the use of **Foundation Models** [26] toward increasing robustness in robotic systems. Large Language Models are used to detect anomalies [71, 251] and to replan under execution failures [118, 171, 251, 253]. Reward models in the form of visual representations [49, 178] or VLMs [295] could be repurposed for failure detection by thresholding predicted rewards. However, [295] shows that additional fine-tuning is required to obtain reliable reward estimates. Du et al. [69] fine-tunes a VLM for episode-level success classification using a human annotated dataset on the order of 10^5 trajectories. In contrast to this work, we 1) focus on zero-shot assessment with VLMs, 2) seek to detect policy failure amidst task execution, and 3) consider the system-level role of VLMs operating alongside policy-level failure detectors, and as such, assign each detector to a specified category of failure.

2.3 Problem Setup

Failure Detection Our goal is to detect when a generative robot policy $\pi(a|s)$ fails to complete its task. The policy operates within a Markov Decision Process (MDP) with a finite horizon H , but it may terminate upon completion of the task at an earlier timestep. Given an initial state s_0 representative of a new test scenario, executing the policy for t timesteps produces a trajectory $\tau_t = (s_0, a_0, \dots, s_t)$. We define **failure detection** as the task of detecting whether a trajectory rollout τ_H constitutes a failure at the earliest possible timestep t . To do so, we aim to construct a failure detector $f(\tau_t) \rightarrow \{\text{ok}, \text{failure}\}$ that, at each timestep t , can provide a classification as to whether the policy *will fail* if it continues executing for the remaining $H - t$ timesteps of the MDP. Note that the failure detector makes its assessment solely based on the history of observed states and sampled actions up to the current timestep t .

The failure detector may contain parameters that require calibration, such as a detection threshold (as in §2.4.1). Therefore, we assume a scenario in which the policy π is first trained, then validated on test cases where it is expected to perform reliably. This validation process yields a small dataset of M successful trajectories $\mathcal{D}_\tau = \{\tau^i\}_{i=1}^M$ that can be used to calibrate the failure detector f (if it contains parameters). Intuitively, the dataset \mathcal{D}_τ characterizes nominal policy behavior within or near the distribution of states it has been trained on, which helps to ground the assessment of

potentially OOD trajectories at test time.

We measure failure detection performance in terms of true positive rate (TPR), true negative rate (TNR), and detection time (DT). We count a true positive if the failure detector raises a warning at any timestep in a trajectory where the policy fails, the earliest of which counts as the detection time. We count a true negative if the failure detector never raises a warning in a trajectory where the policy succeeds. We refer to §A.2.4 for supporting definitions of policy failure and key performance metrics.

Policy Formulation We consider the setting where the policy π is stochastic and predicts a sequence of actions (also referred to as an *action chunk* [305]) for the next h timesteps. That is, the action sequence sampled at the t -th timestep, $a_t \sim \pi(\cdot|s_t)$, consists of h actions $a_t := (a_{t|t}, a_{t+1|t}, \dots, a_{t+h-1|t})$, where the notation $a_{t+i|t}$ denotes the action prediction for time $t+i$ generated at timestep t (as in [28]). The actions $a_{\cdot|t} \in \mathcal{A}$ may correspond to e.g., end-effector poses or velocities. To control the robot, we sample an action sequence and execute the first $k < h$ actions, $a_{t:t+k|t}$, after which we re-evaluate the policy at timestep $t+k$. We visualize this receding horizon rollout for $k=1$ in Fig. 2.2. Notably, a_t and a_{t+k}

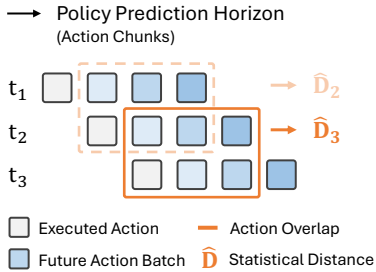


Figure 2.2: Action sequence prediction overlap during policy rollout.

contain actions that temporally overlap for $h-k$ timesteps (i.e., at $a_{t+k:t+h-1|t}$ and $a_{t+k:t+h-1|t+k}$).

Several recently proposed policy architectures achieve state-of-the-art performance by sampling action sequences using generative models [40, 201, 305], to which our approach is generically applicable. Here, we specify the failure detection problem for diffusion policies (DP) [40], which a) are stable to train and b) address action multimodality by representing the policy distribution with a denoising diffusion probabilistic model (DDPM) [111]. We note that the computationally intensive, iterative nature of the denoising process makes it challenging to directly apply existing OOD detection methodologies (e.g., [239]) to diffusion policies for failure detection, thus motivating several of our design decisions. Further details on the training and properties of these models are provided in §A.2.2.

2.4 Proposed Approach: Sentinel

The failure behavior of a generative policy by OOD conditions can be highly diverse, and we therefore argue that the desiderata for a failure detector may vary between qualitative types of failures. Accordingly, we propose to split the failure detection task into two complementary failure categories.

The first is the detection of failures resulting from erratic policy behavior, which may cause a robot to end up in states that are difficult or costly to reset from, knock over objects, or lead to safety hazards. Therefore, it is important to detect erratic behavior as quickly as possible (§2.4.1).

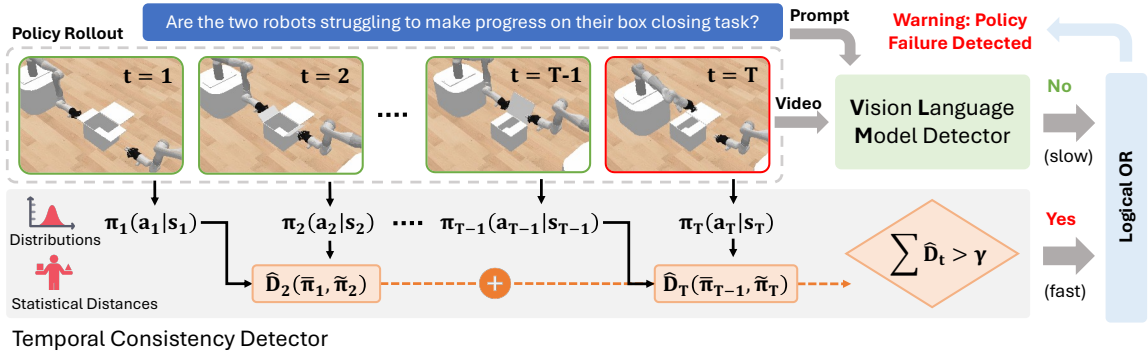


Figure 2.3: **Overview of Sentinel.** The images depict a policy rollout for timesteps $t = 1, \dots, T$. Temporal Consistency Detector: At each timestep t , the state s_t is passed to the generative policy to obtain action distributions π_t between which statistical distances \hat{D}_t are computed to measure temporal consistency. The statistical distances are summed up to the current timestep T (as in Eq. 2.1) and thresholded by γ to detect policy failure. Vision-Language Model (VLM) Detector: The VLM classifies whether the policy is failing to make progress on its task given a video up to timestep T and a description of the task. Execution stops if either detector raises a warning.

The second category is the detection of failures in which the policy struggles to make progress on its task (hereafter referred to as *task progression failures*) but does so in a temporally consistent manner. For example, the policy may confidently place an object in the wrong location. Here, we must observe the robot over a longer period of time to identify that the policy is not making progress towards task completion (§2.4.2).

The **key insight** of our approach is that by defining one failure category as the complement of the other, it becomes trivial to combine failure detectors to form an accurate overall detection pipeline whilst satisfying the requirements of each failure category. Our full pipeline, **Sentinel**, is shown in Fig. 2.3.

2.4.1 STAC: Detecting Erratic Failures with Temporal Consistency

When a policy operates in nominal, in-distribution settings, it should complete its task in a temporally consistent manner. For example, a policy may plan to avoid an obstacle on the right or on the left, but not jitter between the two options. Moreover, as noted in [40], training a diffusion policy that predicts action sequences rather than individual actions encourages temporal consistency between action predictions.

Therefore, we propose to construct a quantifiable measure of temporal action consistency to detect whether the policy is behaving erratically, and hence, is likely to fail at the task. However, the multimodal distributional nature of DPs makes it difficult to directly compare two sampled actions $a_t \sim \pi(a_t|s_t)$ and $a_{t+k} \sim \pi(a_{t+k}|s_{t+k})$, e.g., throughout execution. This is because the actions may differ substantially along their prediction horizon when the policy commits or switches

between different action modes, or simply due to randomness in sampling. Instead, we quantify erratic policy behavior with statistical measures of temporal action consistency (**STAC**, which we term our approach).

Let $\bar{\pi}_t := \pi(a_{t+k:t+h-1}|t|s_t)$ and $\tilde{\pi}_{t+k} := \pi(a_{t+k:t+h-1}|t+k|s_{t+k})$ be the marginal action distributions of the temporally overlapping actions between timesteps t and $t+k$. We compute the temporal consistency between two contiguous timesteps t and $t+k$ as $\hat{D}(\bar{\pi}_t, \tilde{\pi}_{t+k}) \geq 0$, where \hat{D} denotes the chosen statistical distance function (e.g., maximum mean discrepancy, KL-divergence)¹. In addition, we propose to take the cumulative sum of statistical distances along a trajectory as a measure of the overall temporal consistency in a policy rollout. At each policy-inference timestep $t = jk$ with $j \in \{0, 1, \dots\}$, we compute the temporal consistency score as

$$\eta_t := \sum_{i=0}^{j-1} \hat{D}(\bar{\pi}_{ik}, \tilde{\pi}_{(i+1)k}). \quad (2.1)$$

Computing the consistency score in a cumulative manner has two advantages over thresholding the distance at each timestep individually. Firstly, it allows us to detect cases where the temporal consistency metric \hat{D} is marginally larger than usual throughout the episode (e.g., jitter). Secondly, it allows us to detect instances where the policy is temporally inconsistent more often than in nominal scenarios.

At runtime, we raise a failure warning at the moment that η_t exceeds a failure detection threshold γ , which we calibrate offline using the validation dataset of successful trajectories \mathcal{D}_τ . Here, we first compute the cumulative temporal consistency scores throughout the entirety of the lengths $H_i \leq H$ of trajectories in \mathcal{D}_τ , yielding $\{\eta_{H_i}^i\}_{i=1}^M$. Then, we set the threshold γ to the $1 - \delta$ quantile of $\{\eta_{H_i}^i\}_{i=1}^M$, where $\delta \in (0, 1)$ is a hyperparameter. Intuitively, this ensures that the false positive rate (FPR)—the probability that we raise a false alarm and terminate on any trajectory that is i.i.d. with respect to \mathcal{D}_τ —remains low, such that any warnings are likely failures. We can formalize this intuition using recent results from conformal prediction [10, 176]:

Proposition 1 (STAC has low FPR). *Let P_τ denote the distribution of success trajectories in the validation dataset $\mathcal{D}_\tau = \{\tau^i\}_{i=1}^M \stackrel{\text{iid}}{\sim} P_\tau$. Then, the FPR—the probability of raising a false alarm at*

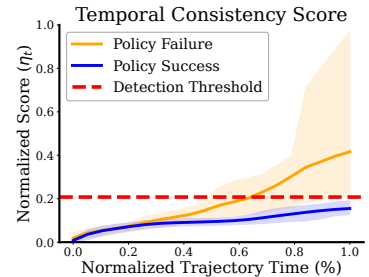


Figure 2.4: Temporal consistency scores grow faster when the policy fails. Error bars indicate the 5-th and 95-th score quantiles.

¹Due to the iterative denoising procedure of the diffusion policy, analytically computing a distance $D(\bar{\pi}_t, \tilde{\pi}_{t+k})$ is challenging, as evaluating the densities of $\bar{\pi}_t$ and $\tilde{\pi}_{t+k}$ requires marginalizing out the intermediate diffusion steps and the non-overlapping actions. Instead, we approximate D with its empirical counterpart \hat{D} by sampling a batch of action sequences (parallelized on a GPU) at each timestep t and $t+k$ rather than a single action sequence.

any point during an i.i.d. test trajectory $\tau \sim P_\tau$ of length $H' \leq H$ —is at most δ :

$$\text{FPR} := \mathbb{P}_{P_\tau}(\exists 0 \leq t \leq H' \text{ s.t. } \eta_t > \gamma) \leq \delta.$$

We refer to §A.1.1 for additional details on STAC and §A.4 for a full statement and proof of Proposition 1.

2.4.2 Detecting Task Progression Failures with VLMs

A policy operating in out-of-distribution settings may not always fail by exhibiting erratic behavior that we can detect with STAC (§2.4.1). For example, suppose the policy confidently commits to the wrong plan or produces approximately constant outputs. Detecting such failures requires an understanding as to whether or not the policy is progressing on its task, which necessitates a more comprehensive analysis of the robot’s behavior within the context of its task specification. Therefore, we propose to use VLMs to monitor the task progress of the policy by providing them with the robot’s image observations up to the current timestep as a video. We do so because recent work has shown that high-capacity VLMs possess robotics relevant knowledge and contextual reasoning abilities [69, 84, 162, 200, 295].

We formulate the detection of task progression failures as a chain-of-thought (CoT) [281], video question answering (QA) task [11, 293], reflecting current best practices in prompting. To capture a notion of *task progress*, the VLM must reason across time and in the context of the policy’s task. Thus, we construct a prompt that contains a description of the task and the VLM’s role as a runtime monitor. We query the VLM online using the text prompt and the history of observed images (i.e., a video) $I_{0:t} := (I_0, I_{\nu k}, I_{2\nu k}, \dots, I_t)$ up to the current timestep t , where ν determines the frequency of the images relative to the execution horizon k of the DP (§2.3). Differentiating between partial progress and task failure can be ambiguous for a slow moving robot, and thus, we also specify the current elapsed time t and the time limit for the task H . This enables the VLM to gauge whether the rate at which the robot is executing will result in a timely task completion. After performing a CoT analysis, the VLM concludes with a classification in $\{\text{ok}, \text{failure}\}$. For additional details on the VLM and prompt, please see §A.1.2.

At the time of writing, cloud-querying a state-of-the-art VLM for video QA incurs significant latency (e.g., GPT-4o’s mean response time was 14.0s). However, we emphasize that VLM inference latency is a lesser concern for detecting task progression failures because they are likely to occur at longer timescales and do not require urgent intervention. In contrast, we assign the rapid detection of erratic failures to STAC (§2.4.1). Notably, the fast and slow detection requirements of our complementary failure categories mean that STAC and the VLM can operate at different timescales, offering potential benefits such as reduced costs and a lower likelihood of false positives when they run in parallel (Fig. 2.3).

2.5 Experiments

We conduct a series of experiments to test our failure detection framework. These experiments take place in both simulation and the real world (Fig. 2.1), and host an extensive list of baselines. We refer to §A.2 for a detailed description of our environments, hardware setup, baselines, and evaluation protocol.

Environments. We include the **PushT** domain from [40] to evaluate the detection of failures under action multimodality. The **Close Box** and **Cover Object** domains involve two mobile manipulators and thus present the challenge of a high-dimensional, 14 degree-of-freedom action space. We additionally conduct hardware experiments with a mobile manipulator for a nonprehensile **Push Chair** task. This task presents greater dynamic complexity than the simulation domains [226]. At test time, we generate OOD scenarios by randomizing a) the scale and dimensions of objects in **PushT** and **Close Box** and b) the pose of the object in **Cover Object** and **Push Chair** beyond the policy’s demonstration data.

Baselines. We evaluate Sentinel (i.e., both STAC and the VLM) against baselines representative of multiple methodological categories in the OOD detection literature [250]. Intuitively, these categories represent different formulations of the failure detector’s score function, responsible for computing the per-timestep scores that are then summed to compute the trajectory score as in Eq. 2.1. We consider score functions based on the embedding similarity of observed states *w.r.t.* \mathcal{D}_τ [158], the reconstruction error of actions sampled from the DP [94], and the output variance of the DP. To strengthen the comparison, we introduce a new baseline that uses the DDPM loss (Eq. A.1) on re-noised actions sampled from the DP as the failure detector’s score function. Where applicable, we implement temporal consistency variants of these baselines to ablate the design of STAC. Further details on these baselines are provided in §A.2.3.

Evaluation Protocol. We train a DP for each environment and use standard settings for the DP’s prediction and execution horizon [40]. We use the same calibration and evaluation protocol across all failure detection methods. That is, we calibrate detection thresholds to the 95-th quantile of scores in a dataset $\mathcal{D}_\tau = \{\tau^i\}_{i=1}^M$ of $M = 50$ in-distribution rollouts for each simulated task and $M = 10$ in-distribution rollouts for the real-world task. Finally, we report standard detection metrics including TPR, TNR, Mean Detection Time, Accuracy, and Balanced Accuracy, following the definitions in §2.3.

2.6 Results

STAC detects diffusion policy failures in multimodal domains. Fig. 2.5 (Left) compares STAC against the best performing method of each baseline category in the **PushT** domain. Here, STAC is the only method to achieve a balanced accuracy of over 90%, indicating that temporal consistency (or lack thereof) is strongly correlated with success (or failure). Alternative output

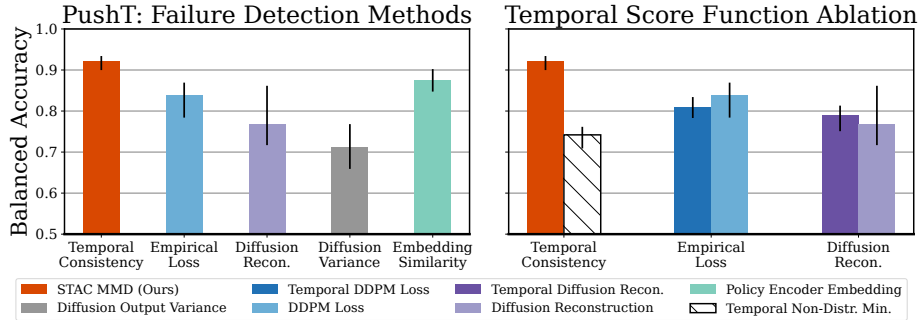


Figure 2.5: **Detecting failures in PushT.** Left: Our failure detector (**STAC**) which measures the temporal consistency of a generative policy outperforms several families of out-of-distribution detectors. Right: The best performance comes from measuring temporal consistency with statistical distance functions; augmenting baselines with temporal consistency does not always increase their performance.

metrics, such as the DP’s output variance, do not perform well because both successes and failures can exhibit high-variance outputs in multimodal domains. Interestingly, the embedding similarity approach performs strongly, which indicates that state dissimilarity *w.r.t.* the calibration dataset happens to be correlated with failure in this domain.

Statistical measures of action similarity enable temporal consistency detection. Fig. 2.5 (Right) ablates the design decisions of **STAC**. First, we observe that augmenting baselines with temporal consistency will at most marginally increase their performance. Second, using a non-statistical distance function (e.g., min. distance) to measure temporal action consistency performs worse than the baselines because it omits action multimodality. Thus, it is the combination of statistical distance functions with temporal consistency that yields the best result. We refer to §A.3.1 for an extended ablation of **STAC**.

STAC accounts for OOD failures and generalization. Results on the **Close Box** domains are shown in Table 2.1. **STAC** attains the highest accuracy in aggregate (96%). However, two of our newly proposed baselines—using the DDPM loss (Eq. A.1) and a temporal reconstruction variant of [94]—also perform well, perhaps due to a decrease in action multimodality relative to **PushT**. Notably, we find that embedding similarity methods conflate OOD states with policy failure, resulting in false positives when the policy succeeds OOD. In contrast, **STAC** effectively differentiates OOD successes from failures.

VLMs must reason across time. In Table 2.1, we find that a state-of-the-art VLM (GPT-4o) struggles to identify task success when given only a single image. Instead, it must observe the robot over the extent of a policy rollout to more accurately reason about task progression and changes in state (resulting in a 91% TNR). While erratic failures are time-sensitive, they are visually more subtle and thus difficult for the VLM to detect (77% TPR). The robot takes more obviously wrong actions (e.g., stalling, drifting astray) in task progression failures (Fig. 2.6). As expected, the VLM has a significantly slower detection time relative to **STAC**, further highlighting **STAC**’s value at

Category 1: Erratic Failures		Close Box: In-Distribution (Policy Success Rate: 91%)			Close Box: Out-of-Distribution (Policy Success Rate: 41%)			Close Box: Combined (Policy Success Rate: 67%)		
Failure Detector		TPR \uparrow	TNR \uparrow	Det. Time (s) \downarrow	TPR \uparrow	TNR \uparrow	Det. Time (s) \downarrow	TPR \uparrow	TNR \uparrow	Accuracy \uparrow
Diffusion	Temporal Non-Distr. Min.	1.00	0.97	5.00	1.00	0.27	12.35	1.00	0.77	0.85
	Diffusion Recon. [94]	0.33	0.95	13.60	0.40	1.00	17.08	0.37	0.96	0.76
	Temporal Diffusion Recon.	1.00	0.96	8.47	0.92	1.00	15.75	0.92	0.97	0.95
	DDPM Loss (Eq. A.1)	1.00	0.90	8.27	1.00	0.94	14.54	1.00	0.91	0.94
	Temporal DDPM Loss	1.00	0.95	7.53	1.00	0.37	13.66	1.00	0.79	0.86
	Diffusion Output Variance	0.33	0.94	14.00	0.28	1.00	17.27	0.26	0.96	0.72
Embed.	Policy Encoder	0.25	0.98	16.27	1.00	0.00	1.59	0.94	0.70	0.78
	CLIP Pretrained	1.00	0.95	15.73	1.00	0.00	8.20	1.00	0.68	0.79
	ResNet Pretrained	1.00	0.95	17.87	1.00	0.00	15.51	1.00	0.68	0.79
STAC	STAC For. KL (Ours)	1.00	0.90	6.60	0.99	0.85	14.04	0.99	0.89	0.92
	STAC Rev. KL (Ours)	1.00	0.95	7.60	0.93	0.97	15.12	0.93	0.96	0.95
	STAC MMD* (Ours)	1.00	0.94	7.20	0.99	0.93	14.72	0.99	0.94	0.96
VLM	GPT-4o Image QA	1.00	0.00	23.20	1.00	0.00	23.20	1.00	0.00	0.29
	GPT-4o Video QA* (Ours)	1.00	0.89	21.20	0.69	0.95	21.02	0.77	0.91	0.87
Sentinel (STAC MMD* + GPT-4o Video QA*)		1.00	0.86	5.47	1.00	0.90	14.25	1.00	0.87	0.91

Table 2.1: **Detecting erratic policy failures in the Close Box domain.** Results are averaged over 3 random seeds. Our temporal consistency detector, STAC, accounts for when a policy fails (**high true positive rate**) and when it generalizes to out-of-distribution test cases (**high true negative rate**), in contrast to embedding-based methods that associate state atypicality with policy failure (**low true negative rate**). Select baselines that accurately detect erratic policy failures in this domain experience a decrease in performance under multimodal conditions (i.e., PushT, as shown in Fig. 2.5), whereas STAC continues to exhibit **strong performance** across multiple domains. VLMs **must reason** over video to attain high true negative rates, as is necessary to combine them with STAC (see Fig. 2.6). Sentinel, which runs STAC and the VLM monitor in parallel, detects 100% of erratic policy failures in this domain.

quickly detecting erratic behavior.

Sentinel: Combining STAC and VLMs for system-level performance increases. We evaluate our failure detectors on distribution shifts that primarily lead to task progression failures in the **Cover Object** and **Close Box** domains. The result is shown in Fig. 2.6. STAC achieves a low TPR (44%) when the policy fails in a temporally consistent manner, whereas the VLM (GPT-4o for **Close Box**, Claude for **Cover Object**) accurately detects task progression failures. As a result, their combination (Sentinel) achieves a 93% TPR whilst incurring only a 7% increase in FPR. The rise in detection time indicates that both STAC (fast) and the VLM (slow) are contributing to the detection of failures.

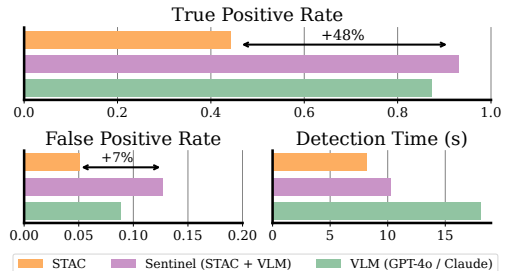


Figure 2.6: **Detecting task progression failures.** Combining VLMs with STAC yields an accurate overall detector (Sentinel) for both task progression and erratic failures (Table 2.1). See §A.3.2 for extended results and analysis.

Sentinel detects real-world, generative policy failures. We evaluate Sentinel on the **Push Chair** task across 10 successful and 10 failed policy rollouts. The results are shown in Table 2.2. When calibrated on only 10 successful in-distribution rollouts, STAC detects 80% of policy failures and raises only one false alarm (90% TNR). The VLM exhibits stronger performance in the real world (90% TPR, 100% TNR) than it does in the simulation domains, perhaps because real-world images constitute a lesser domain gap for visual reasoning compared to images rendered in simulation.

Overall, Sentinel achieves a 95% detection accuracy, highlighting its efficacy for detecting failures in real-world robotic settings.

Discussion. Holistic analysis of Table 2.1, Fig. 2.6, and Table 2.2 shows that we can easily combine STAC and the VLM to yield a performant overall detector for both erratic and task progression failures, particularly because both detectors achieve a high overall TNR. Since all the baselines may 1) show low accuracy on either of the erratic failure domains (i.e., the multi-modal **PushT** and **Close Box** domains) or 2) yield a low TNR, it is unclear how to combine them with other detectors in a way that outperforms Sentinel.

Failure Detector	TPR \uparrow	TNR \uparrow	Det. Time (s) \downarrow
Diffusion Output Variance	0.60	0.90	10.67
Temporal Non-Distr. Min.	0.70	0.80	9.52
STAC Rev. KL (Ours)	0.80	0.90	9.83
GPT-4o Video QA (Ours)	0.90	1.00	12.89
Sentinel (STAC + GPT-4o)	1.00	0.90	9.60

Table 2.2: **Detecting real-world failures.** Sentinel demonstrates strong failure detection performance on the real-world Push Chair task, achieving an overall accuracy of 95%.

2.7 Conclusion

In this chapter, we investigate the problem of failure detection for generative robot policies. We propose Sentinel, a runtime monitor that splits the failure detection task into two categories: 1) Erratic failures, which we detect by measuring the statistical change of a policy’s action distributions over time; 2) task progression failures, where we use Vision-Language Models to assess whether the policy is consistently taking actions that do not solve the task. Our results highlight the importance of targeting complementary failure categories with specialized detectors. Future work includes the use of Sentinel to monitor high-capacity policies [146, 201], inform data collection, and accelerate policy learning.

2.8 Limitations and Future Work

We summarize the limitations of our approach and opportunities for future investigation:

1. **Failure categories.** While categorizing erratic and task progression failures leads to accurate detection of failures across the domains we consider, these two failure categories may not be exhaustive. In the future, introducing additional categories or further partitioning existing ones might provide a broader coverage of failures, allow for more efficient failure detection, and inform mitigation strategies.
2. **Detection guarantees.** Furthermore, our approach does not provide formal guarantees on detecting failures. However, providing such guarantees would require data of both successful and unsuccessful policy rollouts to calibrate the detector [176].

3. **Combining detectors.** Although our detectors attain low false positive rates in aggregate, taking the union of their predictions may, in the worst case, increase the risk of false alarms. Thus, exploring more sophisticated ways to combine complementary failure detectors is a possible point of extension.
4. **Failure prediction.** Finally, our approach is not targeted at predicting failures before they occur, but instead focuses on detecting failures as they occur.

Chapter 3

Understanding Policy Behavior through Training Data

3.1 Introduction

In [Chapter 2](#), we examined how policy reliability can be improved through deployment-time failure detection, enabling systems to identify when learned behaviors are likely to break down. While such mechanisms are essential for mitigating unsafe outcomes, they offer limited insight into *why* failures occur. This chapter addresses this limitation from a data-centric perspective, motivated by the observation that a policy’s deployment-time behavior is fundamentally shaped by the quality and composition of its training data—yet this relationship often remains opaque. Accordingly, we seek to elucidate how individual training demonstrations contribute to downstream outcomes, such as closed-loop task success or failure, thereby providing principled insight into the underlying causes of policy behavior.

More broadly, while some of the largest breakthroughs in deep learning have emerged from architectural innovations, data often remains an underrecognized yet critical driver of a model’s overall performance. The success of scaling vision and language models has been followed by a rising interest in data attribution [[72](#), [97](#), [205](#)]*—*methods that causally link model behavior to training data*—*and in automatic data curation algorithms [[8](#), [157](#), [264](#)], grounded in the idea that not all data points contribute equally, or even positively, to a model’s performance. As the robotics community continues to scale imitation learning and robotics datasets become increasingly diverse [[47](#), [143](#)], developing a deeper understanding of (i) how demonstration data shapes policy behavior and (ii) how we can extract maximum utility from training datasets will be imperative to advancing policy performance toward reliable, open-world deployment.

Curating data for robot imitation learning has been the focus of several recent works [[33](#), [109](#), [151](#)].

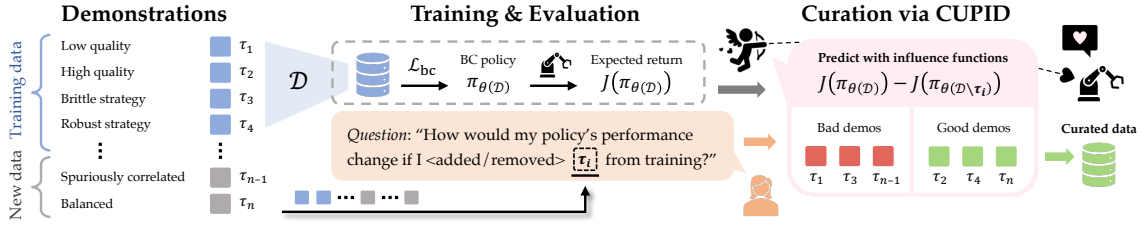


Figure 3.1: We present **CUPID**, a robot data curation method that leverages influence functions to predictively answer counterfactual questions about the effect of each demonstration on downstream policy performance. More details can be found on the CUPID website: <https://cupid-curation.github.io>.

A common approach retains demonstrations deemed most valuable under a heuristic, *task-agnostic quality* metric, resulting in a smaller dataset curated offline [109]. This approach typically rests on the implicit assumption that the designed quality metric aligns well with the policy’s downstream performance—an assumption that may not hold uniformly across diverse robotics tasks. While recent efforts attempt to learn *performance-correlated* heuristics using online policy experience [33], they do not establish strong causal links between training data and policy behavior. As a result, these methods risk misattributing the root cause of policy success or failure with respect to the training data [61].

In this chapter, we formally define data curation in imitation learning as the problem of identifying which expert demonstrations maximally contribute to the policy’s expected return. We then introduce CUPID (CURating Performance-Influencing Demonstrations), a data curation method that directly targets this objective by leveraging influence functions [147, 148]—a technique popularized in the data attribution literature [103]—to identify which demonstrations influenced a policy’s predictions during closed-loop execution. We show that a demonstration’s influence on expected return decomposes into a tractable sum over its state-action transitions and can be efficiently approximated using a REINFORCE-style estimator [258] given a set of policy rollouts. Ranking demonstrations by their estimated performance impact facilitates curation in two settings: (a) filtering existing demonstrations from training sets and (b) selecting high-impact demonstrations from newly collected or pre-collected data—whereas prior work focuses solely on filtering [33, 109]. Finally, while our approach offers a general and effective standalone signal for curating demonstration data, we investigate its combined use with task-agnostic quality metrics (also derived from influence scores), identifying conditions under which the integration of performance- and quality-based metrics strengthens or weakens overall curation performance.

Our contributions are three-fold: (1) We formulate robot data curation as the problem of valuating demonstrations in accordance with their downstream impact on policy performance; (2) We propose CUPID, a novel approach for curating imitation learning datasets based on influence functions, causally linking demonstrations to the policy’s expected return; (3) We characterize the conditions

under which the integration of task-agnostic quality metrics strengthens performance-based data curation, providing practical insights into when such integration is beneficial. Extensive simulation and hardware experiments show that curation with CUPID significantly improves policy performance in mixed-quality regimes, even when using only a fraction of the training data. Moreover, it identifies robust strategies under test-time distribution shifts and can disentangle spurious correlations in training data that hinder generalization—all by observing policy outcomes alone, without requiring additional supervision.

3.2 Related Work

Data Curation in Robotics. Assembling larger and more diverse datasets has been central to scaling efforts in robot imitation learning [25, 29, 47, 143, 146, 201, 309], yet how to extract greater utility from these datasets remains an open question. Several works have explored data augmentation [181, 184, 254, 299, 300] and mixture optimization [108]. Only recently has attention shifted to valuating individual demonstrations for data curation [33, 109, 151]. Hejna et al. [109] estimate demonstration quality offline via mutual information—without considering policy performance—while Chen et al. [33] train classifiers to distinguish successful and failed rollouts across policy checkpoints. In contrast, we directly measure the causal influence of each demonstration on the policy’s expected return, providing a signal that (a) does not require observing both successes and failures, (b) uses only a single policy checkpoint, (c) is robust to spurious correlations in the policy’s rollout distribution, and (d) naturally extends to selecting new data, whereas [33, 109] only filter existing data. Concurrent work includes DataMIL [60], which uses datamodels to select from large multi-task datasets with an offline metric, whereas we focus on single-task curation with an influence measure that directly reflects closed-loop returns from online policy rollouts.

Data Attribution outside Robotics. Data attribution methods model the relationship between training data and learned behavior, with applications in model interpretability [205, 235], data valuation [45, 90], machine unlearning [89], and more [179]. Recent work has focused on improving the accuracy of data attribution methods [15, 20, 120], such as influence functions [147, 148], and extending them to increasingly complex generative architectures [88, 97, 307]. A related line of research explores improving language model pre-training [72] and fine-tuning [73, 172, 288] through data selection. However, these settings typically assume aligned training and evaluation objectives (i.e., prediction loss) and access to test-time labels. In contrast, robot imitation learning involves an objective mismatch: policies are trained via supervised learning but evaluated through closed-loop environment interactions, where task success depends on many sequential predictions and ground-truth action labels are unavailable at test-time.

3.3 Background: Data Attribution via Influence Functions

At a high-level, **the goal of data attribution** methodologies is to explicitly relate model performance and behavior to the training data, so that we can answer *counterfactual* questions about the contribution of training samples towards test-time predictions. Consider a standard supervised learning setting, where we fit model parameters θ on a given training dataset $\mathcal{D} := \{z^1, \dots, z^n\}$ of input-label pairs $z^i = (x^i, y^i) \in \mathcal{Z}$ with $\theta(\mathcal{D}) = \arg \min_{\theta'} \{\mathcal{L}(\theta'; \mathcal{D}) := \frac{1}{n} \sum_{i=1}^n \ell(z^i; \theta')\}$. Moreover, let $f(\hat{z}; \theta) \in \mathbb{R}$ be any chosen performance metric on a test sample $\hat{z} = (\hat{x}, \hat{y}) \in \mathcal{Z}$ given model parameters θ (e.g., cross-entropy loss for a classifier). Then, a data attribution method $\Psi^{\text{out}} : \mathcal{Z} \times \mathcal{Z} \rightarrow \mathbb{R}$ aims to approximate the change in the performance metric f if we were to exclude sample z^i from the model’s training data. That is, we aim to design Ψ^{out} such that $\Psi^{\text{out}}(\hat{z}, z^i) \approx f(\hat{z}; \theta(\mathcal{D} \setminus \{z^i\})) - f(\hat{z}; \theta(\mathcal{D}))$.

The influence function is a data attribution technique that approximates Ψ^{out} *without* retraining any models [103]. Consider perturbing the training objective as $\mathcal{L}_{\epsilon, z}(\theta'; \mathcal{D}) := \mathcal{L}(\theta'; \mathcal{D}) + \epsilon \ell(z, \theta')$, where we add an infinitesimal weight ϵ on the loss of some sample z to \mathcal{L} . The *influence function* estimates the change in the performance metric f as a function of ϵ with a first-order Taylor approximation as

$$\Psi_{\text{inf}}(\hat{z}, z) := \left. \frac{df(\hat{z}; \theta)}{d\epsilon} \right|_{\epsilon=0} = -\nabla_{\theta} f(\hat{z}; \theta(\mathcal{D}))^{\top} H_{\theta}^{-1} \nabla_{\theta} \ell(z; \theta(\mathcal{D})), \quad (3.1)$$

where $H_{\theta} = \frac{1}{n} \sum_{i=1}^n \nabla_{\theta}^2 \ell(z^i; \theta(\mathcal{D}))$ denotes the Hessian of the training loss¹ [147]. Therefore, we can use the influence function to directly approximate the *leave-one-out* influence Ψ^{out} of a sample $z^i \in \mathcal{D}$ as $\Psi_{\text{inf}}^{\text{out}}(\hat{z}, z^i) := -\frac{1}{n} \Psi_{\text{inf}}(\hat{z}, z^i)$. In addition, for $z \notin \mathcal{D}$ we similarly define the *add-one-in* influence as $\Psi_{\text{inf}}^{\text{in}}(\hat{z}, z) := \frac{1}{n} \Psi_{\text{inf}}(\hat{z}, z) \approx f(\hat{z}; \theta(\mathcal{D} \cup \{z\})) - f(\hat{z}; \theta(\mathcal{D}))$ with z excluded from the Hessian H_{θ} .

3.4 Problem Formulation

Imitation Learning (IL): Our objective is to understand how demonstration data contributes to closed-loop performance in robot imitation learning. Thus, we consider a Markov Decision Process $\langle \mathcal{S}, \mathcal{A}, \mathcal{T}, R, \rho_0 \rangle$ with state space \mathcal{S} , action space \mathcal{A} , transition model \mathcal{T} , reward model R , initial state distribution ρ_0 , and finite horizon H . We train a policy π_{θ} to minimize a behavior cloning (BC) objective, i.e., $\theta = \arg \min_{\theta'} \{\mathcal{L}_{\text{bc}}(\theta'; \mathcal{D}) := \frac{1}{|\mathcal{D}|H} \sum_{\xi^i \in \mathcal{D}} \sum_{(s,a) \in \xi^i} \ell(s, a; \pi_{\theta'})\}$, using a dataset of n expert demonstrations $\mathcal{D} = \{\xi^1, \dots, \xi^n\}$. Each demonstration $\xi^i = ((s_0^i, a_0^i), \dots, (s_H^i, a_H^i))$ consists of a state-action trajectory where the robot successfully completes the task. We treat a trajectory $\tau = (s_0, a_0, \dots, s_H)$ as either a *success* or a *failure*, corresponding to the binary returns $R(\tau) = 1$ and $R(\tau) = -1$ respectively.

¹ To reduce the computational cost of Eq. 3.1, we use TRAK [205], which leverages random projections and a Gauss-Newton Hessian approximation for efficient influence estimation. This also makes the influence function amenable to the non-smooth, non-convex loss functions in practical deep learning problems, so we assume Eq. 3.1 is well-defined throughout this chapter.

Therefore, in IL, we train the policy π_θ to match the distribution of successful behaviors in \mathcal{D} , rather than directly maximize its expected return $J(\pi_\theta) := \mathbb{E}_{p(\tau|\pi_\theta)}[R(\tau)]$. As a result, the policy’s performance is intimately linked to the relative suboptimality of the demonstration data—a function of its quality and composition—not just to validation losses, model capacity, or bias-variance tradeoffs. This makes it extremely challenging to systematically improve performance. Recent works underscore that simply scaling demonstration collection may result in datasets that contain substantial redundancies and behaviors that may actually harm policy performance, even though $R(\xi^i) = 1$ for all demonstrations $\xi^i \in \mathcal{D}$ [21].

Robot Data Curation: While several recent works propose intuitive measures of quality to curate data, we find that such heuristics can misalign with how deep models actually learn, sometimes even worsening test-time performance compared to randomly choosing samples (see §3.6). Therefore, we first formally define robot data curation as the problem of identifying demonstration data that maximizes the policy’s closed-loop performance. In particular, assume that we have a *base policy* π_θ trained on the demonstration data \mathcal{D} . We consider two settings that are essential to a policy debugging toolchain. The first is that of *data filtering*, where our goal is to identify and remove redundant or harmful demonstrations from \mathcal{D} that may be limiting the performance of the base policy π_θ .

Task 1 (Filter- k demonstrations). Let $\Xi_k^- = \{S \subseteq \mathcal{D} \mid |S| = k\}$ denote all possible k -demonstration subsets of the training dataset $\mathcal{D} = \{\xi^1, \dots, \xi^n\}$, where $k \leq n$. Determine which k demonstrations should be removed from \mathcal{D} to maximize policy performance with respect to the task objective J . That is, find

$$S^* = \arg \max_{S \in \Xi_k^-} J(\pi_\theta) \quad \text{s.t.} \quad \theta = \arg \min_{\theta'} \mathcal{L}_{bc}(\theta'; \mathcal{D} \setminus S).$$

The second is that of *data selection*, where we seek to guide the subselection of new demonstration data to maximally improve our base policy, given a fixed budget.

Task 2 (Select- k demonstrations). Let $\Xi_k^+ = \{S \subseteq \mathcal{H} \mid |S| = k\}$ denote all possible k -demonstration subsets of a holdout dataset $\mathcal{H} = \{\xi^1, \dots, \xi^{n'}\}$, where $k \leq n'$. Determine which k demonstrations should be added to \mathcal{D} from \mathcal{H} to maximize policy performance with respect to the task objective J . That is, find

$$S^* = \arg \max_{S \in \Xi_k^+} J(\pi_\theta) \quad \text{s.t.} \quad \theta = \arg \min_{\theta'} \mathcal{L}_{bc}(\theta'; \mathcal{D} \cup S).$$

In **Task 2**, we consider the problem of identifying the most impactful trajectories from a newly collected batch of demonstrations or from an existing pre-collected dataset, akin to performing quality control.

Policy Testing & Evaluation: To make progress on **Task 1** and **Task 2**, we assume access to

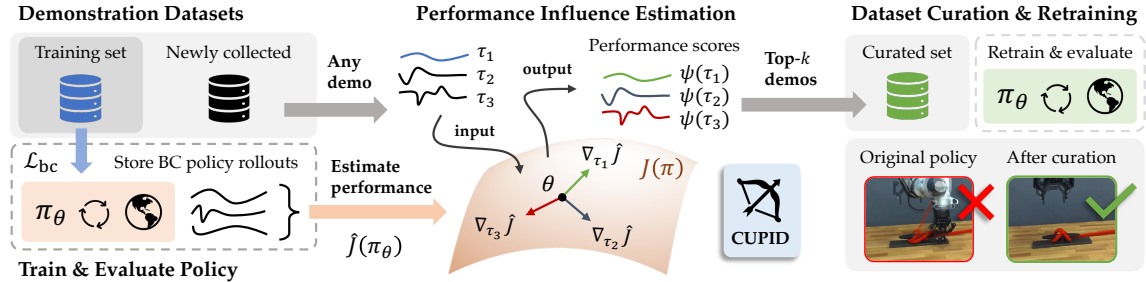


Figure 3.2: **Data curation with CUPID.** Upon training a policy on a set of demonstrations using behavior cloning, we evaluate it online to collect closed-loop rollout trajectories and estimate the policy’s expected return. CUPID ranks demonstration based on their measured influence on this performance estimate and selects the top- k . Thus, curating with CUPID results in a dataset of demonstrations that most strongly influences closed-loop policy success.

a small dataset of m rollouts $\mathcal{D}_\tau = \{\tau^1, \dots, \tau^m\} \stackrel{\text{iid}}{\sim} p(\tau|\pi_\theta)$ of the base policy π_θ along with their associated returns $\{R(\tau^1), \dots, R(\tau^m)\}$ to estimate $J(\pi_\theta)$. This aligns with how we currently evaluate policies in practice [272], despite lacking principled strategies to leverage evaluations towards BC policy improvement.

3.5 CUPID: Curating Performance-Influencing Demonstrations

In the literature, the desiderata for curating demonstration data appears diverse and often context specific, with recent works valuating demonstrations upon heuristic measures of similarity [33], compatibility [83], uncertainty [48], and information gain [109]. **The key insight** of our approach is that solving curation problems, i.e., **Task 1** and **Task 2** (§3.4), requires causally connecting training data to the policy’s closed-loop performance. Therefore, we first adapt techniques from data attribution, as defined in §3.3, to directly compute the influence of a training demonstration on the performance of a policy. This allows us to use our *performance influence* to directly curate data in alignment with our objectives.

3.5.1 Demonstration-Performance Influence

While existing data attribution methods can trace validation losses back to the training set \mathcal{D} for curation purposes, the BC loss is not always reflective of a policy’s closed-loop performance [222]. Thus, we must first develop an analogous notion of the influence function to capture the impact of a *demonstration trajectory* on the *closed-loop performance* of an imitation learning policy. To do so, we group the BC training objective into trajectory-level losses by introducing $\ell_{\text{traj}}(\xi; \pi_{\theta'}) := \frac{1}{H} \sum_{(s,a) \in \xi} \ell(s, a; \pi_{\theta'})$, so that $\mathcal{L}_{\text{bc}}(\theta'; \mathcal{D}) = \frac{1}{|\mathcal{D}|} \sum_{\xi^i \in \mathcal{D}} \ell_{\text{traj}}(\xi^i; \pi_{\theta'})$. We now formally define the

performance influence of a demonstration as the application of the influence function (see Eq. 3.1) on the policy’s expected return:

Definition 1 (Performance Influence). *Let ξ be a demonstration of interest. Suppose we train a policy π_θ to minimize the perturbed BC objective $\mathcal{L}_{\text{bc}}^{\epsilon, \xi}(\theta'; \mathcal{D}) := \mathcal{L}_{\text{bc}}(\theta'; \mathcal{D}) + \epsilon \ell_{\text{traj}}(\xi; \pi_{\theta'})$. Then, demonstration ξ ’s **performance influence** is the derivative of the policy’s expected return $J(\pi_\theta)$ with respect to the weight ϵ . That is,*

$$\Psi_{\pi\text{-inf}}(\xi) := \left. \frac{dJ(\pi_\theta)}{d\epsilon} \right|_{\epsilon=0} = -\nabla_\theta J(\pi_\theta)^\top H_{\text{bc}}^{-1} \nabla_\theta \ell_{\text{traj}}(\xi; \pi_\theta),$$

where $H_{\text{bc}} := \nabla_\theta^2 \mathcal{L}_{\text{bc}}(\theta; \mathcal{D})$ denotes the Hessian of the BC objective.

In essence, **Definition 1** enables us to predictively answer the counterfactual: “How would the policy’s expected return change if we upweighted—or by negating, downweighted—the loss on a demonstration ξ during training?” While **Definition 1** neatly aligns with the standard definition of the influence function in Eq. 3.1—using J as the performance metric and ℓ_{traj} as the demonstration-level loss—we distinguish the *performance influence* from the standard influence function [147] for two key reasons: (1) The performance influence attributes the *outcome* of a policy’s sequential decisions to time-series demonstrations, whereas the existing techniques discussed in §3.3 only relate an individual labeled prediction to a single training sample; (2) We cannot directly compute $\Psi_{\pi\text{-inf}}$ because the policy’s expected return $J(\pi_\theta)$ depends on the unknown transition dynamics and reward function. To alleviate these challenges, we show that we can decompose the *performance influence* into influence scores of individual action predictions, which we define as the *action influence*.

Definition 2 (Action Influence). *The **action influence** of a state-action pair (s, a) on a test state-action pair (s', a') is the influence of (s, a) on the policy’s log-likelihood $\log \pi_\theta(a'|s')$. That is,*

$$\Psi_{a\text{-inf}}((s', a'), (s, a)) := -\nabla_\theta \log \pi_\theta(a'|s')^\top H_{\text{bc}}^{-1} \nabla_\theta \ell(s, a; \pi_\theta). \quad (3.2)$$

The advantage of the *action influence* is that we can easily compute the quantities in Eq. 3.2 given the policy weights θ and the training demonstrations \mathcal{D} , e.g., using the attribution methods discussed in §3.3. However, we emphasize that computing *action influences* over state-action samples from a policy rollout $\tau \sim p(\tau|\pi_\theta)$ only tells us what demonstration data led to the policy taking those actions, without ascribing value to the resulting outcome (e.g., success or failure). We now show that the performance influence decomposes into the sum of individual action influences, weighted by the trajectory return $R(\tau)$.

Proposition 2. *Assume that $\theta(\mathcal{D}) = \arg \min_{\theta'} \mathcal{L}_{\text{bc}}(\theta'; \mathcal{D})$, that \mathcal{L}_{bc} is twice differentiable in θ , and*

that $H_{bc} \succ 0$ is positive definite (i.e., $\theta(\mathcal{D})$ is not a saddle point)¹. Then, it holds that²

$$\Psi_{\pi\text{-inf}}(\xi) = \mathbb{E}_{\tau \sim p(\tau|\pi_\theta)} \left[\frac{R(\tau)}{H} \sum_{(s', a') \in \tau} \sum_{(s, a) \in \xi} \Psi_{a\text{-inf}}((s', a'), (s, a)) \right]. \quad (3.3)$$

In brief, we prove [Proposition 2](#) using the log-derivative trick underlying policy gradient methods [[258](#), [283](#)] to decompose $\Psi_{\pi\text{-inf}}$ into $\Psi_{a\text{-inf}}$ (see [§B.4.1](#) for proof). Because [Proposition 2](#) relates the performance influence to the average action influence that a demonstration ξ has on the closed-loop distribution of policy rollouts, [Proposition 2](#) directly provides a method to estimate $\Psi_{\pi\text{-inf}}$:

Estimate $\Psi_{\pi\text{-inf}}$: First, evaluate the policy π_θ online to gather a set of rollouts $\mathcal{D}_\tau = \{\tau^1, \dots, \tau^m\} \stackrel{\text{iid}}{\sim} p(\tau|\pi_\theta)$ and their associated returns $\{R(\tau^1), \dots, R(\tau^m)\}$. Then, construct an empirical estimate of the performance influence $\widehat{\Psi}_{\pi\text{-inf}}$ using [Eq. 3.3](#), by averaging action influences across the rollouts in \mathcal{D}_τ .

We illustrate the performance influence in [Fig. 3.2](#) and summarize its estimation procedure in [Algorithm 1](#).

Algorithm 1 Performance Influence

- 1: **Input:** Policy π_θ , training data \mathcal{D} , demonstration ξ , data attribution method Ψ
 - 2: Collect rollouts $\mathcal{D}_\tau = \{\tau^1, \dots, \tau^m\} \stackrel{\text{iid}}{\sim} p(\tau|\pi_\theta)$ and returns $\{R(\tau^1), \dots, R(\tau^m)\}$
 - 3: Use Ψ, \mathcal{D} to compute $\Psi_{a\text{-inf}}((s', a'), (s, a))$ for all $(s', a') \in \mathcal{D}_\tau, (s, a) \in \xi$
 - 4: Estimate $\widehat{\Psi}_{\pi\text{-inf}}(\xi) := \frac{1}{m} \sum_{\tau^i \in \mathcal{D}_\tau} \frac{R(\tau^i)}{H} \sum_{(s', a') \in \tau^i} \sum_{(s, a) \in \xi} \Psi_{a\text{-inf}}((s', a'), (s, a))$.
 - 5: **Output:** Estimated performance influence $\widehat{\Psi}_{\pi\text{-inf}}(\xi)$
-

3.5.2 Data Curation with Performance Influence

In this section, we leverage the performance influence $\Psi_{\pi\text{-inf}}$, which we developed in [§3.5.1](#), to curate data towards the filtering and selection tasks ([Task 1](#) and [Task 2](#)) defined in [§3.4](#). In particular, we use the estimates of $\Psi_{\pi\text{-inf}}$ to make the following first-order Taylor approximations on the *leave-one-out* and *add-one-in* influence (as defined in [§3.3](#)) of a demonstration trajectory as

$$\Psi_{\pi\text{-inf}}^{\text{out}}(\xi) := -\frac{\widehat{\Psi}_{\pi\text{-inf}}(\xi)}{|\mathcal{D}|} \approx J(\pi_{\theta(\mathcal{D} \setminus \{\xi\})}) - J(\pi_{\theta(\mathcal{D})}), \quad \Psi_{\pi\text{-inf}}^{\text{in}}(\xi) := \frac{\widehat{\Psi}_{\pi\text{-inf}}(\xi)}{|\mathcal{D}|} \approx J(\pi_{\theta(\mathcal{D} \cup \{\xi\})}) - J(\pi_{\theta(\mathcal{D})}).$$

Then, we use the *leave-one-out* and *add-one-in* influences to counterfactually estimate the change in expected return when removing or adding a set of demonstrations S with a linear approximation as $\Delta \widehat{J}(\pi_{\theta(\mathcal{D} \setminus S)}) \propto \frac{1}{|S|} \sum_{\xi \in S} \Psi_{\pi\text{-inf}}^{\text{out}}(\xi)$ and $\Delta \widehat{J}(\pi_{\theta(\mathcal{D} \cup S)}) \propto \frac{1}{|S|} \sum_{\xi \in S} \Psi_{\pi\text{-inf}}^{\text{in}}(\xi)$. As a result, optimally curating data under our approximate linear model on policy performance simply entails selecting the least influential demonstrations from the training data \mathcal{D} —in the case of data filtering—or selecting the most influential demonstrations from a new set of demonstrations \mathcal{H} —in the case of data selection:

²Note that the fraction $1/H$ appears from the assumption that all trajectories have equal length, which we make purely for notational simplicity without loss of generality. We refer to [§B.4.2](#) for the variable length case.

Task 1: Filter- k Demonstrations**Task 2: Select- k Demonstrations**

$$S_{\text{out}}^* = \arg \text{top-}k(\{\Psi_{\pi\text{-inf}}^{\text{out}}(\xi^i) : \xi^i \in \mathcal{D}\}), \quad (3.4) \quad S_{\text{in}}^* = \arg \text{top-}k(\{\Psi_{\pi\text{-inf}}^{\text{in}}(\xi^i) : \xi^i \in \mathcal{H}\}). \quad (3.5)$$

We note that by linearly approximating policy performance changes using $\Psi_{\pi\text{-inf}}$, we construct what is commonly termed a (linear) *datamodel* [121]. As shown in NLP [72], using such first-order approximations for data curation can often greatly improve model performance over manual notions of quality.

3.5.3 Additional Quality Metrics

In §3.5.1, we constructed a method to estimate $\Psi_{\pi\text{-inf}}$ from a dataset of policy rollouts \mathcal{D}_τ by relying on policy gradient methods. Therefore, the estimated performance influence $\hat{\Psi}_{\pi\text{-inf}}$ becomes increasingly noisy as we reduce the number of rollouts m to evaluate the policy—akin to the high variance problem of the REINFORCE algorithm. To complement the analysis in §3.5.1, we explore the integration of a *reward-agnostic, heuristic* demonstration quality metric based on the action influence scores $\Psi_{a\text{-inf}}$:

$$\Psi_{\text{qual}}(\xi; \mathcal{D}_\tau) := \frac{1}{m} \sum_{\tau \in \mathcal{D}_\tau} \max_{(s', a') \in \tau} \min_{(s, a) \in \xi} \Psi_{a\text{-inf}}((s', a'), (s, a)) - \min_{(s', a') \in \tau} \max_{(s, a) \in \xi} \Psi_{a\text{-inf}}((s', a'), (s, a)). \quad (3.6)$$

We base the quality score Eq. 3.6 on the intuition that we should penalize demonstrations containing outlier or noisy influence scores [147, Sec. 5.2], [109]. As such, we posit that this heuristic can reduce variance on tasks requiring precise motion, yet introduce bias uncorrelated with performance in other settings. Thus, in §3.6, we investigate when the quality score can complement $\Psi_{\pi\text{-inf}}$ to curate data by taking their convex combination, $\alpha\Psi_{\pi\text{-inf}} + (1 - \alpha)\Psi_{\text{qual}}$, ablating $\alpha = 1$ (CUPID) and $\alpha = 1/2$ (CUPID-QUALITY).

3.6 Experiments

We conduct a series of experiments to test the efficacy of CUPID alongside state-of-the-art baselines for robot data curation. These experiments take place across three simulated tasks from the RoboMimic benchmark suite [183] and three real-world tasks with a Franka FR3 manipulator (see Fig. 3.4). These tasks comprise a taxonomy of settings where data curation may benefit policy performance. For a detailed description of our tasks, datasets, baselines, evaluation protocol, and hardware setup, please refer to §B.2

Evaluation. We study the filter- k (Task 1) and select- k (Task 2) curation tasks wherever applicable. For statistical significance, we start filter- k and select- k from random $\sim 2/3$ and $\sim 1/3$ subsets in RoboMimic (300 demonstrations per task total), and random $\sim 9/10$ and $\sim 4/10$ subsets on Franka tasks (120-160 demonstrations per task total), respectively. We use the official convolutional-based diffusion policy implementation [40] for all tasks to measure the effect of curation

on a state-of-the-art policy architecture. Details on the influence function computation for diffusion models are provided in §B.1. We also consider the official π_0 implementation [25] for real-world tasks. To reflect practical constraints, we limit the rollout budget (i.e., the number of rollouts in $\mathcal{D}_\tau = \{\tau^i\}_{i=1}^m$ a curation algorithm may use, as described in §3.4) to $m = 100$ and $m = 25$ for simulated and real-world tasks, respectively. We report policy success rates over 500 rollouts averaged over the last 10 policy checkpoints for simulated tasks, and 25 rollouts performed with the last checkpoint for real-world tasks.

Baselines. We consider baselines from several methodological categories: DemInf [109]—applicable only to filter- k (Task 1)—curates data offline (i.e., without rollouts) by maximizing mutual information, promoting diverse and predictable demonstrations; Demo-SCORE [33] trains binary classifiers to distinguish states from successful and failed rollouts, retaining demonstrations with a high average state success probability; Success Similarity is a custom method that ranks demonstrations by their average state similarity to successful rollouts; Random chooses demonstrations uniformly at random; Oracle approximates an upper bound on performance by curating data with privileged access to ground-truth demonstration labels, e.g., indicating demonstration quality, strategy robustness, or other properties.

3.6.1 Setting 1: Improving Policy Performance in Mixed-Quality Regimes

We first study curation of mixed-quality datasets, where training on lower-quality demonstrations may degrade policy performance [109, 183]. We use the “Lift,” “Square,” and “Transport” tasks from RoboMimic’s multi-human (MH) task suite, which provides ground-truth quality labels for demonstrations. The “Lift” and “Square” tasks contain three quality tiers {“low”, “medium”, “high”}, while the more complex bi-manual “Transport” task contains six quality tiers {“low-low”, “low-medium”, ...}. On hardware, we design the “Figure-8” task (Fig. 3.4(a)), where the robot must tie a simplified cleat hitch—a knot that follows a figure-8 pattern—requiring precise manipulation of a deformable rope.

RoboMimic analysis. Fig. 3.3 presents the RoboMimic benchmark results: the top row shows data quality trends for filter- k and select- k across varying k , while the bottom row reports success rates of diffusion policies trained on the corresponding curated datasets. As expected, we first observe that DemInf—which targets demonstration quality—curates datasets of the highest overall quality by RoboMimic’s ground-truth labels for filter- k (top row, Fig. 3.3). However, policies trained on data curated by CUPID consistently match or outperform those of DemInf (bottom row, Fig. 3.3). This indicates that human perception of demonstration quality does not necessarily correspond to data that maximizes downstream policy success. Second, we find the state similarity heuristics employed by Demo-SCORE and Success Similarity to be relatively ineffective in challenging mixed-quality regimes, where successful and failed rollouts exhibit similar states. Lastly, CUPID-QUALITY, which evenly balances demonstration quality and downstream performance impact (§3.5.3), attains the

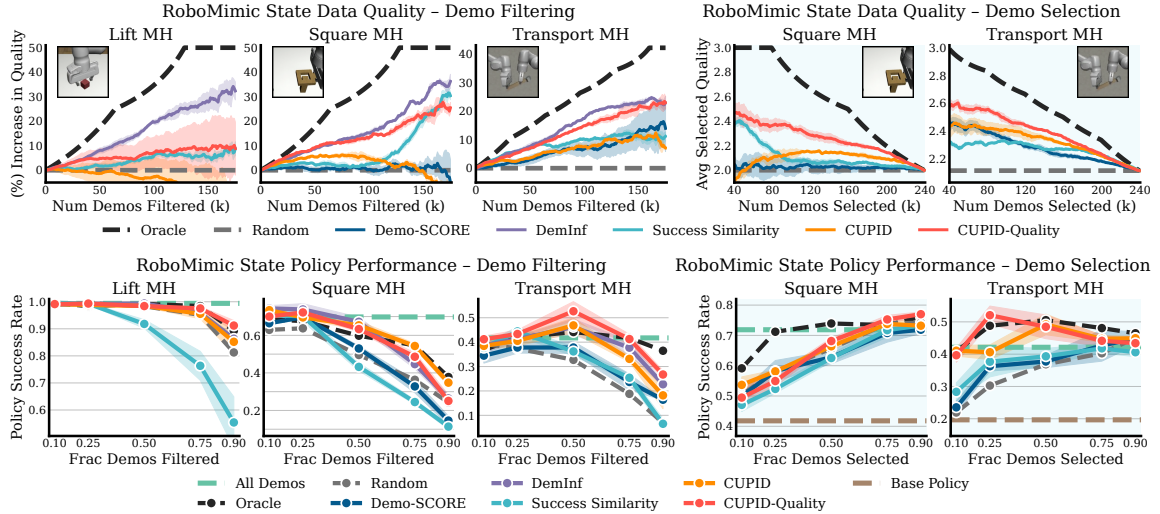


Figure 3.3: RoboMimic mixed-quality curation results. **Top: Data Quality.** Baselines often prioritize demonstration quality (e.g., DemInf [109]), but higher demonstration quality does always translate to higher policy success rates. In contrast, CUPID targets demonstrations that most strongly contribute to downstream policy performance. **Bottom: Policy Performance.** Diffusion policies trained on data curated by CUPID achieve higher success rates than baselines, despite using demonstrations of perceived lower quality. Although combining performance and quality measures (CUPID-QUALITY) yields the best policies on mixed-quality datasets, quality measures can degrade performance in other settings (see Fig. 3.4). Results are averaged over 3 random seeds (500 policies trained across settings). Success rates are computed over 50 rollouts from the last 10 checkpoints (500 rollouts total).

highest policy success rates—surpassing the Oracle in 3/5 cases, and achieving an even higher success rate than the official diffusion policy [40] on “Transport MH” while using fewer than (i) 33% of the original 300 demonstrations and (ii) 10% of the model parameters. We provide an extended discussion of the RoboMimic results in §B.3.1.

Figure-8 analysis. Fig. 3.4(a) shows diffusion policy results on the real-world “Figure-8” task. First, CUPID improves over the base policy’s success rate by 38% (averaged over filtering and selection). Second, as in RoboMimic, CUPID-QUALITY further strengthens curation performance, corroborating the utility of quality metrics (Eq. 3.6) in mixed-quality regimes. As shown in Fig. 3.5(a) (filtering; see §B.3.5 for selection), both CUPID and CUPID-QUALITY successfully retain high-quality demonstrations, whereas baselines such as Demo-SCORE discard some in favor of lower-quality demonstrations. Overall, training on lower-quality demonstrations appears to adversely affect policy performance on the “Figure-8” task.

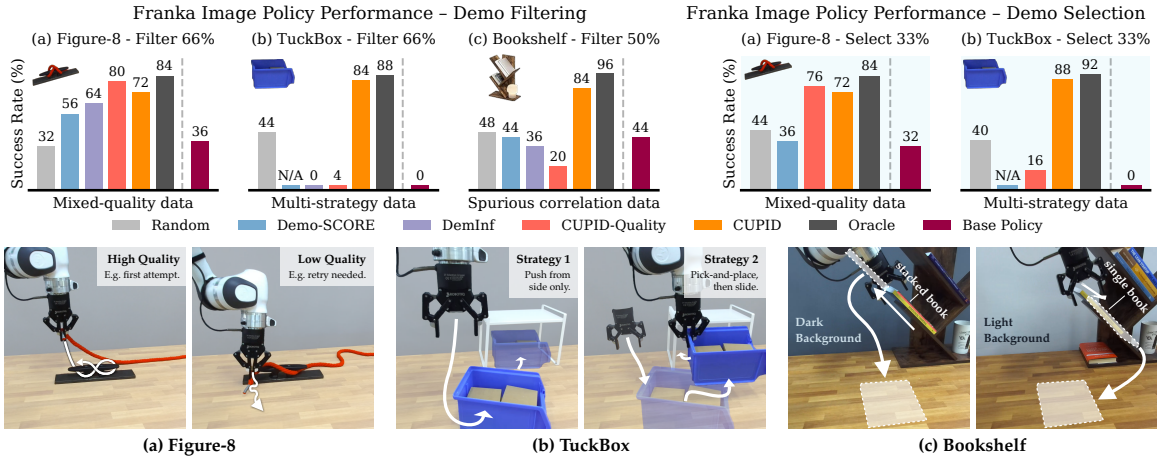
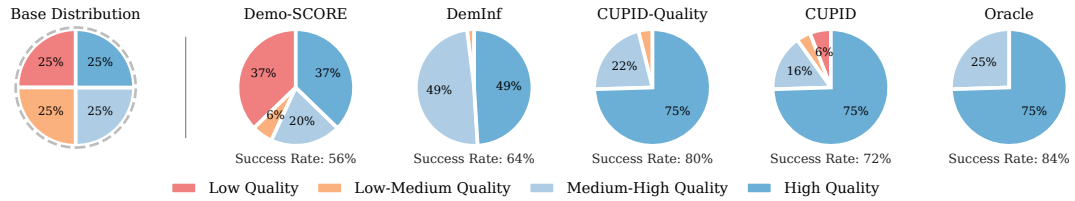


Figure 3.4: **Franka real-world diffusion policy performance.** CUPID, which curates demonstrations *w.r.t.* policy performance, improves success rates on mixed-quality datasets, identifies robust strategies, and disentangles spurious correlations that hinder performance. Although quality measures (e.g., DemInf, CUPID-QUALITY) help in mixed-quality settings (Figure-8; Fig. 3.3), they degrade performance when higher-quality demonstrations induce brittle strategies at test time (TuckBox), or when quality is not the primary factor limiting policy success (Bookshelf). Overall, curating data based on performance (CUPID) maintains robustness across these settings.

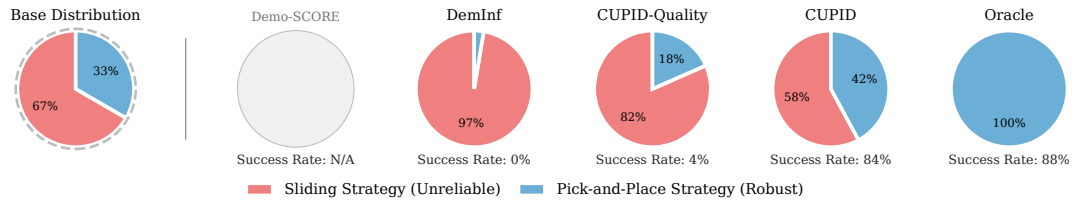
3.6.2 Setting 2: Identifying Robust Test-time Strategies from Policy Failures

Heterogeneous imitation learning datasets may contain multiple strategies for solving a task, some of which can fail under distribution shifts at deployment. We design a real-world “TuckBox” task, where a robot must tuck a recycling bin under a receptacle by (i) sliding or (ii) first repositioning it via pick-and-place (see Fig. 3.4(b)). The dataset contains a 2:1 ratio of sliding to pick-and-place demonstrations, making sliding the dominant strategy. At test time, we induce an imperceptible distribution shift by altering the bin’s mass distribution, rendering sliding unreliable. In this setting, curation aims to rebalance the dataset to promote strategies that are more robust to unforeseen shifts at deployment.

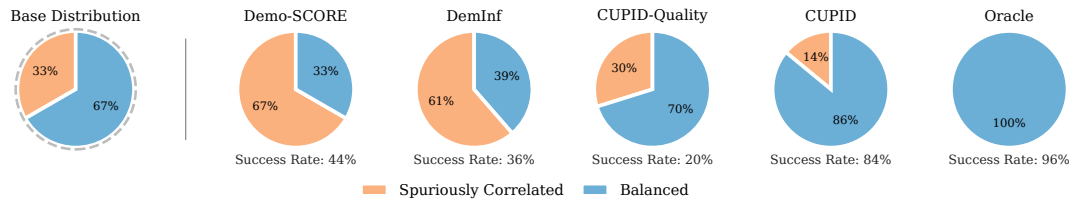
TuckBox analysis. Fig. 3.4(b) shows the diffusion policy results on “TuckBox.” Due to the strategy imbalance, the base policy exclusively exhibits the sliding behavior, resulting in a 100% failure rate under the distribution shift. This immediately invalidates the use of Demo-SCORE, which requires both successful and failed rollouts. In contrast, CUPID does not require observing successes: by linking failures to the demonstrations that influenced them, curating with CUPID yields a policy that exhibits increased pick-and-place behavior, performing comparably (84%-88% success rate) to the Oracle. In contrast, both DemInf and CUPID-QUALITY incorrectly associate the higher-variance pick-and-place demonstrations with lower quality, resulting in more uniform filtering across strategies (see Fig. 3.5(b)). As a result, policies trained on data curated by these baselines default to the brittle



(a) **Figure-8:** Distribution of curated demonstrations after *filtering* 66%. Higher-quality demos are better.



(b) **TuckBox:** Distribution of curated demonstrations after *filtering* 66%. Pick-and-place demos are better.



(c) **Bookshelf:** Distribution of curated demonstrations after *filtering* 50%. Balanced data is better.

Figure 3.5: **Franka diffusion policy curated dataset distributions for filtering (Task 1).** CUPID filters out lower-quality demonstrations (Figure-8), brittle strategies (TuckBox), and spuriously correlated examples (Bookshelf), improving policy performance across tasks. While curation heuristics employed by baselines may be effective in some cases (e.g., DemInf and CUPID-QUALITY in Figure-8), they can lead to suboptimal pruning in others.

sliding strategy at deployment.

3.6.3 Setting 3: Disentangling Spurious Correlations in Demonstration Data

Spurious correlations in training data may cause a policy to rely on non-causal features, hindering generalization to variations in the input or task [61]. We design a real-world “Bookshelf” task, where a robot must extract a target book via (i) horizontal or (ii) vertical pulling motion, depending on whether another book is stacked above the target book. While both strategies are equally represented in the training set, each co-occurs more frequently with a certain background color (see Fig. 3.4(c)). At evaluation, we test the policy under slight variations in the number and position of distractor books, while keeping the white background fixed—the correlate associated with the horizontal pulling

behavior.

Bookshelf analysis. Diffusion policy results are shown in Fig. 3.4(c). The base policy achieves only a 44% success rate, as the presence of the white background often causes the policy to extract the target book horizontally despite another book being stacked on top (causing it to fall). Interestingly, by training classifiers to distinguish failed from successful states, Demo-SCORE appears to misattribute failure to the presence of rollout correlates (the stacked book) rather than causal factors (the white background). In contrast, CUPID attains an 84% success rate by identifying demonstrations that causally drive failure—in this case, horizontal pulling motion with a white background—enabling dataset rebalancing that mitigates the effect of spurious correlations (see Fig. 3.5(c)). As in §3.6.2, DemInf and CUPID-QUALITY incorrectly prioritize the lower-variance horizontal pulling motion, yielding negligible performance gains.

3.7 Discussion and Ablations

3.7.1 How Is Curation Performance Affected by Properties of the Data and Task?

Our mixed-quality curation experiments (Fig. 3.3 and Fig. 3.4(a)) reveal that while curation strengthens performance on “Transport MH” and “Figure-8” (i.e., a fraction of the demonstrations harm policy performance), removing almost *any* demonstration degrades performance on “Square MH” (i.e., all demonstrations appear important). In contrast, only about 15% of the dataset is necessary to maximize performance on “Lift MH” (i.e., the dataset is highly redundant)³. These results indicate that the potential benefits of data curation depend on properties of both the data and the task. For example, one possible hypothesis is that curation is most effective in complex, precision-critical settings (e.g., “Transport MH”), whereas for tasks with greater tolerance for error (e.g., “Lift MH”), state-of-the-art policies [40] appear less sensitive to—and may even benefit from—training on lower-quality demonstrations.

3.7.2 How Many Policy Rollouts Are Required for Effective Curation with CUPID?

CUPID uses a REINFORCE-style estimator to compute the performance influence of each demonstration (Eq. 3.3) for curation. Thus, the accuracy of estimated performance influences depends on the number of policy rollouts. While REINFORCE [258] often yields high-variance gradient estimates under limited rollout budgets, e.g., in reinforcement learning contexts [95], we highlight that our curation objective imposes a lower fidelity requirement: since curation with CUPID involves top- k selection (§3.5.2), it

³Note that Fig. 3.3 does not include select- k curation results for “Lift MH” because the base policy already achieves a 100% success rate, leaving no further room for improvement by selecting additional demonstrations.

suffices to rank helpful demonstrations above harmful ones (requiring fewer rollouts) rather than to estimate performance influence precisely (requiring many rollouts). As shown in Fig. 3.6, the ranking of demonstrations stabilizes with approximately $m \in [25, 50]$ rollouts on “Lift MH” and “Square MH,” and $m \in [50, 100]$ rollouts on “Transport MH.” Similarly, we use only $m = 25$ rollouts for our real-world Franka tasks (Fig. 3.4). These results support the practicality of CUPID under realistic rollout budgets, while noting that more complex tasks (e.g., “Transport MH”) may benefit from a greater number of rollouts.

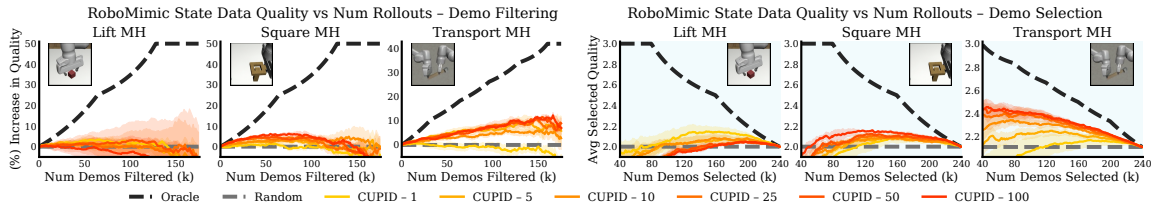


Figure 3.6: **CUPID ablation on the number of policy rollouts.** Performance influences (Eq. 3.3) converge with $m \in [25, 50]$ rollouts on “Lift MH” and “Square MH” (yielding similar quality trends), and $m \in [50, 100]$ rollouts on “Transport MH,” validating the practical applicability of CUPID under realistic rollout budgets. Curation is performed on diffusion policies. Results are averaged over 3 random seeds. Errors bars represent standard error.

3.7.3 Can Data Curated for Single-Task Policies Strengthen Generalist Policy Performance?

In Fig. 3.7, we show that datasets curated by CUPID for single-task diffusion policies can significantly improve the fine-tuned performance of a generalist Vision-Language-Action (VLA) model, π_0 [25]. While CUPID is, in principle, tailored to the specific policy used during rollouts, it consistently identifies low-quality, stochastic behaviors in “Figure-8” and unreliable strategies in “TuckBox” (Fig. 3.5)—both intrinsic properties of the data. Filtering these poorer demonstrations (or selecting better ones) is thereby likely to improve the performance *any* policy.

This highlights a promising direction to alleviate the computational cost of CUPID in large-scale settings: use smaller, single-task policies to curate datasets for larger, multi-task models.

VLA Robustness. Fig. 3.7 also suggests that scaling the pre-training of VLA models does not inherently enable them to leverage their generalist knowledge to, e.g., *ignore* low-quality behaviors or brittle strategies in demonstration data. That is, data curation still appears important for VLA post-training.

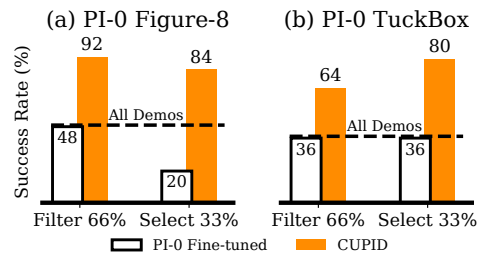


Figure 3.7: Data curated for single-task diffusion policies improves π_0 [25] post-training performance. Additional results in Fig. B.8.

3.8 Conclusion

In this chapter, we study the problem of data curation for robot imitation learning. We present CUPID, a novel data curation method that uses influence functions to measure the causal impact of a demonstration on the policy’s closed-loop performance. Our results highlight the general utility of performance-based curation for two key curation tasks—filtering existing training demonstrations and subselecting new demonstrations—and across diverse curation settings, where a policy’s test-time performance varies with the choice of training data.

Among many key problems in robotics, it is inherently difficult to develop strong intuitions about how training data influences downstream policy behavior, and to delineate why a policy trained exclusively on expert demonstration data would exhibit suboptimal performance at deployment. We hope this investigation spurs continued interest in pursuit of these questions.

3.9 Limitations and Future Work

We summarize the limitations of our approach and opportunities for future investigation:

1. **Curation tasks.** The curation tasks considered in this chapter ([Task 1](#) and [Task 2](#)) aim to curate performance-maximizing datasets for a specified filtering or selection quantity of demonstrations k . Determining the suitable quantity of demonstrations to curate represents a possible point of extension.
2. **Data properties.** Critically, future work should further investigate how properties of the data dictate the extent to which curation can improve policy performance, as discussed in [§3.7.1](#).
3. **Data explainability.** Our methods focus on curating existing demonstrations as a first step. However, future work may seek to interpret the properties of influential demonstrations to actively inform subsequent data collection efforts—for example, by providing instructions to data collectors.
4. **Selection methods.** While the *greedy* selection procedures used in [Eq. 3.4](#) and [Eq. 3.5](#) are tractable to optimize and often improve over quality- and similarity-based measures [\[72\]](#), they ignore the interactions between demonstrations in the curated set [\[121, 148\]](#). This can temper performance gains when the size of the curated set is large. Future work should investigate higher-order approximations that consider the joint diversity of the curated dataset, as is common in the active learning literature (e.g., [\[233, Sec. 4.3\]](#)).
5. **Larger datasets.** Estimating performance influences over the full demonstration dataset incurs a computational cost comparable to that of policy training. Reducing this expense in large-scale settings is an important future direction. For example, one could approximate group

effects [148] via random sampling or limit influence estimation to smaller data subsets identified using coarse-grained heuristics.

6. **Estimator variance.** Finally, although we observe stable performance from CUPID across curation settings, the use of the REINFORCE estimator may result in high variance influence scores, e.g., when the number of policy rollouts is small. In such settings, variance reduction techniques, such as those typically used in reinforcement learning [95], may further improve the fidelity of our influence scores.

Part II

Policy Coordination and Planning

Chapter 4

Coordinating Policy Sequences for Long-Horizon Tasks

4.1 Introduction

In the preceding chapters, we examined how deployment-time monitoring and data-centric interpretability mechanisms can help safeguard learned policies, diagnose failures, and improve the reliability of individual behaviors. However, many everyday tasks—such as rearranging a table, shelving kitchenware, or packing objects—are inherently *long-horizon*: they require the successful execution of a sequence of behaviors rather than a single action in isolation. This chapter focuses on a critical challenge that arises when independently learned behaviors are composed. That is, subtle dependencies between behaviors emerge when they are sequenced, potentially rendering downstream behaviors infeasible. As a result, achieving reliable outcomes for multi-step, real-world tasks requires robots to explicitly reason about and coordinate these dependencies at deployment time.

Consider the example in [Fig. 4.1](#), where the robot needs to retrieve an object outside of its workspace by first using an L-shaped hook to pull the target object closer. How the robot picks up the hook affects whether the target object will be reachable. Traditionally, planning actions to ensure the geometric feasibility of a sequential manipulation task is handled by motion planning [[155](#), [265](#), [266](#)], which typically requires full observability of the environment state and knowledge of its dynamics. Learning-based approaches [[13](#), [130](#), [229](#)] can acquire skills without this privileged information. However, using independently learned skills to perform unseen long-horizon manipulation tasks is an unsolved problem. The skills could be myopically executed one after another to solve a simpler subset of tasks, but solving more complex tasks requires planning with these skills to ensure the feasibility of the entire skill sequence.

Prior work focuses on sequencing skills at *train time* to solve a small set of sequential manipulation

Greedy execution



Planning with STAP (Ours)



Figure 4.1: Sequential manipulation tasks often contain geometric dependencies between actions. In this example, the robot needs to use the hook to pull the block into its kinematic workspace so it is close enough to pick up. The top row shows how greedy execution of skills results in the robot picking up the hook in a way that prevents it from reaching the block. We present a method for planning with skills to maximize long-horizon success without the need to train the skills on long-horizon tasks. More details can be found on the STAP website: <https://sites.google.com/stanford.edu/stap>. © 2023 IEEE.

tasks [57, 292]. To contend with long-horizons, these methods often learn skills [53] that consist of a policy and parameterized manipulation primitive [75]. The policy predicts the parameters of the primitive, thereby governing its motion. Such methods are *task-specific* in that they need to be trained on skill sequences that reflect the tasks they might encounter at test time. In our framework, we assume that a task planner provides a novel sequence of skills at *test time* that will then be grounded with parameters for manipulation primitives through optimization. This makes our method *task-agnostic*, as skills can be sequenced to solve long-horizon tasks not seen during training.

At the core of our method, *Sequencing Task-Agnostic Policies* (STAP), we use Q-functions to optimize the parameters of manipulation primitives in a given sequence. Policies and Q-functions for each skill are acquired through off-the-shelf Reinforcement Learning. We then define a planning objective to maximize all Q-functions in a skill sequence, ensuring its geometric feasibility. To evaluate downstream Q-functions of future skills, we learn a dynamics model that can predict future states. We also use *Uncertainty Quantification* (UQ) to avoid visiting states that are *Out-Of-Distribution* (OOD) for the learned skills. We train all of these components independently per skill, making it easy to gradually expand a library of skills without the need to retrain existing ones.

Our contributions are three-fold: we propose 1) a framework to train an extensible library of

task-agnostic skills, 2) a planning method that optimizes arbitrary sequences of skills to solve long-horizon tasks, and 3) a method to solve Task and Motion Planning (TAMP) problems with learned skills. In extensive experiments, we demonstrate that planning with STAP promotes long-horizon success on tasks with complex geometric dependencies between actions. We also demonstrate that our framework works on a real robot.

4.2 Related Work

4.2.1 Robot Skill Learning

How to represent and acquire composable manipulation skills is a widely studied problem in robotics. A broad class of methods uses Learning from Demonstration (LfD) [13]. Dynamic Movement Primitives (DMPs) [141, 206, 230] are a form of LfD that learns the parameters of dynamical systems encoding movements [119, 152, 189, 268]. More recent extensions integrate DMPs with deep neural networks to learn more flexible policies [16, 17]—for instance, to build a large library of skills from human video demonstrations [238]. Skill discovery methods instead identify action patterns in offline datasets [237] and either distill them into policies [7, 236] or extract skill priors for use in downstream tasks [208, 248]. Robot skills can also be acquired via active learning [54], Reinforcement Learning (RL) [134, 135, 174, 215, 240], and offline RL [32].

An advantage of our planning framework is that it is agnostic to the types of skills employed, requiring only that it is possible to predict the probability of the skill’s success given the current state and action. Here, we learn skills [53] that consist of a policy and a parameterized manipulation primitive [75]. The actions output by the policy are the parameters of the primitive determining its motion. In STAP, we will use the Q-functions of the policy to optimize suitable parameters [134, 238] for a sequence of manipulation primitives.

4.2.2 Long-Horizon Robot Planning

Once manipulation skills have been acquired, using them to perform sequential manipulation tasks remains an open challenge. [9, 133, 137, 193] propose data-driven methods to determine the *symbolic* feasibility of skills and only control their timing, while we seek to ensure the *geometric* feasibility of skills by controlling their trajectories. Other techniques rely on task planning [116, 284], subgoal planning [247], or meta-adaptation [115, 291] to sequence learned skills to novel long-horizon goals. However, the tasks considered in these works do not feature rich geometric dependencies between actions that necessitate motion planning or skill coordination.

The options framework [259] and the parameterized action Markov Decision Process (MDP) [188] train a high-level policy to engage low-level policies [14, 196] or primitives [42, 57, 199, 273] towards long-horizon goals. [234] proposes a hierarchical RL method that uses the value functions of lower-level

policies as the state space for a higher-level RL policy. Our approach is also related to model-based RL methods which jointly learn dynamics and reward models to guide planning [46, 76, 101], policy search [102, 126], or combine both [231, 289]. While these methods demonstrate that policy hierarchies and model-based planning can enable RL to solve long-horizon problems, they are typically trained in the context of a single task. In contrast, we seek to *plan* with lower-level skills to solve tasks never seen before.

Closest in spirit to our approach is that of Xu et al. [292], Deep Affordance Foresight (DAF), which proposes to learn a dynamics model, skill-centric affordances (value functions), and a skill proposal network that serves as a higher-level RL policy. We identify several drawbacks with DAF: first, because DAF relies on multi-task experience for training, generalizing beyond the distribution of training tasks may be difficult; second, the dynamics, affordance models, and skill proposal network need to be trained synchronously, which complicates expanding the current library of trained skills; third, their planner samples actions from uniform random distributions, which prevents DAF from scaling to high-dimensional action spaces and long horizons. STAP differs in that our dynamics, policies, and affordances (Q-functions) are learned independently per skill. Without any additional training, we combine the skills at planning time to solve unseen long-horizon tasks. We compare our method against DAF in the planning experiments (§4.7.2).

4.2.3 Task and Motion Planning

TAMP solves problems that require both symbolic and geometric reasoning [87, 265]. DAF learns a skill proposal network to replace the typical task planner in TAMP, akin to [275]. Another prominent line of research learns components of the TAMP system, often from a dataset of precomputed solutions [43, 63, 65, 243, 277, 278]. The problems we consider involve complex geometric dependencies between actions that are typical in TAMP. However, STAP only performs geometric reasoning and by itself is not a TAMP method. We demonstrate in experiments (§4.7.3) that STAP can be combined with symbolic planners to solve TAMP problems.

4.3 Problem Setup

4.3.1 Long-Horizon Planning

Our objective is to solve long-horizon manipulation tasks that require sequential execution of learned skills. These skills come from a skill library $\mathcal{L} = \{\psi^1, \dots, \psi^K\}$, where each skill ψ^k consists of a parameterized manipulation primitive [75] ϕ^k and a learned policy π^k . A primitive $\phi^k(a^k)$ takes in parameters a^k and executes a series of motor commands on the robot, while a policy $\pi^k(a^k | s^k)$ is trained to predict a distribution of suitable parameters a^k from the current state s^k . For example, the $\text{Pick}(a, b)$ skill may have a primitive which takes as input an end-effector pose and executes a

trajectory to pick up object a , where the robot first moves to the commanded pose, closes the gripper to grasp a , and then lifts a off of b . The learned policy π^k for this skill will then try to predict end-effector poses to pick up a .

We assume access to a high-level planner that computes *plan skeletons* (i.e. skill sequences) to achieve a high-level goal. STAP aims to solve the problem of turning plan skeletons into geometrically feasible *action plans* (i.e. parameters for each manipulation primitive in the plan skeleton).

STAP is agnostic to the choice of high-level planner. For instance, it can be used in conjunction with Planning Domain Definition Language (PDDL) [190] task planners to perform hierarchical TAMP [132]. In this setup, the task planner and STAP will be queried numerous times to find multiple plan skeletons grounded with optimized action plans. STAP will also evaluate each action plan’s probability of success (i.e. its geometric feasibility). After some termination criterion is met, such as a timeout, the candidate plan skeleton and action plan with the highest probability of success is returned.

4.3.2 Task-Agnostic Policies

We aim to learn policies $\{\pi^1, \dots, \pi^K\}$ for the skill library \mathcal{L} that can be sequenced by a high-level planner in arbitrary ways to solve any long-horizon task. We call these policies task-agnostic because they are not trained to solve a specific long-horizon task. Instead, each policy π^k is associated with a skill-specific contextual bandit (i.e. a single timestep MDP)

$$\mathcal{M}^k = (\mathcal{S}^k, \mathcal{A}^k, T^k, R^k, \rho^k), \quad (4.1)$$

where \mathcal{S}^k is the state space, \mathcal{A}^k is the action space, $T^k(s'^k | s^k, a^k)$ is the transition model, $R^k(s^k, a^k, s'^k)$ is the binary reward function, and $\rho^k(s^k)$ is the initial state distribution. Given a state s^k , the policy π^k produces an action a^k , and the state evolves according to the transition model $T^k(s'^k | s^k, a^k)$. Thus, the transition model encapsulates the execution of the manipulation primitive ϕ^k (§4.3.1).

A long-horizon domain is one in which each timestep involves the execution of a single policy, and it is specified by

$$\overline{\mathcal{M}} = (\mathcal{M}^{1:K}, \overline{\mathcal{S}}, \overline{T}^{1:K}, \overline{\rho}^{1:K}, \Gamma^{1:K}), \quad (4.2)$$

where $\mathcal{M}^{1:K}$ is the set of MDPs whose policies can be executed in the long-horizon domain, $\overline{\mathcal{S}}$ is the state space of the long-horizon domain, $\overline{T}^k(\overline{s}' | \overline{s}, a^k)$ is an extension of dynamics $T^k(s'^k | s^k, a^k)$ that models how the entire long-horizon state evolves with action a^k , $\overline{\rho}^k(\overline{s})$ is an extension of initial state distributions $\rho^k(s^k)$ over the long-horizon state space, and $\Gamma^k : \overline{\mathcal{S}} \rightarrow \mathcal{S}^k$ is a function that maps from the long-horizon state space to the state space of policy k . We assume that the dynamics $T^k(s'^k | s^k, a^k)$, $\overline{T}^k(\overline{s}' | \overline{s}, a^k)$ and initial state distributions $\rho^k(s^k)$, $\overline{\rho}^k(\overline{s}^k)$ are unknown.

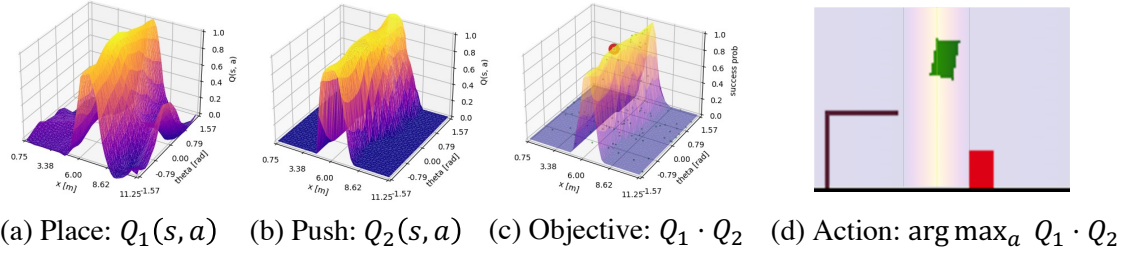


Figure 4.2: Planning in a 2D toy domain. The agent needs to get the green block under the brown receptacle with two skills: Place() and Push() that operate on the horizontal position x of the green block. Plots (a) and (b) show the Q-functions across (x, θ) for each skill. Place() is only trained to get the green block on the ground, so the planner must determine $a = x$ s.t. Push() is unobstructed. The optimal action maximizes the probability of long-horizon task success (Eq. 4.3), approximated by the product of Q-functions in plot (c). © 2023 IEEE.

Note that while the policies may have different state spaces \mathcal{S}^k , policy states s^k must be obtainable from the long-horizon state space $\bar{\mathcal{S}}$ via $s^k = \Gamma^k(\bar{s})$. This is to ensure that the policies can be used together in the same environment to perform long-horizon tasks. In the base case, all the state spaces are identical and Γ^k is simply the identity function. Another case is that \bar{s} is constructed as the concatenation of all $s^{1:K}$ and $\Gamma^k(\bar{s})$ extracts the slice in \bar{s} corresponding to s^k .

4.4 Sequencing Task-Agnostic Policies

Given a task in the form of a sequence of skills to execute, our planning framework constructs an optimization problem with the policies, Q-functions, and dynamics models of each skill. Solving the optimization problem results in parameters for all manipulation primitives in the skill sequence such that the entire sequence’s probability of success is maximized.

We formalize our planning methodology in this section and outline its implementation in §4.5. Lastly, we describe our procedure for training modular skill libraries in §4.6.

4.4.1 Grounding Skill Sequences with Action Plans

We assume that we are given a plan skeleton of skills $\tau = [\psi_1, \dots, \psi_H] \in \mathcal{L}^H$ (hereafter denoted by $\tau = \psi_{1:H}$) that should be successfully executed to solve a long-horizon task. Let \mathcal{M}_h with subscript h denote the MDP corresponding to the h -th skill in the sequence—in contrast to \mathcal{M}^k with superscript k , which denotes the k -th MDP in the skill library. A long-horizon task is considered successful if every skill reward r_1, \dots, r_H received during execution is 1.

Given an initial state $\bar{s}_1 \in \bar{\mathcal{S}}$, our problem is to ground the plan skeleton $\tau = \psi_{1:H}$ with an action plan $\xi = [a_1, \dots, a_H] \in \mathcal{A}_1 \times \dots \times \mathcal{A}_H$ that maximizes the probability of succeeding at the long-horizon task. This is framed as an optimization problem $\arg \max_{a_{1:H}} J$, where the maximization

objective J is the task success probability

$$J(a_{1:H}; \bar{s}_1) = p(r_1 = 1, \dots, r_H = 1 \mid \bar{s}_1, a_{1:H}).$$

Here, $r_{1:H}$ are the skill rewards received at each timestep.

With the long-horizon dynamics models $\bar{T}^k(\bar{s}' \mid \bar{s}, a^k)$, the objective can be cast as the expectation

$$J = \mathbb{E}_{\bar{s}_{2:H} \sim \bar{T}_{1:H-1}} [p(r_1 = 1, \dots, r_H = 1 \mid \bar{s}_{1:H}, a_{1:H})].$$

By the Markov assumption, rewards are conditionally independent given states and actions. We can express the probability of task success as the product of reward probabilities

$$J = \mathbb{E}_{\bar{s}_{2:H} \sim \bar{T}_{1:H-1}} [\prod_{h=1}^H p(r_h = 1 \mid \bar{s}_h, a_h)].$$

Because the skill rewards are binary, the skill success probabilities are equivalent to Q-values:

$$\begin{aligned} p(r_h = 1 \mid \bar{s}_h, a_h) &= \mathbb{E}_{\bar{s}_{h+1} \sim \bar{T}_h} [r_h \mid \bar{s}_h, a_h] \\ &= Q_h(\Gamma_h(\bar{s}_h), a_h). \end{aligned}$$

The final objective is expressed in terms of Q-values:

$$J = \mathbb{E}_{\bar{s}_{2:H} \sim \bar{T}_{1:H-1}} [\prod_{h=1}^H Q_h(\Gamma_h(\bar{s}_h), a_h)]. \quad (4.3)$$

This planning objective is simply the product of Q-values evaluated along the trajectory $(\bar{s}_1, a_1, \dots, \bar{s}_H, a_H)$, where the states are predicted by the long-horizon dynamics model: $\bar{s}_2 \sim \bar{T}_1(\cdot \mid \bar{s}_1, a_1), \dots, \bar{s}_H \sim \bar{T}_{H-1}(\cdot \mid \bar{s}_{H-1}, a_{H-1})$.¹

4.4.2 Ensuring Action Plan Feasibility

A plan skeleton $\tau = \psi_{1:H}$ is feasible only if, for every pair of consecutive skills ψ_i and ψ_j , there is a non-zero overlap between the terminal state distribution of i and the initial state distribution of j . More formally,

$$\mathbb{E}_{\bar{s}_i \sim \bar{\rho}_i, a_i \sim \mathcal{A}_i, \bar{s}_j \sim \bar{\rho}_j} [\bar{T}_i(\bar{s}_j \mid \bar{s}_i, a_i)] > 0, \quad (4.4)$$

where $\bar{\rho}_i$ and $\bar{\rho}_j$ are the initial state distributions for skills ψ_i and ψ_j , respectively, and a_i is uniformly distributed with respect to action space \mathcal{A}_i for skill ψ_i . Given a state $\bar{s}_i \sim \bar{\rho}_i$, it is part of the

¹One might consider maximizing the *sum* of Q-values instead of the product, but this may not reflect the probability of task success. For example, if we want to optimize a sequence of ten skills, consider a plan that results in nine Q-values of 1 and one Q-value of 0, for a total sum of 9. One Q-value of 0 would indicate just one skill failure, but this is enough to cause a failure for the entire task. Compare this to a plan with ten Q-values of 0.9. This plan has an equivalent sum of 9, but it is preferable because it has a non-zero probability of succeeding.

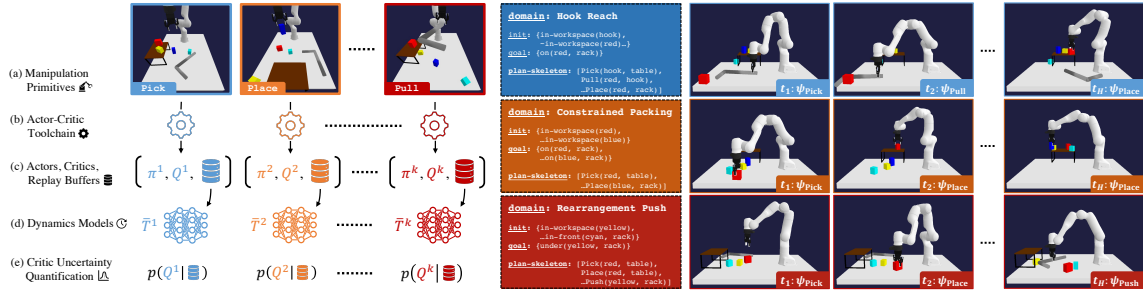


Figure 4.3: **Left:** Training pipeline. We train each skill independently on single-step environments with skill-specific rewards. We use the experience collected by each skill to train (1) a dynamics model and (2) a SCOD [239] model to predict OOD critic inputs per skill. The benefit of training each skill independently is that we can easily add skills to the library or even mix skill acquisition strategies (e.g. RL, imitation learning, and handcrafted skills). Our planning framework ensures that the skills can be composed to solve any long-horizon task even if the skills were not explicitly trained to perform those tasks. **Right:** Example evaluation tasks. We evaluate our method on 9 tasks: 3 Hook Reach tasks, where the robot needs to use the hook to bring objects closer, 3 Constrained Packing tasks, where the robot needs to place blocks on the rack, and 3 Rearrangement Push tasks, where the robot needs to remove obstacles to push a target block under the rack. The 9 tasks feature a range of geometric complexities and plan skeleton lengths. © 2023 IEEE.

planner’s job to determine an action a_i that induces a valid subsequent state $\bar{s}_j \sim \bar{p}_j$ if one exists. Failing to do so constitutes an OOD event for skill ψ_j , where the state \bar{s}_j has drifted beyond the region of the state space where $Q_j(\Gamma_j(\bar{s}_j), a_j)$ is well-defined and ψ_j is executable.

Neglecting state distributional shift over an action plan ξ may degrade the quality of objective function J with spuriously high Q-values (Eq. 4.3). Moreover, Eq. 4.4 cannot be explicitly computed to determine the validity of actions because the initial state distributions of all skills $\bar{\rho}^k(\bar{s}^k)$ are unknown. We can detect OOD states (and actions) by performing UQ on the Q-functions $Q^k(s^k, a^k)$. Filtering out Q-values with high uncertainty would result in action plans ξ that are robust (i.e. have low uncertainty) while maximizing the task feasibility objective. We discuss efficient methods for training UQ models on learned Q-functions in §4.6.3.

4.5 Planning Action Sequences

To find action sequences that maximize the probability of long-horizon task success (Eq. 4.3), we use sampling-based optimization techniques: shooting and cross-entropy method (CEM) [223]. In shooting, we simply sample action plans $\xi = a_{1:H} \in \mathcal{A}_1 \times \dots \times \mathcal{A}_H$ and select the one with the highest predicted objective score. CEM is an extension of shooting that iteratively refines the action sampling distribution to fit a fraction of the population with the highest objective scores.

Sampling action plans from uniform distributions may be sufficient for small action spaces and short skill sequences. However, this strategy suffers from the curse of dimensionality and may not scale desirably to the large action spaces and long skill sequences that we consider. Meanwhile, directly

executing actions $a^k \sim \pi^k(\cdot|s^k)$ from policies that are trained to solve skill-specific tasks produces myopic behavior that rarely succeeds for long-horizon tasks with complex geometric dependencies between actions.

The policies can be leveraged to initialize a sampling-based search by producing an action plan that is likely to be closer to an optimal plan than one sampled uniformly at random. We therefore use two variants of shooting and CEM, termed policy shooting and policy CEM, which sample actions from Gaussian distributions $a^k \sim \mathcal{N}(\pi^k(s^k), \sigma)$, where the mean is the action predicted by the policy and the standard deviation is a planning hyperparameter.

4.6 Training Skills

4.6.1 Policies and Q-functions

One of the key advantages of our approach is that the policies can be trained independently and then composed at test time to solve unseen sequential tasks. For each skill ψ_k , we want to obtain a policy $\pi^k : \mathcal{S}^k \rightarrow \mathcal{A}^k$ that solves the task specified by the skill-specific MDP \mathcal{M}^k (Eq. 4.1), along with a Q-function Q^k modeling the policy’s expected success

$$Q^k(s^k, a^k) = \mathbb{E}_{s'^k \sim T^k(\cdot | s^k, a^k)} [R^k(s^k, a^k, s'^k)].$$

Our framework is agnostic to the method for acquiring the policy and Q-function. Many deep RL algorithms are able to simultaneously learn the policy (i.e. actor) and Q-function (i.e. critic) with unknown dynamics [79, 165]. We therefore leverage off-the-shelf RL algorithms to learn a policy and Q-function for each skill (Fig. 4.3 - Left (c)). In our experiments, we specifically use Soft Actor-Critic (SAC) [100]. For other policy acquisition methods, policy evaluation can be performed to obtain a Q-function after a policy has been learned.

4.6.2 Dynamics

The dynamics models are used to predict future states at which each downstream Q-function in the plan skeleton will be evaluated. We learn a deterministic model $\bar{T}^k(\bar{s}, a^k)$ for each skill ψ_k using the single-step forward prediction loss

$$L_{\text{dynamics}}(\bar{T}^k; \bar{s}, a^k, \bar{s}') = \left\| \bar{T}^k(\bar{s}, a^k) - \bar{s}' \right\|_2^2.$$

Each dynamics model \bar{T}^k is trained on the state transition experience (\bar{s}, a^k, \bar{s}') collected during the training of policy π^k (§4.6.1), stored in the replay buffer \mathcal{D}^k (Fig. 4.3 - Left (d)). Training our dynamics models on existing state transitions is efficient and circumvents the challenges associated with learning dynamics in the context of a long-horizon task [126].

4.6.3 Uncertainty Quantification

Measuring the epistemic uncertainty over the Q-values allows us to identify when dynamics-predicted states and planned actions drift OOD for downstream critics Q^k . We leverage recent advances in neural network UQ to obtain an explicit Gaussian posterior predictive distribution

$$p(Q^k \mid s^k, a^k, \mathcal{D}^k; w^k) = \mathcal{N}(\mu_{Q^k}, \sigma_{Q^k}; w^k) \quad (4.5)$$

with sketching curvature for OOD detection (SCOD) [239]. SCOD computes the weights w^k that parameterizes the posterior distribution over each critic Q^k using only the experience $(\bar{s}, a^k) \sim \mathcal{D}^k$ collected over the course of training policy π^k (Fig. 4.3 - Left (e)). An advantage of SCOD over common UQ techniques [80, 82] is that it imposes no train-time dependencies on any algorithms used in our framework.

4.7 Experiments

In our experiments, we test the following hypotheses:

- H1** Maximizing the product of learned Q-functions (Eq. 4.3) translates to maximizing long-horizon task success.
- H2** Skills trained with our framework are able to generalize to unseen long-horizon tasks by optimizing Eq. 4.3.
- H3** Our planning method can be combined with a task planner and UQ (Eq. 4.5) to solve TAMP problems.

We evaluate our method on a 3D manipulation domain with 4 skills: $\text{Pick}(a, b)$: pick a from b ; $\text{Place}(a, b)$: place a onto b ; $\text{Pull}(a, \text{hook})$: pull a into the robot’s workspace with a *hook*; and $\text{Push}(a, \text{hook})$: push a with a *hook*.

The long-horizon state space $\bar{\mathcal{S}}$ is a sequence of low-dimensional object states that contains information such as 6D poses. The policy state spaces \mathcal{S}^k are constructed so that the first m object states correspond to the m arguments of the corresponding skill. For example, a state for the policy of $\text{Pick}(\text{box}, \text{rack})$ will contain first the *box*’s state, then the *rack*’s state, followed by a random permutation of the remaining object states. The policy action spaces \mathcal{A}^k are all 4D. For example, a policy-predicted action for $\text{Pick}(a, b)$ specifies the 3D grasp position of the end-effector relative to the target a and orientation about the world z -axis.

Our evaluation is on 9 different long-horizon tasks (i.e. plan skeletons τ). The tasks cover a range of symbolic and geometric complexities (Fig. 4.3 - Right), with plan skeleton lengths ranging from 4 to 10 skills. Each task involves geometric dependencies between actions, which motivates the need

for planning. We use 100 randomly generated instances (i.e. object configurations) for evaluation on each task.

4.7.1 Product of Q-Functions Approximates Task Success (H1)

We test **H1** by comparing STAP to an **Oracle** baseline that runs forward simulations with policy shooting to find action plans that achieve ground-truth task success. Our method uses learned Q-functions and dynamics to predict task success as the product of Q-functions. We expect that planning with this objective will come close to matching the task success upper bound provided by **Oracle**.

We compare several planning methods: **Policy Shooting** and **Policy CEM**, which use the learned policies to initialize the action sampling distributions (§4.5), as well as **Random Shooting** and **Random CEM**, which use uniform action priors. We also compare with **Greedy**, which does not plan but greedily executes the skills. The evaluation metrics are ground-truth task success, sub-goal completion rate (what percentage of skills in a plan are successfully executed), and predicted task success computed from Eq. 4.3.

Due to the significant amount of time required to run forward simulations for **Oracle**, we limit the number of sampled trajectories evaluated during planning to 1000 for all methods. This is not enough to succeed at the most complex tasks, and thus, we evaluate on the simplest task from the Hook Reach and Constrained Packing domains.

The results from both tasks are averaged and presented in Fig. 4.4. As expected, **Oracle** achieves the highest success rate, although not perfect because 1000 samples are not enough to solve all of the tasks. **Policy CEM** nearly matches **Oracle**’s success rate, which demonstrates that maximizing the product of Q-functions is a good proxy for maximizing task success. **Policy CEM** also exhibits a low success prediction error, which demonstrates that the learned Q-functions and dynamics generalize well to these unseen long-horizon tasks. Meanwhile, planning with these learned models runs 4 orders of magnitude faster than **Oracle** and does not require ground-truth knowledge about the environment state or dynamics.

Policy Shooting performs slightly worse than **Policy CEM**, which demonstrates CEM’s strength in finding local maxima through iterative refinement. **Random CEM** and **Random Shooting** perform quite poorly, indicating that the planning space is too large (16D for these tasks) for random sampling. **Greedy** performs strongly, perhaps indicating that these simpler tasks can be solved without planning.

4.7.2 STAP Skills Generalize to Long-Horizon Tasks (H2)

In this experiment, we test the ability of our framework to solve 9 long-horizon tasks with geometric dependencies between actions. We compare against DAF [292], a state-of-the-art method for learning to solve TAMP problems. As task planning is outside the scope of this chapter, we omit DAF’s

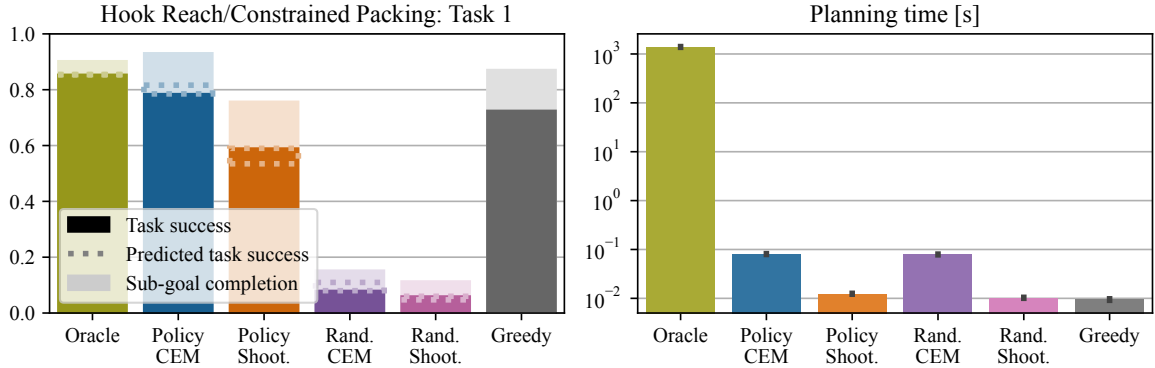


Figure 4.4: A small-scale experiment comparing the performance of our method to **Oracle** planning. The left plot shows the average success rates across two domains (Hook Reach and Constrained Packing). The dark bars indicate the ground truth task success, and the light bars indicate sub-goal completion rate, which measures how close the plan was to successfully completing the task. The predicted task success computed from the product of Q-values is indicated by a dotted line. Our method with **Policy CEM** is able to nearly match the success rate of **Oracle** while taking 4 orders of magnitude less time, as shown in the plot on the right. © 2023 IEEE.

skill proposal network and compare only to the skills trained with DAF (**DAF-Skills**), which are comprised of dynamics and affordance models. DAF’s planning objective is similar to ours, except that it evaluates the product of affordances rather than Q-functions. We give **DAF-Skills** the same plan skeleton τ that is given to our method and augment DAF’s shooting planner with CEM for a more even comparison.

Like other model-based RL methods, DAF requires training on a set of long-horizon tasks that is representative of the evaluation task distribution. We therefore train one **DAF-Skills** model per task (9 total) and run evaluation on the same task. We also test the ability of these models to generalize to the other two tasks within the same domain (**DAF-Gen**). Since **DAF-Skills** is trained on its evaluation task, we expect it to perform at least as well as STAP, if not better. However, we expect **DAF-Gen** to perform slightly worse than STAP, since the evaluation tasks differ from the training tasks, even if they are similar. We train all models for 48 hours each and allow 1000 samples per dimension for planning.

The results are presented in Fig. 4.5. Our method with **Policy CEM** achieves competitive success rates with **DAF-Skills** on 4 out of the 9 tasks and outperforms it on 2 tasks with highly complex action dependencies (Rearrangement Push). While **DAF-Gen** matches the performance of **Policy CEM** on 2 tasks, it gets relatively low success on the others. This indicates that skills trained on one long-horizon task may not effectively transfer to other tasks with similar action dependencies. Our method of training skills in independent environments and then generalizing to long-horizon tasks via planning is efficient from a training perspective, since the same trained skills can be used for all downstream tasks.

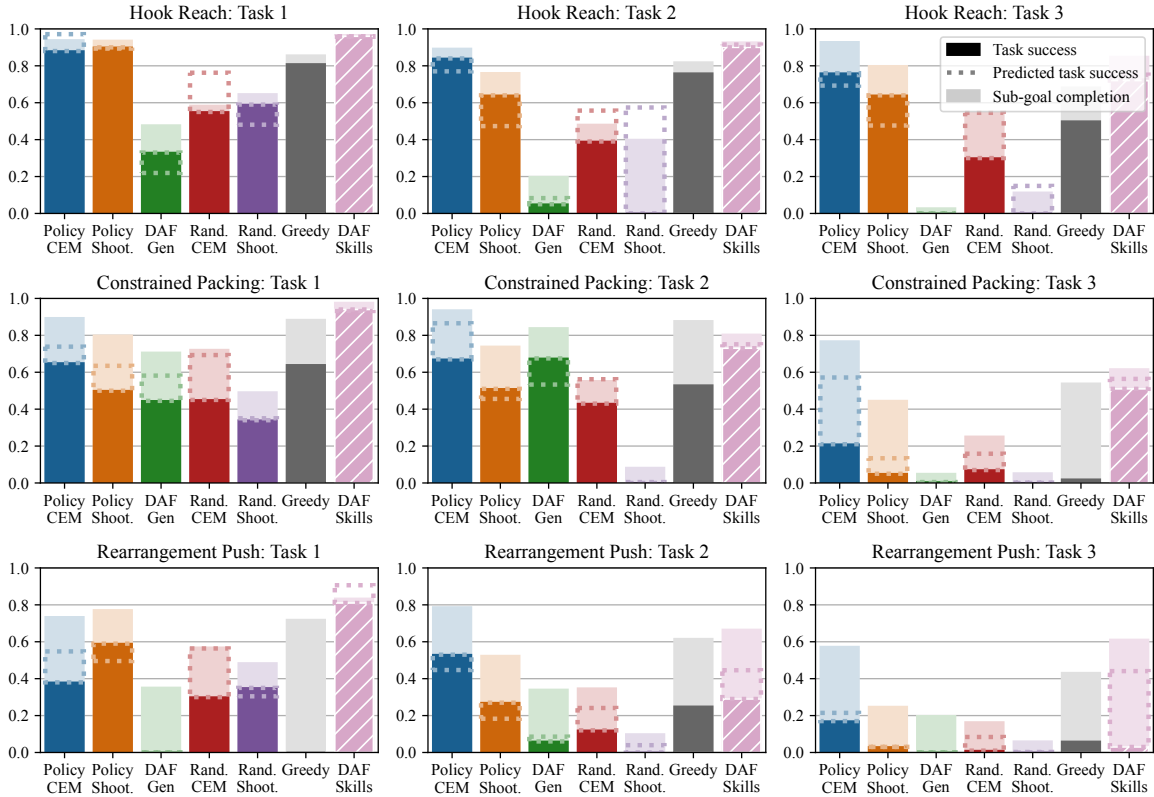


Figure 4.5: Planning experiment with 3 domains, each with 3 tasks. Our method with **Policy CEM** is able to generalize to all of these tasks without ever seeing them during training. On 6 out of the 9 tasks, our method either matches or outperforms **DAF-Skills**, which is trained directly on the evaluation task. **DAF-Gen** shows the generalization performance of the **DAF-Skills** models when evaluated on unseen tasks within the same domain. © 2023 IEEE.

4.7.3 STAP Can be Extended for TAMP with UQ (H3)

In this experiment, we combine our framework with a PDDL task planner as described in §4.3.1 and evaluate it on two TAMP problems. In Hook Reach, the robot needs to decide the best way to pick up a block, which may or may not be in its workspace. In Constrained Packing, the robot needs to place a fixed number of objects on the rack but is free to choose among any of the objects on the table. To mimic what the robot might find in an unstructured, real-world environment, some of these objects are distractor objects that are initialized in ways not seen by the skills during training (e.g. the blocks can be stacked, placed behind the robot base, or tipped over). The task planner may end up selecting these distractor objects for placing on the rack, but since the skills have not been trained to handle these objects, their predicted success (Q-values) may be unreliable. UQ is particularly important for such scenarios, so we introduce **SCOD Policy CEM**, which filters out candidate action plans with high uncertainty in the predicted task success score (Eq. 4.3). That is,

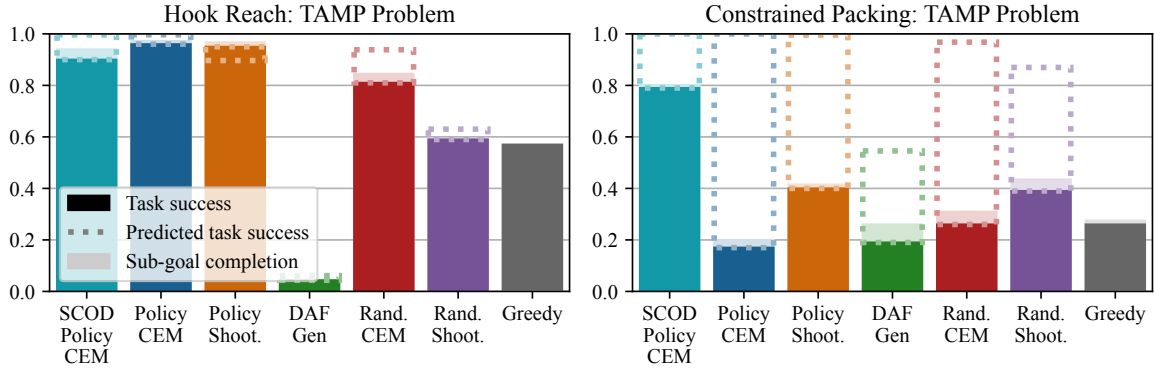


Figure 4.6: Integration of our planning framework with task planning and UQ to solve TAMP problems. The poor performance of the methods without SCOD in the Constrained Packing problem highlights the importance of UQ when attempting to solve unseen TAMP problems with learned skills. © 2023 IEEE.

the n action plans with the highest skill uncertainties (Eq. 4.5) are not considered for execution.

The results are presented in Fig. 4.6. **Policy CEM** achieves 97% success on the Hook Reach TAMP problem, while **SCOD Policy CEM** suffers a slight performance drop. However, for Constrained Packing, which contains OOD states, **SCOD Policy CEM** strongly outperforms the other methods. Exploring different ways to integrate UQ into our planning framework is a promising direction for future work.

4.7.4 Real-World Sequential Manipulation

We demonstrate that skills trained with our framework can be used to perform sequential manipulation tasks in a real robot environment. We take RGB-D images from a Kinect v2 camera and use manually tuned color thresholds to segment objects in the scene. With these segmentations, we estimate object poses using the depth image, which is then used to construct the initial environment state \bar{s}_1 . Qualitative results are provided in the supplementary video.

4.8 Conclusion

We present a framework for sequencing task-agnostic policies that have been trained independently. The key to generalization is planning actions that maximize the probability of long-horizon task success, which we model using the product of learned Q-values. This requires learning a dynamics model to predict future states and using UQ to filter out OOD states that the skills do not support. The result is a library of skills that can be composed to solve arbitrary long-horizon tasks with complex geometric dependencies between actions.

4.8.1 Future Work

Future work includes the investigation of methods for scaling skills to high-dimensional observations, combining the library of learned skills with a set of handcrafted skills, and exploring planning objectives that capture other desirable properties of trajectories, beyond their geometric feasibility.

Chapter 5

Searching for Feasible Policy Sequences from Language

5.1 Introduction

In [Chapter 4](#), we examined a central challenge in solving real-world, long-horizon tasks with learned behavior policies: even when individual behaviors can be executed reliably, unmodeled dependencies between them may critically affect the feasibility and success of an entire sequence. To address this, we introduced a method that estimates the success probability of a given policy sequence and uses this estimate to coordinate policy outputs at deployment time. This chapter builds on that foundation by observing that, for many tasks, multiple candidate sequences of behaviors may achieve the same goal. Generating such sequences—commonly referred to as task planning or symbolic planning—and selecting those with the highest likelihood of success therefore represents an additional avenue for improving reliability. Because (1) tasks are often most naturally specified in language (e.g., “shelve the dishes”), and (2) pretrained foundation models possess broad, internet-scale knowledge relevant to everyday activities, we explore the use of *Large Language Models* as symbolic planners to flexibly generate and search over candidate policy sequences directly from natural language task descriptions.

Long-horizon robot planning is traditionally formulated as a joint symbolic and geometric reasoning problem, where the symbolic reasoner is supported by a formal logic representation (e.g. first-order logic [1]). Such systems can generalize within the logical planning domain specified by experts. However, many desirable properties of plans that can be conveniently expressed in language by non-expert users may be cumbersome to specify in formal logic. Examples include the specification of user intent or preferences.

The emergence of Large Language Models (LLMs) [26] as a task-agnostic reasoning module presents a promising pathway to general robot planning capabilities. Several recent works [6, 118, 163, 286]

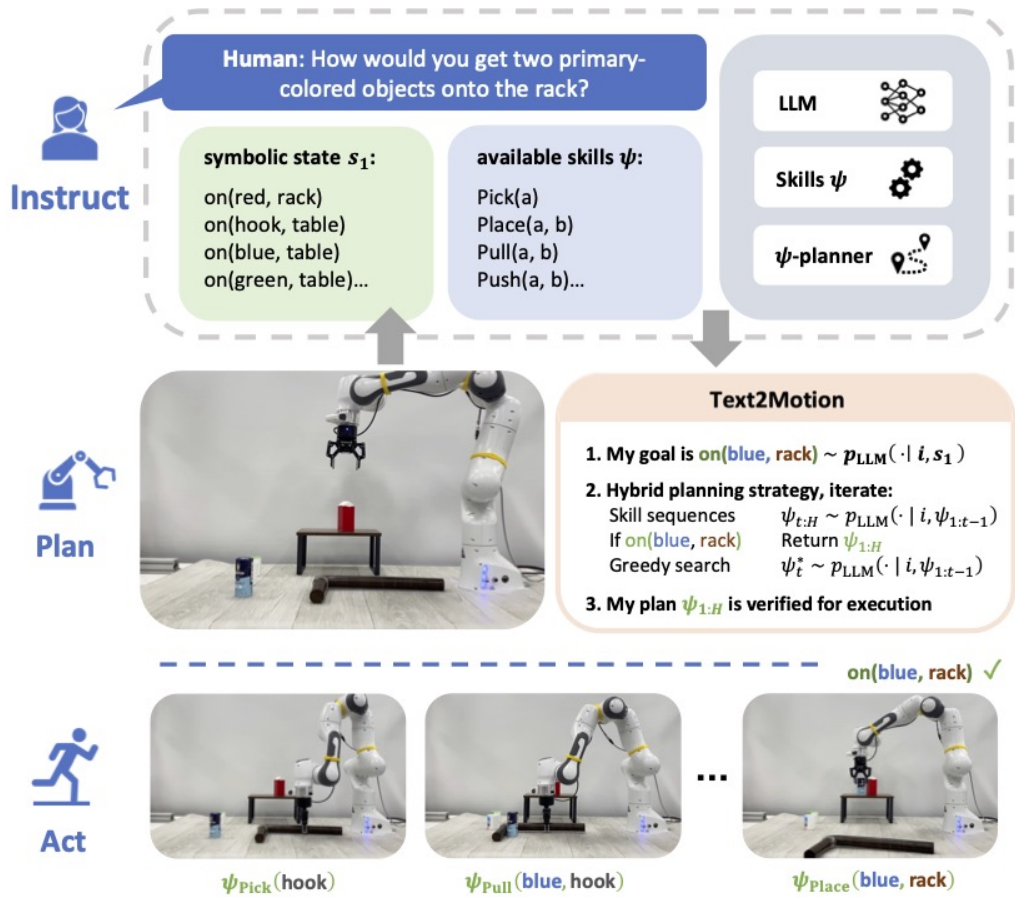


Figure 5.1: To carry out the instruction “get two primary-colored objects onto the rack,” the robot must apply symbolic reasoning over the scene description and language instruction to deduce what skills should be executed to acquire a second primary-colored object, after noticing that a red object is already on the rack (i.e. `on(red, rack)`). It must also apply geometric reasoning to ensure that skills are sequenced in a manner that is likely to succeed. Unlike prior work [6, 118] that myopically executes skills at the current timestep, Text2Motion constructs *sequences* of skills and coordinates their geometric dependencies with geometric feasibility planning [3]. Upon planning the skill sequence `Pick(hook)`, `Pull(blue, hook)`, `Pick(blue)`, `Place(blue, rack)`, our method computes a grasp position on the hook that enables pulling the blue object into the robot workspace so that it can be successfully picked up in the next step. More details can be found on the Text2Motion website: <https://sites.google.com/stanford.edu/text2motion>. © 2023 Springer Nature.

capitalize on their ability to perform task planning for robot systems without needing to manually specify symbolic planning domains. Nevertheless, these prior approaches adopt myopic or open-loop execution strategies, trusting LLMs to produce correct plans without verifying them on the symbolic or geometric level. Such strategies are challenged in long-horizon settings, where the task planning abilities of even the most advanced LLMs appear to degrade [269], and the overall success of a

seemingly correct task plan depends as well on how it is executed to ensure long-horizon feasibility. Therefore, we ask in this chapter: how can we verify the correctness and feasibility of LLM-generated plans prior to execution?

We propose **Text2Motion**, a language-based planning framework that interfaces an LLM with a library of learned skills and a geometric feasibility planner [3] to solve complex sequential manipulation tasks (Fig. 5.1). Our contributions are two-fold: (i) a hybrid LLM planner that synergistically integrates shooting-based and search-based planning strategies to construct geometrically feasible plans for tasks not seen by the skills during training; and (ii) a plan termination method that infers goal states from a natural language instruction to verify the completion of plans before executing them. We find that our planner achieves a success rate of 82% on a suite of challenging table top manipulation tasks, while prior language-based planning methods achieve a 13% success rate.

5.2 Related Work

5.2.1 Language for Robot Planning

Language is increasingly being explored as a medium for solving long-horizon robotics problems. For instance, *Language-conditioned policies* (LCPs) are not only used to learn short-horizon skills [125, 128, 238, 241, 242, 257], but also long-horizon policies [29, 58, 191]. However, LCPs require expensive data collection and training procedures if they are to generalize to a wide distribution of long-horizon tasks with diverse instructions.

Several recent works leverage the generative qualities of LLMs by prompting them to predict long-horizon plans. [117] grounds an LLM planner to admissible action sets for task planning, [168, 246] explore the integration of LLMs with PDDL [1], and [252, 279] focuses on task-level replanning with LLMs. Tangential works shift the representation of plans from action sequences to code [163, 249, 271, 301] and embed task queries, robot actions, solution samples, and fallback behaviors as programs in the prompt. In contrast to these works, which primarily address challenges in task planning with LLMs, we focus on verifying LLM-generated plans for feasibility on the geometric level.

Closest in spirit to our approach are SayCan [6] and Inner Monologue (IM) [118] which at each timestep score the *usefulness* and *feasibility* of all possible skills and execute the one with the highest score. Termination occurs when the score of the stop “skill” is larger than any other. IM provides additional sources of feedback to the LLM in the form of skill successes and task-progress cues.

While SayCan and IM are evaluated on a diverse range of tasks, there are several limitations that impede their performance in the settings we study. First, by only myopically executing the next skill at each timestep, they may fail to account for geometric dependencies that exist over the extent of a skill sequence. For an example, see Fig. 5.1. Second, they do not explicitly predict a multi-step plan, which prevents verification of desired properties or outcomes prior to execution. Examples of such

properties could include whether the final state induced by the plan satisfies symbolic constraints or whether the plan adheres to safety criteria. Lastly, these methods ignore the uncertainty of skill feasibility predictions (i.e. affordances), which [3] demonstrates is important when sequencing learned skills to solve long-horizon tasks. By addressing these limitations, **Text2Motion** outperforms SayCan and IM by a large margin on tasks with geometric dependencies, as demonstrated in the experiments.

5.2.2 Task and Motion Planning

Task and Motion Planning (TAMP) refers to a problem setting in which a robot solves long-horizon tasks through symbolic and geometric reasoning [87, 131]. The hierarchical approach [132] characterizes the most common family of solution methods. Such methods typically employ a) a symbolic task planner [27, 110] to produce a candidate plan skeleton, and b) a motion planner to verify the plan skeleton for its geometric feasibility and compute a motion trajectory subject to robot and environmental constraints [62, 86, 265].

For complex tasks, classical TAMP solvers [24, 59, 86, 132, 153, 265] may iterate between task planning and motion planning for minutes until a plan is found. To amortize planning costs, works learn sampling distributions [3, 144, 145, 277, 292], visual feasibility heuristics [63, 64, 66], low-level controllers [65, 245], or state sparsifiers [43, 243], from datasets of solutions computed by classical TAMP solvers. Another line of works learn symbolic representations for TAMP [9, 44, 52, 149, 150, 244, 245, 278], often from task-specific symbolic transition experience.

As is common in TAMP, **Text2Motion** also assumes knowledge of task-relevant objects and their poses in order to plan feasible trajectories for long-horizon tasks. However, central to our investigation is the use of LLMs instead of symbolic task planners often used in TAMP [87], and language as convenient medium to express tasks that may be cumbersome to specify in formal logic (e.g. user preferences [286]). Accordingly, we address early challenges concerning the reliable use of LLMs (discussed in §5.2.1) in the long-horizon settings typically solved by TAMP. **Text2Motion** thereby presents several qualitative differences from TAMP: i) the ability to interpret free-form language instructions for the construction of multi-step plans, and ii) the capacity to reason over an unrestricted set of object classes and object properties, both of which are supported by the commonsense knowledge of LLMs [31]. We leave the extension of our framework to open-world settings (e.g. via environment exploration [34] or interaction [51]) to future work.

5.3 Problem Setup

We aim to solve long-horizon sequential manipulation problems that require symbolic and geometric reasoning from a natural language instruction i and the initial state of the environment s_1 . We assume a closed-world setting, whereby the initial state s_1 contains knowledge of task-relevant objects

and their poses as provided by an external perception system (§D.4.1). Fulfillment of the instruction i corresponds to achieving a desired goal configuration of the task-relevant objects which can be symbolically expressed with a closed set of predicates (§D.2.1).

5.3.1 LLM and Skill Library

We assume access to an LLM and a library of skills $\mathcal{L}^\psi = \{\psi^1, \dots, \psi^N\}$. Each skill ψ consists of a policy $\pi(a|s)$ and a parameterized manipulation primitive $\phi(a)$ [75], and is associated with a contextual bandit, or a single-timestep Markov Decision Process (MDP):

$$\mathcal{M} = (\mathcal{S}, \mathcal{A}, T, R, \rho), \quad (5.1)$$

where \mathcal{S} is the state space, \mathcal{A} is the action space, $T(s'|s, a)$ is the transition model, $R(s, a, s')$ is the binary reward function, and $\rho(s)$ is the initial state distribution. When a skill ψ is executed, an action $a \in \mathcal{A}$ is sampled from its policy $\pi(a|s)$ and fed to its primitive $\phi(a)$, which consumes the action and executes a series of motor commands on the robot. If the skill succeeds, it receives a binary reward of r (or $-r$ if it fails). We subsequently refer to policy actions $a \in \mathcal{A}$ as *parameters* for the primitive, which, depending on the skill, can represent grasp poses, placement locations, and pulling or pushing distances (§D.1.1).

A timestep in our environment corresponds to the execution of a single skill. We assume that each skill comes with a language description and that methods exist to obtain its policy $\pi(a|s)$, Q-function $Q^\pi(s, a)$, and dynamics model $T^\pi(s'|s, a)$. Our framework is agnostic to the approach used to obtain these models. We also assume a method to convey the environment state $s \in \mathcal{S}$ to the LLM as natural language.

5.3.2 The Planning Objective

Our objective is to find a plan in the form of a sequence of skills $[\psi_1, \dots, \psi_H]$ (for notational convenience, we hereafter represent sequences with range subscripts, e.g. $\psi_{1:H}$) that is both likely to satisfy the instruction i and can be successfully executed from the environment’s initial state s_1 . This objective can be expressed as the joint probability of skill sequence $\psi_{1:H}$ and binary rewards $r_{1:H}$ given the instruction i and initial state s_1 :

$$\begin{aligned} p(\psi_{1:H}, r_{1:H} \mid i, s_1) \\ = p(\psi_{1:H} \mid i, s_1) p(r_{1:H} \mid i, s_1, \psi_{1:H}). \end{aligned} \quad (5.2)$$

The first term in this product $p(\psi_{1:H} \mid i, s_1)$ considers the probability that the skill sequence $\psi_{1:H}$ will satisfy the instruction i from a symbolic perspective. However, a symbolically correct skill sequence may fail during execution due to kinematic constraints of the robot or geometric dependencies

spanning the skill sequence. We must also consider the *success probability* of the skill sequence $\psi_{1:H}$ captured by the second term in this product $p(r_{1:H} \mid i, s_1, \psi_{1:H})$. The success probability depends on the parameters $a_{1:H}$ fed to the underlying sequence of primitives $\phi_{1:H}$ that control the robot’s motion:

$$p(r_{1:H} \mid i, s_1, \psi_{1:H}) = p(r_{1:H} \mid s_1, a_{1:H}). \quad (5.3)$$

Eq. 5.3 represents the probability that skills $\psi_{1:H}$ achieve rewards $r_{1:H}$ when executed from initial state s_1 with parameters $a_{1:H}$; which is independent of the instruction i . If just one skill fails (reward $\neg r$), then the entire plan fails.

5.3.3 Geometric Feasibility Planning

The role of geometric feasibility planning is to maximize the success probability (Eq. 5.3) of a skill sequence $\psi_{1:H}$ by computing an optimal set of parameters $a_{1:H}$ for the underlying primitive sequence $\phi_{1:H}$. This process is essential for finding plans that maximize the overall planning objective in Eq. 5.2. In our experiments, we leverage Sequencing Task-Agnostic Policies (STAP) [3].

STAP resolves geometric dependencies across the skill sequence $\psi_{1:H}$ by maximizing the product of step reward probabilities of parameters $a_{1:H}$:

$$a_{1:H}^* = \arg \max_{a_{1:H}} \mathbb{E}_{s_{2:H}} \left[\prod_{t=1}^H p(r_t \mid s_t, a_t) \right], \quad (5.4)$$

where future states $s_{2:H}$ are predicted by dynamics models $s_{t+1} \sim T^{\pi_t}(\cdot \mid s_t, a_t)$. Note that the reward probability $p(r_t \mid s_t, a_t)$ is equivalent to the Q-function $Q^{\pi_t}(s_t, a_t)$ for skill ψ_t in a contextual bandit setting with binary rewards (Eq. 5.1). The success probability of the optimized skill sequence $\psi_{1:H}$ is thereby approximated by the product of Q-functions evaluated from initial state s_1 along a sampled trajectory $s_{2:H}$ with parameters $a_{1:H}^*$:

$$p(r_{1:H} \mid s_1, a_{1:H}) \approx \prod_{t=1}^H Q^{\pi_t}(s_t, a_t^*). \quad (5.5)$$

In principle, our framework is agnostic to the specific approach used for geometric feasibility planning, requiring only that it is compatible with the skill formalism defined in §5.3.1 and provides a reliable estimate of Eq. 5.3.

5.4 Methods

The core idea of our approach is to ensure the geometric feasibility of an LLM task plan—and thereby its correctness—by predicting the success probability (Eq. 5.3) of learned skills that are sequenced according to the task plan. In the following sections, we outline two strategies for planning with



Figure 5.2: **SHOOTING and GREEDY-SEARCH planning overview.** Both SHOOTING and GREEDY-SEARCH planners use the LLM to predict the set of valid goal states given the user’s natural language instruction and a description of the current state of the environment. These predicted goals are used to decide when the instruction is satisfied and planning can terminate. **Left:** The SHOOTING strategy uses the LLM to propose full skill sequences first and then runs geometric feasibility planning afterwards. As shown in the experiments, this approach fails when the space of candidate task plans is large but few skill sequences are geometrically feasible. **Right:** In the GREEDY-SEARCH strategy, the LLM is used to propose K candidate skills with the top LLM scores. The geometric feasibility planner then evaluates the feasibility of each candidate skill, and the one with the highest product of LLM and geometric feasibility scores is selected. The successor state of this skill is predicted by the geometric feasibility planner’s dynamics model. If the successor state does not satisfy any of the predicted goals, then it is given to the LLM to plan the next skill. If a goal is satisfied, then the planner returns the skill sequence for execution. By interleaving LLM task planning with geometric feasibility planning at each planning iteration, GREEDY-SEARCH is able to reliably find feasible plans across the different families of tasks we study in the experiments. © 2023 Springer Nature.

LLMs and learned skills: a shooting-based planner and a search-based planner. We then introduce the full planning algorithm, **Text2Motion**, which synergistically integrates the strengths of both strategies. These strategies represent different ways of maximizing the overall planning objective in Eq. 5.2.

5.4.1 Goal Prediction

Plans with high overall objective scores (Eq. 5.2) are not guaranteed to satisfy their instruction. Consider the instruction “move all the dishes from the table to the sink” issued in an environment with two dishes on the table. While a plan that picks and places one of the two dishes in the sink may have a high language model likelihood and success probability, it fails to satisfy the instruction.

The first step in all planning strategies is to convert the language instruction into a goal condition that can be checked against a candidate sequence of skills. Given an instruction i , a set of objects O in the scene, and a library of predicate classifiers $\mathcal{L}^\chi = \{\chi^1, \dots, \chi^M\}$, we use the LLM to predict a set of $|\mathcal{G}|$ symbolic goal propositions $\mathcal{G} = \{g_1, \dots, g_j\}$ that would satisfy the instruction. Each goal proposition $g \in \mathcal{G}$ is a set of predicates grounded over objects in the scene. Each predicate is a binary-valued function over objects and has a one-to-one correspondence with a predicate classifier $\chi \in \mathcal{L}^\chi$ that implements the predicate (details in §D.2.1). We define a satisfaction function $F_{\text{sat}}^\mathcal{G}(s) : \mathcal{S} \rightarrow \{0, 1\}$ which takes as input a geometric state s and evaluates to 1 if any goal proposition $g \in \mathcal{G}$ predicted by the LLM holds in state s .

A sequence of skills $\psi_{1:H}$ is said to satisfy the instruction i iff:

$$\exists s \in s_{2:H+1} : F_{\text{sat}}^{\mathcal{G}}(s) = 1, \quad (5.6)$$

where the future states $s_{2:H+1}$ are predicted by the geometric feasibility planner (see §5.3.3). If $F_{\text{sat}}^{\mathcal{G}}(s_t)$ evaluates to 1 for a geometric state s_t at timestep $t \leq H + 1$, then the planner returns the subsequence of skills $\psi_{1:t-1}$ for execution.

Algorithm 2 Shooting-based LLM planner

```

1: globals:  $\mathcal{L}^\psi, \mathcal{L}^x, \text{SATFUNC}, \text{LLM}, \text{STAP}$ 
2: function SHOOTING( $i, s_1, \mathcal{G}; K$ )
3:    $F_{\text{sat}}^{\mathcal{G}} \leftarrow \text{SATFUNC}(\mathcal{G}, \mathcal{L}^x)$  ▷ Goal checker
4:    $\{\psi_{1:H}^{(j)}\}_{j=1}^K \leftarrow \text{LLM}(i, s_1, \mathcal{G}, K)$  ▷ Gen. plans
5:    $C = \{\}$  ▷ Init. candidate set
6:   for  $j = 1 \dots K$  do
7:      $s_{2:H+1}^{(j)}, a_{1:H}^{(j)} \leftarrow \text{STAP}(s_1, \psi_{1:H}^{(j)}, \mathcal{L}^\psi)$ 
8:     if  $F_{\text{sat}}^{\mathcal{G}}(s_t^{(j)}) == 1$  for  $t \leq H + 1$  then
9:        $\psi_{1:t-1}^{(j)} \leftarrow \psi_{1:H}^{(j)}[: t - 1]$  ▷ Slice plan
10:       $C \leftarrow C \cup \{j\}$  ▷ Add to candidate set
11:    end if
12:    Compute  $p_{\text{success}}^{(j)}$  via Eq. 5.5
13:  end for
14:  Filter OOD plans from  $C$  as per Eq. 5.13
15:  if  $C == \emptyset$  then
16:    raise planning failure
17:  end if
18:   $j^* = \arg \max_{j \in C} p_{\text{success}}^{(j)}$ 
19:  return  $\psi_{1:t-1}^{(j^*)}$  ▷ Return best plan
20: end function

```

5.4.2 Shooting-Based Planning

The planner is responsible for finding geometrically feasible plans that satisfy the goal condition predicted by the LLM (§5.4.1). To this end, the first strategy we propose is a shooting-based planner, termed **SHOOTING** (see Fig. 5.2, Left), which takes a single-step approach to maximizing the overall planning objective in Eq. 5.2. **SHOOTING**'s process is further outlined in Algorithm 2. **SHOOTING** requires querying the LLM only once to generate K candidate skill sequences $\{\psi_{1:H}^1, \dots, \psi_{1:H}^K\}$ in an open-ended fashion. Each candidate skill sequence is processed by the geometric feasibility planner which returns an estimate of the sequence's success probability (Eq. 5.5) and its predicted future state trajectory $s_{2:H+1}$. Skill sequences that satisfy the goal condition (Eq. 5.6) are added to a candidate set. Invalid skill sequences as determined by §5.4.5 are filtered-out of the candidate set. If the candidate set is not empty, **SHOOTING** returns the skill sequence with the highest success probability, or raises a planning failure otherwise.

5.4.3 Search-Based Planning

We propose a second planner, **GREEDY-SEARCH** (see Fig. 5.2, Right), which at each planning iteration ranks candidate skills predicted by the LLM and adds the top scoring skill to the running plan.

This iterative approach can be described as a decomposition of the planning objective in Eq. 5.2 by timestep t :

$$\begin{aligned} p(\psi_{1:H}, r_{1:H} \mid i, s_1) \\ = \prod_{t=1}^H p(\psi_t, r_t \mid i, s_1, \psi_{1:t-1}, r_{1:t-1}). \end{aligned} \quad (5.7)$$

We define the joint probability of ψ_t and r_t in Eq. 5.7 as the skill score S_{skill} :

$$S_{\text{skill}}(\psi_t) = p(\psi_t, r_t \mid i, s_1, \psi_{1:t-1}, r_{1:t-1}),$$

which we factor using conditional probabilities:

$$\begin{aligned} S_{\text{skill}}(\psi_t) &= p(\psi_t \mid i, s_1, \psi_{1:t-1}, r_{1:t-1}) \\ &\quad p(r_t \mid i, s_1, \psi_{1:t}, r_{1:t-1}). \end{aligned} \quad (5.8)$$

Each planning iteration of **GREEDY-SEARCH** is responsible for finding the skill ψ_t that maximizes the skill score (Eq. 5.8) at timestep t .

Skill usefulness: The first factor of Eq. 5.8 captures the *usefulness* of a skill generated by the LLM with respect to satisfying the instruction. We define the skill usefulness score S_{llm} :

$$S_{\text{llm}}(\psi_t) = p(\psi_t \mid i, s_1, \psi_{1:t-1}, r_{1:t-1}) \quad (5.9)$$

$$\approx p(\psi_t \mid i, s_{1:t}, \psi_{1:t-1}). \quad (5.10)$$

In Eq. 5.10, the probability of the next skill ψ_t (Eq. 5.9) is cast in terms of the predicted state trajectory $s_{2:t}$ of the running plan $\psi_{1:t-1}$, and is thus independent of prior rewards $r_{1:t-1}$. We refer to §D.3.1 for a detailed derivation of Eq. 5.10.

At each planning iteration t , we optimize $S_{\text{llm}}(\psi_t)$ by querying an LLM to generate K candidate skills $\{\psi_t^1, \dots, \psi_t^K\}$. We then compute the usefulness scores $S_{\text{llm}}(\psi_t^k)$ by summing the token log-probabilities of each skill’s language description (visualized in §5.5.3). These scores represent the likelihood that ψ_t^k is the correct skill to execute from a language modeling perspective to satisfy instruction i .

Skill feasibility: The second factor of Eq. 5.8 captures the *feasibility* of a skill generated by the

Algorithm 3 Search-based LLM planner

```

1: globals:  $\mathcal{L}^\psi, \mathcal{L}^\chi, \text{SATFUNC}, \text{LLM}, \text{STAP}$ 
2: function GREEDY-SEARCH( $i, s_1, \mathcal{G}; K, d_{\max}$ )
3:    $F_{\text{sat}}^\mathcal{G} \leftarrow \text{SATFUNC}(\mathcal{G}, \mathcal{L}^\chi)$  ▷ Goal checker
4:    $\Psi = []; \tau = [s_1]$  ▷ Init. running plan
5:   while  $\text{len}(\Psi) < d_{\max}$  do
6:      $\Psi, \tau \leftarrow \text{GREEDY-STEP}(i, s_1, \mathcal{G}, \Psi, \tau, K)$ 
7:     if  $F_{\text{sat}}^\mathcal{G}(\tau[-1]) == 1$  then
8:       return  $\Psi$  ▷ Return goal-reaching plan
9:     end if
10:  end while
11:  raise planning failure
12: end function
13: function GREEDY-STEP( $i, s_1, \mathcal{G}, \Psi, \tau; K$ )
14:   $t = \text{len}(\Psi) + 1$  ▷ Curr. planning iteration
15:   $\{\psi_t^{(j)}\}_{j=1}^K \leftarrow \text{LLM}(i, \tau, \mathcal{G}, K)$  ▷ Gen. skills
16:   $C = \{\}$  ▷ Init. candidate set
17:  for  $j = 1 \dots K$  do
18:     $\psi_{1:t}^{(j)} \leftarrow \Psi.append(\psi^{(j)})$ 
19:     $s_{2:t+1}^{(j)}, a_{1:t}^{(j)} \leftarrow \text{STAP}(s_1, \psi_{1:t}^{(j)}, \mathcal{L}^\psi)$ 
20:    Compute  $S_{\text{llm}}(\psi_t^{(j)})$  via Eq. 5.10
21:    Compute  $S_{\text{geo}}(\psi_t^{(j)})$  via Eq. 5.12
22:     $S_{\text{skill}}(\psi_t^{(j)}) \leftarrow S_{\text{llm}}(\psi_t^{(j)}) \times S_{\text{geo}}(\psi_t^{(j)})$ 
23:    if  $\psi_t^{(j)}$  is not OOD then ▷ As per Eq. 5.13
24:       $C \leftarrow C \cup \{j\}$  ▷ Add to candidate set
25:    end if
26:  end for
27:   $j^* = \arg \max_{j \in C} S_{\text{skill}}(\psi_t^{(j)})$ 
28:  return  $\psi_{1:t}^{(j^*)}, s_{1:t+1}^{(j^*)}$  ▷ Return running plan
29: end function

```

LLM. We define the skill feasibility score S_{geo} :

$$S_{\text{geo}}(\psi_t) = p(r_t \mid i, s_1, \psi_{1:t}, r_{1:t-1}) \quad (5.11)$$

$$\approx Q^{\pi_t}(s_t, a_t^*), \quad (5.12)$$

where Eq. 5.12 approximates Eq. 5.11 by the Q-value evaluated at predicted future state s_t with optimized parameter a_t^* , both of which are computed by the geometric feasibility planner. We refer to §D.3.2 for a detailed derivation of Eq. 5.12.

Skill selection: The skill feasibility score (Eq. 5.12) and skill usefulness score (Eq. 5.10) are then multiplied to produce the overall skill score (Eq. 5.8) for each of the K candidate skills $\{\psi_t^1, \dots, \psi_t^K\}$. Invalid skills as determined by §5.4.5 are filtered-out of the candidate set. Of the remaining skills, the one with the highest skill score ψ_t^* is added to the running plan $\psi_{1:t-1}$. If the predicted geometric state s_{t+1} that results from skill ψ_t^* satisfies the predicted goal condition (Eq. 5.6), the skill sequence

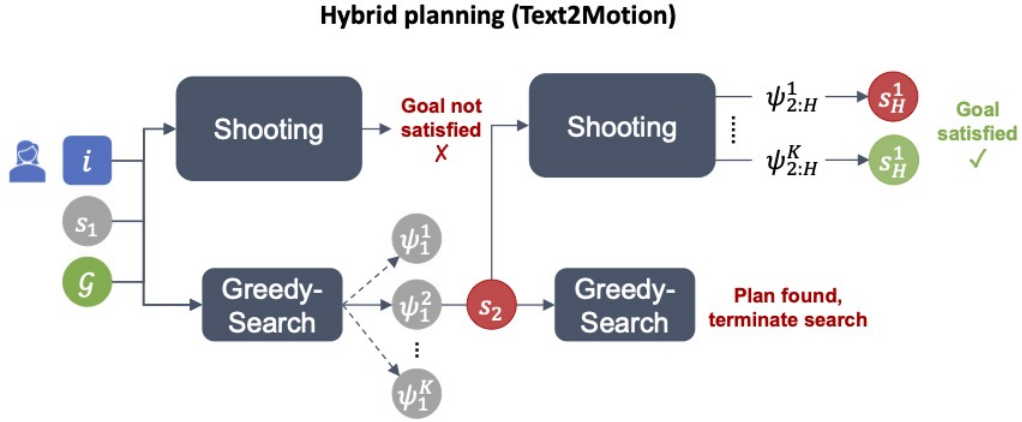


Figure 5.3: **Proposed hybrid planner**. After predicting goals for a given instruction, Text2Motion iterates the process: i) invoke SHOOTING to plan full skill sequences, and if no goal-reaching plan is found, ii) take a GREEDY-SEARCH step and check if executing the selected “best” skill would reach the goal. Note that the entire planning process occurs before execution. See Fig. 5.2 for a visualization of the SHOOTING and GREEDY-SEARCH planners. © 2023 Springer Nature.

$\psi_{1:t}$ is returned for execution. Otherwise, s_{t+1} is used to initialize planning iteration $t + 1$. The process repeats until the planner returns or a maximum search depth d_{\max} is met raising a **planning failure**. This process is outlined in Algorithm 3.

The baselines we compare to [6, 118] only consider the feasibility of skills ψ_t^k in the current state s_t . In contrast, **GREEDY-SEARCH** considers the feasibility of skills ψ_t^k in the context of the planned sequence $\psi_{1:t-1}$ via geometric feasibility planning.

5.4.4 Text2Motion

We present **Text2Motion**, a hybrid planning algorithm that inherits the strengths of both shooting-based and search-based planning strategies. In particular, **SHOOTING** offers efficiency when geometrically feasible skill sequences can be easily predicted by the LLM given the initial state and the instruction. **GREEDY-SEARCH** serves as a reliable fall-back strategy that can determine what skills are feasible at the current timestep, should **SHOOTING** fail to find a plan. A visualization is provided in Fig. 5.3.

At each planning iteration t , **Text2Motion** optimistically invokes **SHOOTING** to plan K candidate skill sequences. If **SHOOTING** raises a planning failure, then **Text2Motion** falls back to a single step of **GREEDY-SEARCH**, which adds the skill ψ_t^* with the highest skill score (Eq. 5.8) to the running plan $\psi_{1:t-1}$. The geometric feasibility planner predicts the state s_{t+1} that would result from executing ψ_t^* . If state s_{t+1} satisfies the goal condition (Eq. 5.6), the skill sequence $\psi_{1:t}$ is returned for execution. Otherwise, the next planning iteration starts by invoking **SHOOTING** on predicted state s_{t+1} . The process repeats until the planner returns or a maximum search depth d_{\max} is met.

Algorithm 4 Text2Motion hybrid planner

```

1: globals:  $\mathcal{L}^x$ , SATFUNC, SHOOTING, GREEDY-STEP
2: function TEXT2MOTION( $i, s_1, \mathcal{G}; K, d_{\max}$ )
3:    $F_{\text{sat}}^{\mathcal{G}} \leftarrow \text{SATFUNC}(\mathcal{G}, \mathcal{L}^x)$ 
4:    $\Psi = []; \tau = [s_1]$  ▷ Goal checker
5:   while  $\text{len}(\Psi) < d_{\max}$  do ▷ Init. running plan
6:     try
7:       return SHOOTING( $i, \tau, \mathcal{G}, K$ )
8:     catch planning failure
9:      $\Psi, \tau \leftarrow \text{GREEDY-STEP}(i, s_1, \mathcal{G}, \Psi, \tau, K)$ 
10:    if  $F_{\text{sat}}^{\mathcal{G}}(\tau[-1]) == 1$  then
11:      return  $\Psi$ 
12:    end if
13:  end try
14: end while
15:  raise planning failure
16: end function

```

Text2Motion is outlined in [Algorithm 4](#).

5.4.5 Out-of-Distribution Detection

During planning, the LLM may propose skills that are out-of-distribution (OOD) given a state s_t and optimized parameter a_t^* . For instance, a symbolically incorrect skill, like Place(dish, table) when the dish is not in hand, may end up being selected if we rely on learned Q-values, since the Q-value for an OOD input can be spuriously high. We therefore reject plans that contain an OOD skill.

We consider a skill ψ_t to be OOD if the variance of its Q-value ([Eq. 5.12](#)) predicted by an ensemble [[154](#)] exceeds a calibrated threshold ϵ^{ψ_t} :

$$F_{\text{OOD}}(\psi_t) = \mathbb{1}(\text{Var}_{i \sim 1:B} [Q_i^{\pi_t}(s_t, a_t^*)] \geq \epsilon^{\psi_t}), \quad (5.13)$$

where $\mathbb{1}$ is the indicator function and B is the ensemble size. We refer to [§D.1.2](#) for details on calibrating OOD thresholds ϵ^{ψ} .

5.5 Experiments

We conduct experiments to test four hypotheses:

H1 Geometric feasibility planning is a necessary ingredient when using LLMs and robot skills to solve manipulation tasks with geometric dependencies from a natural language instruction.

H2 GREEDY-SEARCH is better equipped to solve tasks with partial affordance perception (as defined in [§5.5.4](#)) compared to SHOOTING.

H3 **Text2Motion**’s hybrid planner inherits the strengths of shooting- and search-based strategies.

H4 *A priori* goal prediction is a more reliable plan termination strategy than stop scoring.

The following subsections describe the baseline methods we compare against, details on LLMs and prompts, the tasks over which planners are evaluated, and performance metrics we report.

5.5.1 Baselines

We compare **Text2Motion** with a series of language-based planners, including the proposed **SHOOTING** and **GREEDY-SEARCH** strategies. For consistency, we use the same skill library \mathcal{L}^ψ , with independently trained policies π and Q-functions Q^π , the OOD rejection strategy (§5.4.5) and, where appropriate, the dynamics models $T^\pi(s, a)$ and geometric feasibility planner (§5.3.3) across all methods and tasks.

SAYCAN-GS: We implement a cost-considerate variant of SayCan [6] with a module dubbed **GENERATOR-SCORER** (GS). At each timestep t , SayCan ranks *all possible* skills by $p(\psi_t | i, \psi_{1:t-1}) \cdot V^{\pi_t}(s_t)$, before executing the top scoring skill (Scorer). However, the cost of ranking skills scales unfavorably with the number of scene objects \mathcal{O} and skills in library \mathcal{L}^ψ . **SAYCAN-GS** limits the pool of skills considered in the ranking process by querying the LLM for the K most useful skills $\{\psi_t^1, \dots, \psi_t^K\} \sim p(\psi_t | i, \psi_{1:t-1})$ (Generator) before engaging Scorer. Execution terminates when the score of the stop “skill” is larger than the other skills.

INNERMONO-GS: We implement the *Object + Scene* variant of Inner Monologue [118] by providing task-progress scene context in the form of the environment’s symbolic state. We acquire **INNERMONO-GS** by equipping [118] with **GENERATOR-SCORER** for cost efficiency. LLM skill likelihoods are equivalent to those from **SAYCAN-GS** except they are now also conditioned on the visited state history $p(\psi_t | i, s_{1:t}, \psi_{1:t-1})$.

5.5.2 Large Language Model

We use two pretrained language models, both of which were accessed through the OpenAI API: i) `text-davinci-003`, a variant of the InstructGPT [204] language model family which is finetuned from GPT-3 with human feedback and ii) the Codex model [36] (specifically, `code-davinci-002`). For the **SHOOTING** planner, we empirically found `text-davinci-003` to be the most capable at open-ended generation of skill sequences. For all other queries, we use `code-davinci-002` as it was found to be reliable. We do not train or finetune the LLMs and only use few shot prompting.

5.5.3 Prompt Engineering

The in-context examples are held consistent across all methods and tasks in the prompts passed to the LLM. We provide an example of the prompt structure used to query **GREEDY-SEARCH** for

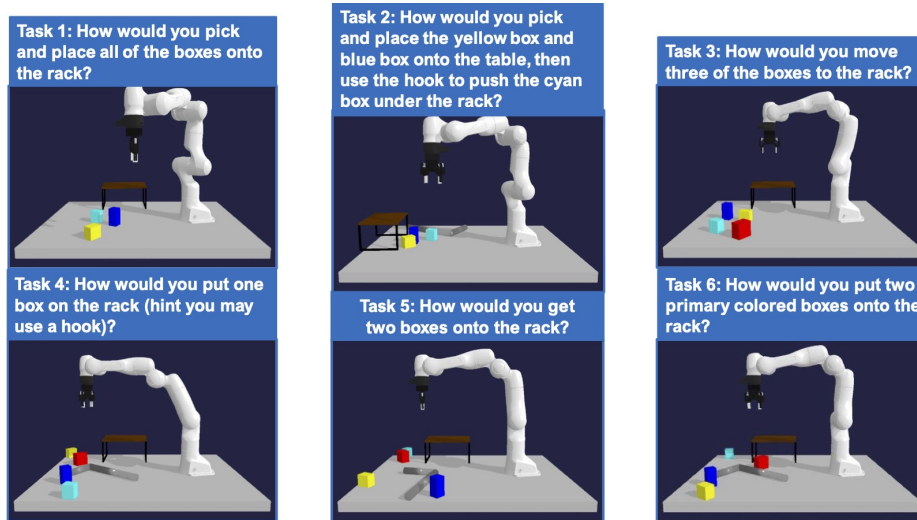


Figure 5.4: **TableEnv manipulation evaluation task suite.** We evaluate the performance of all methods on tasks based on the above manipulation domain. The tasks considered vary in terms of difficulty and each task contains a subset of three properties: being long horizon (Tasks 1, 2, 3, 5, 6), containing lifted goals (Tasks 4, 5, 6), and having partial affordance perception (Tasks 4, 5, 6). During evaluation, we randomize the geometric parameters of each task. © 2023 Springer Nature.

$K = 5$ skills at the first planning iteration (prompt template is in black and LLM output is in orange):

```

Available scene objects: ['table', 'hook', 'rack', 'yellow box', 'blue box', 'red box']

Object relationships: ['inhand(hook)', 'on(yellow box, table)', 'on(rack, table)', 'on(blue box, table)']

Human instruction: How would you push two of the boxes to be under the rack?

Goal predicate set: [['under(yellow box, rack)', 'under(blue box, rack)'], ['under(blue box, rack)', 'under(red box, rack)'], ['under(yellow box, rack)', 'under(red box, rack)']]

Top 5 next valid robot actions (python list): ['push(yellow box, rack)', 'push(red box, rack)', 'place(hook, table)', 'place(hook, rack)', 'pull(red box, hook)']

```

The prompt above chains the output of two queries together: one for goal prediction (§5.4.1), and another for skill generation (§5.4.3). To compute the skill usefulness (Eq. 5.10), we replace Top 5 next valid robot actions with Executed action:, append the language description of the generated skill (e.g. Push(yellow box, rack)), and sum token log-probabilities. We provide the full set of in-context examples in the Appendix (§D.2.2).

5.5.4 Task Suite

We construct a suite of evaluation tasks (Fig. 5.4) in a table-top manipulation domain. Each task includes a natural language instruction i and initial state distribution $\rho(s)$ from which geometric task instances are sampled. For the purpose of experimental evaluation only, tasks also contain a ground-truth goal criterion to evaluate whether a plan has satisfied the corresponding task instruction. Finally, each task contains subsets of the following properties:

- **Long-horizon (LH):** Tasks that require skill sequences $\psi_{1:H}$ of length six or greater to solve. For example, Task 1 in Fig. 5.4 requires the robot to pick and place three objects for a total of six skills. In our task suite, **LH** tasks also contain geometric dependencies that span across the sequence of skills which are unlikely to be resolved by myopically executing each skill. For example, Task 2 (Fig. 5.4) requires the robot to pick and place obstructing boxes (i.e. blue and yellow) to enable a collision-free push of the cyan box underneath the rack using the hook.
- **Lifted goals (LG):** Goals are expressed over object classes rather than object instances. For example, the lifted goal instruction “move three boxes to the rack” specifies an object class (i.e. boxes) rather than an object instance (e.g. the red box). This instruction is used for Task 3 (Fig. 5.4). Moreover, **LG** tends to correspond to planning tasks with many possible solutions. For instance, there may only be a single solution to the non-lifted instruction “fetch me the red box and the blue box,” but an LLM must contend with more options when asked to, for example, “fetch any two boxes.”
- **Partial affordance perception (PAP):** Skill affordances cannot be perceived solely from the spatial relations described in the initial state s_1 . For instance, Task 5 (Fig. 5.4) requires the robot to put two boxes onto the rack. However, the scene description obtained through predicate classifiers \mathcal{L}^x (described in §5.4.1) and the instruction i do not indicate whether it is necessary to use a hook to pull an object closer to the robot first.

5.5.5 Evaluation and Metrics

Text2Motion, **SHOOTING**, **GREEDY-SEARCH**: We evaluate these language planners by marking a plan as successful if, upon execution, they reach a final state s_{H+1} that satisfies the instruction i of a given task. A plan is executed only if the geometric feasibility planner predicts a state that satisfies the inferred goal conditions (§5.4.1).

Two failure cases are tracked: i) planning failure: the method does not produce a sequence of skills $\psi_{1:H}$ whose optimized parameters $a_{1:H}^*$ (Eq. 5.4) results in a state that satisfies $F_{\text{sat}}^{\mathcal{G}}$ within a maximum plan length of d_{max} ; ii) execution failure: the execution of a plan that satisfies $F_{\text{sat}}^{\mathcal{G}}$ does not achieve the ground-truth goal of the task.

Since the proposed language planners use learned dynamics models to optimize parameters $a_{1:H}$ with respect to (potentially erroneous) future state predictions $s_{2:H}$, we perform the low-level

execution of the skill sequence $\psi_{1:H}$ in closed-loop fashion. Thus, upon executing the skill ψ_t at timestep t and receiving environment feedback s_{t+1} , we call STAP [3] to perform geometric feasibility planning on the remaining planned skills $\psi_{t+1:H}$. We do not perform task-level replanning, which would involve querying the LLM at timestep $t + 1$ for a new sequence of skills $\psi_{t+1:H}$.

SAYCAN-GS & INNERMONO-GS: These myopic agents execute the next best admissible skill ψ_t at each timestep t without looking-ahead. Hence, we evaluate them in a closed-loop manner for a maximum of d_{\max} steps. We mark a run as a success if the agent issues the `stop` skill and the current state s_t satisfies the ground-truth goal. Note that this comparison is advantageous for these myopic agents because they are given the opportunity to perform closed-loop replanning at the task-level (e.g. re-attempting a failed skill), whereas task-level replanning does not occur for **Text2Motion**, **SHOOTING**, or **GREEDY-SEARCH**. This advantage does not lead to measurable performance gains on the challenging evaluation domains that we consider.

Reported metrics: We report success rates and subgoal completion rates for all methods. Success rates are averaged over ten random seeds per task, where each seed corresponds to a different geometric instantiation of the task (§5.5.4). Subgoal completion rates are computed over all plans by measuring the number of steps an *oracle planner* would take to reach the ground-truth goal from a planner’s final state. To further delineate the performance of **Text2Motion** from **SHOOTING** and **GREEDY-SEARCH**, we also report the percentages of planning and execution failures.

5.6 Results

5.6.1 Feasibility Planning Is Required to Solve Tasks with Geometric Dependencies (H1)

Our first hypothesis is that performing geometric feasibility planning on task plans output by the LLM is essential to task success. To test this hypothesis, we compare methods that use geometric feasibility planning (**Text2Motion**, **SHOOTING**, **GREEDY-SEARCH**) against myopic methods that do not (**SAYCAN-GS** and **INNERMONO-GS**).

Instructions i provided in the first two planning tasks (**LH**) allude to skill sequences that, if executed appropriately, would solve the task. In effect, the LLM plays a lesser role in contributing to plan success, as its probabilities are conditioned to mimic the skill sequences in i . On such tasks, **Text2Motion**, **SHOOTING** and **GREEDY-SEARCH** which employ geometric feasibility planning over skills sequences better contend with geometric dependencies prevalent in **LH** tasks and thereby demonstrate higher success rates.

In contrast, the myopic baselines (**SAYCAN-GS** and **INNERMONO-GS**) fail to surpass success rates of 20%, despite completing between 50%-80% of the subgoals (Fig. 5.5). This result is anticipated as the feasibility of downstream skills requires coordination with earlier skills in the sequence, which these methods do not consider. As the other tasks combine aspects of **LH** with **LG** and **PAP**, it

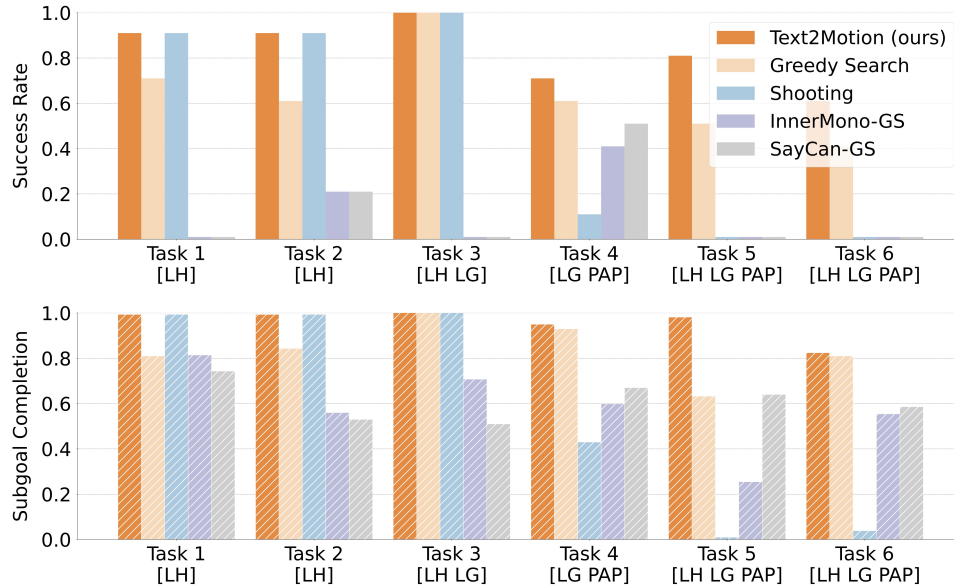


Figure 5.5: **Results on the TableEnv manipulation domain** with 10 random seeds for each task. **Top:** Our method (Text2Motion) significantly outperforms all baselines on tasks involving partial affordance perception (Task 4, 5, 6). For tasks without partial affordance perception, the methods that use geometric feasibility planning (Text2Motion, SHOOTING, GREEDY-SEARCH) convincingly outperform the methods (SAYCAN-GS and INNERMONO-GS) that do not. We note that SHOOTING performs well on the tasks without partial affordance perception as it has the advantage of outputting *multiple* goal-reaching candidate plans and selecting the one with the highest execution success probability. **Bottom:** Methods without geometric feasibility planning tend to have high sub-goal completion rates but very low success rates. This divergence arises because it is possible to make progress on tasks without resolving geometric dependencies in the earlier timesteps; however, failure to account for geometric dependencies results in failure of the overall task. © 2023 Springer Nature.

remains difficult for **SAYCAN-GS** and **INNERMONO-GS** to find solutions.

Surprisingly, we see that **SAYCAN-GS** closely matches the performance of **INNERMONO-GS**, which is additionally provided with descriptions of all states encountered during execution (as opposed to just the initial scene description). This result suggests that explicit language feedback does not contribute to success on our tasks when considered in isolation from plan feasibility.

5.6.2 Search-Based Reasoning Is Required for PAP Tasks (H2)

Our second hypothesis is that search-based reasoning is required to solve the **PAP** family of tasks (defined in §5.5.4). We test this hypothesis by comparing **GREEDY-SEARCH** and **SHOOTING**, which represent two distinct approaches to combining symbolic and geometric reasoning to maximize the overall planning objective (Eq. 5.2). **SHOOTING** uses Q-functions of skills to optimize K skill

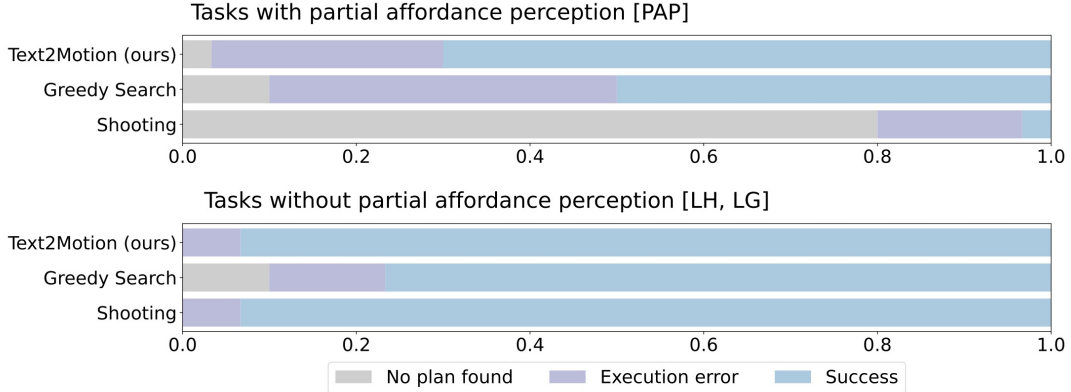


Figure 5.6: **Failure modes of language-based planners on two categories of tasks.** In this plot, we analyse the various types of failure modes that occur with Text2Motion, SHOOTING and GREEDY-SEARCH when evaluated on tasks with partial affordance perception (PAP; see §5.5.4 for an explanation) and tasks without partial affordance perception (non-PAP). **Top:** For the PAP tasks, SHOOTING incurs many planning failures because the space of possible plans is large but only few can be feasibly executed. In contrast, GREEDY-SEARCH uses value functions during search to narrow down the space of plans to those that are feasible. Text2Motion relies on GREEDY-SEARCH as a fallback if SHOOTING fails, and thus can also contend with PAP tasks. **Bottom:** For the non-PAP tasks, SHOOTING outperforms GREEDY-SEARCH. We attribute this difference to SHOOTING’s ability to output multiple task plans while GREEDY-SEARCH can only output a single plan. Finally, Text2Motion matches the performance of SHOOTING as it also outputs and selects among multiple task plans. © 2023 Springer Nature.

sequences (Eq. 5.4) after they are generated by the LLM. GREEDY-SEARCH uses Q-functions as skill feasibility heuristics (Eq. 5.12) to guide search while a skill sequence is being constructed.

In the first two tasks (LH, Fig. 5.5), we find that SHOOTING achieves slightly higher success rates than GREEDY-SEARCH, while both methods achieve 100% success rates in the third task (LH + LG). This result indicates a subtle advantage of SHOOTING when multiple feasible plans can be directly inferred from i and s_1 . SHOOTING can capitalize on diverse orderings of K generated skill sequences (including the one specified in i) and select the one with the highest success probability (Eq. 5.3). For example, Task 1 (Fig. 5.4) asks the robot to put three boxes onto the rack; SHOOTING allows the robot to test multiple different skill sequences while GREEDY-SEARCH only outputs a single plan. This advantage is primarily enabled by bias in the Q-functions: Eq. 5.5 may indicate that Place(dish, rack) then Place(cup, rack) is more geometrically complex than Place(cup, rack) then Place(dish, rack), while they are geometric equivalents.

The plans considered by GREEDY-SEARCH at planning iteration t share the same sequence of predecessor skills $\psi_{1:t-1}$. This affords limited diversity for the planner to exploit. However, GREEDY-SEARCH has a significant advantage when solving the PAP family of problems (Fig. 5.5, Tasks 4-6). Here, skill sequences with high success probabilities (Eq. 5.3) are difficult to infer directly

Hybrid planning breakdown	Task 4	Task 5	Task 6
% SHOOTING only	14%	0%	0%
% GREEDY-SEARCH only	0%	0%	0%
% Combination	86%	100%	100%
Avg. GREEDY-SEARCH Steps	1.0	2.6	3.0
Avg. Plan Length	5.0	7.0	7.0

Table 5.1: **Ablation on hybrid planning method.** We analyze the usage percentages of both SHOOTING and GREEDY-SEARCH in successful plans found by our hybrid planner (see Fig. 5.3). We find that, as tasks increase in difficulty (Task 4, 5, 6), the majority of solutions involve a combination of both planners. This result indicates that shooting-based and search-based planning strategies play complementing roles in the success of Text2Motion. © 2023 Springer Nature.

from i , s_1 , and the in-context examples provided in the prompt. As a result, SHOOTING incurs an 80% planning failure rate, while GREEDY-SEARCH finds plans over 90% of the time (Fig. 5.6). In terms of success, GREEDY-SEARCH solves 40%-60% of the PAP tasks, while SHOOTING achieves a 10% success rate on Task 4 (LG + PAP) and fails to solve any of the latter two tasks (LH + LG + PAP). Moreover, SHOOTING does not meaningfully advance on any subgoals, unlike SAYCAN-GS and INNERMONO-GS, which consider the geometric feasibility of skills at each timestep (albeit, myopically).

5.6.3 Hybrid Planning Integrates the Strengths of Shooting-Based and Search-Based Methods (H3)

Our third hypothesis is that shooting-based planning and search-based planning have complementing strengths that can be unified in a hybrid planning framework. We test this hypothesis by comparing the performance of Text2Motion against SHOOTING and GREEDY-SEARCH.

The results are presented in Fig. 5.5. We find that Text2Motion matches the performance of SHOOTING on tasks that do not consist of PAP (Task 1, 2, 3). This is expected because SHOOTING does not exhibit planning failures on these tasks (Fig. 5.6) and Text2Motion starts by invoking SHOOTING, which results in their identical performance. However, on tasks with PAP (Task 4, 5, 6) we observe that Text2Motion succeeds more often than GREEDY-SEARCH. This suggests that interleaving SHOOTING and GREEDY-SEARCH at each planning iteration enables Text2Motion to consider a more diverse set of goal-reaching solutions. This result is corroborated in Fig. 5.6, where we see that Text2Motion incurs fewer planning and execution failures than GREEDY-SEARCH.

In Table 5.1, we further analyze the usage percentages of SHOOTING and GREEDY-SEARCH within successful plans executed by Text2Motion. The results show that, for tasks involving PAP, over 90% of solutions involve a combination of both shooting- and search-based strategies, which

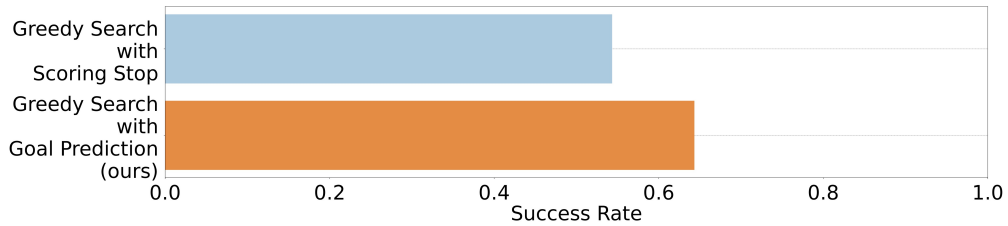


Figure 5.7: **Ablation on termination method: goal proposition prediction vs stop scoring.** We compare the performance of GREEDY-SEARCH using two different plan termination methods: using the LLM to predict goals *a priori* (ours) and scoring a stop skill [6] during search. We present results averaged across all six tasks and ten seeds for each variation (120 experiments in total). We find that terminating planning when LLM-predicted goals are satisfied results in a 10% boost in success rate over stop scoring. © 2023 Springer Nature.

confirms our third hypothesis.

5.6.4 Plan Termination Is Made Reliable via Goal Prediction (H4)

Our fourth hypothesis is that predicting goals from instructions *a priori* and selecting plans based on their satisfaction (§5.4.1) is more reliable than scoring plan termination with a dedicated stop skill at each timestep. We test this hypothesis in an ablation experiment (Fig. 5.7), comparing our plan termination method to that of SayCan and Inner Monologue’s, while keeping all else constant for our GREEDY-SEARCH planner. We run 120 experiments (two variations, six tasks, and ten seeds each) in total on the TableEnv Manipulation task suite. The results in Fig. 5.7 suggest that, for the tasks we consider, our proposed goal prediction method leads to 10% higher success rates than the scoring baseline.

We also note the apparent advantages of both techniques. First, goal prediction is more efficient than scoring stop as the former requires only one LLM query, whereas the latter needs to be queried at every timestep. Second, goal prediction offers interpretability over stop scoring, as it is possible to inspect the goal that the planner is aiming towards prior to execution. Nonetheless, stop scoring does provide benefits in terms of expressiveness, as its predictions are not constrained to any specific output format. This advantage, however, is not captured in our evaluation task suite, which at most require conjunctive (\wedge) and disjunctive (\vee) goals. For instance, “Stock two boxes onto the rack” could correspond to $(\text{on}(\text{red box}, \text{rack}) \wedge \text{on}(\text{blue box}, \text{rack})) \vee (\text{on}(\text{yellow box}, \text{rack}) \wedge \text{on}(\text{cyan box}, \text{rack}))$, while in theory, stop scoring can represent all goals expressible in language.

5.7 Conclusion

We present a language-based planning framework that combines LLMs, learned skills, and geometric feasibility planning to solve long-horizon robotic manipulation tasks containing geometric dependencies. **Text2Motion** constructs a task- and motion-level plan and verifies that it satisfies a natural language instruction by testing planned states against inferred goals. In contrast to prior language planners, our method verifies that its plan satisfies the instruction before executing any actions in the environment. **Text2Motion** represents a hybrid planning formalism that optimistically queries an LLM for long-horizon plans and falls back to a reliable search strategy should optimistic planning fail. As a result, **Text2Motion** inherits the strengths of both shooting-based and search-based planning formalisms.

Our results highlight the following: (i) geometric feasibility planning is important when using LLMs and learned skills to solve sequential manipulation tasks from natural language instructions; (ii) search-based reasoning can contend with a family of tasks where the space of possible plans is large but only few are feasible; (iii) shooting-based and search-based planning strategies can be synergistically integrated in a hybrid planner that outperforms its constituent parts; (iv) terminating plans based on inferred symbolic goals is more reliable than prior LLM scoring techniques.

5.8 Limitations and Future Work

We summarize the limitations of our approach and opportunities for future investigation:

1. **LLM likelihoods:** We observed an undesirable pattern emerge in the planning phase of **GREEDY-SEARCH** and the execution phase of **SAYCAN-GS** and **INNERMONO-GS**, where *recency bias* [306] would cause the LLM to produce unreliable likelihoods (Eq. 5.10), inducing a cyclic state of repeating feasible skills. While we mitigate such failures by combining **GREEDY-SEARCH** and **SHOOTING** in the hybrid **Text2Motion** algorithm, leveraging calibration techniques to increase the reliability LLM likelihoods [37, 161] may improve the performance search-based planning over long-horizons.
2. **Skill library:** As with other methods that use skill libraries, **Text2Motion** is reliant on the fidelity of the learned skills, their value functions, and the ability to accurately predicted future states with dynamics models. Thus, incorporating skills that operate on high-dimensional observations (e.g. images [238]) into our framework may require adopting techniques for stable long-term predictions in these observation spaces [67].
3. **Runtime complexity:** **Text2Motion** is mainly comprised of learned components, which comes with its associated efficiency benefits. Nonetheless, runtime complexity was not a core focus of this investigation, and STAP [3] was frequently called during planning, increasing the overall planning time. LLMs also impose an inference bottleneck as each API query

(§5.5.2) requires 2-10 seconds, but we anticipate improvements with advances in both LLM inference techniques and in methods that distill LLM capabilities into smaller, cost-efficient models [267]. Thus, there remains opportunities to increase the plan-time efficiency of our method, for instance, by warm starting geometric feasibility planning with solutions cached in earlier planning iterations [282].

4. **Closed-world assumptions:** Our framework operates in a closed-world setting (§5.3), where we assume to know which objects are task-relevant and the poses of objects are estimated by an external perception system at the time of receiving a language instruction. Extending **Text2Motion** to open-world settings may necessitate exploring [34] or interacting [51] with the environment to discover objects that are not initially observable, and training skills to support a diverse set of real-world objects [125, 136]. This could be accomplished by integrating **Text2Motion** as part of a broader planning system, where it is used to produce feasible and verified plans to subgoals, while building knowledge of the environment in unobserved or partially observable regions during the execution of those subgoals. The use of Visual Question and Answering (VQA) [308] and multi-modal foundation models that are visually grounded [68, 202] also holds promise. Such models may support scaling **Text2Motion** to higher-dimensional observation spaces and potentially serve as a substitutes for closed-world components used in our framework (e.g. detecting a variable number of predicates using VQA).

Chapter 6

Conclusion

6.1 Summary of Contributions and Findings

Continued progress in general-purpose learned policies for robot control suggests a trajectory toward increasingly broad deployment across industrial settings and everyday human environments, where reliability is critical. This dissertation advances the perspective that deployment-time reliability is a *property* that emerges from deliberately designed, complementary mechanisms that operate *around* learned policies—reinforcing them at points of fragility and providing practical insight into their behavior to enable systematic improvement. We have examined several such mechanisms, including: (1) runtime failure detection and intervention [5], (2) data-centric interpretation of policy behavior and performance [4], and (3) composition and coordination of learned behaviors for real-world, long-horizon tasks [2, 3]—the key contributions and findings of which we summarize below.

Monitoring Policies for Runtime Failure Detection (Sentinel): In [Chapter 2](#), we studied the problem of detecting imminent deployment-time failures of learned robot policies and introduced Sentinel, a runtime monitoring framework for generative policy architectures that detected failures without requiring any failure data. The central insight was that policy failures manifested across multiple timescales—ranging from local behavioral inconsistencies to global stagnation in task progress—and were therefore best captured by a hierarchy of specialized, complementary detectors. Across both simulation and real-world experiments, Sentinel detected 18% more failures than any individual monitoring approach alone, while enabling earlier and more reliable intervention.

Understanding Policy Behavior through Training Data (CUPID): In [Chapter 3](#), we investigated the opaque relationship between closed-loop policy behavior and training data. We introduced CUPID, a data-centric interpretability framework that leveraged influence functions to estimate how individual training demonstrations affected a policy’s expected return. The key insight was that deployment-time performance could be meaningfully interpreted—and systematically improved—by attributing outcomes such as task success or failure to specific training examples,

enabling counterfactual reasoning about data quality and composition. Empirically, CUPID reliably identified the demonstrations most influential to policy performance and achieved state-of-the-art results while using less than 50% of the available training data.

Coordinating Policy Sequences for Long-Horizon Tasks (STAP): In [Chapter 4](#), we examined how individually learned behaviors often failed when composed to solve long-horizon tasks, due to unmodeled dependencies that compromise sequence feasibility. To address this, we introduced STAP, a framework that coordinated sequences of learned policies by explicitly estimating and optimizing their joint success probability at deployment time. The key insight was that this joint success probability could be captured as the product of Q-functions—models learned during policy training—whose optimization automatically resolved dependencies between behaviors. STAP significantly improved long-horizon task success in complex environments and achieved up to four orders of magnitude faster planning than baselines that relied on simulation for future prediction.

Searching for Feasible Policy Sequences from Language (Text2Motion): In [Chapter 5](#), we studied the problem of solving long-horizon manipulation tasks specified in natural language, where multiple candidate behavior sequences may satisfy the goal semantically but differ in feasibility. We introduced Text2Motion, a language-based task and motion planning framework that used LLMs to generate candidate policy sequences and feasibility-aware estimates from STAP to guide their selection. The key insight was that interleaving high-level language-guided search with low-level feasibility estimation was essential for reliably solving tasks with large combinatorial search spaces. Empirically, Text2Motion significantly outperformed prior language-based planning approaches, achieving a 69% improvement in success rate across a suite of long-horizon manipulation tasks.

Together, these contributions constitute an articulated exploration into improving the reliability of learned policies at deployment. Each addresses a distinct yet complementary challenge that inevitably arises when robot systems transition from controlled laboratory settings to the open-ended variability of the real world.

6.2 Directions for Future Work

There remain many promising avenues for future investigation. Several reflect key extensions of the methodologies developed in this dissertation—monitoring, interpreting, and coordinating policies—and are discussed in the future work sections of their respective chapters. We focus here on a set of new directions that have received comparatively less attention in the study of policy reliability.

Robotics World Models: A core challenge for policy reliability is that training-time metrics such as validation loss are often weak predictors of closed-loop performance at deployment [222] (e.g., policies with lower validation loss do not necessarily achieve higher task success on a real robot). However, directly evaluating policy behavior in closed loop is expensive and inherently unscalable [19], since finite test conditions cannot reflect the breadth of variability a policy will encounter over

its deployment lifetime. High-fidelity world models offer a promising path toward more reliable policies by enabling low-cost, closed-loop evaluation of policy behavior in imagination, reducing reliance on real-world testing [211, 263]. Furthermore, building controllable world models—as in autonomous driving research [164, 175, 185, 217, 260]—could support systematic stress-testing of policies under rare, unexpected, or safety-critical scenarios, enabling targeted robustness evaluation and policy improvement [38]. Recent work has begun exploring the integration of world models in the deployment loop to steer [287] or filter policy actions [232], while more expressive models that capture distributions over future states under partial observability could enable policies to anticipate and avoid failure modes before they occur. Given the computational cost of forward prediction, such approaches may benefit from fast-slow architectures that selectively invoke expensive look-ahead when policy uncertainty is high.

Hierarchical Policy Architectures: Hierarchical design has long played a central role in robotics, with its benefits clearly demonstrated in autonomous driving [139, 276] and task and motion planning systems [87, 132]. By stratifying decision-making and control across multiple levels of abstraction and timescales, hierarchical architectures enable coordinated, intelligent, and robust runtime behavior [192]. While earlier efforts toward general-purpose policies unified high-level reasoning and low-level control within a single model (e.g., reasoning-based VLAs [22, 300]), more recent work has gravitated toward system-1–system-2 architectures [261], which pair a slower, high-level planning policy with a fast, reactive control policy. Such architectures may offer several advantages for deployment-time reliability. First, high-capacity system-2 models can support reliability-enhancing functions such as failure monitoring [70], online correction [167], and fallback intervention [251]—capabilities that have already shown promise in handling unexpected and safety-critical scenarios [81]. Second, as discussed in [Chapter 3](#), policy failures are often difficult to diagnose and remediate; modular architectures may improve interpretability by isolating failures to specific components (e.g., planning versus control), enabling more targeted improvement. Lastly, while the approaches discussed in [Chapter 4](#) and [Chapter 5](#) employed hierarchies for sequencing single-step primitive policies, integrating more advanced, closed-loop policies such as VLAs for task and motion planning remains an open problem.

Explainability and Mechanistic Interpretability: While [Chapter 3](#) established a quantitative link between deployment-time policy behavior and the training data that influenced policy predictions, such approaches do not surface conceptual, human-interpretable insight into why a policy succeeds or fails. This limits our ability to derive actionable guidance from closed-loop evaluation data, which may be used to efficiently debug and improve policies through fine-grained data curation [4], determine what data should be collected next [303], or construct evidence-based safety cases prior to deployment. Early work on explainability has begun to characterize policy failure modes [227, 228], and initial mechanistic interpretability approaches have explored concept-based steering of policy behavior at deployment time [105]. However, these efforts only scratch the surface of the types of questions such

methods could address. Promising future work lies in identifying new reliability-critical problems that explainability and interpretability are well suited to, and in developing new ways to apply these tools to learned policies—beyond post hoc analysis or manual concept probing.

6.3 Concluding Remarks

This dissertation casts deployment as an emerging problem category in robot learning—one whose importance will grow as policy capabilities mature and robots move beyond controlled laboratory settings. We have argued that reliability is a central desideratum for learned robot policies and demonstrated that it can be systematically advanced by addressing complementary challenges arising from the uncertainty, diversity, and complexity of real-world environments. Looking ahead, emerging tools and models open promising research directions for further strengthening deployment-time reliability, moving the field toward a future of safe and trustworthy robot deployment at scale.

Appendix A

Additional Details: Sentinel

Appendix Overview: Unpacking Failure Modes of Generative Policies

The appendix offers additional details with respect to the implementation of our failure detection framework (§A.1), the experiments conducted (§A.2), along with extended results and analysis (§A.3), and finally, supporting derivations (§A.4) for our proposed failure detectors. **Qualitative results** and a **video abstract** are made available at <https://sites.google.com/stanford.edu/sentinel>.

A.1	Method Details: Sentinel	79
A.1.1	Temporal Consistency Detection with STAC	80
A.1.2	Runtime Monitoring with Vision Language Models	82
A.2	Experiment Details	86
A.2.1	Environments	86
A.2.2	Diffusion Policies	88
A.2.3	Baselines	89
A.2.4	Evaluation Protocol	94
A.3	Additional Results	96
A.3.1	Ablation Experiments on STAC	96
A.3.2	Extended Results: VLM Runtime Monitor	97
A.4	Derivations	101

A.1 Method Details: Sentinel

As shown in Fig. 2.3, the **Sentinel** runtime monitoring framework consists of the parallel operation of two complementary failure detectors, each assigned to the detection of a particular failure category

of generative policies. The first is a temporal consistency detector that monitors for erratic policy behavior via statistical temporal action consistency (STAC) measures. The second is a Vision Language Model (VLM) that monitors for failure of the policy to make progress on its task. In this section, we provide additional details *w.r.t.* the implementation of STAC (§A.1.1) and the VLM runtime monitor (§A.1.2).

A.1.1 Temporal Consistency Detection with STAC

Background To summarize §2.3, STAC assumes the use of a stochastic policy π that, at each policy-inference timestep t , predicts an action sequence for the next h timesteps as $a_{t:t+h-1|t} \sim \pi(\cdot|s_t)$, executes the first k actions $a_{t:t+k|t}$, before re-evaluating the policy at timestep $t+k$. Between two contiguous inference timesteps t and $t+k$, sampled action sequences $a_{t+k:t+h-1|t}$ and $a_{t+k:t+h-1|t+k}$ (both in $\mathbb{R}^{(h-k) \times |\mathcal{A}|}$) overlap for $h-k$ timesteps. At a high-level, STAC seeks to quantify *how much* a generative policy’s action distributions are changing over time. It does this by computing statistical distances between the distributions of overlapping actions, i.e., given $\bar{\pi}_t := \pi(a_{t+k:t+h-1|t}|s_t)$ and $\tilde{\pi}_{t+k} := \pi(a_{t+k:t+h-1|t+k}|s_{t+k})$, we compute $D(\bar{\pi}_t, \tilde{\pi}_{t+k})$.

Hypothesis Our central hypothesis is that large statistical distances correlate with downstream policy failure. Intuitively, a predictive policy can be likened to possessing an internal world model that simulates how robot actions affect environment states. When the policy is in distribution, we expect this world model to be accurate, thus resulting in smaller statistical distances. More concretely, if the policy’s internal model of state s_{t+k} at timestep t coincides with the actual observed state s_{t+k} at timestep $t+k$, the distribution of actions $\tilde{\pi}_{t+k}$ should be well-represented by the distribution $\bar{\pi}_t$. As a result, the distance $D(\bar{\pi}_t, \tilde{\pi}_{t+k})$ will be small (for the right choice of statistical distance function D). Conversely, when the policy is out of distribution (OOD), its internal model of state s_{t+k} at timestep t may be inaccurate, yielding a divergence between $\bar{\pi}_t$ and $\tilde{\pi}_{t+k}$ and a larger statistical distance.

Implementation Details As mentioned in §2.4.1, we propose to approximate $D(\bar{\pi}_t, \tilde{\pi}_{t+k})$ with an empirical distance function \hat{D} instead of computing it analytically, as doing so presents the challenge of marginalizing out both the non-overlapping actions (between timesteps t and $t+k$) and the intermediate steps of the diffusion process [255]. We found the following approximations to work well in practice:

- Maximum Mean Discrepancy (MMD) with radial basis function (RBF) kernels. We compute

$$\begin{aligned} \hat{D}(\bar{\pi}_t, \tilde{\pi}_{t+k}) &= \mathbb{E}_{a_t, a'_t \sim \bar{\pi}_t} [k(a_t, a'_t)] + \mathbb{E}_{a_{t+k}, a'_{t+k} \sim \tilde{\pi}_{t+k}} [k(a_{t+k}, a'_{t+k})] \\ &\quad - 2\mathbb{E}_{a_t \sim \bar{\pi}_t, a_{t+k} \sim \tilde{\pi}_{t+k}} [k(a_t, a_{t+k})], \quad \text{where } k(x, y; \beta_1) = \exp\left(-\frac{\|x-y\|^2}{\beta_1}\right). \end{aligned}$$

Here, $k : \mathbb{R}^{(h-k) \times |\mathcal{A}|} \times \mathbb{R}^{(h-k) \times |\mathcal{A}|} \rightarrow \mathbb{R}$ computes the similarity between two overlapping action sequences, and β_1 denotes the bandwidth of the RBF kernel. The expectations are taken over a batch of B action sequences sampled from the generative policy.

- Forward KL-divergence via Kernel Density Estimation (KDE) of the policy distributions:

$$\hat{D}(\bar{\pi}_t, \tilde{\pi}_{t+k}) = \mathbb{E}_{a_{t+k} \sim \tilde{\pi}_{t+k}} \left[\log \frac{p(a_{t+k})}{q(a_{t+k})} \right],$$

where p and q are KDEs of $\tilde{\pi}_{t+k}$ and $\bar{\pi}_t$ fit on a batch of B action sequences sampled from each policy distribution, respectively. As before, we use Gaussian RBF kernels of the form $k(x, y; \beta_2)$, where β_2 denotes the bandwidth of the RBF kernels used for KDE.

- Reverse KL-divergence via KDE of the policy distributions:

$$\hat{D}(\bar{\pi}_t, \tilde{\pi}_{t+k}) = \mathbb{E}_{a_t \sim \bar{\pi}_t} \left[\log \frac{p(a_t)}{q(a_t)} \right],$$

where p and q are KDEs of $\bar{\pi}_t$ and $\tilde{\pi}_{t+k}$ fit on a batch of B action sequences sampled from each distribution, respectively, and all other parameters follow the forward KL definitions.

Hyperparameters The batch size B , MMD bandwidth β_1 , and KDE bandwidth β_2 are hyperparameters that we select for a given environment. As expected, we found that larger batch sizes are necessary for accurate mean embeddings and density estimates in domains with higher degrees of multimodality (e.g., $B = 256$ action sequences for **PushT** and **Push Chair**). We also found that using either default settings or dynamic calibration techniques are sufficient to obtain suitable MMD and KDE bandwidth parameters β_1 and β_2 , respectively. For example, setting β_2 in proportion to the maximum eigenvalue of the covariance of overlapping actions $a_{t+k:t+h-1|}$ sampled from $\bar{\pi}_t$ and $\tilde{\pi}_{t+k}$ worked well in multimodal domains. Further details on hyperparameters are provided in [Table A.1](#).

Hyperparameters	PushT (↑ Multimodality)	Close Box & Cover Object (↓ Multimodality)	Push Chair (↑ Multimodality)
MMD + KDE batch size (B)	256	32	256
MMD bandwidth (β_1)	Median Heuristic [96, 195]	$1.0/ \mathcal{A} $	Median Heuristic
KDE bandwidth (β_2)	$\sqrt{\lambda_{\max}(\text{Cov}(a_{t+k:t+h-1 }))}$	1.0	$\sqrt{\lambda_{\max}(\text{Cov}(a_{t+k:t+h-1 }))}$
Policy action space (\mathcal{A})	Linear Velocity	2 x (Linear + Angular Velocity)	1 x (Linear + Angular Velocity)
Policy prediction horizon (h)	16	16	16
Policy execution horizon (k)	8	4	4

Table A.1: **Hyperparameters settings** for temporal consistency detection with STAC.

Additional Design Choices There are several additional settings that one could adjust to increase STAC’s detection performance on their task. First, filtering components of the policy’s action space that are either noisy or discrete can increase the quality of the statistical distance score function. For example, the policy’s action space in our robotic manipulator domains include end-effector linear

and angular velocities, as well as a binary gripper command. However, when computing statistical distances, we omit all binary gripper commands. Next, reducing the execution horizon k of the generative policy to compare action distributions that are closer in time can mitigate excessively large statistical distances in highly dynamic or stochastic environments. Likewise, comparing action distributions over a shorter prediction horizon h may be suitable if the tails of predicted action sequences e.g., exhibit high variance.

A.1.2 Runtime Monitoring with Vision Language Models

As described in §2.4.2, we formulate the detection of task progression failures as a chain-of-thought (CoT) [281], video question answering (Video QA) [293] task with VLMs. Below, we provide details on the implementation of our VLM runtime monitor and the prompt templates used in our experiments.

Vision Language Models In extended experiments (§A.3.2), we include variants of the VLM runtime monitor based on several models: OpenAI’s GPT-4o, Anthropic’s Claude 3.5 Sonnet, and Google’s Gemini 1.5 Pro [216]. At the time of writing, these represent the current state-of-the-art VLMs for complex, multimodal reasoning tasks. We use consistent prompts across all models, however, we slightly vary the implementation of the monitor to reflect the suggested best practices of each VLM.

Implementation Details We propose to query the VLM online with a parsed text prompt describing the runtime monitoring task and the history of images (i.e., a video) $I_{0:t} := (I_0, I_{\nu k}, I_{2\nu k}, \dots, I_t)$ captured by the robot’s camera system up to the current timestep t . Here, the hyperparameter ν specifies the frequency of the images relative to the execution horizon k of the generative policy (§2.3) for generality, as the video may be captured at a much higher frame rate than the policy’s execution rate. In experiments, simply setting $\nu \in \{1, 2\}$ provided sufficient granularity for the VLM to identify the motion of the robot.

By making non-blocking API calls, the VLM runtime monitor can operate at relatively high frequencies. For example, the VLM can be queried at each policy-inference timestep $t = jk$ for $j \in \{0, 1, \dots\}$ (i.e., at STAC’s detection frequency) to provide a failure classification. However, depending on the task, doing so may neither be necessary nor desirable for two reasons. First, because task progression failures are likely to occur at longer timescales than erratic failures, querying the VLM at a reduced frequency might provide time for meaningful changes in state to occur. In turn, this would reduce redundancy in the VLM’s predictions e.g., if no meaningful changes in state occurred since the last time it was queried. Second, while STAC—a statistical output monitor—can be evaluated at negligible cost (computationally and monetarily), querying state-of-the-art, closed-source VLMs may come with considerable expense. Since task progression failures are unlikely to require immediate intervention (in contrast to erratic failures), querying the VLM less often than STAC

could be preferable. In experiments, we queried the VLM to detect task progression failures twice per episode.

The prompt template consists of three parts: 1) a brief description of the VLM’s role as the runtime monitor of a robotic manipulator system, which it must execute by analyzing the attached video; 2) a description of the robot’s task, the total amount of time that has elapsed¹, and time limit for the task (corresponding to the MDP horizon H in §2.3); 3) instructions to elicit a CoT response, ensuring that the VLM describes and analyzes the motion of the robot and all task-relevant objects and outputs a classification that can be easily parsed. To remove ambiguity over the expected behavior of the robot and what constitutes task completion, we make sure that the task description is sufficiently detailed:

```
task_descriptions:
  cover: "hide the white box by covering it with the black blanket. The white box is located
    somewhere in front of the two robot arms and does not move. The black blanket starts directly
    in between the two robot arms"
  close: "close the white box by folding in the two smaller white side lids and the bigger white back
    lid. The white box is located in between the two robot arms and does not move. The robots
    should concurrently approach the side lids and push both side lids up, followed by approaching
    the back lid and folding up the back lid with both arms, without grasping the lids with the
    grippers"
  push_chair: "push the black chair into the circular table. The black chair starts directly in front
    of the robot. The robot should push black chair in a relatively straight line, without the
    chair rotating to the left or to the right, so that the seat of the chair is properly tucked
    under the circular table"
```

We elicit a four-step CoT response from the VLM that 1) generates a set of task-relevant questions whose correct answers would fully characterize the motion of the robot and all task-relevant objects in the video, 2) answers the task-relevant questions while providing fine-grained visual details, 3) analyzes the questions, answers, and elapsed time to identify whether the robot is making progress towards task completion within the episode time limit, and 4) concludes with an overall classification in {ok, failure}. Interestingly, we found that prompting the VLM to generate its own questions instead of manually specifying them leads to more accurate descriptions of the video and ensuing predictions.

Prompt Template (Video QA)

¹Online runtime monitoring requires the VLM to differentiate whether a) the robot is still in progress of executing the task correctly (i.e., partial progress) or whether b) the robot will fail to complete the task (e.g., by stalling in a partially completed state). Differentiating between partial progress and task failure can be ambiguous for a slow moving robot, and thus, providing the VLM with the current elapsed time serves as a reference to gauge whether or not the rate at which the robot is executing the task will result in a timely task completion.

You are the runtime monitor for an autonomous mobile manipulator robot capable of solving common household tasks. A camera system captures a series of image frames (i.e., a video) of the robot executing its current task online. The image frames are captured at approximately 1Hz. As a runtime monitor, your job is to analyze the video and identify whether the robot is a) in progress of executing the task or b) failing to execute the task, for example, by acting incorrectly or unsafely.

The robot's current task is to {DESCRIPTION}. The robot may take up to {TIME_LIMIT} seconds to complete this task. The current elapsed time is {TIME} seconds.

Format your output in the following form:

[start of output]

Questions: First, generate a set of task-relevant questions that will enable you to understand the full, detailed motion of the robot and all task-relevant objects from the beginning to the end of the accompanying video.

Answers: Second, precisely answer the generated questions, providing fine-grained visual details that will help you accurately assess the current state of progress on the task.

Analysis: Assess whether the robot is clearly failing at the task. Since the video only represents the robot's progress up to the current timestep and the robot moves slowly, refrain from making a failure classification unless the robot is unlikely to complete the task in the allotted time. Explicitly note the amount of time that has passed in seconds and compare it with the time limit (e.g., x out of {TIME_LIMIT} seconds). Finally, based on the questions, answers, analysis, and elapsed time, decide whether the robot is in progress, or whether the robot will fail to complete its task in the remaining time (if any).

Overall assessment: {CHOICE: [ok, failure]}

[end of output]

Rules:

1. If you see phrases like {CHOICE: [choice1, choice2]}, it means you should replace the entire phrase with one of the choices listed. For example, replace the entire phrase '{CHOICE: [A, B]}' with 'B' when choosing option B. Do NOT enclose your choice in '{' '}' brackets. If you are not sure about the value, just use your best judgement.
2. Do NOT forget to conclude your analysis with an overall assessment. As indicated above with '{CHOICE: [ok, failure]}', your only options for the overall assessment are 'ok' or 'failure'.
3. Always start the output with [start of output] and end the output with [end of output].

Prompt Ensembling

The Video QA failure detection task requires comprehensive and detailed reasoning of over potentially long sequences of images, which, at the time of writing, is a challenge for even the most capable VLMs. As such, we can expect the performance of the VLM runtime monitor to degrade when it is deployed in domains that are visually OOD *w.r.t.* the VLM's training data (e.g., images rendered in simulation or captured from unusual camera poses). In these settings, the VLM runtime monitor may

provide a reasonable but imperfect signal on task progression failures, resulting in misclassifications.

To strengthen the reliability of our VLM runtime monitor, we propose a simple prompt ensembling strategy [209], whereby we construct multiple Video QA prompts, query the VLM with each prompt, and take the overall failure classification to be the *majority vote* of the predictions across all prompts. Intuitively, if the failure detectors associated with each individual prompt are fairly accurate to begin with, the resulting majority-vote detector will have an even higher probability of correctness.

In experiments, we only found it necessary to use prompt ensembling in the **Cover Object** domain. We construct two variants of the Video QA prompt (3 prompts total), each of which follow a similar CoT structure while including additional information to diversify the VLM’s reasoning. The first prompt variant, **Video QA + Success Video**, includes a video of a successful policy rollout for the current task. This allows the VLM to distinguish off-nominal policy behavior at test time from nominal policy behavior illustrated in the example video. The second prompt variant, **Video QA + Goal Images**, includes example images of the scene at the end of successful policy rollouts, which serve as a visual reference for task completion. In accordance with the assumptions of our framework, these prompt variants only require data associated with policy success to detect unknown failures at test time.

Prompt Template (Video QA + Success Video)

```
You are the runtime monitor... # Same as Video QA
```

```
To inform your analysis, you will be provided with an example video that shows the full motion of the robot and all task-relevant objects when the task is successfully executed. For example, the last image frame in the example video will show what the scene should look like at the end of a successfully executed task. By comparing the current video with the example video, you may be able to visually distinguish when the robot is failing at the task versus when it is making steady progress or has completed.
```

```
The robot’s current task is... # Same as Video QA
```

```
Questions: First, generate a set of task-relevant questions that will enable you to understand the full, detailed motion of the robot and all task-relevant objects from the beginning to the end of the accompanying video. In addition, generate questions that will enable you to identify any key similarities or differences between the current video and the example success video.
```

```
Answers: Second, precisely answer... # Same as Video QA
```

Prompt Template (Video QA + Goal Images)

You are the runtime monitor... # Same as Video QA

To inform your analysis, you will be provided with several example images that show what the scene (i. e., the robot and all task-relevant objects) should look like at the end of a successfully executed task. By comparing the last few image frames of the current video with these example images, you may be able to visually distinguish when the robot is failing at the task versus when it is making steady progress or has completed.

The robot’s current task is... # Same as Video QA

Questions: First, generate a set of task-relevant questions that will enable you to understand the full, detailed motion of the robot and all task-relevant objects from the beginning to the end of the accompanying video. In addition, generate questions that will enable you to identify any key similarities or differences between the current video and the example images of successfully completed tasks.

Answers: Second, precisely answer... # Same as Video QA

A.2 Experiment Details

A.2.1 Environments

We provide additional details on the environments used to evaluate Sentinel. These environments vary in terms of their data distribution (e.g., multimodal or high-dimensional actions) and support different types of distribution shift (e.g., object scale, pose, dynamics), under which the behavior of generative diffusion policies can be methodically studied. The environments are visualized in [Fig. A.1](#).

Simulation Domains

PushT Domain The policy is tasked with pushing a planar “T”-shaped object into a goal configuration. A trajectory is considered successful if the overlap between the “T”-shaped object and its goal exceeds 90% within 300 environment steps. The action space is the 2-DoF linear velocity of the end-effector. We generate OOD test scenarios by non-uniformly randomizing the scale and dimensions of the “T”-shaped object beyond the randomizations contained in the policy’s demonstration data. The policy tends to fail by converging to a locally optimal configuration, where the “T” overlaps with its goal but in an incorrect orientation. Since the task can be solved in a number of ways, we include this domain to evaluate the performance of various score functions in the presence of action multimodality. We refer to [40] for the process of generating demonstration data in this domain.

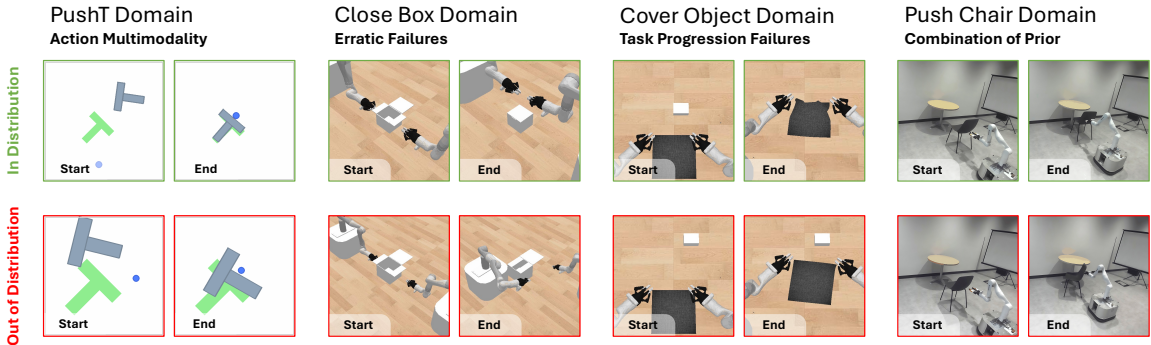


Figure A.1: **Evaluation Domains.** We evaluate our failure detection framework across three simulation domains and one real-world domain. These domains provide coverage over different data distributions (e.g., action multimodality, high-dimensional actions) and modes of generative policy failure. For example, generative policies tend to fail erratically in the **Close Box** domain, but smoothly in the **Cover Object** domain. An effective failure detector should be performant across multiple domains, which entails coverage over heterogeneous failure modes.

Close Box Domain The policy is tasked with closing a box that has three lids. A trajectory is considered successful if all three lids are closed within 120 environment steps (24 seconds). The action space is the 14-DoF linear + angular velocities and gripper commands for the end-effectors of two mobile manipulators. Demonstration data is generated by an oracle policy that sets a series of waypoints for the end-effectors based on the initial state. We generate OOD test scenarios by non-uniformly randomizing the scale of the box beyond the randomizations contained in the policy’s demonstration data. The policy tends to fail erratically when the robots e.g., collide with the box or its lids, however, task progression failures may also occur. This domain is primarily used to evaluate the detection of erratic policy failures on a bi-manual robotic system with a high-dimensional action space.

Cover Object Domain The policy is tasked with covering a rigid object with a cloth. A trajectory is considered successful if over 75% of the object is covered by the cloth within 64 environment steps (13 seconds). The action space and process of generating demonstration data is identical to that of **Close Box**. We generate OOD test scenarios by non-uniformly randomizing the position of the object beyond the randomizations contained in the policy’s demonstration data. The policy tends to fail by releasing the cover before reaching the object. Hence, this domain is used to evaluate the detection of task progression failures, where reasoning over longer durations is required to assess task progress.

Real-World Domains

Mobile Robot Setup We use a holonomic mobile base equipped with a Kinova Gen3 7-DoF arm. A single ZED 2 camera is fixed in the workspace to capture visual observations for the generative policy. The ZED 2 camera first generates a partial-view point cloud of the environment, from which we segment task-relevant objects using the Grounded Segment Anything Model [219] based on a natural language description related to the task. The segmented point cloud serves as the visual input to the policy. Additionally, we use a motion capture system to track the pose of the mobile base. During evaluation, the policy processes the point clouds, predicts a sequence of 16 actions, of which the first 4 are executed on the robot. The mobile manipulator robot then maneuvers its arm according to these commands, adjusting the pose of the base if the end-effector moves outside a pre-defined workspace.

Push Chair Domain The policy is tasked with tucking a chair into a table using a single-arm mobile manipulation platform. A trajectory is considered successful if the seat of the chair is properly tucked under the table by the end of the policy rollout. The action space is the 7-DoF linear + angular velocities and gripper command for the end-effector of the mobile manipulator robot. Demonstration data is extracted from human videos: we use an off-the-shelf hand detection model [207], an object segmentation model [39, 219], and a stereo-to-depth model to extract human hand poses and object point clouds from a subsampled set of frames in each of the 15 human demonstration videos. We generate OOD test scenarios by randomizing the initial pose of the chair beyond the randomizations contained in the demonstration data. The policy tends to fail erratically if the chair rotates away in either direction when pushed, but such failures are also visually apparent. Therefore, this task is used to test the efficacy of both STAC and the VLM runtime monitor in a dynamically complex [226], real-world setting.

A.2.2 Diffusion Policies

We train a diffusion policy (DP) for each environment, using 200 demonstrations for the **PushT** domain, 50 demonstrations for each of the **Close Box** and **Cover Object** domains, and 15 demonstrations for the real-world **Push Chair** domain. In a DP, actions are generated by iteratively denoising an initially random action $a_t^N \sim \mathcal{N}(0, 1)$ over N steps as a_t^N, \dots, a_t^0 , where a_t^i with a superscript i denotes the generated action sequence at the i -th denoising iteration. In an imitation learning setting, the DP’s noise prediction network ϵ_θ is trained to predict the random noise ϵ^i added to actions drawn from a dataset of expert demonstrations $\mathcal{D}_{\text{train}}$ by minimizing

$$\mathcal{L}_{\text{ddpm}} := \mathbb{E}_{(s, a^0) \sim \mathcal{D}_{\text{train}}, \epsilon^i, i} [\|\epsilon^i - \epsilon_\theta(\sqrt{\bar{\alpha}_i} a^0 + \sqrt{1 - \bar{\alpha}_i} \epsilon^i, s, i)\|^2], \quad (\text{A.1})$$

where the constants $\bar{\alpha}_i$ depend on the chosen noise schedule of the diffusion process.

To increase the salience of distribution shift *w.r.t.* the position and scale of objects, we use point clouds as inputs to the policy instead of RGB images (i.e., a 5% increase in object scale may not be salient in an image). For simulation experiments, we use a diffusion policy architecture identical to the original paper [40] except for the visual encoder, where we substitute the ResNet-based encoder for a PointNet-based one: a 4-layer PointNet++ encoder [210] with hidden dimension 128. The output of this encoder is concatenated with the proprioceptive inputs and then fed to the noise prediction network. For real-world experiments, we use the recently proposed EquiBot diffusion policy architecture [296], which additionally incorporates SIM(3) equivariance into the diffusion process. We use EquiBot to evaluate our failure detectors on a current state-of-the-art approach for learning generative policies in the real world. All diffusion policies produce an action over $N = 100$ denoising iterations. Unless otherwise specified, we use standard settings for the prediction h and execution horizon k of the diffusion policy.

A.2.3 Baselines

We outline the implementation details of our baselines as introduced in §2.5. First, with the exception of the VLM runtime monitors, all evaluated failure detection methods consist of computing a score $S(\cdot)$ at each policy-inference timestep in a rollout, taking the cumulative sum of scores up to the current timestep t , and then checking if the cumulative sum exceeds a calibrated threshold to detect policy failure. As such, the baselines differ in their *score function*, i.e., how they compute the per-timestep scores that are then summed and thresholded. Intuitively, a good score function should be well-correlated with policy failure, that is, it should output small values when the policy is succeeding and large ones when it is failing. For example, Fig. 2.4 demonstrates that STAC holds this property. We baseline against an extensive suite of score functions, some of which we newly introduce for the case of generative diffusion policies, and others that are common in the OOD detection literature [250].

STAC Baselines (Policy-Level Monitors)

- **Policy Encoder Embedding** quantifies the dissimilarity of the current point cloud observation o_t *w.r.t.* to the point clouds in the calibration dataset of M successful policy rollouts $\mathcal{D}_\tau = \{\tau^i\}_{i=1}^M$ (as described in §2.3) within the embedding space of the policy’s encoder (here, o_t denotes the point cloud input to the policy, which includes the point cloud at the current and previous timestep). More concretely, let E be the policy’s encoder, $z_t = E(o_t)$ be the current point cloud embedding, and $\mathcal{D}_z = E(\mathcal{D}_\tau)$ be the embeddings of all point clouds contained in the calibration dataset. We compute the per-timestep score as the Mahalanobis distance

$$S(z_t; \mathcal{D}_z) = \sqrt{(z_t - \mu_z)^T \Sigma_{zz}^{-1} (z_t - \mu_z)}, \quad (\text{A.2})$$

where μ_z is the mean and Σ_{zz} is the covariance of the embeddings in \mathcal{D}_z . At test time, we raise a failure warning if the cumulative score η_t exceeds a calibrated detection threshold γ

$$\eta_t > \gamma, \quad \text{where} \quad \eta_t = \sum_{i=0}^{j-1} S(z_i; \mathcal{D}_z), \quad t = jk.$$

Here, γ is set to the $1 - \delta$ quantile of cumulative scores computed over the calibration trajectories $\{\eta_{|\tau^i|}^i\}_{i=1}^M$, where $\tau^i \in \mathcal{D}_\tau$. Importantly, when computing the calibration scores η^i , we do so in a *leave-trajectory-out* fashion: i.e., for a point cloud $o_t \in \tau^i$ where $\tau^i \in \mathcal{D}_\tau$, we compute the per-timestep score as $S(E(o_t); E(\mathcal{D}_\tau \setminus \tau^i))$. This ensures that the dissimilarity of observation o_t is computed *w.r.t.* trajectories other than its own, which a) aligns with how scores are computed at test time and b) ensures that calibration scores are not trivially low.

We experimented with alternatives to the Mahalanobis distance in Eq. A.2, substituting it with top- k scoring for $k \in \{1, 5, 10\}$ based on cosine similarity and L2 distance metrics. However, we found the Mahalanobis distance to be the most stable. We also evaluated variants of this baseline that compute the dissimilarity of the full policy state s_t (including both the point cloud embedding and the robots’ end-effector poses), but found equivalent performance.

- **CLIP Pretrained Embedding** quantifies the dissimilarity of the current image observation I_t *w.r.t.* to the images in the calibration dataset $\mathcal{D}_\tau = \{\tau^i\}_{i=1}^M$ within the embedding space of a pretrained CLIP encoder [213]. The score function (Eq. A.2) and calibration process are identical to those of **Policy Encoder Embedding**. Importantly, the encoder used here is trained with a representation learning objective, which results in a structured embedding space and more interpretable embedding similarity scores. In our experiments, we use the open-source clip-vit-base-patch32 version of CLIP without any fine-tuning.
- **ResNet Pretrained Embedding** is identical to **CLIP Pretrained Embedding**, except it quantifies image-space dissimilarity using embeddings from a ResNet18 pretrained model [106].
- **Temporal Non-Distributional Minimum** is similar to STAC (§A.1.1) in that it seeks to compute a consistency score between overlapping actions $a_{t+k:t+h-1|t}$ and $a_{t+k:t+h-1|t+k}$ sampled from the generative policy at contiguous policy-inference timesteps t and $t+k$, respectively. However, it does so by using a non-statistical distance function. In particular, this baseline computes the per-timestep temporal consistency score at timestep $t+k$ as

$$S(s_{t+k}) = \min_{b \in \{1..B\}} \left\| a_{t+k:t+h-1|t} - a_{t+k:t+h-1|t+k}^b \right\|,$$

where $a_{t+k:t+h-1|t+k}^b \sim \tilde{\pi}_{t+k}(\cdot | s_{t+k})$. That is, we sample a batch of B action sequences at timestep $t+k$, compute their L2 distances *w.r.t.* the overlapping actions of the previously executed action sequence $a_{t+k:t+h-1|t}$, and return the L2 distance associated with the most

similar action sequence. Intuitively, this baseline attempts to find the closest action sequence at timestep $t + k$ to the previously executed action sequence, while STAC attempts to quantify how well the action distribution $\tilde{\pi}_{t+k}$ at timestep $t + k$ is represented in the distribution $\bar{\pi}_t$ at timestep t . The values of B are provided in [Table A.1](#). The calibration and runtime procedures of this baseline are identical to those of STAC ([§2.4.1](#)).

- **Diffusion Reconstruction** adapts the diffusion-based OOD detection approach of Graham et al. [94] for the case of diffusion policies. Specifically, this baseline computes the reconstruction error on re-noised action sequences sampled from the diffusion policy as

$$S(s_t) = \mathbb{E}_{a^0 \sim \pi(\cdot | s_t), \epsilon^i, i} \left[\left\| a^0 - \epsilon_\theta^{i:0} (\sqrt{\bar{\alpha}_i} a^0 + \sqrt{1 - \bar{\alpha}_i} \epsilon^i, s_t) \right\|^2 \right], \quad (\text{A.3})$$

where $\epsilon_\theta^{i:0}$ denotes the reverse diffusion process from the i -th denoising iteration to the 0-th iteration, resulting in the reconstructed action. We approximate the expectation in [Eq. A.3](#) over a batch of $B = 256$ action sequences sampled from the diffusion policy, each re-noised for $i \in \{5, 10, 25, 50\}$ forward diffusion steps (also referred to as *reconstruction depths*). We experimented with several sets of reconstruction depths and found comparable performance. We note that this baseline comes with significant computational expense as it needs to perform the denoising process multiple times: i.e., if we would like to compute R reconstructions, this baseline is approximately R times more expensive than a single reverse diffusion process. The calibration and runtime procedures of this baseline are identical to those of STAC ([§2.4.1](#)).

- **Temporal Diffusion Reconstruction** is a temporal variant of **Diffusion Reconstruction** that also computes the reconstruction error on re-noised action sequences sampled from the diffusion policy, but reconstructs the action sequences conditioned on the previous state s_t as

$$S(s_t, s_{t+k}) = \mathbb{E}_{a_{t+k:t+h-1|t+k}^0 \sim \tilde{\pi}_{t+k}, \epsilon^i, i} \left[\left\| \hat{a}^0 - \epsilon_\theta^{i:0} (\sqrt{\bar{\alpha}_i} \hat{a}^0 + \sqrt{1 - \bar{\alpha}_i} \epsilon^i, s_t) \right\|^2 \right].$$

Here, \hat{a}^0 denotes the action sequence over which reconstructions are computed, concatenating the first k (executed) actions sampled at timestep t with following $h - k$ (predicted) actions sampled at timestep $t + k$: that is, $\hat{a}^0 = a_{t:t+k|t} \oplus a_{t+k:t+h-1|t+k}^0$. This step is necessary to ensure that the denoising process conditioned on s_t only considers actions within the policy’s prediction horizon. This baseline represents an alternative form of temporal consistency. Intuitively, it asks whether action sequences sampled at timestep $t + k$ would also be sampled at timestep t , to which the answer is likely yes if the policy is in distribution, and likely no if the policy is OOD—because the marginal distributions conditioned on s_t versus s_{t+k} may be different. The hyperparameters of this baseline follow those of **Diffusion Reconstruction**.

- **DDPM Loss** computes the empirical DDPM loss on re-noised action sequences sampled from

the diffusion policy as

$$S(s_t) = \mathbb{E}_{a^0 \sim \pi(\cdot | s_t), \epsilon^i, i} \left[\left\| \epsilon^i - \epsilon_\theta(\sqrt{\bar{\alpha}_i} a^0 + \sqrt{1 - \bar{\alpha}_i} \epsilon^i, s_t, i) \right\|^2 \right].$$

Here, the expectation is taken over a batch of $B = 256$ sampled action sequences and 10 sampled denoising iterations $i \sim \mathcal{U}[0, N)$, where N is the total number of denoising iterations (§A.2.2). We can think of this baseline as a more efficient version of **Diffusion Reconstruction**, since it directly quantifies the diffusion policy’s performance on its training task without the need to reconstruct actions over numerous denoising iterations. The calibration and runtime procedures of this baseline are identical to those of STAC (§2.4.1).

- **Temporal DDPM Loss** is a temporal variant of **DDPM Loss** that also computes the empirical DDPM loss on re-noised action sequences sampled from the diffusion policy, but does so conditioned on the previous state s_t as

$$S(s_t, s_{t+k}) = \mathbb{E}_{a_{t+k:t+h-1|t+k}^0 \sim \tilde{\pi}_{t+k}, \epsilon^i, i} \left[\left\| \epsilon^i - \epsilon_\theta(\sqrt{\bar{\alpha}_i} \hat{a}^0 + \sqrt{1 - \bar{\alpha}_i} \epsilon^i, s_t, i) \right\|^2 \right],$$

where $\hat{a}^0 = a_{t:t+k|t} \oplus a_{t+k:t+h-1|t+k}^0$ (as defined in **Temporal Diffusion Reconstruction**). The hyperparameters of this baseline follow those of **DDPM Loss**, over which it is expected to offer advantages via temporal consistency.

- **Diffusion Output Variance** computes the variance over B action sequences sampled from the diffusion policy and thresholds it *w.r.t.* the $1 - \delta$ quantile of sample variances computed over the calibration dataset \mathcal{D}_τ . This baseline reflects an alternative output metric to temporal consistency that can be monitored to detect policy failure. While computing output variances might bear resemblance to ensemble methods [154], we note that this approach does not quantify epistemic model uncertainty. Doing so would require training multiple diffusion policies and performing inference with each at test time, which we avoid due to computational expense. The hyperparameters of this baseline are identical to those of STAC (see Table A.1).

Discussion on Baselines First, we highlight that the embedding-based approaches predict failure solely based on the dissimilarity or atypicality of the current state. Hence, these baselines are not *policy aware*: they may raise failure warnings for states that are dissimilar from those contained in the calibration dataset \mathcal{D}_τ without understanding how the policy behaves in those states. In some cases, the policy may still succeed or generalize to minor distribution shifts in state, causing the detection performance of these baselines to significantly diminish. The reconstruction-based approaches may account for the generalization characteristics of the policy but come with computational expense, which may prohibit their use in real-time settings. The DDPM loss approaches present the next best alternative to STAC, as their score functions coincide with the diffusion policy’s training task and

can be computed at negligible computational cost. However, we note that the DDPM loss baseline is specific to diffusion policies, whereas STAC is agnostic to the generative policy formulation.

VLM Baselines (Task-Level Monitors)

As described in §2.4.2, we propose to monitor the task progress of a generative policy by zero-shot prompting a VLM to analyze a video of the robot’s execution up to the current timestep. We contrast the performance of our Video QA approach with a variation, Image QA, that queries the VLM using only I_t , the image recorded at the current timestep t , rather than the full video $I_{0:t}$. This baseline is used to evaluate the importance of video-based reasoning compared to single images. We construct the Image QA prompt by minimally modifying the Video QA prompt (§A.1.2) as shown below:

Prompt Template (Image QA)

You are the runtime monitor for an autonomous mobile manipulator robot capable of solving common household tasks. A camera system captures image frames (at approximately 1Hz) of the robot executing its current task online. As a runtime monitor, your job is to analyze the most recent image frame and identify whether the robot is a) in progress of executing the task or b) failing to execute the task, for example, by acting incorrectly or unsafely.

The robot’s current task is to {DESCRIPTION}. The robot may take up to {TIME_LIMIT} seconds to complete this task. The current elapsed time is {TIME} seconds.

Format your output in the following form:

[start of output]

Questions: First, generate a set of task-relevant questions that will enable you to thoroughly analyze the image frame and identify what actions the robot has taken so far.

Answers: Second, precisely answer the generated questions, providing fine-grained visual details that will help you accurately assess the current state of progress on the task.

Analysis: Assess whether the robot is clearly failing at the task. Since the image frame only represents the robot’s progress up to the current timestep and the robot moves slowly, refrain from making a failure classification unless the robot takes unsafe actions or is unlikely to complete the task in the allotted time. Explicitly note the amount of time that has passed in seconds and compare it with the time limit (e.g., x out of {TIME_LIMIT} seconds). Finally, based on the questions, answers, analysis, and elapsed time, decide whether the robot is in progress, or whether the robot will fail to complete its task in the remaining time (if any).

Overall assessment: {CHOICE: [ok, failure]}

[end of output]

Rules:

1. If you see phrases like {CHOICE: [choice1, choice2]}, it means you should replace the entire phrase with one of the choices listed. For example, replace the entire phrase '{CHOICE: [A, B]}' with 'B' when choosing option B. Do NOT enclose your choice in '{' '}' brackets. If you are not sure about the value, just use your best judgement.

2. Do NOT forget to conclude your analysis with an overall assessment. As indicated above with '{CHOICE: [ok, failure]}', your only options for the overall assessment are 'ok' or 'failure'.
3. Always start the output with [start of output] and end the output with [end of output].

A.2.4 Evaluation Protocol

Definition: Policy Failure

Consider a policy $\pi(a|s)$ that operates within a finite-horizon Markov Decision Process (MDP): a 5-tuple $\langle \mathcal{S}, \mathcal{A}, T, R, H \rangle$, where \mathcal{S} and \mathcal{A} are the state and action spaces, $T(s'|s, a)$ is the transition model, $R(s, a, s')$ is the reward model, and H is the MDP horizon. Given an initial state s_0 representative of a new test scenario, executing the policy for t timesteps produces a trajectory $\tau_t = (s_0, a_0, \dots, s_t)$. The trajectory’s *return* is defined as the cumulative sum of rewards: $R(\tau_t) = \sum_{t'=0}^{t-1} R(s_{t'}, a_{t'}, s_{t'+1})$.

We define **policy failure** simply in terms of task completion. More formally, given a defined success threshold R_τ , the policy fails if the return on its trajectory τ_t does not exceed the success threshold within the MDP horizon: $R(\tau_t) < R_\tau$ where $t \geq H$. In the simplest case, the success threshold R_τ equals 1, and the reward model $R(s, a, s')$ equals 1 *iff* the task is complete at state s' . For example, if the robot is tasked with picking up a cup and receives a reward of 1 only once the cup is firmly grasped. In experiments, we adhere to this definition of policy failure and threshold trajectory returns as $R(\tau_H) < R_\tau$ to compute ground-truth labels for whether or not a policy failed in a trajectory τ_H .

Relation to failure detection: In §2.3, we provide a definition of the failure detection task—to detect whether a trajectory τ_H constitutes a policy failure at the earliest possible timestep t —that is different from detecting the specific timestep at which (or before) the policy “fails.” Doing so removes the need to manually specify task-specific failure criteria required to e.g., label each timestep in a trajectory. While the goal of our failure detectors is thus to flag failure episodes, it is still beneficial to catch failures at the earliest possible timestep, which is why a) our above definition of policy failure is formulated in terms of a partial trajectory τ_t up to the current timestep $t \leq H$ of the MDP, b) we propose an online detection scheme that monitors for failure at each timestep t based on the trajectory up to the current timestep (i.e., $f(\tau_t) \rightarrow \{\text{ok}, \text{failure}\}$), and c) we report the detection time as a performance metric.

Constructing the Calibration Dataset

Calibrating STAC and its baselines requires a small dataset of successful policy rollouts $\mathcal{D}_\tau = \{\tau^i\}_{i=1}^M$, which provide grounding on the nominal, in-distribution behavior of the policy. This allows us to evaluate the test-time behavior of a potentially failing policy *w.r.t.* its known nominal behavior.

Calibration Data Quality We found it important to ensure the quality of trajectories $\tau^i \in \mathcal{D}_\tau$. Specifically, trajectories in which the policy succeeds but in an undesired or unacceptable manner

should not be used for calibration. For example, the policy may solve the **Close Box** task (Fig. A.1) but damage the lids of the box in the process. Including such a trajectory in the calibration dataset would define this behavior as *nominal* and degrade the sensitivity of the detectors at test time. Returning to our example, the detectors may not raise a failure warning if the policy damages a box at test time.

Collecting the Calibration Dataset In practice, such a calibration dataset could be collected during a policy validation phase prior to deployment. For instance, we collect $M = 50$ successful policy rollouts for each simulation domain, manually filtering episodes where the policy succeeded with unacceptable behavior (e.g., with jitter). We hypothesize that the performance of the detectors *w.r.t.* the number of rollouts M is task specific. For example, a smaller calibration dataset may be sufficient for tasks with low variability (i.e., in a single, structured environment), while a larger dataset may be necessary if the policy is to be deployed at scale. We note, however, that increasing the calibration dataset size may be desirable to achieve stronger conformal guarantees on the detector’s FPR (as derived in §A.4).

Calibrating on Demonstration Data Finally, in attempt to eliminate the need to collect an additional calibration dataset of successful policy rollouts, we experimented with variants of STAC that directly calibrated on trajectories contained in the policy’s demonstration dataset. However, doing so led to a significant increase in the detector’s FPR. We attribute this to the well-known covariate shift problem for imitation learned policies [221, 222]. That is, their prediction error increases quadratically on states induced under the policy, causing the detectors’ to mistake successful test-time rollouts for failures.

Testing and Evaluation

Instead of evaluating the failure detectors online (i.e., during policy rollouts), we collect several test datasets of policy rollouts, which consist of both successes and failures. Each trajectory is labeled either success or failure by thresholding the return at the final state of the episode (as detailed in §A.2.4). We then perform offline evaluation of the failure detectors by invoking them at each timestep of the trajectory, which allows us to identify the first timestep at which the detectors issue a warning.

Reported Metrics

We expand on the metrics outlined in §2.3. We first define a *positive* as a trajectory where the policy fails and a *negative* as a trajectory where the policy succeeds. A true positive is counted if the failure detector raises a warning at any timestep in a trajectory where the policy fails. A true negative is counted if the failure detector never raises a warning in a trajectory where the policy succeeds. The

definitions for false positive and false negative follow accordingly. Detection time is defined as the earliest timestep in which the failure detector raises a warning in a trajectory where the policy fails.

In our experiments, we report true positive rate (TPR), true negative rate (TNR), false positive rate (FPR), detection time (DT), accuracy, and balanced accuracy. TPR measures the number of true positives (detected failures) over total number of positives (failures). TNR measures the number of true negatives (detected successes) over total number of negatives (successes). FPR measures the number of false positives (false alarms) over the total number of negatives (successes). Accuracy and balanced accuracy account for both the TPR and TNR of the detector. However, we report balanced accuracy when the test set contains a non-negligible imbalance of positive and negative trajectories.

A.3 Additional Results

A.3.1 Ablation Experiments on STAC

Does STAC’s performance depend on the policy’s prediction and execution horizon?

We conduct an ablation study on the **PushT** domain to test how the performance of STAC varies with respect to the prediction horizon h and execution horizon k of the diffusion policy. Together, the prediction and execution horizons determine the number of temporally overlapping action components (i.e., between $a_{t+k:t+h-1|t}$ and $a_{t+k:t+h-1|t+k}$) that are statistically compared by STAC, while the execution horizon governs how far apart in time the action distributions $\bar{\pi}_t$ and $\tilde{\pi}_{t+k}$ are generated.

The result is shown in Fig. A.2. We find that STAC (MMD) performs comparatively across execution horizons of $k = 4$ and $k = 8$, but performs best with the standard diffusion policy settings of $k = 8$ and $h = 16$ (used for the main result in Fig. 2.5). The detector’s performance drops when using the smallest execution horizon of $k = 2$. We attribute this to the relatively small amount of environment change that occurs within two execution steps, which causes $\bar{\pi}_t$ and $\tilde{\pi}_{t+k}$ to be similarly distributed and leads to overly conservative statistical distances. This is reflected in our results, where the detectors attain $> 95\%$ TNRs across various execution horizons, but using $k = 2$ leads to a significant drop in TPR to 61%, while $k = 4$ and $k = 8$ attain TPRs of 78% and 95%, respectively.

To further ablate the choice of policy prediction horizon, we conduct a similar study on the simulated **Close Box** and real-world **Push Chair** domains. The result is shown in Table A.2, where we find that STAC is quite robust to the choice of prediction horizon, while the best result is achieved by using the standard setting of $h = 16$.

Overall, STAC’s performance may vary with the policy’s execution horizon, but is relatively stable

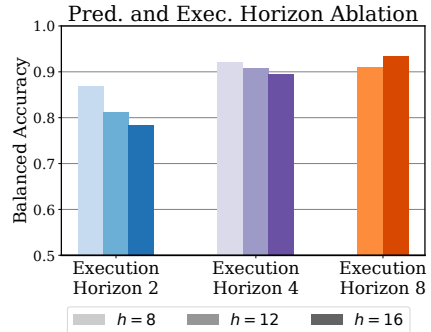


Figure A.2: Performance variation of STAC subject to different policy prediction and execution horizons in **PushT**.

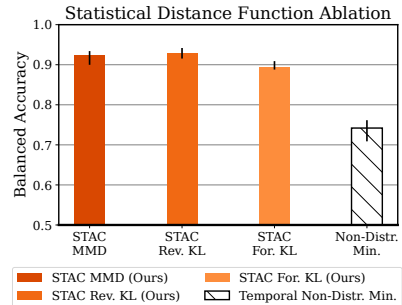
	Domain	Pred. Horizon (h)	TPR \uparrow	TNR \uparrow	Accuracy \uparrow
Sim.	Close Box	8	0.92	0.94	0.93
	Close Box	12	0.88	1.00	0.93
	Close Box	16	0.96	1.00	0.98
Real	Push Chair	8	1.00	0.80	0.90
	Push Chair	12	0.80	0.80	0.80
	Push Chair	16	0.80	0.90	0.85

Table A.2: STAC ablation on policy prediction horizon h .

across choices of the policy’s prediction horizon. The fact that we calibrate STAC and deploy it with the same prediction horizon may normalize the influence of this parameter at test time.

How does STAC’s performance vary with the choice of statistical distance function?

Fig. A.3 ablates STAC’s performance across various choices of statistical distance functions in the **PushT** domain. Here, we find that STAC performs comparably across common choices like maximum mean discrepancy (MMD) with RBF kernels and KL-divergence via kernel density estimation (details in §A.1.1). This finding is corroborated in Table A.3, where all variants of STAC attain a detection accuracy of over 90% in the **Close Box** domain. In contrast, we observe a large performance drop when using a non-statistical distance function (“Temporal Non-Distr. Min”; §A.2.3) to measure temporal action consistency. This performance drop can be attributed to stochastic multimodality of the generative policy, which makes it challenging to sample individual actions that are similar to those at preceding timesteps during policy rollout. Because the non-statistical distance function is more sensitive than statistical distance functions to stochasticity in action sampling, we see an increased occurrence of false alarms.

Figure A.3: Performance variation of STAC based on the choice of statistical distance function in **PushT**.

A.3.2 Extended Results: VLM Runtime Monitor

To supplement the analysis provided in §2.6, we herein focus on the performance of our VLM runtime monitor and its complementary role to STAC for the detection of erratic and task progression failures.

Erratic Failure Analysis Table A.3 presents the extended results of our experiments on the **Close Box** domain, where we aim to detect erratic policy failures that result from OOD scaling of the box. We run several evaluations of our VLM runtime monitor, varying the choice of VLM (GPT-4o, Claude 3.5 Sonnet, Gemini 1.5 Pro [216]) and prompt template (Video QA, Image QA). Since erratic failures in this domain are assigned to STAC—which detects 99% of them—we would

like the VLM to avoid raising false alarms so as to keep the overall FPR of Sentinel low when the two detectors are combined.

Category 1: Erratic Failures		Close Box: In-Distribution (Policy Success Rate: 91%)			Close Box: Out-of-Distribution (Policy Success Rate: 41%)			Close Box: Combined (Policy Success Rate: 67%)		
Failure Detector		TPR \uparrow	TNR \uparrow	Det. Time (s) \downarrow	TPR \uparrow	TNR \uparrow	Det. Time (s) \downarrow	TPR \uparrow	TNR \uparrow	Accuracy \uparrow
Diffusion	Temporal Non-Distr. Min.	1.00	0.97	5.00	1.00	0.27	12.35	1.00	0.77	0.85
	Diffusion Recon. [94]	0.33	0.95	13.60	0.40	1.00	17.08	0.37	0.96	0.76
	Temporal Diffusion Recon.	1.00	0.96	8.47	0.92	1.00	15.75	0.92	0.97	0.95
	DDPM Loss (Eq. A.1)	1.00	0.90	8.27	1.00	0.94	14.54	1.00	0.91	0.94
	Temporal DDPM Loss	1.00	0.95	7.53	1.00	0.37	13.66	1.00	0.79	0.86
	Diffusion Output Variance	0.33	0.94	14.00	0.28	1.00	17.27	0.26	0.96	0.72
Embed.	Policy Encoder	0.25	0.98	16.27	1.00	0.00	1.59	0.94	0.70	0.78
	CLIP Pretrained	1.00	0.95	15.73	1.00	0.00	8.20	1.00	0.68	0.79
	ResNet Pretrained	1.00	0.95	17.87	1.00	0.00	15.51	1.00	0.68	0.79
STAC	STAC For. KL	1.00	0.90	6.60	0.99	0.85	14.04	0.99	0.89	0.92
	STAC Rev. KL	1.00	0.95	7.60	0.93	0.97	15.12	0.93	0.96	0.95
	STAC MMD*	1.00	0.94	7.20	0.99	0.93	14.72	0.99	0.94	0.96
VLM	GPT-4o Image QA	1.00	0.00	23.20	1.00	0.00	23.20	1.00	0.00	0.29
	GPT-4o Video QA*	1.00	0.89	21.20	0.69	0.95	21.02	0.77	0.91	0.87
	Gemini 1.5 Pro Image QA	1.00	0.00	21.20	1.00	0.00	23.20	1.00	0.00	0.29
	Gemini 1.5 Pro Video QA	1.00	0.57	17.20	1.00	0.50	20.20	1.00	0.55	0.68
	Claude 3.5 Sonnet Image QA	1.00	0.06	23.20	0.69	0.10	23.20	0.77	0.07	0.27
	Claude 3.5 Sonnet Video QA	0.83	0.31	23.20	0.44	0.40	23.20	0.55	0.35	0.40
Sentinel (STAC MMD* + GPT-4o Video QA*)		1.00	0.86	5.47	1.00	0.90	14.25	1.00	0.87	0.91

Table A.3: **Extended results on detecting erratic failures in the Close Box domain.** Our temporal consistency detector, STAC, detects 99% of erratic failures exhibited by diffusion policies. VLMs raise many false alarms when prompted with just a single image (Image QA), whereas performing Video QA (Ours) leads to a stark increase in TNR across all models. Performance also varies across the choice of VLM; GPT-4o is the most reliable in this domain, in contrast to other VLMs that struggle to accurately characterize the robot’s task progress in the video. Overall, Sentinel detects 100% of failures, while combining STAC and the VLM increases false alarms to 13%.

We first discuss the poor performance of the Image QA baseline. When prompted with just a single image, we find that all VLMs struggle to distinguish policy successes from failures and thereby do not exceed a TNR of 7%. Without observing the initial state (i.e., the box with its lids open) and the actions of the robot, the VLM is unable to identify the lids of the box and whether they have been closed. Thus, once the task’s time limit is exceeded, the VLM simply declares failure. We iterated on several prompts that included detailed questions in attempt to coerce the VLM to reason about the location of the box and its lids, but this yielded negligible changes in performance. As a result, all the outputs of the Image QA baseline resemble the following example of a false positive:

Analysis: The current observation shows the manipulator’s arms positioned near the white box, with the grippers open and not grasping the lids. The two smaller white side lids and the bigger white back lid of the box are not visible, suggesting they are not yet folded. The elapsed time is 30 out of 30 seconds, which means the robot has reached the time limit for completing the task. Given that the lids are not folded and the task is not completed, the robot is clearly failing the task.

Overall assessment: failure

Prompting the VLMs in a Video QA setup (§A.1.2) results in a strict increase in TNR across all models. Although, depending on the domain, we clearly observe that some VLMs show better visual reasoning performance than others. On the **Close Box** domain, GPT-4o generates relatively coherent descriptions of the videos, whereas Claude 3.5 Sonnet and Gemini 1.5 Pro often e.g., confuse closed lids for open lids or fail to recognize that the robot has made any significant progress. While this performance discrepancy is difficult to explain, two potential reasons are: a) the **Close Box** task can require reasoning over long videos (i.e., 20-30 image frames) and, while the VLMs’ large context windows are accommodating, the VLMs may still be susceptible to recency bias [306]; b) the images rendered in this domain might be better represented in the training data of one VLM (GPT-4o, in this case) compared to others.

Task Progression Failure Analysis In the context of VLM runtime monitoring, task progression failures differ from erratic failures in that they are more visually apparent and hence simpler for the VLM to interpret. For example, the policy takes more obviously incorrect actions, e.g., clearly misplacing the cover in the **Cover Object** domain (see Fig. A.1), but it does so in a temporally consistent manner that goes unnoticed by STAC. Therefore, under task progression failures, we require the VLM to attain both a high TPR and TNR, whereas we are mainly concerned with TNR under erratic failures. The extended results of our task progression failure experiments are shown in Table A.4 for the **Cover Object** domain and Table A.5 for the **Close Box** domain, the two of which are aggregated in Fig. 2.6.

Category 2: Task Progression Failures		Cover Object: In-Distribution (Policy Success Rate: 98%)			Cover Object: Out-of-Distribution (Policy Success Rate: 3%)			Cover Object: Combined (Policy Success Rate: 56%)		
		TPR ↑	TNR ↑	Det. Time (s) ↓	TPR ↑	TNR ↑	Det. Time (s) ↓	TPR ↑	TNR ↑	Accuracy ↑
DIF.	Temporal Non-Distr. Min.	1.00	0.93	2.40	0.06	1.00	7.60	0.09	0.93	0.56
	Diffusion Output Variance	0.00	0.77	-	0.00	1.00	-	0.00	0.77	0.44
	STAC For. KL	1.00	0.95	2.40	0.03	1.00	6.40	0.06	0.95	0.56
	STAC Rev. KL	1.00	0.93	2.40	0.03	1.00	6.40	0.06	0.93	0.55
STAC	STAC MMD*	1.00	0.93	2.40	0.09	1.00	7.73	0.12	0.93	0.58
VLM	GPT-4o Image QA	1.00	0.07	12.00	1.00	0.00	11.03	1.00	0.07	0.47
	GPT-4o Video QA	1.00	0.05	5.60	1.00	0.00	10.06	1.00	0.05	0.46
	Gemini 1.5 Pro Image QA	1.00	0.05	12.00	0.91	0.00	11.15	0.91	0.05	0.42
	Gemini 1.5 Pro Video QA	1.00	0.00	5.60	1.00	0.00	7.54	1.00	0.00	0.44
	Claude 3.5 Sonnet Image QA	1.00	0.81	12.00	0.70	1.00	12.00	0.71	0.82	0.77
	Claude 3.5 Sonnet Video QA	1.00	0.84	12.00	0.79	1.00	12.00	0.79	0.84	0.82
	Claude 3.5 Sonnet Video QA + Success Video	1.00	0.77	12.00	0.94	1.00	11.59	0.94	0.77	0.85
	Claude 3.5 Sonnet Video QA + Goal Images	1.00	0.93	5.60	0.76	1.00	11.74	0.76	0.93	0.86
	Claude 3.5 Sonnet Prompt Ensemble* (see §A.1.2)	1.00	0.93	12.00	0.85	1.00	12.00	0.85	0.93	0.90
	Sentinel (STAC MMD* + Claude 3.5 Sonnet Video QA)	1.00	0.79	2.40	0.82	1.00	8.68	0.82	0.80	0.81
	Sentinel (STAC MMD* + Claude 3.5 Sonnet Prompt Ensemble*)	1.00	0.88	2.40	0.88	1.00	8.69	0.88	0.89	0.88

Table A.4: **Extended results on detecting task progression failures in the Cover Object domain.** STAC only detects 12% of task progression failures (i.e., when the policy fails in a temporally consistent manner), which highlights the need for VLM runtime monitoring. Claude 3.5 Sonnet exhibits the most reliable detection performance in this domain, however, we use a prompt ensembling technique (details in §A.1.2) to reduce the number of false positives. Overall, Sentinel detects 88% of failures whilst raising 11% false alarms.

Among the VLMs considered, we find that Claude 3.5 Sonnet exhibits the best performance in the **Cover Object** domain (Table A.4), achieving a 79% TPR and an 84% TNR when prompted in a Video QA setup. Qualitative analysis of the responses from GPT-4o and Gemini 1.5 Pro reveals that

they misinterpret the videos and thus raise an excessive number of false alarms. As expected, STAC achieves an appreciable 93% TNR, but only detects 12% of task progression failures. The combination of STAC and Claude 3.5 Sonnet Video QA performs amicably (82% TPR, 80% TNR) but can be improved in terms of reducing the number of false positives, the majority of which are raised by the VLM. Here, we show that the prompt ensembling strategy discussed in §A.1.2 strengthens the reliability of our VLM runtime monitor (“Claude 3.5 Sonnet Prompt Ensemble”), increasing the TNR to 93%. Finally, the combination of this improved VLM runtime monitor with STAC results in a version of Sentinel that detects 88% of failures whilst raising a more acceptable number of false alarms (11%).

Category 2: Task Progression Failures		Close Box: In-Distribution (Policy Success Rate: 85%)			Close Box: Out-of-Distribution (Policy Success Rate: 0%)			Close Box: Combined (Policy Success Rate: 40%)		
Failure Detector		TPR \uparrow	TNR \uparrow	Det. Time (s) \downarrow	TPR \uparrow	TNR \uparrow	Det. Time (s) \downarrow	TPR \uparrow	TNR \uparrow	Accuracy \uparrow
Diff.	Temporal Non-Distr. Min.	1.00	0.97	4.67	0.67	-	7.46	0.71	0.97	0.82
	Diffusion Output Variance	0.00	1.00	-	0.28	-	11.57	0.25	1.00	0.55
STAC	STAC For. KL	1.00	0.97	5.07	0.61	-	8.14	0.65	0.97	0.78
	STAC Rev. KL	1.00	0.97	6.13	0.61	-	10.11	0.65	0.97	0.78
	STAC MMD*	1.00	0.97	5.47	0.61	-	9.06	0.65	0.97	0.78
VLM	GPT-4o Image QA	1.00	0.00	23.20	1.00	-	22.68	1.00	0.00	0.60
	GPT-4o Video QA*	1.00	0.89	21.20	0.87	-	22.00	0.88	0.89	0.89
	Gemini 1.5 Pro Image QA	1.00	0.00	21.20	0.96	-	23.20	0.96	0.00	0.57
	Gemini 1.5 Pro Video QA	1.00	0.57	17.20	0.98	-	15.47	0.98	0.57	0.82
	Claude 3.5 Sonnet Image QA	1.00	0.06	23.20	0.78	-	23.20	0.81	0.06	0.51
	Claude 3.5 Sonnet Video QA	0.83	0.31	23.20	0.80	-	23.20	0.81	0.31	0.61
Sentinel (STAC MMD* + GPT-4o Video QA*)		1.00	0.86	5.47	0.96	-	12.20	0.96	0.86	0.92

Table A.5: **Extended results on detecting task progression failures in the Close Box domain.** Here, STAC detects considerably more task progression failures than in the **Cover Object** domain, yet 35% of failures are left undetected. As in Table A.3, we find that video-based reasoning is necessary for VLMs to attain high TNRs, with GPT-4o showing the best performance. Overall, Sentinel detects 96% of failures whilst raising 14% false alarms.

The results in Table A.5 reaffirm the following **key takeaways**: a) image-based VLM reasoning is insufficient for understanding the robot’s task progress, thus resulting in low TNRs; b) the VLMs’ performances vary across domains, with GPT-4o and Claude 3.5 Sonnet performing the best in the **Close Box** and **Cover Object** domains, respectively; c) STAC and the VLM runtime monitor play complementary roles toward a performant overall failure detector across domains. We expect the performance of our VLM runtime monitor (and thus Sentinel) to improve with the future release of more capable VLMs [35], which may also eliminate the discrepancies among VLMs noted above.

Discussion: Why combine failure detectors by taking the union of their predictions?

Our full failure detector, Sentinel, combines STAC and the VLM by taking the union of their predictions (i.e., the “Logical OR” in Fig. 2.3), which, in the worst case, compounds their false positive rates by applying the union bound. However, doing so follows from several design considerations:

- **Importance weighting:** We explicitly define one failure category as the complement of the other and assign a specialized detector to each because it is extremely difficult to design a single detector that captures highly heterogeneous failure modes. Thus, by using the “OR” operation, we are placing *equal importance* on the two proposed failure categories. We note

that our failure detector’s primary purpose is to detect unseen failures at deployment time: i.e., we do not assume any data of robot failures to calibrate the detector, which may be necessary to tune importance weights for different detectors. Furthermore, importance weights that are optimal on one dataset may perform poorly on failure modes not represented in that data.

- **Performance interpretability:** Using a simple scheme to combine detectors makes it easy to interpret a) the runtime behavior of the combined detector and b) which individual detectors are contributing to performance and when. For example, using the logical “OR” implies that Sentinel’s overall FPR remains acceptably low if both STAC and the VLM runtime monitor have low FPRs. STAC achieves a provably low FPR (§A.4), while strategies exist to reduce the VLM’s FPR through e.g., prompt ensembling (§A.1.2) or conformal calibration [218]. Thus, we can expect a low FPR when the detectors are combined. We can similarly interpret Sentinel’s TPR performance, as exemplified in our experimental analysis. Ease of performance interpretation may not hold true with more sophisticated schemes for combining detectors.
- **Runtime constraints:** In practice, STAC (fast) and the VLM runtime monitor (slow) come with different inference-time latencies and may need to run at distinct timescales. Thus, our logical “OR” combination only applies at overlapping timesteps and otherwise allows each failure detector to flag independently, i.e., without synchronizing their detection rates. This flexibility is crucial, as more sophisticated combination schemes could encounter issues if e.g., unexpected network latencies result in delayed responses from a cloud-hosted VLM.

Nevertheless, we note that more sophisticated combination schemes might offer advantages, such as improved detection performance or scalability when integrating additional detectors. Exploring such schemes that align with the above design considerations represents a valuable direction for future work.

A.4 Derivations

To validate our design choices, we show that STAC’s score function and calibration procedure in §2.4.1 provably result in a low FPR. To do so, we apply recently popularized tools from conformal prediction because they are sample efficient and distribution free, meaning that they do not require distributional assumptions on the trajectory rollouts. Our guarantee is a direct application of the standard results in split conformal prediction [10], but to ensure the self-containedness of this manuscript, we first briefly reintroduce the core concepts in conformal prediction (taken from [10]) using the notation in Chapter 2.

Background on Conformal Inference In its most basic form, conformal prediction aims to construct a prediction set \mathcal{C} that will contain the true value of a new test point X_{test} with a user

defined probability of at least $1 - \delta$ [10]. To do so, a conformal algorithm requires 1) a sequence of calibration samples $\{X^i\}_{i=1}^M$ with all samples $X^1, \dots, X^M, X_{\text{test}}$ i.i.d. and 2) a conformity score function $\eta(X) \in \mathbb{R}$. Intuitively, conformal methods use $\{\eta(X^i)\}_{i=1}^M$ to identify how likely $\eta(X_{\text{test}})$ is to lie within the range of a $1 - \delta$ fraction of the calibration samples (i.e., how well X_{test} conforms to the calibration data). We emphasize that this approach ensures that we construct a valid prediction set \mathcal{C} , regardless of the choice of conformity score and without knowing any properties of the data generating distribution:

Theorem 1 (Adapted from Thm. D.1 in [10]). *Let $\mathcal{D}_{\text{calib}} = \{X^1, \dots, X^M\}$ be a calibration dataset and let X_{test} be a test sample. Suppose that the samples in $\mathcal{D}_{\text{calib}}$ and X_{test} are independent and identically distributed (i.i.d.). Then, defining*

$$\gamma := \inf \left\{ \xi \in \mathbb{R} : \frac{|\{i : \eta(X^i) \leq \xi\}|}{M} \geq \frac{\lceil (M+1)(1-\delta) \rceil}{M} \right\}$$

as the $\frac{\lceil (M+1)(1-\delta) \rceil}{M}$ empirical quantile of the calibration data ensures that

$$\mathbb{P}(\eta(X_{\text{test}}) \leq \gamma) \geq 1 - \delta.$$

Here, $\lceil \cdot \rceil$ denotes the ceiling function.

Conformal guarantee of STAC The base split conformal procedure outlined by **Theorem 1** requires that the samples used for calibration and test are i.i.d. This is not the case for states and actions observed sequentially within a trajectory, complicating the analysis of applying STAC at each timestep within a trajectory. Thus, to resolve this issue and provide a guarantee when we sequentially apply STAC on the correlated state-action pairs within a trajectory, we calibrate the detector using the consistency scores generated across full trajectories in §2.4.1. This allows us to rigorously bound the FPR using **Theorem 1**.

Proposition 3 (STAC has low FPR). *Let $\mathcal{D}_\tau = \{\tau^i\}_{i=1}^M \stackrel{\text{iid}}{\sim} P_\tau$ be the validation dataset of successful trajectories, each consisting of $H_i \leq H$ timesteps and drawn i.i.d. from the closed-loop nominal distribution P_τ . For notational simplicity, assume that any trajectory has a length divisible by k (i.e., $H_i \bmod k = 0$). Moreover, let η_t be defined as the STAC temporal consistency score at some timestep $0 \leq t \leq H$ in Eq. 2.1 and set γ equal to the empirical $\frac{\lceil (M+1)(1-\delta) \rceil}{M}$ quantile of the terminal STAC scores $\{\eta_{H_i}^i\}_{i=1}^M$ of the trajectories in \mathcal{D}_τ . Then, the false positive rate—that is, the probability that we raise a false alarm at any point during a new successful test trajectory $\tau \sim P_\tau$ of length $H' \leq H$ —is at most δ :*

$$\text{FPR} := \mathbb{P}_{P_\tau}(\exists 0 \leq t \leq H' \text{ s.t. } \eta_t > \gamma) \leq \delta. \quad (\text{A.4})$$

Proof. Let $H' \leq H$ be the length of the test trajectory τ . If there is no distribution shift, i.e., when the test trajectory τ is i.i.d. with respect to $\mathcal{D}_\tau \stackrel{\text{iid}}{\sim} P_\tau$, it holds that $\eta_{H'}$ and $\{\eta_{H_i}^i\}_{i=1}^M$ are i.i.d.

Therefore, by [Theorem 1](#), we have that

$$\mathbb{P}_{P_\tau}(\eta_{H'} > \gamma) \leq \delta.$$

Moreover, since we define $\eta_t = \sum_{i=0}^{j-1} \hat{D}(\tilde{\pi}_{ik}, \tilde{\pi}_{(i+1)k})$ for $t = jk$ in [Eq. 2.1](#) and since $\hat{D}(\cdot, \cdot) \geq 0$ because it is a statistical distance, it follows that η_t is increasing. That is, $\eta_0 \leq \eta_k \leq \eta_{2k} \leq \dots \leq \eta_{H'}$. Therefore, if η_t crosses the threshold γ at any time, it also holds that $\eta_{H'} > \gamma$. This immediately implies the proposition, as we then have that

$$\mathbb{P}_{P_\tau}(\exists 0 \leq t \leq H' \text{ s.t. } \eta_t > \gamma) = \mathbb{P}_{P_\tau}(\eta_{H'} > \gamma) \leq \delta.$$

□

We conclude this section with three remarks:

1. We only bound the FPR, which ensures that our algorithm does not raise a false alarm with high probability, so that any warnings likely correspond to an OOD scenario. We do so because a system that frequently raises false alarms is impractical to use. Our calibration approach does not guarantee the detection of failures, nor does it guarantee that we do not issue false alarms on OOD successes, as this is not possible without any distributional assumptions on the OOD scenarios or without using failure data for calibration [[177](#)]. Instead, we empirically find that our temporal consistency score performs amicably at detecting failures in our experiments.
2. [Proposition 3](#) only certifies that the FPR of STAC is low. We make no claims on combined performance of STAC and the VLM, as VLM represents a black-box classifier. Future work could investigate methodologies to jointly calibrate an ensemble of failure detectors.
3. Conformal guarantees, like those in [Theorem 1](#) and [Proposition 3](#), are *marginal* with respect to the calibration data. That is, they may not hold exactly when given a particular calibration dataset, but if we were to sample thousands of calibration datasets, the guarantees would hold on average. Thus, as expected, STAC does not exactly satisfy [Eq. A.4](#) in our results, as compute budgets restricted our experiments to repetitions on a limited number of random seeds.

Appendix B

Additional Details: CUPID

Appendix Overview – Curating Data your Robot Loves with Influence Functions

The appendix offers additional details *w.r.t.* the implementation of CUPID (§B.1), the experiments conducted (§B.2), along with extended results and analysis (§B.3), and finally, supporting derivations for our data curation methods (§B.4). Videos and code are made available at: <https://cupid-curation.github.io>.

B.1	Implementation Details	105
B.1.1	Influence Functions for Diffusion Policies	105
B.1.2	CUPID Hyperparameters	107
B.1.3	Combining Score Functions	107
B.2	Experimental Setup	108
B.2.1	Hardware Setup	108
B.2.2	Policy Architectures	108
B.2.3	Tasks and Datasets	109
B.2.4	Baseline Details	111
B.3	Additional Results and Analysis	112
B.3.1	Extended Discussion on RoboMimic Results (§3.7.1)	112
B.3.2	Ablation on Number of Policy Rollouts in RoboMimic (§3.7.2)	113
B.3.3	Additional Data Quality Results in RoboMimic	114
B.3.4	Data Filtering Curation Distributions in Franka Real-World	115
B.3.5	Data Selection Curation Distributions in Franka Real-World	116
B.3.6	Additional Results for Franka PI-0: Curated Dataset Transfer (§3.7.3)	117
B.4	Derivations	119

B.4.1	Proof of Proposition 2	119
B.4.2	Derivation of Performance Influence for Variable Length Trajectories	119

B.1 Implementation Details

B.1.1 Influence Functions for Diffusion Policies

For ease of reference in this section, we restate the definition of the action influence ([Definition 2](#)) and the proposition establishing performance influence ([Proposition 2](#)), both originally introduced in [§3.5](#).

Restatement of [Definition 2](#). *The action influence of a state-action pair (s, a) on a test state-action pair (s', a') is the influence of (s, a) on the policy’s log-likelihood $\log \pi_\theta(a'|s')$. That is,*

$$\Psi_{a\text{-inf}}((s', a'), (s, a)) := -\nabla_\theta \log \pi_\theta(a'|s')^\top H_{\text{bc}}^{-1} \nabla_\theta \ell(s, a; \pi_\theta).$$

Restatement of [Proposition 2](#). *Assume that $\theta(\mathcal{D}) = \arg \min_{\theta'} \mathcal{L}_{\text{bc}}(\theta'; \mathcal{D})$, that \mathcal{L}_{bc} is twice differentiable in θ , and that $H_{\text{bc}} \succ 0$ is positive definite (i.e., $\theta(\mathcal{D})$ is not a saddle point)¹. Then, it holds that*

$$\Psi_{\pi\text{-inf}}(\xi) = \mathbb{E}_{\tau \sim \mathcal{P}(\tau | \pi_\theta)} \left[\frac{R(\tau)}{H} \sum_{(s', a') \in \tau} \sum_{(s, a) \in \xi} \Psi_{a\text{-inf}}((s', a'), (s, a)) \right].$$

where $\Psi_{\pi\text{-inf}}(\xi)$ is the **performance influence** of a demonstration ξ (as introduced in [Definition 1](#)).

Computing the Action Influence

Although [Proposition 2](#) provides a clean mechanism to attribute policy performance to its training data by leveraging influence scores on action log-likelihoods, computing $\nabla_\theta \log \pi_\theta(a'|s')$ (in the action influence $\Psi_{a\text{-inf}}$) for diffusion-based policy architectures is nontrivial due to the iterative denoising process [[111](#), [256](#)]. Instead, various works outside robotics propose to approximate the log-likelihood with the denoising loss $\ell(s', a'; \pi_\theta)$ for the purpose of data attribution [[88](#)], because the denoising loss is proportionate to the variational lower bound on $\log \pi_\theta(a'|s')$. In [§3.6](#), we apply a similar approximation to perform data attribution on state-of-the-art diffusion policies [[40](#)], which we describe below.

Diffusion Policy: Consider the standard diffusion policy architecture [[40](#)]. An action $a := a^0$ is generated by iteratively denoising an initially random action $a^T \sim \mathcal{N}(0, 1)$ over T steps as a^T, \dots, a^0 using a noise prediction network ϵ_θ , where a^i denotes the generated action at the i -th denoising iteration. Following the imitation learning setting described in [§3.4](#), the parameters θ of the noise prediction network ϵ_θ are fit to the BC objective as $\theta = \arg \min_{\theta'} \{\mathcal{L}_{\text{bc}}(\theta'; \mathcal{D}) := \frac{1}{|\mathcal{D}|H} \sum_{\xi^i \in \mathcal{D}} \sum_{(s, a) \in \xi^i} \ell(s, a; \pi_{\theta'})\}$. Here, the noise prediction network ϵ_θ is trained to predict random

noise $\epsilon^i \sim \mathcal{N}(0, 1)$ added to the action a at randomly sampled timesteps $i \sim \mathcal{U}[0, T)$ of the diffusion process using the loss function ℓ defined as

$$\ell(s, a; \pi_{\theta'}) := \mathbb{E}_{\epsilon^i, i} [\|\epsilon^i - \epsilon_{\theta'}(\sqrt{\bar{\alpha}_i}a + \sqrt{1 - \bar{\alpha}_i}\epsilon^i, s, i)\|^2], \quad (\text{B.1})$$

where the constants $\bar{\alpha}_i$ depend on the chosen noise schedule of the diffusion process.

Influence Approximations: Since the denoising loss ℓ in Eq. B.1 is proportionate to the variational lower bound on the action log-likelihood $\log \pi_{\theta}(a|s)$, it may seem intuitive to substitute $\nabla_{\theta} \log \pi_{\theta}(a'|s')$ with $-\nabla_{\theta} \ell(s', a'; \pi_{\theta})$ —assuming gradient alignment—to approximate the action influence (Eq. 3.2) as

$$\Psi_{a\text{-inf}}((s', a'), (s, a)) \approx \nabla_{\theta} \ell(s', a'; \pi_{\theta})^{\top} H_{\text{bc}}^{-1} \nabla_{\theta} \ell(s, a; \pi_{\theta}). \quad (\text{B.2})$$

A similar approach is taken by Georgiev et al. [88] for attributing the generations of image-based diffusion models. However, consistent with more recent results in the data attribution literature [166, 307], we find this approximation to work poorly in practice, with highly influential training samples $(s, a) \in \mathcal{D}$ rarely reflecting the test-time transitions $(s', a') \in \tau$ over which the action influences are computed. Instead, we follow the approach of Zheng et al. [307], which entails replacing both $\log \pi_{\theta}(a'|s')$ and $\ell(s, a; \pi_{\theta})$ in Eq. 3.2 with a surrogate, label-agnostic output function $\ell_{\text{square}}(s, a; \pi_{\theta}) := \mathbb{E}_{\epsilon^i, i} [\|\epsilon_{\theta}(\sqrt{\bar{\alpha}_i}a + \sqrt{1 - \bar{\alpha}_i}\epsilon^i, s, i)\|^2]$, making our final approximation of the action influence

$$\Psi_{a\text{-inf}}((s', a'), (s, a)) \approx \nabla_{\theta} \ell_{\text{square}}(s', a'; \pi_{\theta})^{\top} H_{\text{square}}^{-1} \nabla_{\theta} \ell_{\text{square}}(s, a; \pi_{\theta}). \quad (\text{B.3})$$

Here, $H_{\text{square}} = \frac{1}{|\mathcal{D}|H} \sum_{\xi^i \in \mathcal{D}} \sum_{(s, a) \in \xi^i} \nabla_{\theta} \ell_{\text{square}}(s, a; \pi_{\theta}) \nabla_{\theta} \ell_{\text{square}}(s, a; \pi_{\theta})^{\top}$ is the Gauss-Newton approximation of the Hessian—as introduced by Martens [187] and applied for stable and efficient influence estimation in [15, 205]—under the surrogate output function ℓ_{square} .

Additional Remarks: While the use of ℓ_{square} may seem counterintuitive at first, it offers three key advantages for computing action influences:

1. Leave-one-out influences (§3.3) computed using ℓ_{square} (Eq. B.3) are empirically found to correlate better with actual changes in a diffusion model’s loss—i.e., the difference $\ell(s', a'; \pi_{\theta(\mathcal{D} \setminus (s, a))}) - \ell(s', a'; \pi_{\theta(\mathcal{D})})$ —than those computed using the loss ℓ (Eq. B.2) [307].
2. Theoretical analysis also shows that ℓ_{square} more closely aligns with a distributional formulation of the leave-one-out influence compared to the loss ℓ [166]. In the case of diffusion policies, this distributional formulation would seek to design $\Psi_{a\text{-inf}}$ such that it approximates the *leave-one-out divergence* $\Psi_{a\text{-inf}}((s', a'), (s, a)) \approx D_{\text{KL}}(\pi_{\theta(\mathcal{D})}(a'|s') || \pi_{\theta(\mathcal{D} \setminus (s, a))}(a'|s'))$.
3. Using ℓ_{square} significantly reduces the computational cost of computing action influences for policies with high-dimensional action spaces, because the ℓ^2 -norm collapses the model’s

prediction into a scalar $\|\epsilon_\theta(\sqrt{\bar{\alpha}_i}a + \sqrt{1 - \bar{\alpha}_i}\epsilon^i, s, i)\|^2$. As a result, computing Eq. B.3 requires only a single model gradient $\nabla_\theta \ell_{\text{square}}$ per training and test sample. In contrast, while the technique proposed by Lin et al. [166] offers a more accurate estimate of the leave-one-out divergence $D_{\text{KL}}(\pi_{\theta(\mathcal{D})}(a'|s') || \pi_{\theta(\mathcal{D} \setminus (s,a))}(a'|s'))$, its computational cost scales linearly with the dimensionality of the model’s output, which may be prohibitive.

Accuracy-Efficiency Tradeoff: We note that our approach for computing the performance influence of a demonstration (Eq. 3.3) is agnostic to the choice of influence estimation technique [88, 166, 194, 290, 307], allowing practitioners to trade off between accuracy and efficiency based on available computational resources, and enabling integration of improved data attribution methods (e.g., [120]) in the future.

B.1.2 CUPID Hyperparameters

We use the same set of hyperparameters for CUPID and CUPID-QUALITY across all experiments.

Performance Influence (Eq. 3.3): For all tasks, we define the trajectory return to be $R(\tau) = 1$ if τ completes the task and $R(\tau) = -1$ otherwise. As a result, every rollout trajectory $\tau \sim p(\cdot | \pi_\theta)$ provides information on the utility of each demonstration toward the policy’s closed-loop performance. We also found CUPID to work with alternative return definitions—for example, focusing solely on successful rollouts by setting $R(\tau) = 0$ when τ fails. However, such choices may increase sample complexity.

Action Influence (Eq. B.3): The action influence requires computing the gradient of an expectation $\nabla_\theta \ell_{\text{square}}(s, a; \pi_\theta) = \nabla_\theta \mathbb{E}_{\epsilon^i, i} [\|\epsilon_\theta(\sqrt{\bar{\alpha}_i}a + \sqrt{1 - \bar{\alpha}_i}\epsilon^i, s, i)\|^2]$. For all tasks, we approximate the expectation using a batch of $B = 64$ samples $(\epsilon^{(b)}, i^{(b)})$, where $\epsilon^{(b)} \sim \mathcal{N}(0, 1)$ and $i^{(b)} \sim \mathcal{U}[0, T]$ are sampled independently.

Data Attribution: We leverage TRAK [205] to efficiently compute action influences as defined in Eq. B.3. First, TRAK uses random projections $\mathbf{P} \sim \mathcal{N}(0, 1)^{p \times d}$, where p is the number of model parameters and $d \ll p$ is the specified projection dimension, to reduce the dimensionality of the gradients as $g_\theta = \mathbf{P}^\top \nabla_\theta \ell_{\text{square}}$ while preserving their inner products $g_\theta \cdot g_\theta \approx \nabla_\theta \ell_{\text{square}} \cdot \nabla_\theta \ell_{\text{square}}$ [129]. Second, TRAK ensembles influence scores over C independently trained models (i.e., from different seeds) to account for non-determinism in learning. In our experiments, we use the standard projection dimension $d = 4000$ and minimize computational cost by using only a single policy checkpoint $C = 1$, noting that ensembling over $C > 1$ policy checkpoints is likely to improve the accuracy of our influence scores.

B.1.3 Combining Score Functions

For ease of exposition in §3.5.3, we express the overall score of a demonstration as the convex combination of its performance influence and its quality score $\alpha \Psi_{\pi\text{-inf}} + (1 - \alpha) \Psi_{\text{qual}}$, where $\alpha = 1$

and $\alpha \in [0, 1]$ instantiates CUPID and CUPID-QUALITY, respectively. Here, we additionally note that taking weighted combinations of score functions requires first normalizing them to equivalent scales. Hence, our implementation uniformly normalizes demonstration scores within the range $[0, 1]$ (i.e., producing an absolute ranking of demonstrations) for each score function $\Psi_{\pi\text{-inf}}$ and Ψ_{qual} before combining them. This simple approach can be applied to combine an arbitrary number of demonstration score functions.

B.2 Experimental Setup

B.2.1 Hardware Setup

As depicted in Fig. 3.4, our hardware experiments involve a Franka FR3 manipulator robot. We use a single ZED 2 camera to capture RGB-D observations and disregard the depth information. Our image-based policies process 256×256 downsampled RGB observations and predict sequences of end-effector poses for the manipulator, which are tracked using operational space control [142].

B.2.2 Policy Architectures

Diffusion Policy (DP): We use the original diffusion policy implementation¹ from Chi et al. [40]. Specifically, we use the convolutional-based diffusion policy architecture for efficiency. For state-based tasks (e.g., in RoboMimic; Fig. 3.3), actions are generated solely using the noise prediction network ϵ_{θ} as described in §B.1.1. However, for image-based tasks (e.g., on hardware; Fig. 3.4), the policy π_{θ} contains two sets of parameters $\theta = (\theta_o, \theta_a)$ corresponding to a ResNet-18 encoder E_{θ_o} and the noise prediction network ϵ_{θ_a} . When scoring demonstrations, we compute action influences (Eq. B.3) over all available policy parameters θ , noting that one might also consider using a subset of the parameters, e.g., those of the noise prediction network or an alternative action head, under reduced computational budgets.

Other optimizations: In preliminary experiments, we found that the original diffusion policy (a) was heavily over-parameterized and (b) converged in performance much earlier in training than the specified maximum number of epochs. Thus, to accelerate experimentation in RoboMimic (Fig. 3.3), we (a) manually determined the smallest model size that performed similarly to the original policy and (b) adjusted the maximum number of epochs to the point where additional training would result in no further performance gains. Importantly, we keep the model size and training epochs consistent across all curation methods for a given RoboMimic task. For real-world hardware experiments, we use the same model size and limit the number of training steps to 200K across all tasks, similar to Hejna et al. [109]. All other diffusion policy hyperparameters are consistent with the original implementation [40].

¹DP’s open-source implementation: https://github.com/real-stanford/diffusion_policy.

Generalist Robot Policy (π_0): We fine-tune Physical Intelligence’s π_0 Vision-Language-Action (VLA) policy² via Low-Rank Adaptation (LoRA) [114] on the “Figure-8” and “Tuck-Box” tasks. To ensure the post-trained policy’s performance is solely a result of the properties of the curated dataset used for training, we use the standard fine-tuning parameter configuration from Black et al. [25] and keep all hyperparameters fixed across experiments (see Table B.1). We trained on 2 NVIDIA RTX 4090 GPUs, which took approximately 15 hours under the configuration in Table B.1. In initial experiments, we found that training for 30K steps was necessary to compensate for mismatch between our robot’s action space (target end-effector poses tracked via operational space control) and the action spaces used to pre-train the base π_0 policy (absolute joint angles). In addition, we found that using a descriptive prompt for the task was necessary to yield performant policies. We kept these prompts fixed across training, evaluation, and all curation settings. For the “TuckBox” task, we used the instruction “Move the blue box underneath the white shelf” to avoid biasing the policy towards a particular behavior mode (e.g., “sliding” or “pick-and-place”). For the “Figure-8” task, we used the instruction “Pick up the red rope, then tie a figure 8,” where we found the two-step instruction to increase performance over shorter instructions like “Tie the cleat.” Similar to the diffusion policy experiment, we fine-tune a separate π_0 model for each curation task—filter- k (Task 1) and select- k (Task 2)—using their corresponding base demonstration datasets. We then fine-tune additional π_0 models on datasets curated by our methods.

Hyperparameter	Value
Training steps	30,000
Batch size	16
Optimizer	AdamW
Learning rate schedule	Cosine decay
EMA	Disabled
Action chunk length	50 steps
Control frequency	10 Hz
Image resolution	224 × 224
Observation history	1 frame
VLM backbone LoRA	Rank = 16, α = 16
Action expert LoRA	Rank = 32, α = 32

Table B.1: **Hyperparameter configuration** used for π_0 [25] post-training.

B.2.3 Tasks and Datasets

Here, we provide additional details regarding our real-world hardware tasks and their corresponding datasets. We refer to Mandlekar et al. [183] for details on the simulated RoboMimic benchmark.

Figure-8: A brief description of the task is provided in §3.6.1. The “Figure-8” dataset contains 160 demonstrations evenly split across four *quality tiers*. Higher quality demonstrations complete the task at a constant rate without errors, while lower-quality demonstrations vary in progression rate [5] and include retry or recovery behaviors. Therefore, the “Figure-8” task intends to reflect a practical setting where demonstrations of varying properties are introduced during data collection, whether organically or deliberately, e.g., to improve policy robustness to recoverable failures [56]. Therefore, we expect curation algorithms that distinguish demonstrations upon notions of quality (e.g., predictability [109]) to perform well on this task, which is consistent with our findings in Fig. 3.4(a) and Fig. 3.7(a).

² π_0 ’s open-source implementation: <https://github.com/Physical-Intelligence/openpi>.

TuckBox: A brief description of the task is provided in §3.6.2. As mentioned, the “TuckBox” dataset contains 120 demonstrations split 2:1 between two subsets: 80 demonstrations solve the task by sliding the box under the receptacle, while 40 demonstrations first reposition the box in front of the receptacle via pick-and-place. Although the sliding strategy appears more smooth and involves just a single step, it is rendered unreliable by imperceptible test-time distribution shifts to the box’s mass distribution. As such, “TuckBox” stands conceptually opposite to “Figure-8,” whereby attending to heuristic properties of demonstrations (e.g., quality) may result in poor curation performance (as shown in Fig. 3.4(b)).

Bookshelf: A brief description of the task is provided in §3.6.3. To summarize, the robot must extract a target book that is either shelved alone—affording a simple, horizontal pulling motion—or with another book stacked on top of it (i.e., a *bookstack*). In the bookstack case, the robot must extract the target book using a vertical pulling motion, such that the stacked book does not fall off the shelf in the process (see Fig. 3.4(c)). In total, the “Bookshelf” dataset contains 120 demonstrations split across three subsets: (a) 60 demonstrations feature the target book shelved alone with a white background, (b) 20 demonstrations feature the bookstack with a white background, and (c) 40 demonstrations feature the bookstack with a dark background. All subsets feature task-irrelevant distractor books on other shelves.

Spurious correlations in training data: Although the vertical pulling solution to the bookstack case is demonstrated in scenes with both white and dark backgrounds, the disproportionate number of demonstrations in subset (a) versus subset (b) spuriously correlates the horizontal pulling motion with the white background. Such spurious correlations may result in *causal confusion* [61], where the policy ignores the bookstack, attends the white background, and executes the failing horizontal strategy.

Spurious correlations in rollout data: Like “TuckBox,” “Bookshelf” represents another limiting case for curating data with quality metrics [109]. However, it also presents an additional challenge for methods that seek to curate data using online experience [33]. For example, approaches that attend to differences in states between successful and failed policy rollouts may be susceptible to spurious correlations in the rollout data. Consider the simple case: if we were to observe successful rollouts when the target book is shelved alone and failed rollouts when another book is stacked above the target, then training a classifier (i.e., as in Demo-SCORE [33]) to distinguish successful from failed states may wrongly attribute failures to the presence of the stacked book. Curating demonstrations with such a classifier would, in turn, worsen the spurious correlation in the training data. Thus, we posit that handling more challenging cases of spurious correlations in real-world data will require methods that *causally attribute* the outcomes of observed test-time experiences to the training data, such as CUPID.

B.2.4 Baseline Details

DemInf: We use the official implementation³ provided by Hejna et al. [109]. We note that DemInf curates data offline—that is, without using any policy rollouts—and is at present only applicable to the demonstration filtering setting (i.e., filter- k , as defined in Task 1).

Demo-SCORE: We construct our own implementation based on the description provided by the authors [33]. Given our assumed fixed budget of $m = 100$ rollouts for RoboMimic experiments (§3.6), we collect 25 rollouts from $C = 4$ policy checkpoints throughout training. We train three-layer MLP classifiers with hidden dimensions [16, 16, 16] on the first three rollout sets, and select the best classifier via cross-validation on the last 25 rollouts, as described in [33]. Since we reduce the rollout budget to $m = 25$ rollouts for hardware experiments (§3.6), we collect 25 rollouts from the last $C = 1$ policy checkpoint. We then train a single ResNet-18 encoder and three-layer classification head with hidden dimensions [32, 32, 32] on 20 of the rollouts, leaving 5 validation rollouts to monitor for overfitting. We train all classifiers with a heavy dropout of 0.3 and an AdamW weight decay of 0.1 to prevent overfitting, in alignment with [33]. Although Chen et al. [33] only test Demo-SCORE for demonstration filtering, we extend its use for demonstration selection (i.e., select- k , as defined in Task 2).

Success Similarity: We design a custom robot data curation algorithm that, similar to Demo-SCORE, values demonstrations based on a heuristic measure of similarity *w.r.t.* successful policy rollouts. Instead of training classifiers, Success Similarity measures the average state-embedding similarity of a demonstration *w.r.t.* all successful rollouts as

$$S(\xi; \mathcal{D}_\tau) = - \sum_{\tau \in \mathcal{D}_\tau} \left[\mathbf{1}(R(\tau) = 1) \cdot \frac{1}{H^2} \sum_{s' \in \tau} \sum_{s \in \xi} D(\phi(s'), \phi(s)) \right],$$

where the indicator function $\mathbf{1}$ evaluates to 1 if rollout τ is successful and 0 otherwise, H is the assumed length of all demonstrations $\xi \in \mathcal{D}$ and rollouts $\tau \in \mathcal{D}_\tau$ for notational simplicity, ϕ is the state embedding function, and D is a specified distance function over state embeddings [251], such as the Mahalanobis, L2, or cosine distance. For image-based states, we experimented with various embedding functions ϕ , including ResNet [106], DINOv2 [203], and the policy’s vision encoder [5], and ultimately found the policy’s vision encoder to work best in RoboMimic. The embedding function is set to identity for low-dimensional states (i.e., $\phi(s) = s$). Lastly, the distance function D is chosen for compatibility with ϕ : e.g., L2 distance for policy encoder embeddings and cosine distance for DINOv2 embeddings.

Comparison to Performance Influence (CUPID): One can interpret Success Similarity as replacing the action influence $\Psi_{a\text{-inf}}((s', a'), (s, a))$ (Eq. 3.2) with a state-based proxy $-D(\phi(s'), \phi(s))$ in an attempt to estimate the performance contribution of a demonstration (Eq. 3.3). In our RoboMimic experiments (Fig. 3.3), this approach performs comparably to Demo-SCORE and, in some cases, even

³DemInf open-source implementation: <https://github.com/jhejna/demonstration-information>.

outperforms it—without requiring the training of any additional models. However, Success Similarity performs consistently worse than CUPID across all tasks, supporting prior findings that influence functions offer a substantially stronger causal signal than heuristic measures of similarity [205].

Oracle: For each task, the Oracle method represents a best attempt to curate data assuming privileged access to ground-truth demonstration labels. For the RoboMimic and “Figure-8” tasks, the Oracle ranks demonstrations in descending order of quality, choosing high-quality demonstrations before low-quality demonstrations. For the “TuckBox” task, the Oracle first chooses all demonstrations exhibiting the more robust pick-and-place strategy before any demonstration exhibiting the more brittle sliding strategy. Lastly, for the “Bookshelf” task, the Oracle chooses demonstrations to minimize the effect of the *known* spurious correlation (i.e., horizontal pulling motion in the presence of a white background), resulting in a more balanced curated dataset. These definitions of the Oracle apply identically to the filter- k (Task 1) and select- k (Task 2) curation tasks studied throughout this chapter.

Additional baselines: We implement a number of additional custom baselines that one might try in practice, such as curating data based on policy loss, policy uncertainty, state diversity, and action diversity. However, we exclude them from our experiments given their relatively poor performance.

B.3 Additional Results and Analysis

We present additional results and ablations for our RoboMimic and Franka real-world tasks that were cut from the main text due to space constraints.

B.3.1 Extended Discussion on RoboMimic Results (§3.7.1)

We provide an extended discussion on §3.7.1 for our RoboMimic simulation results.

Performance versus Data Quality: One of our key findings is that the performance of a state-of-the-art policy does not strictly correlate with the *perceived quality* of its training data. Factors such as redundancy, balance, and coverage of the dataset all play a role in determining policy performance. This is illustrated in the Oracle filter- k results (left three plots of Fig. 3.3). While the top row shows a monotonic increase in average dataset quality as lower-quality demonstrations are filtered out, the bottom row reveals (1) a consistent performance drop for diffusion policies on 2 out of 3 tasks, and (2) as expected, performance degradation when too many demonstrations are removed. Similar analysis applies to the select- k setting. These results highlight two important points: First, the impact of dataset curation should not be judged by quality labels alone, but by the downstream performance of models trained on curated datasets. Second, determining how much data to curate (i.e., the k in filter- k and select- k) remains another key challenge for effective data curation in practice.

Performance versus Task Complexity: We evaluate curation performance across three RoboMimic tasks of increasing complexity—“Lift MH,” “Square MH,” and “Transport MH.” On the simplest task,

“Lift MH,” diffusion policies achieve 100% success despite training on all demonstrations, indicating that low-quality demonstrations have minimal impact and can be safely filtered. We observe a similar trend for the moderately difficult “Square MH” task, where the policy benefits from access to all demonstrations regardless of their quality. However, performance degrades more quickly as demonstrations are filtered, suggesting increased sensitivity to data quantity due to the task’s higher complexity relative to “Lift MH.” Finally, on the challenging “Transport MH” task, which requires precise bi-manual coordination, both CUPID and CUPID-QUALITY significantly outperform the base policy. These results suggest that curation of mixed-quality datasets is most beneficial for complex, precision-critical tasks, where training on lower-quality data is more likely to hinder performance.

B.3.2 Ablation on Number of Policy Rollouts in RoboMimic (§3.7.2)

We conduct an ablation study in RoboMimic evaluating the quality of datasets curated by CUPID and CUPID-QUALITY under varying numbers of rollouts, $m \in \{1, 5, 10, 25, 50, 100\}$. The results for state-based and image-based diffusion policies are shown in Fig. B.1 and Fig. B.2, respectively. For “Lift MH” and “Square MH,” performance influences (Eq. 3.3) stabilize around $m \in [25, 50]$, yielding quality trends similar to those obtained with $m = 100$. For “Transport MH,” quality trends continue to evolve until approximately $m \in [50, 100]$ rollouts, indicating that more rollouts are beneficial for accurate influence estimation in complex task settings—where curation has the greatest effect on performance.

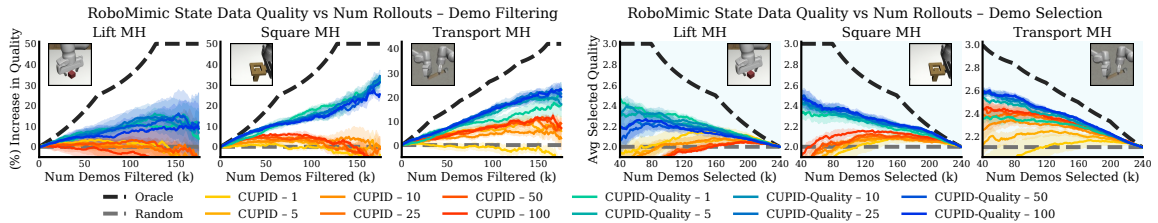


Figure B.1: RoboMimic state ablation: Data quality trends under varying number of rollouts. Performance influences (Eq. 3.3) converge around $m \in [25, 50]$ rollouts for “Lift MH” and “Square MH” (yielding similar quality trends), but continue to evolve until $m \in [50, 100]$ rollouts for “Transport MH.” Curation performed on state-based diffusion policies. Results are averaged over 3 random seeds. Errors bars represent the standard error.

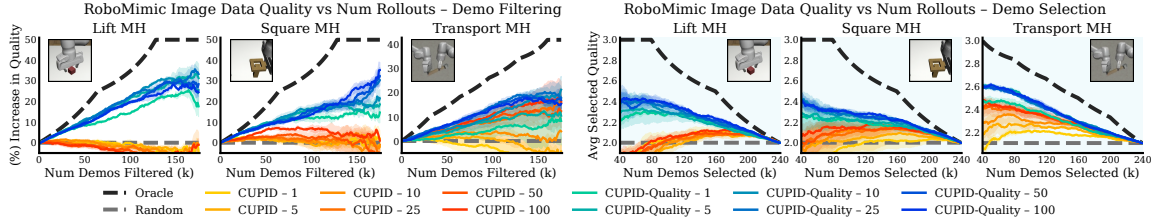


Figure B.2: RoboMimic image ablation: Data quality trends under varying number of rollouts. Performance influences (Eq. 3.3) converge around $m \in [25, 50]$ rollouts for “Lift MH” and “Square MH” (yielding similar quality trends), but continue to evolve until $m \in [50, 100]$ rollouts for “Transport MH.” Curation performed on image-based diffusion policies. Results are averaged over 3 random seeds. Errors bars represent the standard error.

B.3.3 Additional Data Quality Results in RoboMimic

We provide full data quality results in RoboMimic. Fig. B.3 is identical to the top row of Fig. 3.3 in the main text, but also includes data quality trends for select- k curation on “Lift MH.” Fig. B.4 shows data quality results for image-based diffusion policies. We do not retrain image-based policies on curated datasets (as in the bottom row of Fig. 3.3) due to the substantial computational resources required.

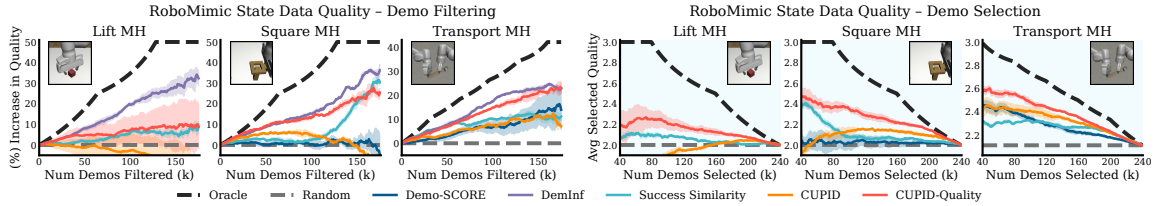


Figure B.3: RoboMimic state data quality results. Curation performed on state-based diffusion policies. Results are averaged over 3 random seeds. Errors bars represent the standard error.

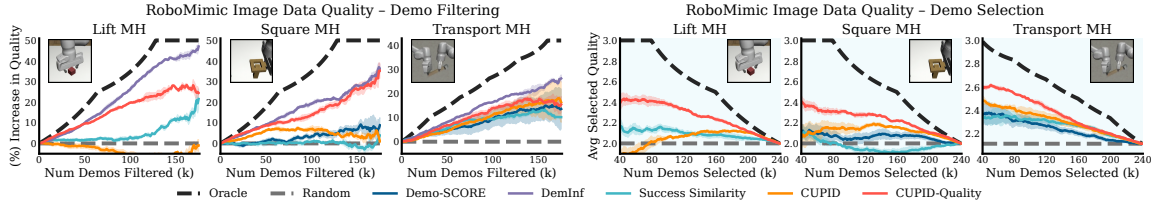
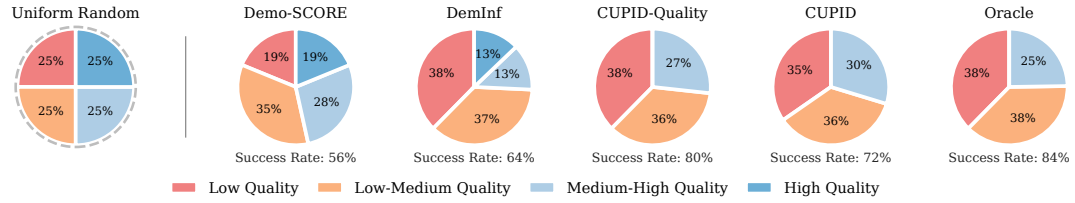
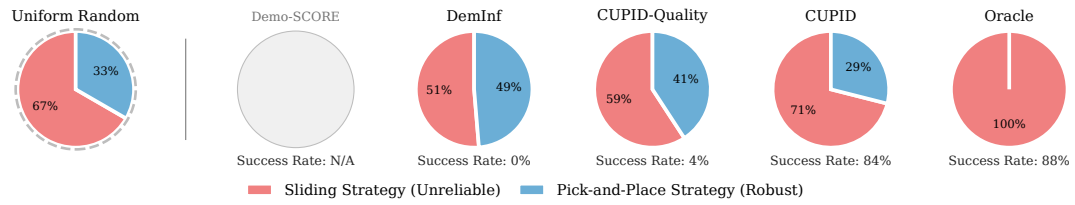


Figure B.4: RoboMimic image data quality results. Curation performed on image-based diffusion policies. Results are averaged over 3 random seeds. Errors bars represent the standard error.

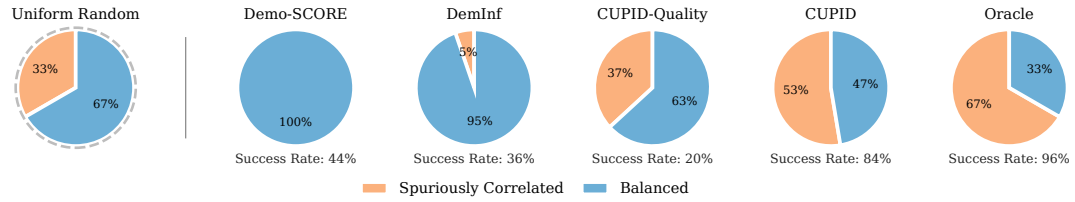
B.3.4 Data Filtering Curation Distributions in Franka Real-World



(a) **Figure-8:** Distribution of demonstrations *filtered*. Filtering lower-quality demos is better.



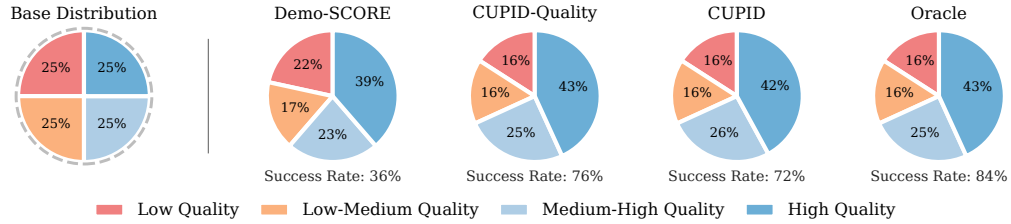
(b) **TuckBox:** Distribution of demonstrations *filtered*. Filtering sliding demos is better.



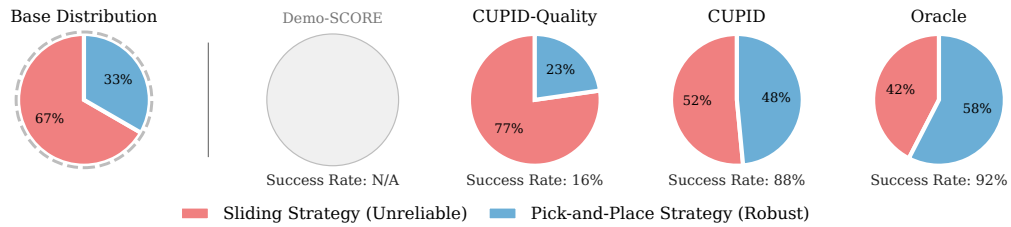
(c) **Bookshelf:** Distribution of demonstrations *filtered*. Filtering spurious correlations is better.

Figure B.5: Franka diffusion policy – distribution of demonstrations filtered (S^* in Task 1). See Fig. 3.5 for distributions of the corresponding curated datasets used for policy training.

B.3.5 Data Selection Curation Distributions in Franka Real-World

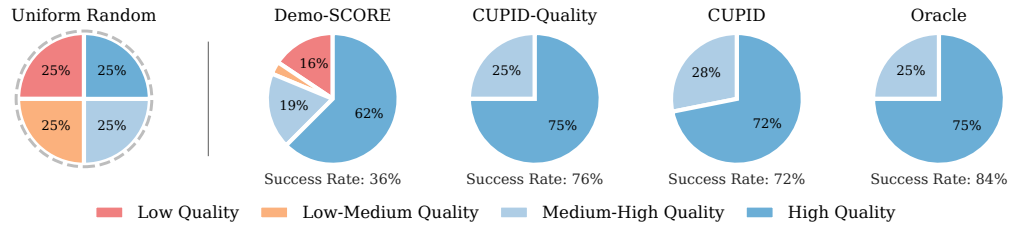


(a) **Figure-8:** Distribution of curated demonstrations after *selecting* 33%. Higher-quality demos are better.

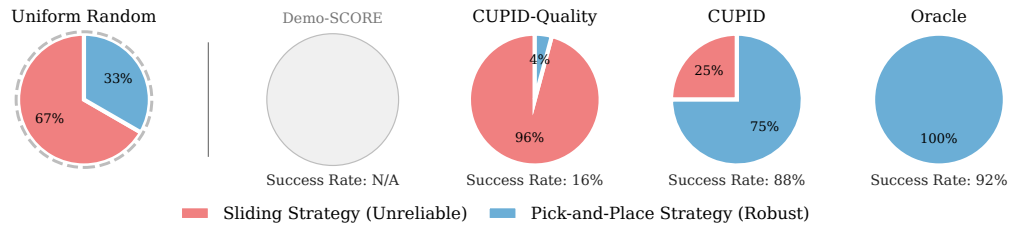


(b) **TuckBox:** Distribution of curated demonstrations after *selecting* 33%. Pick-and-place demos are better.

Figure B.6: **Franka diffusion policy curated dataset distributions for selection (Task 2).** CUPID selects higher-quality demonstrations (Figure-8) and robust strategies (TuckBox), improving policy performance across tasks (see Fig. 3.4). While curation heuristics employed by baselines may be effective in some cases (e.g., CUPID-QUALITY in Figure-8), they can lead to suboptimal selection in others.



(a) **Figure-8:** Distribution of demonstrations *selected*. Selecting higher-quality demos is better.



(b) **TuckBox:** Distribution of demonstrations *selected*. Selecting pick-and-place demos is better.

Figure B.7: **Franka diffusion policy – distribution of demonstrations selected (S^* in Task 2).** See Fig. B.6 for distributions of the corresponding curated datasets used for policy training.

B.3.6 Additional Results for Franka PI-0: Curated Dataset Transfer (§3.7.3)

Fig. B.8 contains the full results of our π_0 ablation (Fig. 3.7), including the performance of π_0 [25] trained on datasets curated by CUPID and CUPID-QUALITY for both the “Figure-8” and “TuckBox” tasks.

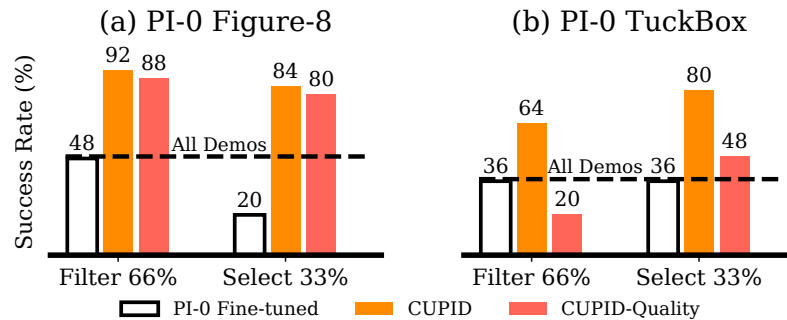


Figure B.8: Data curated for single-task diffusion policies improves π_0 [25] post-training performance. As in Fig. 3.4, quality measures (CUPID-QUALITY) may degrade performance when higher-quality demonstrations induce brittle strategies at test time (TuckBox), whereas curating based on performance (CUPID) is robust across settings.

In this experiment, we investigate two questions: (1) Can datasets curated with one policy architecture result in increased performance when used to train another policy with a different architecture? (2) How influential is curation for policies that have been pre-trained on large-scale multi-task datasets?

Curation Transfer: Towards the first question, Fig. B.8 shows that datasets curated using diffusion policies significantly increase the performance of fine-tuned π_0 policies relative to fine-tuning on the base, uncurated datasets. We attribute these results to two causes: First, we find that both the diffusion policy and π_0 have sufficient capacity to accurately fit the training data distribution, and thus, they should learn a similar behavior distribution from the training data. This implies that the observed performance gains in Fig. B.8 result from curation transfer between policies. Second, as the ‘‘TuckBox’’ experiment shows in Fig. 3.4(b), our method is able to effectively identify behaviors in the demonstration data that are not robust. While on-policy evaluations (i.e., rollouts) are necessary to identify such brittle behaviors, these are purely properties of the training demonstration data. Therefore, filtering out poor behaviors will increase the performance of any policy. Similarly, on the high-precision ‘‘Figure-8’’ task, filtering out more noisy, low-quality demonstrations is likely to improve performance for any policy.

VLA Robustness: Towards the second question, we find that even when the base policy is pre-trained on a large, diverse, multi-task dataset, curation is still essential to yield strong fine-tuned performance. As shown in Fig. B.8, π_0 policies trained on the base demonstration datasets are unable to reliably complete our tasks. In contrast, policies trained on curated datasets attain significantly higher success rates. As such, our results indicate that simply training VLM-based policies on more data and more tasks does not strictly result in pre-conditioned policies that use their generalist knowledge to ‘‘ignore’’ low-quality behaviors or brittle strategies in demonstration data—i.e., data curation still appears essential.

Concluding Remarks: Overall, these results indicate that using smaller, single-task policies to curate individual datasets, which may then benefit a larger, multi-task policy is a promising direction to alleviate the computational cost of applying our method to generalist policies. Still, we emphasize that datasets curated using our method are not completely *model agnostic*, as the same demonstrations may influence different models in different ways. As such, while π_0 achieves a higher base performance than the diffusion policy, the π_0 policies trained on curated datasets perform similarly to or slightly worse than the diffusion policies (for which those datasets were curated).

B.4 Derivations

B.4.1 Proof of **Proposition 2**

Proof. As presented in §3.3, applying the basic derivation of the influence function¹ in [147] gives us that

$$\begin{aligned}\Psi_{\pi\text{-inf}}(\xi) &:= \left. \frac{dJ(\pi_\theta)}{d\epsilon} \right|_{\epsilon=0} \\ &= -\nabla_\theta J(\pi_\theta)^\top \nabla_\theta^2 \mathcal{L}_{\text{bc}}(\theta; \mathcal{D})^{-1} \nabla_\theta \ell_{\text{traj}}(\xi; \pi_\theta).\end{aligned}$$

Next, note that the standard log-derivative trick underlying policy gradient methods [258, 283] tells us that

$$\nabla_\theta J(\pi_\theta) = \mathbb{E}_{\tau \sim p(\tau|\pi_\theta)} \left[R(\tau) \sum_{(s', a') \in \tau} \nabla_\theta \log \pi_\theta(a'|s') \right].$$

Therefore, since \mathcal{L}_{bc} and ℓ_{traj} are deterministic functions of θ , ξ , and \mathcal{D} , it holds that

$$\Psi_{\pi\text{-inf}}(\xi) = \mathbb{E}_{\tau \sim p(\tau|\pi_\theta)} \left[R(\tau) \sum_{(s', a') \in \tau} -\nabla_\theta \log \pi_\theta(a'|s')^\top H_{\text{bc}}^{-1} \nabla_\theta \ell_{\text{traj}}(\xi; \pi_\theta) \right]$$

by linearity of expectation. Finally, by simply noting that $\ell_{\text{traj}}(\xi; \pi_\theta) = \frac{1}{H} \sum_{(s,a) \in \xi} \ell(s, a; \theta)$ and applying the definition of $\Psi_{a\text{-inf}}$, we have the result:

$$\Psi_{\pi\text{-inf}}(\xi) = \mathbb{E}_{\tau \sim p(\tau|\pi_\theta)} \left[\frac{R(\tau)}{H} \sum_{(s', a') \in \tau} \sum_{(s,a) \in \xi} \Psi_{a\text{-inf}}((s', a'), (s, a)) \right].$$

□

B.4.2 Derivation of Performance Influence for Variable Length Trajectories

In §3.4 and §3.5, we assumed that all trajectories in the demonstration dataset \mathcal{D} were of an equal length H for notational simplicity. Here, we show that without loss of generality, our analysis extends to the case where the length of demonstration trajectories vary. Suppose each demonstration $\xi^i \in \mathcal{D}$ has length H^i , so that the base policy π_θ minimizes the average loss across all samples in the demonstration data, i.e.,

$$\theta = \arg \min_{\theta'} \{ \tilde{\mathcal{L}}_{\text{bc}}(\theta'; \mathcal{D}) := \frac{1}{(\sum_{i=1}^n H^i)} \sum_{\xi^i \in \mathcal{D}} \sum_{(s,a) \in \xi^i} \ell(s, a; \pi_{\theta'}) \}. \quad (\text{B.4})$$

Note that the objective in [Eq. B.4](#) is equivalent to an unweighted BC loss

$$\mathcal{L}'_{\text{bc}}(\theta'; \mathcal{D}) := \sum_{\xi^i \in \mathcal{D}} \sum_{(s,a) \in \xi^i} \ell(s, a; \pi_{\theta'}),$$

which decomposes into its unweighted trajectory losses $\ell'_{\text{traj}}(\xi; \pi_{\theta'}) := \sum_{(s,a) \in \xi} \ell(s, a; \pi_{\theta'})$, so that $\mathcal{L}'_{\text{bc}}(\theta', \mathcal{D}) = \sum_{\xi^i \in \mathcal{D}} \ell'_{\text{traj}}(\xi^i; \pi_{\theta'})$. We can then derive an equivalent statement to [Proposition 2](#) for the unweighted loss functions that applies when the demonstrations have variable length.

Proposition 4. *Assume that $\theta(\mathcal{D}) = \arg \min_{\theta'} \mathcal{L}'_{\text{bc}}(\theta'; \mathcal{D})$, that \mathcal{L}'_{bc} is twice differentiable in θ , and that $H_{\text{bc}} \succ 0$ is positive definite (i.e., $\theta(\mathcal{D})$ is not a saddle point)¹. Then, it holds that*

$$\Psi_{\pi\text{-inf}}(\xi) = \mathbb{E}_{\tau \sim p(\tau|\pi_{\theta})} \left[R(\tau) \sum_{(s',a') \in \tau} \sum_{(s,a) \in \xi} \Psi_{a\text{-inf}}((s', a'), (s, a)) \right]. \quad (\text{B.5})$$

Proof. As presented in [§3.3](#), applying the basic derivation of the influence function¹ in [\[147\]](#) gives us that

$$\begin{aligned} \Psi_{\pi\text{-inf}}(\xi) &:= \left. \frac{dJ(\pi_{\theta})}{d\epsilon} \right|_{\epsilon=0} \\ &= -\nabla_{\theta} J(\pi_{\theta})^{\top} \nabla_{\theta}^2 \mathcal{L}'_{\text{bc}}(\theta; \mathcal{D})^{-1} \nabla_{\theta} \ell'_{\text{traj}}(\xi; \pi_{\theta}). \end{aligned}$$

Next, note that the standard log-derivative trick underlying policy gradient methods [\[258, 283\]](#) tells us that

$$\nabla_{\theta} J(\pi_{\theta}) = \mathbb{E}_{\tau \sim p(\tau|\pi_{\theta})} \left[R(\tau) \sum_{(s',a') \in \tau} \nabla_{\theta} \log \pi_{\theta}(a'|s') \right].$$

Therefore, since \mathcal{L}'_{bc} and ℓ'_{traj} are deterministic functions of θ , ξ , and \mathcal{D} , it holds that

$$\Psi_{\pi\text{-inf}}(\xi) = \mathbb{E}_{\tau \sim p(\tau|\pi_{\theta})} \left[R(\tau) \sum_{(s',a') \in \tau} -\nabla_{\theta} \log \pi_{\theta}(a'|s')^{\top} H_{\text{bc}}^{-1} \nabla_{\theta} \ell'_{\text{traj}}(\xi; \pi_{\theta}) \right]$$

by linearity of expectation. Finally, by simply noting that $\ell'_{\text{traj}}(\xi; \pi_{\theta}) = \sum_{(s,a) \in \xi} \ell(s, a; \theta)$ and applying the definition of $\Psi_{a\text{-inf}}$, we have the result:

$$\Psi_{\pi\text{-inf}}(\xi) = \mathbb{E}_{\tau \sim p(\tau|\pi_{\theta})} \left[R(\tau) \sum_{(s',a') \in \tau} \sum_{(s,a) \in \xi} \Psi_{a\text{-inf}}((s', a'), (s, a)) \right].$$

□

Appendix C

Additional Details: STAP

Appendix – STAP: Sequencing Task-Agnostic Policies

The appendix discusses commonly asked questions about our planning framework and provides details on the manipulation skill library used for planning. Qualitative results and code are made available at <https://sites.google.com/stanford.edu/stap>.

C.1 Discussion and Limitations	121
C.2 Manipulation Skill Library	124
C.2.1 Parameterized Manipulation Primitives	124
C.2.2 Training Manipulation Skills	124

C.1 Discussion and Limitations

Q1: *What enables our planning framework to generalize to unseen tasks?*

A core hypothesis of this investigation is that it is easier to learn *task-agnostic skills* that support long-horizon reasoning than it is to learn a single *long-horizon policy* that can generalize to arbitrary tasks (i.e. skill sequences). This hypothesis is motivated by two facts: 1) the state-action space associated with all possible long-horizon skill sequences grows exponentially $O(c^H)$ with the length H of the skill sequences considered, where c is some constant; 2) adequately exploring this exponentially sized state-action space during the training of a single long-horizon policy, as required to solve arbitrary tasks, is challenging from both a methodology and engineering standpoint. In contrast, the state-action that must be sufficiently explored to plan with STAP grows only linearly $O(K)$ with the number of task-agnostic skills K in the skill library. However, it is essential that STAP’s task-agnostic skills are trained (at least in-part) on states that are likely to occur when solving tasks of interest.

Having learned a library of task-agnostic skills, our method plans with the skills at test-time to maximize the feasibility of a specified sequence of skills. Because the skills have been trained independent of each other and of the planner, every specified sequence of skills can be regarded as an *unseen task* that STAP must generalize to. Our method accomplishes this via optimization of a planning objective (see §4.4.1) in a process that involves the skills’ policies, Q-functions, and dynamics models. Thus, the generality of our method to unseen tasks stems from the compositionality of independently learned skills.

Q2: *Why is STAP useful for Integrated Task and Motion Planning?*

Task and Motion Planning (TAMP) seeks to solve long-horizon tasks by integrating symbolic and geometric reasoning. Symbolic task planners and PDDL are commonly used to produce candidate plan skeletons or skill sequences that satisfy a user-specified symbolic goal. Robotics subroutines, e.g. motion planners, collision checkers, inverse kinematics solvers, are then procedurally invoked to verify the feasibility of the plan skeleton and return a corresponding motion plan.

Different than prior work, STAP presents an avenue to develop general TAMP algorithms centered around learned skills. While in §4.3.1, we use STAP to perform geometric reasoning on candidate skill sequences proposed by a symbolic planner, many other instantiations are possible. For example, success probabilities (Eq. 4.3) predicted by STAP can serve as a geometric feasibility heuristic to guide task planning with classical search algorithms [112] or foundation models [2]. Such TAMP algorithms would inherit the efficiency of planning with STAP, as shown in Fig. 4.4. They would also benefit from the modularity associated with skill libraries, where new skills can be added to support a larger set of tasks and old skills can be updated to improve overall planning performance without the need to modify any other components of the TAMP framework.

Q3: *What would it take to scale STAP to high-dimensional observation spaces?*

Our framework is not limited to the low-dimensional state space described in §4.7, however, several challenges must be addressed in order to use STAP in conjunction with high-dimensional sensory data such as images or 3D point clouds.

- **Skills:** Q-functions must accurately characterize the skill’s success probability given the high-dimensional observation. Challenge: the fidelity of skill Q-functions obtained via model-free Reinforcement Learning (RL) [79, 100] may be too low for long-horizon planning. Potential solution(s): acquire skills from large-scale datasets and couple controllable, data-driven learning methods (e.g. offline RL, imitation learning, supervised learning) with data augmentation techniques.
- **Dynamics:** The planning state space (Eq. 4.2) must be amenable to accurate forward prediction over long-horizon skill sequences. Challenge: predicted high-dimensional states become coarse over long-horizons [76, 285] which complicates their use in manipulation planning settings that demand fine-grained geometric detail. Potential solution(s): leverage pretrained representations for robotics [138, 198] and learn latent dynamic models [102, 292] for forward prediction.

Since STAP is reliant on the quality of the underlying skill library, we expect the capabilities of our method to improve with advancements in robot skill acquisition and visuomotor policies, representation learning, and video prediction for robotics.

Q4: *How else can uncertainty quantification be incorporated into planning?*

In our TAMP experiments (§4.5), we take a filtering-based approach to robustify STAP planning in out-of-distribution scenarios. Specifically, we use Sketching Curvature for Out-of-Distribution Detection (SCOD) [239] for uncertainty quantification (UQ) of Q-functions and disregard the n plans with the most uncertain Q-values at each planning iteration.

While SCOD imposes no train-time dependencies on any algorithms in our framework, its forward pass is computationally and memory intensive and slows planning as a result. For faster planning, UQ alternatives such as deep ensembles [82] or Monte-Carlo dropout [80] can be employed which, in contrast to SCOD, require modifying the algorithms used to learn skills. We further note that the described filtering-based optimization approach can be substituted with more sophisticated planning techniques, several of which have been implemented and verified to work with STAP. For example, we could formulate a distributionally robust variant of our planning objective (Eq. 4.3) to optimize a lower-confidence bound of the Q-values:

$$J(a_{1:H}; \bar{s}_1) = \mathbb{E}_{\bar{s}_{2:H} \sim \bar{T}_{1:H-1}} \left[\prod_{h=1}^H Q_h(\Gamma_h(\bar{s}_h), a_h) - \alpha F_{\text{unc}}(\bar{s}_h, a_h; Q_h, \Gamma_h) \right],$$

where F_{unc} quantifies the uncertainty of Q-function Q_h evaluated at $s_h = \Gamma(\bar{s}_h)$ and a_h , and α is a scalar hyperparameter (e.g. the z-score). The uncertainty function F_{unc} is determined by the choice of UQ method. For deep ensembles, this would correspond to the empirical variance of the ensemble predictions $F_{\text{unc}}(\bar{s}_h, a_h; Q_h, \Gamma_h) = \text{Var}[Q_h(\Gamma_h(\bar{s}_h), a_h)]$. Other choices of F_{unc} include posterior predictive variances provided by SCOD or coherent risk measures such as Conditional Value at Risk (CVaR) [30]. We have experimentally validated such formulations of STAP, and ultimately, the appropriate choice of planning objective and optimization scheme should correspond to the evaluation tasks and domains of interest.

Q5: *What are the main limitations of our method?*

Currently, our method is limited in settings with high degrees of partial observability and stochastic dynamics. Examples include mobile manipulation in unknown environments and interacting with dynamic agents, where it may be intractable to predict future states necessary for look-ahead planning. While these tasks are beyond the scope of this investigation, we note that our method is agnostic to the specific choice of skills and dynamics models, and thus, components that account for stochasticity could be used interchangeably. Instead, we focus on generalization to geometrically challenging manipulation problems.

C.2 Manipulation Skill Library

C.2.1 Parameterized Manipulation Primitives

All variants of STAP interface with a library of manipulation skills $\mathcal{L} = \{\psi^1, \dots, \psi^K\}$. Each skill ψ consists of a learned policy $\pi(a | s)$ and a parameterized manipulation primitive [75] $\phi(a)$. The policy is trained to output parameters $a \sim \pi(a | s)$ that results in successful actuation of the primitive $\phi(a)$ in a contextual bandit setting (Eq. 4.1) with a binary reward function $R(s, a, s')$. Our library consists of four skills, $\mathcal{L} = \{\psi^{\text{Pick}}, \psi^{\text{Place}}, \psi^{\text{Pull}}, \psi^{\text{Push}}\}$, used to solve tasks in simulation and in the real-world. The policies must learn to manipulate objects with different geometries (e.g. π^{Pick} is used for both $\text{Pick}(\text{box})$ and $\text{Pick}(\text{hook})$). We describe the parameterization and reward function of each skill below. A reward of $r = 0$ is provided if any collision occurs with a non-argument object. For example, if ψ^{Place} collides with *rack* while executing $\text{Place}(\text{box}, \text{table})$.

- **Pick(*obj*)**: the parameter a represents the grasp pose of *obj* in the coordinate frame of *obj*. The policy π^{Pick} receives a reward of $r = 1$ if the primitive ϕ^{Pick} successfully grasps and picks up *obj*.
- **Place(*obj*, *rec*)**: the parameter a represents the placement pose of *obj* in the coordinate frame of *rec*. The policy π^{Place} receives a reward of $r = 1$ if the primitive ϕ^{Place} places *obj* stable atop *rec*.
- **Pull(*obj*, *tool*)**: the parameter a represents the initial position, direction, and distance of a pull on *obj* with *tool* in the coordinate frame of *obj*. The policy π^{Pull} receives a reward of $r = 1$ if the primitive ϕ^{Pull} moves *obj* toward the robot by a minimum of $0.05m$.
- **Push(*obj*, *tool*, *rec*)**: the parameter a represents the initial position, direction, and distance of a push on *obj* with *tool* in the coordinate frame of *obj*. The policy π^{Push} receives a reward of $r = 1$ if the primitive ϕ^{Push} moves *obj* away from the robot by a minimum of $0.05m$ and if the final pose of *obj* is underneath *rec*.

C.2.2 Training Manipulation Skills

We use the Soft Actor-Critic [100] (SAC) algorithm with original hyperparameters to simultaneously learn a stochastic policy $\pi(a | s)$ and Q-function $Q^\pi(s, a)$ for each skill ψ . All models are trained for $200k$ single-step episodes and the (s, a, s') transitions are stored in a replay buffer $\mathcal{D}^\psi = \{(s^i, a^i, s'^i)\}_{i=1}^{200k}$ for each skill ψ . The replay buffer data is later used to train the dynamics models $\bar{T}^k(\bar{s}, a^k)$ (§4.6.2) and calibrate the weights w^k used by SCOD for UQ (§4.6.3).

Appendix D

Additional Details: Text2Motion

Overview

The appendix offers additional details with respect to the implementation of **Text2Motion** and language planning baselines (§D.1), the experiments conducted (§D.2), derivations supporting the design of our algorithms (§D.3), and the **real-world planning demonstrations** (§D.4). Qualitative results are made available at <https://sites.google.com/stanford.edu/text2motion>.

D.1	Implementation Details	125
D.1.1	Learning Robot Skills and Dynamics	126
D.1.2	Out-of-Distribution Detection	128
D.1.3	Task Planning with LLMs	129
D.1.4	Geometric Feasibility Planning	129
D.2	Experiment Details	130
D.2.1	Scene Descriptions as Symbolic States	130
D.2.2	In-Context Examples	131
D.3	Derivations	134
D.3.1	Skill Usefulness Derivation	134
D.3.2	Skill Feasibility Derivation	135
D.4	Real World Demonstration	135
D.4.1	Hardware Setup	135
D.4.2	Real-World Robot Demonstration	136

D.1 Implementation Details

The **Text2Motion** planner integrates both **SHOOTING** and **GREEDY-SEARCH** to construct skill sequences that are feasible for the robot to execute in the environment. The planning procedure

relies on four core components: 1) a library of learned robot skills, 2) a method for detecting when a skill is out-of-distribution (OOD), 3) a large language model (LLM) to perform task-level planning, and 4) a geometric feasibility planner that is compatible with the learned robot skills. All evaluated language-based planners use the above components, while **SAYCAN-GS** and **INNERMONO-GS** are myopic agents that do not perform geometric feasibility planning. We provide implementation details of these components in the following subsections.

D.1.1 Learning Robot Skills and Dynamics

Skill library overview: All evaluated language planners interface an LLM with a library of robot skills $\mathcal{L} = \{\psi^1, \dots, \psi^N\}$. Each skill ψ has a language description (e.g. Pick(a)) and is associated with a parameterized manipulation primitive [75] $\phi(a)$. A primitive $\phi(a)$ is controllable via its *parameter* a which determines the motion [142] of the robot’s end-effector through a series of waypoints. For each skill ψ , we train a policy $\pi(a|s)$ to output parameters $a \in \mathcal{A}$ that maximize primitive’s $\phi(a)$ probability of success in a contextual bandit setting (Eq. 5.1) with a skill-specific binary reward function $R(s, a, s')$. We also train an ensemble of Q-functions $Q_{1:B}^\pi(s, a)$ and a dynamics model $T^\pi(s'|s, a)$ for each skill, both of which are required for geometric feasibility planning. We discuss the calibration of Q-function ensembles for OOD detection of skills in §D.1.2.

We learn four manipulation skills to solve tasks in simulation and in the real-world: ψ^{Pick} , ψ^{Place} , ψ^{Pull} , ψ^{Push} . Only a single policy per skill is trained, and thus, the policy must learn to engage the primitive over objects with differing geometries (e.g. π^{Pick} is used for both Pick(box) and Pick(hook)). The state space \mathcal{S} for each policy is defined as the concatenation of geometric state features (e.g. pose, size) of all objects in the scene, where the first n object states correspond to the n skill arguments and the rest are randomized. For example, the state for the skill Pick(hook) would have be a vector of all objects’ geometric state features with the first component of the state corresponding to the hook.

Parameterized manipulation primitives: We describe the parameters a and reward function $R(s, a, s')$ of each parameterized manipulation primitive $\phi(a)$ below. A collision with a non-argument object constitutes an execution failure for all skills, and as a result, the policy receives a reward of 0. For example, π^{Pick} would receive a reward of 0 if the robot collided with box during the execution of Pick(hook).

- Pick(obj): $a \sim \pi^{\text{Pick}}(a|s)$ denotes the grasp pose of obj *w.r.t* the coordinate frame of obj. A reward of 1 is received if the robot successfully grasps obj.
- Place(obj, rec): $a \sim \pi^{\text{Place}}(a|s)$ denotes the placement pose of obj *w.r.t* the coordinate frame of rec. A reward of 1 is received if obj is stably placed on rec.
- Pull(obj, tool): $a \sim \pi^{\text{Pull}}(a|s)$ denotes the initial position, direction, and distance of a pull on obj with tool *w.r.t* the coordinate frame of obj. A reward of 1 is received if obj moves toward

the robot by a minimum of $d_{\text{Pull}} = 0.05m$.

- Push(obj, tool, rec): $a \sim \pi^{\text{Push}}(a|s)$ denotes the initial position, direction, and distance of a push on obj with tool *w.r.t* the coordinate frame of obj. A reward of 1 is received if obj moves away from the robot by a minimum of $d_{\text{Push}} = 0.05m$ and if obj ends up underneath rec.

Dataset generation: All planners considered in Chapter 5 rely on accurate Q-functions $Q^\pi(s, a)$ to estimate the feasibility of skills proposed by the LLM. This places a higher fidelity requirement on the Q-functions than typically needed to learn a reliable policy, as the Q-functions must characterize both skill success (feasibility) and failure (infeasibility) at a given state. Because the primitives $\phi(a)$ reduce the horizon of policies $\pi(a|s)$ to a single timestep, and the reward functions are $R(s, a, s') \in \{0, 1\}$, the Q-functions can be interpreted as binary classifiers of state-action pairs. Thus, we take a staged approach to learning the Q-functions Q^π , followed by the policies π , and lastly the dynamics models T^π .

Scenes in our simulated environment are instantiated from a symbolic specification of objects and spatial relations, which together form a symbolic state. The goal is to learn a Q-function that sufficiently covers the state-action space of each skill. We generate a dataset that meets this requirement in four steps: a) enumerate all valid symbolic states; b) sample geometric scene instances s per symbolic state; c) uniformly sample actions over the action space $a \sim \mathcal{U}^{[0,1]^d}$; (d) simulate the states and actions to acquire next states s' and compute rewards $R(s, a, s')$. We slightly modify this sampling strategy to maintain a minimum success-failure ratio of 40%, as uniform sampling for more challenging skills such as Pull and Push seldom emits a success ($\sim 3\%$). We collect 1M (s, a, s', r) tuples per skill of which 800K of them are used for training (\mathcal{D}_t), while the remaining 200K are used for validation (\mathcal{D}_v). We use the same datasets to learn the Q-functions Q^π , policies π , and dynamics models T^π for each skill.

Model training: We train an ensemble of Q-functions with mini-batch gradient descent and logistic regression loss. Once the Q-functions have converged, we distill their returns into stochastic policies π through the maximum-entropy update [99]:

$$\pi^* \leftarrow \arg \max_{\pi} \mathbb{E}_{(s,a) \sim \mathcal{D}_t} [\min(Q_{1:B}^\pi(s, a)) - \alpha \log \pi(a|s)].$$

Instead of evaluating the policies on \mathcal{D}_v , which contains states for which no feasible action exists, the policies are synchronously evaluated in an environment that exhibits only feasible states. This simplifies model selection and standardizes skill capabilities across primitives. All Q-functions achieve precision and recall rates of over 95%. The average success rates of the converged policies over 100 evaluation episodes are: π_{Pick} with 99%, π_{Place} with 90%, π_{Pull} with 86%, π_{Push} with 97%.

We train a deterministic dynamics model per skill using the forward prediction loss:

$$L_{\text{dynamics}}(T^\pi; \mathcal{D}_t) = \mathbb{E}_{(s,a,s') \sim \mathcal{D}_t} \|T^\pi(s, a) - s'\|_2^2.$$

The dynamics models converge to within millimeter accuracy on the validation split.

Hyperparameters: The Q-functions, policies, and dynamics models are MLPs with hidden dimensions of size [256, 256] and ReLU activations. We train an ensemble of $B = 8$ Q-functions with a batch size of 128 and a learning rate of $1e^{-4}$ with a cosine annealing decay [173]. The Q-functions for Pick, Pull, and Push converged on \mathcal{D}_v in 3M iterations, while the Q-function for Place required 5M iterations. We hypothesize that this is because classifying successful placements demands carefully attending to the poses and shapes of all objects in the scene so as to avoid collisions. The policies are trained for 250K iterations with a batch size of 128 and a learning rate of $1e^{-4}$, leaving all other parameters the same as [99]. The dynamics models are trained for 750K iterations with a batch size of 512 and a learning rate of $5e^{-4}$; only on successful transitions to avoid the noise associated with collisions and truncated episodes. The parallelized training of all models takes approximately 12 hours on an Nvidia Quadro P5000 GPU and 2 CPUs per job.

D.1.2 Out-of-Distribution Detection

The training dataset described in §D.1.1 contain both successes and failures for symbolically valid skills like Pick(box). However, when using LLMs for robot task planning, it is often the case that the LLM will propose symbolically invalid skills, such as Pick(table), that neither the skill’s policy, Q-functions, or dynamics model have observed in training. We found that a percentage of out-of-distribution (OOD) queries would result in erroneously high Q-values, causing the invalid skill to be selected. Attempting to execute such a skill leads to control exceptions or other failures.

Whilst there are many existing techniques for OOD detection of deep neural networks, we opt to detect OOD queries on the learned Q-functions via deep ensembles due to their ease of calibration [154]. A state-action pair is classified as OOD if the empirical variance of the predicted Q-values is above a determined threshold:

$$F_{\text{OOD}}(\psi) = \mathbb{1} \left(\text{Var}_{i \sim 1:B} [Q_i^\pi(s, a)] \geq \epsilon^\psi \right),$$

where each threshold ϵ^ψ is unique to skill ψ .

To determine the threshold values, we generate an a calibration dataset of 100K symbolically invalid states and actions for each skill. The process takes less than an hour on a single CPU as the actions are infeasible and need not be simulated in the environment (i.e. rewards are known to be 0). We compute the mean and variance of the Q-ensemble for each (s, a) sample in both the training dataset (in-distribution inputs) and the calibration dataset (out-of-distribution inputs), and produce two histograms by binning the computed ensemble variances by the ensemble means. We observe that the histogram of variances corresponding to OOD inputs is uniform across all Q-value bins and

is an order of magnitude large than the ensemble variances computed over in-distribution inputs. This allows us to select thresholds ϵ^ψ which are low enough to reliably detect OOD inputs, yet will not be triggered for in-distribution inputs: $\epsilon^{\text{Pick}} = 0.10$, $\epsilon^{\text{Place}} = 0.12$, $\epsilon^{\text{Pull}} = 0.10$, and $\epsilon^{\text{Push}} = 0.06$.

D.1.3 Task Planning with LLMs

Text2Motion, **GREEDY-SEARCH**, and the myopic planning baselines **SAYCAN-GS** and **INNERMONO-GS** use `code-davinci-002` [36] to generate and score skills, while **SHOOTING** queries `text-davinci-003` [204] to directly output full skill sequences. In our experiments, we used a temperature setting of 0 for all LLM queries.

To maintain consistency in the evaluation of various planners, we allow **Text2Motion**, **SAYCAN-GS**, and **INNERMONO-GS** to generate $K = 5$ skills $\{\psi_t^1, \dots, \psi_t^K\}$ at each timestep t . Thus, every search iteration of **GREEDY-SEARCH** considers five possible extensions to the current running sequence of skills $\psi_{1:t-1}$. Similarly, **SHOOTING** generates $K = 5$ skill sequences.

As described in §5.4.3, skills are selected at each timestep t via a combined usefulness and geometric feasibility score:

$$\begin{aligned} S_{\text{skill}}(\psi_t) &= S_{\text{llm}}(\psi_t) \cdot S_{\text{geo}}(\psi_t) \\ &\approx p(\psi_t \mid i, s_{1:t}, \psi_{1:t-1}) \cdot Q^{\pi_t}(s_t, a_t^*), \end{aligned}$$

where **Text2Motion**, **GREEDY-SEARCH**, and **SHOOTING** use geometric feasibility planning (details below in §D.1.4) to compute $S_{\text{geo}}(\psi_t)$, while **SAYCAN-GS** and **INNERMONO-GS** use the current value function estimate $V^{\pi_t}(s_t) = \mathbb{E}_{a_t \sim \pi_t}[Q^{\pi_t}(s_t, a_t)]$. We find that in both cases, taking $S_{\text{llm}}(\psi_t)$ to be the SoftMax log-probability score produces a winner-takes-all effect, causing the planner to omit highly feasible skills simply because their associated log-probability was marginally lower than the LLM-likelihood of another skill. Thus, we dampen the SoftMax operation with a β -coefficient to balance the ranking of skills based on both feasibility and usefulness. We found $\beta = 0.3$ to work well.

D.1.4 Geometric Feasibility Planning

Given a sequence of skills $\psi_{1:H}$, geometric feasibility planning computes parameters $a_{1:H}$ that maximizes the success probability of the underlying sequence of primitives $\phi_{1:H}$. For example, given a skill sequence `Pick(hook)`, `Pull(box, hook)`, geometric feasibility planning would compute a 3D grasp position on the hook that enables a successful pull on the box thereafter.

Text2Motion is agnostic to the method that fulfils the role of geometric feasibility planning. In our experiments we leverage Sequencing Task-Agnostic Policies (STAP) [3]. Specifically, we consider the PolicyCEM variant of STAP, where optimization of the skill sequence’s success probability (Eq. 5.4) is warm started with parameters sampled from the policies $a_{1:H} \sim \pi_{1:H}$. We perform ten iterations of the Cross-Entropy Method [223], sampling 10K trajectories at each iteration and

Task ID	Properties	Instruction
Task 1	LH	How would you pick and place all of the boxes onto the rack?"
Task 2	LH + LG	How would you pick and place the yellow box and blue box onto the table, then use the hook to push the cyan box under the rack?"
Task 3	LH + PAP	How would you move three of the boxes to the rack?"
Task 4	LG + PAP	How would you put one box on the rack?"
Task 5	LH + LG + PAP	How would you get two boxes onto the rack?"
Task 6	LH + LG + PAP	How would you move two primary colored boxes to the rack?"

Table D.1: **TableEnv manipulation task suite**. We use the following shorthands as defined in [Chapter 5](#): LH: Long-Horizon, LG: Lifted Goals, PAP: Partial Affordance Perception. © 2023 Springer Nature.

selecting 10 elites to update the mean of the sampling distribution for the following iteration. The standard deviation of the sampling distribution is held constant at 0.3 for all iterations.

D.2 Experiment Details

We refer to [Table D.1](#) for an overview of the tasks in the TableEnv Manipulation suite.

D.2.1 Scene Descriptions as Symbolic States

For the remainder of this section, we use the following definitions of terms:

- **Predicate:** a binary-valued function over objects that evaluates to true or false (e.g. $\text{on}(a, b)$)
- **Spatial Relation:** a predicate grounded over objects that evaluates to true (e.g. $\text{on}(\text{rack}, \text{table})$)
- **Predicate Classifier:** a function that implements whether a predicate is true or false in the scene. We use hand-crafted predicate classifiers for each spatial relation we model
- **Symbolic State:** the set of all predicates that hold true in the scene
- **Satisfaction Function:** a binary-valued function that takes as input a geometric state, uses the predicate classifiers to detect what predicates hold true in the geometric state, and collects those predicates into a set to form a symbolic state. The satisfaction function evaluates to true if the predicted goals (predicates) hold in the symbolic state

To provide scene context to **Text2Motion** and the baselines, we take a heuristic approach to converting a geometric state s into a basic symbolic state. Symbolic states consist of combinations of one or more of the following predicates: $\text{on}(a, b)$, $\text{under}(a, b)$, and $\text{inhand}(a)$. $\text{inhand}(a) = \text{True}$ when the height of object a is above a predefined threshold. $\text{on}(a, b) = \text{True}$ when i) object a is

above b (determined by checking if the centroid of a’s axis-aligned bounding box is greater than b’s axis-aligned bounding box), ii) a’s bounding box intersects b’s bounding box, and iii) $\text{inhand}(a) = \text{False}$. $\text{under}(a, b) = \text{True}$ when $\text{on}(a, b) = \text{False}$ and a’s bounding box intersects b’s bounding box.

The proposed **goal prediction method** (§5.4.1) outputs goal propositions consisting of combinations of the predicates above which have been grounded over objects (i.e. spatial relations). As an example, for the natural language instruction “Put two of the boxes under the rack” and a symbolic state $[\text{on}(\text{red box}, \text{table}), \text{on}(\text{green box}, \text{rack}), \text{on}(\text{hook}, \text{rack}), \text{on}(\text{blue box}, \text{rack})]$, the LLM might predict the set of three goals $\{[\text{under}(\text{red box}, \text{rack}), \text{under}(\text{blue box}, \text{rack})], [\text{under}(\text{red box}, \text{rack}), \text{under}(\text{green box}, \text{rack})], [\text{under}(\text{green box}, \text{rack}), \text{under}(\text{blue box}, \text{rack})]\}$. We note that objects are neither specified as within or beyond the robot workspace, as we leave it to the skill’s Q-functions to determine feasibility (§D.1.1).

Since planning in high-dimensional observation spaces is not the focus of this investigation, we assume knowledge of objects in the scene and use hand-crafted heuristics to detect spatial relations between objects. There exists several techniques to convert high-dimensional observations into scene descriptions, such as the one used in [302]. We leave exploration of these options to future work.

D.2.2 In-Context Examples

For all experiments and methods, we use the following in-context examples to construct the prompt passed to the LLMs.

```
Available scene objects: ['table', 'hook', 'rack', 'yellow box', 'blue box', 'red box']
Object relationships: ['inhand(hook)', 'on(yellow box, table)', 'on(rack, table)', 'on(blue box, table)']
Human instruction: How would you push two of the boxes to be under the rack?
Goal predicate set: [['under(yellow box, rack)', 'under(blue box, rack)'], ['under(blue box, rack)', 'under(red box, rack)'], ['under(yellow box, rack)', 'under(red box, rack)']]
Top 1 robot action sequences: ['push(yellow box, hook, rack)', 'push(red box, hook, rack)']
```

```
Available scene objects: ['table', 'cyan box', 'hook', 'blue box', 'rack', 'red box']
Object relationships: ['on(hook, table)', 'on(rack, table)', 'on(blue box, table)', 'on(cyan box, table)', 'on(red box, table)']
Human instruction: How would you push all the boxes under the rack?
Goal predicate set: [['under(blue box, rack)', 'under(cyan box, rack)', 'under(red box, rack)']]
Top 1 robot action sequences: ['pick(blue box)', 'place(blue box, table)', 'pick(hook)', 'push(cyan box, hook, rack)', 'place(hook, table)', 'pick(blue box)', 'place(blue box, table)', 'pick(hook)', 'push(blue box, hook, rack)', 'push(red box, hook, rack)']
```

Available scene objects: ['table', 'cyan box', 'red box', 'hook', 'rack']
 Object relationships: ['on(hook, table)', 'on(rack, table)', 'on(cyan box, rack)', 'on(red box, rack)']
 Human instruction: put the hook on the rack and stack the cyan box above the rack - thanks
 Goal predicate set: [['on(hook, rack)', 'on(cyan box, rack)']]
 Top 1 robot action sequences: ['pick(hook)', 'pull(cyan box, hook)', 'place(hook, rack)', 'pick(cyan box)', 'place(cyan box, rack)']

Available scene objects: ['table', 'rack', 'hook', 'cyan box', 'yellow box', 'red box']
 Object relationships: ['on(yellow box, table)', 'on(rack, table)', 'on(cyan box, table)', 'on(hook, table)', 'on(red box, rack)']
 Human instruction: Pick up any box.
 Goal predicate set: [['inhand(yellow box)'], ['inhand(cyan box)']]
 Top 1 robot action sequences: ['pick(yellow box)']

Available scene objects: ['table', 'blue box', 'cyan box', 'hook', 'rack', 'red box', 'yellow box']
 Object relationships: ['inhand(hook)', 'on(red box, rack)', 'on(yellow box, table)', 'on(blue box, table)', 'on(cyan box, rack)', 'on(rack, table)']
 Human instruction: could you move all the boxes onto the rack?
 Goal predicate set: [['on(yellow box, rack)', 'on(blue box, rack)']]
 Top 1 robot action sequences: ['pull(yellow box, hook)', 'place(hook, table)', 'pick(yellow box)', 'place(yellow box, rack)', 'pick(blue box)', 'place(blue box, rack)']

Available scene objects: ['table', 'blue box', 'red box', 'hook', 'rack', 'yellow box']
 Object relationships: ['on(hook, table)', 'on(blue box, table)', 'on(rack, table)', 'on(red box, table)', 'on(yellow box, table)']
 Human instruction: situate an odd number greater than 1 of the boxes above the rack
 Goal predicate set: [['on(blue box, rack)', 'on(red box, rack)', 'on(yellow box, rack)']]
 Top 1 robot action sequences: ['pick(hook)', 'pull(blue box, hook)', 'place(hook, table)', 'pick(blue box)', 'place(blue box, rack)', 'pick(red box)', 'place(red box, rack)', 'pick(yellow box)', 'place(yellow box, rack)']

Available scene objects: ['table', 'cyan box', 'hook', 'red box', 'yellow box', 'rack', 'blue box']

Object relationships: ['on(hook, table)', 'on(red box, table)', 'on(blue box, table)', 'on(cyan box, table)', 'on(rack, table)', 'under(yellow box, rack)']

Human instruction: How would you get the cyan box under the rack and then ensure the hook is on the table?

Goal predicate set: [['under(cyan box, rack)', 'on(hook, table)']]

Top 1 robot action sequences: ['pick(blue box)', 'place(blue box, table)', 'pick(red box)', 'place(red box, table)', 'pick(hook)', 'push(cyan box, hook, rack)', 'place(hook, table)']

Available scene objects: ['table', 'cyan box', 'hook', 'yellow box', 'blue box', 'rack']

Object relationships: ['on(hook, table)', 'on(yellow box, rack)', 'on(rack, table)', 'on(cyan box, rack)']

Human instruction: set the hook on the rack and stack the yellow box onto the table and set the cyan box on the rack

Goal predicate set: [['on(hook, rack)', 'on(yellow box, table)', 'on(cyan box, rack)']]

Top 1 robot action sequences: ['pick(yellow box)', 'place(yellow box, table)', 'pick(hook)', 'pull(yellow box, hook)', 'place(hook, table)']

Available scene objects: ['table', 'cyan box', 'hook', 'rack', 'red box', 'blue box']

Object relationships: ['on(hook, table)', 'on(blue box, rack)', 'on(cyan box, table)', 'on(red box, table)', 'on(rack, table)']

Human instruction: Move the warm colored box to be underneath the rack.

Goal predicate set: [['under(red box, rack)']]

Top 1 robot action sequences: ['pick(blue box)', 'place(blue box, table)', 'pick(red box)', 'place(red box, table)', 'pick(hook)', 'push(red box, hook, rack)']

Available scene objects: ['table', 'blue box', 'hook', 'rack', 'red box', 'yellow box']

Object relationships: ['on(hook, table)', 'on(red box, table)', 'on(blue box, table)', 'on(yellow box, rack)', 'on(rack, table)']

Human instruction: Move the ocean colored box to be under the rack and ensure the hook ends up on the table.

Goal predicate set: [['under(blue box, rack)']]

Top 1 robot action sequences: ['pick(red box)', 'place(red box, table)', 'pick(yellow box)', 'place(yellow box, rack)', 'pick(hook)', 'push(blue box, hook, rack)', 'place(hook, table)']

```

Available scene objects: ['table', 'cyan box', 'hook', 'rack', 'red box', 'blue box']
Object relationships: ['on(hook, table)', 'on(cyan box, rack)', 'on(rack, table)', 'on(red
box, table)', 'inhand(blue box)']
Human instruction: How would you set the red box to be the only box on the rack?
Goal predicate set: [['on(red box, rack)', 'on(blue box, table)', 'on(cyan box, table)']]
Top 1 robot action sequences: ['place(blue box, table)', 'pick(hook)', 'pull(red box, hook)',
'place(hook, table)', 'pick(red box)', 'place(red box, rack)', 'pick(cyan box)', 'place(cyan
box, table)']

```

D.3 Derivations

We provide two derivations to support our approximation of the skill score S_{skill} (used to select skills while planning with **GREEDY-SEARCH** and **Text2Motion**) defined in Eq. 5.8. The skill score is expressed as a product of two terms:

$$S_{\text{skill}}(\psi_t) = p(\psi_t \mid i, s_1, \psi_{1:t-1}, r_{1:t-1}) \quad (\text{D.1})$$

$$p(r_t \mid i, s_1, \psi_{1:t}, r_{1:t-1}).$$

D.3.1 Skill Usefulness Derivation

Eq. 5.9 defines the first term in the skill score product to be the skill *usefulness* score S_{llm} . We derive the approximation of S_{llm} given in Eq. 5.10, which corresponds to quantity we use in our experiments.

$$S_{\text{llm}}(\psi_t) = p(\psi_t \mid i, s_1, \psi_{1:t-1}, r_{1:t-1})$$

$$= \int p(\psi_t \mid i, s_{1:t}, \psi_{1:t-1}, r_{1:t-1})$$

$$p(s_{2:t} \mid i, s_1, \psi_{1:t-1}, r_{1:t-1}) ds_{2:t}$$

$$= \mathbf{E}_{s_{2:t}} [p(\psi_t \mid i, s_{1:t}, \psi_{1:t-1}, r_{1:t-1})] \quad (\text{D.2})$$

$$\approx \mathbf{E}_{s_{2:t}} [p(\psi_t \mid i, s_{1:t}, \psi_{1:t-1})] \quad (\text{D.3})$$

$$\approx p(\psi_t \mid i, s_{1:t}, \psi_{1:t-1}) \quad (\text{D.4})$$

The final expression is given in Eq. D.4. Here, we compute a single sample Monte-Carlo estimate of Eq. D.3 under the future state trajectory $s_2 \sim T^{\pi_1}(\cdot \mid s_1, a_1^*), \dots, s_t \sim T^{\pi_{t-1}}(\cdot \mid s_{t-1}, a_{t-1}^*)$, where $a_{1:t-1}^*$ is computed by STAP [3]. The key insight is that future state trajectories $s_{2:t}$ are only ever sampled after STAP has performed geometric feasibility planning to maximize the *success probability* (Eq. 5.3) of the running plan $\psi_{1:t-1}$. By doing so, we ensure that the future states $s_{2:t}$ correspond to a successful execution of the running plan $\psi_{1:t-1}$, i.e. achieving positive rewards $r_{1:t-1}$. This

supports the independence assumption on rewards $r_{1:t-1}$ used to derive Eq. D.3 from Eq. D.2.

D.3.2 Skill Feasibility Derivation

Eq. 5.11 defines the second term in the skill score product (Eq. D.1) as the skill *feasibility* score S_{geo} . We derive the approximation provided in Eq. 5.12, which is the quantity we use in our experiments.

$$S_{\text{geo}}(\psi_t) = p(r_t \mid i, s_1, \psi_{1:t}, r_{1:t-1}) \quad (\text{D.5})$$

$$= p(r_t \mid s_1, \psi_{1:t}, r_{1:t-1}) \quad (\text{D.6})$$

$$= \int p(r_t \mid s_{1:t}, \psi_{1:t}, r_{1:t-1}) \\ p(s_{2:t} \mid s_1, \psi_{1:t}, r_{1:t-1}) ds_{2:t}$$

$$= \mathbb{E}_{s_{2:t}} [p(r_t \mid s_{1:t}, \psi_{1:t}, r_{1:t-1})] \quad (\text{D.7})$$

$$\approx \mathbb{E}_{s_{2:t}} [p(r_t \mid s_{1:t}, \psi_{1:t})] \quad (\text{D.8})$$

$$= \mathbb{E}_{s_{2:t}} [p(r_t \mid s_{1:t}, a_{1:t}^*)] \quad (\text{D.9})$$

$$= \mathbb{E}_{s_{2:t}} [p(r_t \mid s_t, a_t^*)] \quad (\text{D.10})$$

$$= \mathbb{E}_{s_{2:t}} [Q^{\pi_t}(s_t, a_t^*)] \quad (\text{D.11})$$

$$\approx Q^{\pi_t}(s_t, a_t^*) \quad (\text{D.12})$$

From Eq. D.5 to Eq. D.6, the reward r_t is conditionally independent of the instruction i given the initial state s_1 , running plan $\psi_{1:t}$, and previous rewards $r_{1:t-1}$. As described in §D.3.1, we can use STAP to make an independence assumption on the previous rewards $r_{1:t-1}$ between Eq. D.7 and Eq. D.8. The reward probability in Eq. D.8 depends on the parameters $a_{1:t}^*$ computed by STAP and fed to the underlying primitive sequence $\phi_{1:t}$, which gives Eq. D.9. Eq. D.10 comes from the Markov assumption, and can be reduced to Eq. D.11 by observing that the reward probability $p(r_t \mid s_t, a_t^*)$ is equal to the Q-value $Q^{\pi_t}(s_t, a_t^*)$ in the contextual bandit setting we consider. The final expression given in Eq. D.12, which represents a single sample Monte-Carlo estimate of Eq. D.11 under a sampled future state trajectory $s_2 \sim T^{\pi_1}(\cdot \mid s_1, a_1^*), \dots, s_t \sim T^{\pi_{t-1}}(\cdot \mid s_{t-1}, a_{t-1}^*)$.

D.4 Real World Demonstration

D.4.1 Hardware Setup

We use a Kinect V2 camera for RGB-D image capture and manually adjust the color thresholds to segment objects in the scene. Given the segmentation masks and the depth image, we can estimate object poses to construct the geometric state of the environment. For the skill library, we use the same set of policies, Q-functions, and dynamics models trained in simulation. We run robot experiments

on a Franka Panda robot manipulator.

D.4.2 Real-World Robot Demonstration

Demonstrations of **Text2Motion** operating on a real robot are made available at <https://sites.google.com/stanford.edu/text2motion>.

Bibliography

- [1] Constructions Aeronautiques, Adele Howe, Craig Knoblock, ISI Drew McDermott, Ashwin Ram, Manuela Veloso, Daniel Weld, David Wilkins SRI, Anthony Barrett, Dave Christianson, et al. Pddl| the planning domain definition language. *Technical Report, Tech. Rep.*, 1998.
- [2] Christopher Agia, Kevin Lin, Toki Migimatsu, Marco Pavone, and Jeannette Bohg. Text2motion: From natural language instructions to feasible plans. *Autonomous Robots*, 47(8):1345–1365, 2023.
- [3] Christopher Agia, Toki Migimatsu, Jiajun Wu, and Jeannette Bohg. Stap: Sequencing task-agnostic policies. In *2023 IEEE International Conference on Robotics and Automation (ICRA)*, pages 7951–7958. IEEE, 2023.
- [4] Christopher Agia, Rohan Sinha, Jingyun Yang, Rika Antonova, Marco Pavone, Haruki Nishimura, Masha Itkina, and Jeannette Bohg. Cupid: Curating data your robot loves with influence functions. In Joseph Lim, Shuran Song, and Hae-Won Park, editors, *Proceedings of The 9th Conference on Robot Learning*, volume 305 of *Proceedings of Machine Learning Research*, pages 2907–2932. PMLR, 27–30 Sep 2025.
- [5] Christopher Agia, Rohan Sinha, Jingyun Yang, Ziang Cao, Rika Antonova, Marco Pavone, and Jeannette Bohg. Unpacking failure modes of generative policies: Runtime monitoring of consistency and progress. In Pulkit Agrawal, Oliver Kroemer, and Wolfram Burgard, editors, *Proceedings of The 8th Conference on Robot Learning*, volume 270 of *Proceedings of Machine Learning Research*, pages 689–723. PMLR, 06–09 Nov 2025.
- [6] Michael Ahn, Anthony Brohan, Noah Brown, Yevgen Chebotar, Omar Cortes, Byron David, Chelsea Finn, Keerthana Gopalakrishnan, Karol Hausman, Alex Herzog, et al. Do as i can, not as i say: Grounding language in robotic affordances. *arXiv preprint arXiv:2204.01691*, 2022.
- [7] Anurag Ajay, Aviral Kumar, Pulkit Agrawal, Sergey Levine, and Ofir Nachum. Opal: Offline primitive discovery for accelerating offline reinforcement learning. *International Conference on Learning Representations (ICLR)*, 2021.

- [8] Alon Albalak, Yanai Elazar, Sang Michael Xie, Shayne Longpre, Nathan Lambert, Xinyi Wang, Niklas Muennighoff, Bairu Hou, Liangming Pan, Haewon Jeong, Colin Raffel, Shiyu Chang, Tatsunori Hashimoto, and William Yang Wang. A survey on data selection for language models. *Transactions on Machine Learning Research*, 2024. ISSN 2835-8856. URL <https://openreview.net/forum?id=XfHWcNTShp>.
- [9] Barrett Ames, Allison Thackston, and George Konidaris. Learning symbolic representations for planning with parameterized skills. In *2018 IEEE/RSJ International Conference on Intelligent Robots and Systems (IROS)*, pages 526–533. IEEE, 2018.
- [10] Anastasios N Angelopoulos and Stephen Bates. A gentle introduction to conformal prediction and distribution-free uncertainty quantification. *arXiv preprint arXiv:2107.07511*, 2021.
- [11] Stanislaw Antol, Aishwarya Agrawal, Jiasen Lu, Margaret Mitchell, Dhruv Batra, C Lawrence Zitnick, and Devi Parikh. Vqa: Visual question answering. In *Proceedings of the IEEE international conference on computer vision*, pages 2425–2433, 2015.
- [12] Pasquale Antonante, David I. Spivak, and Luca Carlone. Monitoring and diagnosability of perception systems. In *2021 IEEE/RSJ International Conference on Intelligent Robots and Systems (IROS)*, pages 168–175, 2021. doi: 10.1109/IROS51168.2021.9636497.
- [13] Brenna D Argall, Sonia Chernova, Manuela Veloso, and Brett Browning. A survey of robot learning from demonstration. *Robotics and autonomous systems*, 57(5):469–483, 2009.
- [14] Pierre-Luc Bacon, Jean Harb, and Doina Precup. The option-critic architecture. In *Proceedings of the AAAI Conference on Artificial Intelligence*, volume 31, 2017.
- [15] Juhan Bae, Nathan Ng, Alston Lo, Marzyeh Ghassemi, and Roger B Grosse. If influence functions are the answer, then what is the question? *Advances in Neural Information Processing Systems*, 35:17953–17967, 2022.
- [16] Shikhar Bahl, Mustafa Mukadam, Abhinav Gupta, and Deepak Pathak. Neural dynamic policies for end-to-end sensorimotor learning. *Advances in Neural Information Processing Systems*, 33:5058–5069, 2020.
- [17] Shikhar Bahl, Abhinav Gupta, and Deepak Pathak. Hierarchical neural dynamic policies. *Robotics: Science and Systems*, 2021.
- [18] Andrea Bajcsy, Dylan P Losey, Marcia K O’Malley, and Anca D Dragan. Learning from physical human corrections, one feature at a time. In *Proceedings of the 2018 ACM/IEEE International Conference on Human-Robot Interaction*, pages 141–149, 2018.

- [19] Jose Barreiros, Andrew Beaulieu, Aditya Bhat, Rick Cory, Eric Cousineau, Hongkai Dai, Ching-Hsin Fang, Kunimatsu Hashimoto, Muhammad Zubair Irshad, Masha Itkina, et al. A careful examination of large behavior models for multitask dexterous manipulation. *arXiv preprint arXiv:2507.05331*, 2025.
- [20] Samyadeep Basu, Phil Pope, and Soheil Feizi. Influence functions in deep learning are fragile. In *International Conference on Learning Representations*, 2021. URL <https://openreview.net/forum?id=xHKVVHGDOEk>.
- [21] Suneel Belkhale, Yuchen Cui, and Dorsa Sadigh. Data quality in imitation learning. *Advances in neural information processing systems*, 36:80375–80395, 2023.
- [22] Suneel Belkhale, Tianli Ding, Ted Xiao, Pierre Sermanet, Quan Vuong, Jonathan Tompson, Yevgen Chebotar, Debidatta Dwibedi, and Dorsa Sadigh. RT-H: Action Hierarchies using Language. In *Proceedings of Robotics: Science and Systems*, Delft, Netherlands, July 2024. doi: 10.15607/RSS.2024.XX.049.
- [23] Homanga Bharadhwaj, Jay Vakil, Mohit Sharma, Abhinav Gupta, Shubham Tulsiani, and Vikash Kumar. Roboagent: Generalization and efficiency in robot manipulation via semantic augmentations and action chunking, 2023.
- [24] Julien Bidot, Lars Karlsson, Fabien Lagriffoul, and Alessandro Saffiotti. Geometric backtracking for combined task and motion planning in robotic systems. *Artificial Intelligence*, 247:229–265, 2017.
- [25] Kevin Black, Noah Brown, Danny Driess, Adnan Esmail, Michael Equi, Chelsea Finn, Niccolo Fusai, Lachy Groom, Karol Hausman, Brian Ichter, et al. $\pi 0$: A vision-language-action flow model for general robot control. URL <https://arxiv.org/abs/2410.24164>, 2024.
- [26] Rishi Bommasani, Drew A Hudson, Ehsan Adeli, Russ Altman, Simran Arora, Sydney von Arx, Michael S Bernstein, Jeannette Bohg, Antoine Bosselut, Emma Brunskill, et al. On the opportunities and risks of foundation models. *arXiv preprint arXiv:2108.07258*, 2021.
- [27] Blai Bonet and Héctor Geffner. Planning as heuristic search. *Artificial Intelligence*, 129(1-2): 5–33, 2001.
- [28] Francesco Borrelli, Alberto Bemporad, and Manfred Morari. *Predictive Control for Linear and Hybrid Systems*. Cambridge University Press, 2017.
- [29] Anthony Brohan, Noah Brown, Justice Carbajal, Yevgen Chebotar, Joseph Dabis, Chelsea Finn, Keerthana Gopalakrishnan, Karol Hausman, Alexander Herzog, Jasmine Hsu, Julian Ibarz, Brian Ichter, Alex Irpan, Tomas Jackson, Sally Jesmonth, Nikhil Joshi, Ryan Julian, Dmitry Kalashnikov, Yuheng Kuang, Isabel Leal, Kuang-Huei Lee, Sergey Levine, Yao Lu,

- Utsav Malla, Deeksha Manjunath, Igor Mordatch, Ofir Nachum, Carolina Parada, Jodilyn Peralta, Emily Perez, Karl Pertsch, Jornell Quiambao, Kanishka Rao, Michael S Ryoo, Grecia Salazar, Pannag R Sanketi, Kevin Sayed, Jaspiar Singh, Sumedh Sontakke, Austin Stone, Clayton Tan, Huong Tran, Vincent Vanhoucke, Steve Vega, Quan H Vuong, Fei Xia, Ted Xiao, Peng Xu, Sichun Xu, Tianhe Yu, and Brianna Zitkovich. RT-1: Robotics Transformer for Real-World Control at Scale. In *Proceedings of Robotics: Science and Systems*, Daegu, Republic of Korea, July 2023. doi: 10.15607/RSS.2023.XIX.025.
- [30] Daniel Brown, Scott Niekum, and Marek Petrik. Bayesian robust optimization for imitation learning. *Advances in Neural Information Processing Systems*, 33:2479–2491, 2020.
- [31] Tom Brown, Benjamin Mann, Nick Ryder, Melanie Subbiah, Jared D Kaplan, Prafulla Dhariwal, Arvind Neelakantan, Pranav Shyam, Girish Sastry, Amanda Askell, et al. Language models are few-shot learners. *Advances in neural information processing systems*, 33:1877–1901, 2020.
- [32] Yevgen Chebotar, Karol Hausman, Yao Lu, Ted Xiao, Dmitry Kalashnikov, Jake Varley, Alex Irpan, Benjamin Eysenbach, Ryan Julian, Chelsea Finn, et al. Actionable models: Unsupervised offline reinforcement learning of robotic skills. *International Conference on Machine Learning*, 2021.
- [33] Annie S Chen, Alec M Lessing, Yuejiang Liu, and Chelsea Finn. Curating demonstrations using online experience. *arXiv preprint arXiv:2503.03707*, 2025.
- [34] Boyuan Chen, Fei Xia, Brian Ichter, Kanishka Rao, Keerthana Gopalakrishnan, Michael S Ryoo, Austin Stone, and Daniel Kappler. Open-vocabulary queryable scene representations for real world planning. *arXiv preprint arXiv:2209.09874*, 2022.
- [35] Boyuan Chen, Zhuo Xu, Sean Kirmani, Brian Ichter, Dorsa Sadigh, Leonidas Guibas, and Fei Xia. Spatialvlm: Endowing vision-language models with spatial reasoning capabilities. In *Proceedings of the IEEE/CVF Conference on Computer Vision and Pattern Recognition*, pages 14455–14465, 2024.
- [36] Mark Chen, Jerry Tworek, Heewoo Jun, Qiming Yuan, Henrique Ponde de Oliveira Pinto, Jared Kaplan, Harri Edwards, Yuri Burda, Nicholas Joseph, Greg Brockman, et al. Evaluating large language models trained on code. *arXiv preprint arXiv:2107.03374*, 2021.
- [37] Yangyi Chen, Lifan Yuan, Ganqu Cui, Zhiyuan Liu, and Heng Ji. A close look into the calibration of pre-trained language models. *arXiv preprint arXiv:2211.00151*, 2022.
- [38] Yuxin Chen, Jianglan Wei, Chenfeng Xu, Boyi Li, Masayoshi Tomizuka, Andrea Bajcsy, and Ran Tian. Reimagination with test-time observation interventions: Distractor-robust world model predictions for visual model predictive control. *arXiv preprint arXiv:2506.16565*, 2025.

- [39] Ho Kei Cheng, Seoung Wug Oh, Brian Price, Alexander Schwing, and Joon-Young Lee. Tracking anything with decoupled video segmentation. In *Proceedings of the IEEE/CVF International Conference on Computer Vision*, pages 1316–1326, 2023.
- [40] Cheng Chi, Zhenjia Xu, Siyuan Feng, Eric Cousineau, Yilun Du, Benjamin Burchfiel, Russ Tedrake, and Shuran Song. Diffusion policy: Visuomotor policy learning via action diffusion. *The International Journal of Robotics Research*, page 02783649241273668, 2023.
- [41] Cheng Chi, Zhenjia Xu, Chuer Pan, Eric Cousineau, Benjamin Burchfiel, Siyuan Feng, Russ Tedrake, and Shuran Song. Universal manipulation interface: In-the-wild robot teaching without in-the-wild robots. In *Proceedings of Robotics: Science and Systems (RSS)*, 2024.
- [42] Rohan Chitnis, Shubham Tulsiani, Saurabh Gupta, and Abhinav Gupta. Efficient bimanual manipulation using learned task schemas. In *2020 IEEE International Conference on Robotics and Automation (ICRA)*, pages 1149–1155. IEEE, 2020.
- [43] Rohan Chitnis, Tom Silver, Beomjoon Kim, Leslie Kaelbling, and Tomas Lozano-Perez. Camps: Learning context-specific abstractions for efficient planning in factored mdps. In *Conference on Robot Learning*, pages 64–79. PMLR, 2021.
- [44] Rohan Chitnis, Tom Silver, Joshua B Tenenbaum, Tomas Lozano-Perez, and Leslie Pack Kaelbling. Learning neuro-symbolic relational transition models for bilevel planning. In *2022 IEEE/RSJ International Conference on Intelligent Robots and Systems (IROS)*, pages 4166–4173. IEEE, 2022.
- [45] Sang Keun Choe, Hwijeen Ahn, Juhan Bae, Kewen Zhao, Minsoo Kang, Youngseog Chung, Adithya Pratapa, Willie Neiswanger, Emma Strubell, Teruko Mitamura, et al. What is your data worth to gpt? llm-scale data valuation with influence functions. *arXiv preprint arXiv:2405.13954*, 2024.
- [46] Kurtland Chua, Roberto Calandra, Rowan McAllister, and Sergey Levine. Deep reinforcement learning in a handful of trials using probabilistic dynamics models. *Advances in neural information processing systems*, 31, 2018.
- [47] Open X-Embodiment Collaboration, Abby O’Neill, Abdul Rehman, Abhiram Maddukuri, Abhishek Gupta, Abhishek Padalkar, Abraham Lee, Acorn Pooley, Agrim Gupta, Ajay Mandlekar, Ajinkya Jain, Albert Tung, Alex Bewley, Alex Herzog, Alex Irpan, Alexander Khazatsky, Anant Rai, Anchit Gupta, Andrew Wang, Andrey Kolobov, Anikait Singh, Animesh Garg, Aniruddha Kembhavi, Annie Xie, Anthony Brohan, Antonin Raffin, Archit Sharma, Arefeh Yavary, Arhan Jain, Ashwin Balakrishna, Azyaan Wahid, Ben Burgess-Limerick, Beomjoon Kim, Bernhard Schölkopf, Blake Wulfe, Brian Ichter, Cewu Lu, Charles Xu, Charlotte Le, Chelsea Finn, Chen Wang, Chenfeng Xu, Cheng Chi, Chenguang Huang, Christine Chan,

Christopher Agia, Chuer Pan, Chuyuan Fu, Coline Devin, Danfei Xu, Daniel Morton, Danny Driess, Daphne Chen, Deepak Pathak, Dhruv Shah, Dieter Büchler, Dinesh Jayaraman, Dmitry Kalashnikov, Dorsa Sadigh, Edward Johns, Ethan Foster, Fangchen Liu, Federico Ceola, Fei Xia, Feiyu Zhao, Felipe Vieira Frujeri, Freek Stulp, Gaoyue Zhou, Gaurav S. Sukhatme, Gautam Salhotra, Ge Yan, Gilbert Feng, Giulio Schiavi, Glen Berseth, Gregory Kahn, Guangwen Yang, Guanzhi Wang, Hao Su, Hao-Shu Fang, Haochen Shi, Henghui Bao, Heni Ben Amor, Henrik I Christensen, Hiroki Furuta, Homer Walke, Hongjie Fang, Huy Ha, Igor Mordatch, Ilija Radosavovic, Isabel Leal, Jacky Liang, Jad Abou-Chakra, Jaehyung Kim, Jaimyn Drake, Jan Peters, Jan Schneider, Jasmine Hsu, Jeannette Bohg, Jeffrey Bingham, Jeffrey Wu, Jensen Gao, Jiaheng Hu, Jiajun Wu, Jialin Wu, Jiankai Sun, Jianlan Luo, Jiayuan Gu, Jie Tan, Jihoon Oh, Jimmy Wu, Jingpei Lu, Jingyun Yang, Jitendra Malik, João Silvério, Joey Hejna, Jonathan Booher, Jonathan Tompson, Jonathan Yang, Jordi Salvador, Joseph J. Lim, Junhyek Han, Kaiyuan Wang, Kanishka Rao, Karl Pertsch, Karol Hausman, Keegan Go, Keerthana Gopalakrishnan, Ken Goldberg, Kendra Byrne, Kenneth Oslund, Kento Kawaharazuka, Kevin Black, Kevin Lin, Kevin Zhang, Kiana Ehsani, Kiran Lekkala, Kirsty Ellis, Krishan Rana, Krishnan Srinivasan, Kuan Fang, Kunal Pratap Singh, Kuo-Hao Zeng, Kyle Hatch, Kyle Hsu, Laurent Itti, Lawrence Yunliang Chen, Lerrel Pinto, Li Fei-Fei, Liam Tan, Linxi "Jim" Fan, Lionel Ott, Lisa Lee, Luca Weihs, Magnum Chen, Marion Lepert, Marius Memmel, Masayoshi Tomizuka, Masha Itkina, Mateo Guaman Castro, Max Spero, Maximilian Du, Michael Ahn, Michael C. Yip, Mingtong Zhang, Mingyu Ding, Minhho Heo, Mohan Kumar Srirama, Mohit Sharma, Moo Jin Kim, Naoaki Kanazawa, Nicklas Hansen, Nicolas Heess, Nikhil J Joshi, Niko Suenderhauf, Ning Liu, Norman Di Palo, Nur Muhammad Mahi Shafullah, Oier Mees, Oliver Kroemer, Osbert Bastani, Pannag R Sanketi, Patrick "Tree" Miller, Patrick Yin, Paul Wohlhart, Peng Xu, Peter David Fagan, Peter Mitrano, Pierre Sermanet, Pieter Abbeel, Priya Sundaesan, Qiuyu Chen, Quan Vuong, Rafael Rafailov, Ran Tian, Ria Doshi, Roberto Mart'in-Mart'in, Rohan Bajjal, Rosario Scalise, Rose Hendrix, Roy Lin, Runjia Qian, Ruohan Zhang, Russell Mendonca, Rutav Shah, Ryan Hoque, Ryan Julian, Samuel Bustamante, Sean Kirmani, Sergey Levine, Shan Lin, Sherry Moore, Shikhar Bahl, Shivin Dass, Shubham Sonawani, Shuran Song, Sichun Xu, Siddhant Haldar, Siddharth Karamcheti, Simeon Adebola, Simon Guist, Soroush Nasiriany, Stefan Schaal, Stefan Welker, Stephen Tian, Subramanian Ramamoorthy, Sudeep Dasari, Suneel Belkhale, Sungjae Park, Suraj Nair, Suvir Mirchandani, Takayuki Osa, Tanmay Gupta, Tatsuya Harada, Tatsuya Matsushima, Ted Xiao, Thomas Kollar, Tianhe Yu, Tianli Ding, Todor Davchev, Tony Z. Zhao, Travis Armstrong, Trevor Darrell, Trinity Chung, Vidhi Jain, Vincent Vanhoucke, Wei Zhan, Wenxuan Zhou, Wolfram Burgard, Xi Chen, Xiangyu Chen, Xiaolong Wang, Xinghao Zhu, Xinyang Geng, Xiyuan Liu, Xu Liangwei, Xuanlin Li, Yansong Pang, Yao Lu, Yecheng Jason Ma, Yejin Kim, Yevgen Chebotar, Yifan Zhou, Yifeng Zhu, Yilin Wu, Ying Xu, Yixuan Wang, Yonatan Bisk, Yongqiang Dou, Yoonyoung Cho,

- Youngwoon Lee, Yuchen Cui, Yue Cao, Yueh-Hua Wu, Yujin Tang, Yuke Zhu, Yunchu Zhang, Yunfan Jiang, Yunshuang Li, Yunzhu Li, Yusuke Iwasawa, Yutaka Matsuo, Zehan Ma, Zhuo Xu, Zichen Jeff Cui, Zichen Zhang, Zipeng Fu, and Zipeng Lin. Open X-Embodiment: Robotic learning datasets and RT-X models. In *2024 IEEE International Conference on Robotics and Automation (ICRA)*, pages 6892–6903, 2024. doi: 10.1109/ICRA57147.2024.10611477.
- [48] Yuchen Cui, David Isele, Scott Niekum, and Kikuo Fujimura. Uncertainty-aware data aggregation for deep imitation learning. In *2019 International Conference on Robotics and Automation (ICRA)*, pages 761–767. IEEE, 2019.
- [49] Yuchen Cui, Scott Niekum, Abhinav Gupta, Vikash Kumar, and Aravind Rajeswaran. Can foundation models perform zero-shot task specification for robot manipulation? In *Learning for dynamics and control conference*, pages 893–905. PMLR, 2022.
- [50] Yuchen Cui, Siddharth Karamcheti, Raj Palleti, Nidhya Shivakumar, Percy Liang, and Dorsa Sadigh. No, to the right: Online language corrections for robotic manipulation via shared autonomy. In *Proceedings of the 2023 ACM/IEEE International Conference on Human-Robot Interaction*, pages 93–101, 2023.
- [51] Aidan Curtis, Xiaolin Fang, Leslie Pack Kaelbling, Tomás Lozano-Pérez, and Caelan Reed Garrett. Long-horizon manipulation of unknown objects via task and motion planning with estimated affordances. In *2022 International Conference on Robotics and Automation (ICRA)*, pages 1940–1946. IEEE, 2022.
- [52] Aidan Curtis, Tom Silver, Joshua B Tenenbaum, Tomás Lozano-Pérez, and Leslie Kaelbling. Discovering state and action abstractions for generalized task and motion planning. In *Proceedings of the AAAI Conference on Artificial Intelligence*, volume 36, pages 5377–5384, 2022.
- [53] Bruno Da Silva, George Konidaris, and Andrew Barto. Learning parameterized skills. *International Conference on Machine Learning (ICML)*, 2012.
- [54] Bruno Da Silva, George Konidaris, and Andrew Barto. Active learning of parameterized skills. In *International Conference on Machine Learning*, pages 1737–1745. PMLR, 2014.
- [55] Shreyansh Daftry, Sam Zeng, J. Andrew Bagnell, and Martial Hebert. Introspective perception: Learning to predict failures in vision systems. *2016 IEEE/RSJ International Conference on Intelligent Robots and Systems (IROS)*, pages 1743–1750, 2016. URL <https://api.semanticscholar.org/CorpusID:15394788>.
- [56] Yinpei Dai, Jayjun Lee, Nima Fazeli, and Joyce Chai. Racer: Rich language-guided failure recovery policies for imitation learning. *arXiv preprint arXiv:2409.14674*, 2024.

- [57] Murtaza Dalal, Deepak Pathak, and Russ R Salakhutdinov. Accelerating robotic reinforcement learning via parameterized action primitives. *Advances in Neural Information Processing Systems*, 34:21847–21859, 2021.
- [58] Murtaza Dalal, Ajay Mandlekar, Caelan Garrett, Ankur Handa, Ruslan Salakhutdinov, and Dieter Fox. Imitating task and motion planning with visuomotor transformers. *arXiv preprint arXiv:2305.16309*, 2023.
- [59] Neil T Dantam, Zachary K Kingston, Swarat Chaudhuri, and Lydia E Kavraki. Incremental task and motion planning: A constraint-based approach. In *Robotics: Science and systems*, AnnArbor, Michigan, June 2016. doi: 10.15607/RSS.2016.XII.002.
- [60] Shivin Dass, Alaa Khaddaj, Logan Engstrom, Aleksander Madry, Andrew Ilyas, and Roberto Martín-Martín. Datamil: Selecting data for robot imitation learning with datamodels. *arXiv preprint arXiv:2505.09603*, 2025.
- [61] Pim De Haan, Dinesh Jayaraman, and Sergey Levine. Causal confusion in imitation learning. *Advances in neural information processing systems*, 32, 2019.
- [62] Danny Driess, Ozgur Oguz, and Marc Toussaint. Hierarchical task and motion planning using logic-geometric programming (hlgp). In *RSS Workshop on Robust Task and Motion Planning*, 2019.
- [63] Danny Driess, Jung-Su Ha, and Marc Toussaint. Deep visual reasoning: Learning to predict action sequences for task and motion planning from an initial scene image. *Robotics: Science and Systems*, 2020.
- [64] Danny Driess, Ozgur Oguz, Jung-Su Ha, and Marc Toussaint. Deep visual heuristics: Learning feasibility of mixed-integer programs for manipulation planning. In *2020 IEEE International Conference on Robotics and Automation (ICRA)*, pages 9563–9569. IEEE, 2020.
- [65] Danny Driess, Jung-Su Ha, Russ Tedrake, and Marc Toussaint. Learning geometric reasoning and control for long-horizon tasks from visual input. In *2021 IEEE International Conference on Robotics and Automation (ICRA)*, pages 14298–14305. IEEE, 2021.
- [66] Danny Driess, Jung-Su Ha, and Marc Toussaint. Learning to solve sequential physical reasoning problems from a scene image. *The International Journal of Robotics Research*, 40(12-14): 1435–1466, 2021.
- [67] Danny Driess, Zhiao Huang, Yunzhu Li, Russ Tedrake, and Marc Toussaint. Learning multi-object dynamics with compositional neural radiance fields. In *Proceedings of The 6th Conference on Robot Learning*, volume 205 of *Proceedings of Machine Learning Research*, pages 1755–1768. PMLR, 14–18 Dec 2023.

- [68] Danny Driess, Fei Xia, Mehdi SM Sajjadi, Corey Lynch, Aakanksha Chowdhery, Brian Ichter, Ayzaan Wahid, Jonathan Tompson, Quan Vuong, Tianhe Yu, et al. Palm-e: An embodied multimodal language model. *arXiv preprint arXiv:2303.03378*, 2023.
- [69] Yuqing Du, Ksenia Konyushkova, Misha Denil, Akhil Raju, Jessica Landon, Felix Hill, Nando de Freitas, and Serkan Cabi. Vision-language models as success detectors. In Sarath Chandar, Razvan Pascanu, Hanie Sedghi, and Doina Precup, editors, *Proceedings of The 2nd Conference on Lifelong Learning Agents*, volume 232 of *Proceedings of Machine Learning Research*, pages 120–136. PMLR, 22–25 Aug 2023. URL <https://proceedings.mlr.press/v232/du23b.html>.
- [70] Jiafei Duan, Wilbert Pumacay, Nishanth Kumar, Yi Ru Wang, Shulin Tian, Wentao Yuan, Ranjay Krishna, Dieter Fox, Ajay Mandlekar, and Yijie Guo. Aha: A vision-language-model for detecting and reasoning over failures in robotic manipulation. In Y. Yue, A. Garg, N. Peng, F. Sha, and R. Yu, editors, *International Conference on Learning Representations*, volume 2025, pages 45493–45517, 2025. URL https://proceedings.iclr.cc/paper_files/paper/2025/file/70a06501001e1820fd1eb9ee821302d2-Paper-Conference.pdf.
- [71] Amine Elhafsi, Rohan Sinha, Christopher Agia, Edward Schmerling, Issa AD Nesnas, and Marco Pavone. Semantic anomaly detection with large language models. *Autonomous Robots*, 47(8):1035–1055, 2023.
- [72] Logan Engstrom, Axel Feldmann, and Aleksander Madry. Dsdm: Model-aware dataset selection with datamodels. In *International Conference on Machine Learning*, pages 12491–12526. PMLR, 2024.
- [73] Logan Engstrom, Andrew Ilyas, Benjamin Chen, Axel Feldmann, William Moses, and Aleksander Madry. Optimizing ml training with metagradient descent. *arXiv preprint arXiv:2503.13751*, 2025.
- [74] Alec Farid, David Snyder, Allen Z. Ren, and Anirudha Majumdar. Failure Prediction with Statistical Guarantees for Vision-Based Robot Control. In *Proceedings of Robotics: Science and Systems*, New York City, NY, USA, June 2022. doi: 10.15607/RSS.2022.XVIII.042.
- [75] Javier Felip, Janne Laaksonen, Antonio Morales, and Ville Kyrki. Manipulation primitives: A paradigm for abstraction and execution of grasping and manipulation tasks. *Robotics and Autonomous Systems*, 61(3):283–296, 2013.
- [76] Chelsea Finn and Sergey Levine. Deep visual foresight for planning robot motion. In *2017 IEEE International Conference on Robotics and Automation (ICRA)*, pages 2786–2793. IEEE, 2017.
- [77] Peter Florence, Lucas Manuelli, and Russ Tedrake. Self-supervised correspondence in visuomotor policy learning. *IEEE Robotics and Automation Letters*, 5(2):492–499, 2019.

- [78] Zipeng Fu, Tony Z. Zhao, and Chelsea Finn. Mobile aloha: Learning bimanual mobile manipulation with low-cost whole-body teleoperation. In *arXiv*, 2024.
- [79] Scott Fujimoto, Herke Hoof, and David Meger. Addressing function approximation error in actor-critic methods. In *International conference on machine learning*, pages 1587–1596. PMLR, 2018.
- [80] Yarin Gal and Zoubin Ghahramani. Dropout as a bayesian approximation: Representing model uncertainty in deep learning. In Maria Florina Balcan and Kilian Q. Weinberger, editors, *Proceedings of The 33rd International Conference on Machine Learning*, volume 48 of *Proceedings of Machine Learning Research*, pages 1050–1059, New York, New York, USA, 20–22 Jun 2016. PMLR. URL <https://proceedings.mlr.press/v48/gal16.html>.
- [81] Milan Ganai, Rohan Sinha, Christopher Agia, Daniel Morton, Luigi Di Lillo, and Marco Pavone. Real-time out-of-distribution failure prevention via multi-modal reasoning. In Joseph Lim, Shuran Song, and Hae-Won Park, editors, *Proceedings of The 9th Conference on Robot Learning*, volume 305 of *Proceedings of Machine Learning Research*, pages 283–308. PMLR, 27–30 Sep 2025. URL <https://proceedings.mlr.press/v305/ganai25a.html>.
- [82] M.A. Ganaie, Minghui Hu, A.K. Malik, M. Tanveer, and P.N. Suganthan. Ensemble deep learning: A review. *Engineering Applications of Artificial Intelligence*, 115:105151, 2022. ISSN 0952-1976. doi: <https://doi.org/10.1016/j.engappai.2022.105151>.
- [83] Kanishk Gandhi, Siddharth Karamcheti, Madeline Liao, and Dorsa Sadigh. Eliciting compatible demonstrations for multi-human imitation learning. In Karen Liu, Dana Kulic, and Jeff Ichnowski, editors, *Proceedings of The 6th Conference on Robot Learning*, volume 205 of *Proceedings of Machine Learning Research*, pages 1981–1991. PMLR, 14–18 Dec 2023.
- [84] Jensen Gao, Bidipta Sarkar, Fei Xia, Ted Xiao, Jiajun Wu, Brian Ichter, Anirudha Majumdar, and Dorsa Sadigh. Physically grounded vision-language models for robotic manipulation. In *2024 IEEE International Conference on Robotics and Automation (ICRA)*, pages 12462–12469. IEEE, 2024.
- [85] Jensen Gao, Suneel Belkhale, Sudeep Dasari, Ashwin Balakrishna, Dhruv Shah, and Dorsa Sadigh. A taxonomy for evaluating generalist robot manipulation policies. *IEEE Robotics and Automation Letters*, 2026.
- [86] Caelan Reed Garrett, Tomás Lozano-Pérez, and Leslie Pack Kaelbling. Pddlstream: Integrating symbolic planners and blackbox samplers via optimistic adaptive planning. In *Proceedings of the International Conference on Automated Planning and Scheduling*, volume 30, pages 440–448, 2020.

- [87] Caelan Reed Garrett, Rohan Chitnis, Rachel Holladay, Beomjoon Kim, Tom Silver, Leslie Pack Kaelbling, and Tomás Lozano-Pérez. Integrated task and motion planning. *Annual review of control, robotics, and autonomous systems*, 4:265–293, 2021.
- [88] Kristian Georgiev, Joshua Vendrow, Hadi Salman, Sung Min Park, and Aleksander Madry. The journey, not the destination: How data guides diffusion models. *arXiv preprint arXiv:2312.06205*, 2023.
- [89] Kristian Georgiev, Roy Rinberg, Sung Min Park, Shivam Garg, Andrew Ilyas, Aleksander Madry, and Seth Neel. Attribute-to-delete: Machine unlearning via datamodel matching. In *The Thirteenth International Conference on Learning Representations*, 2025. URL <https://openreview.net/forum?id=3vXpZp0n29>.
- [90] Amirata Ghorbani and James Zou. Data shapley: Equitable valuation of data for machine learning. In *International conference on machine learning*, pages 2242–2251. PMLR, 2019.
- [91] Catherine Glossop, William Chen, Arjun Bhorkar, Dhruv Shah, and Sergey Levine. Cast: Counterfactual labels improve instruction following in vision-language-action models. *arXiv preprint arXiv:2508.13446*, 2025.
- [92] Ken Goldberg. Good old-fashioned engineering can close the 100,000-year “data gap” in robotics, 2025.
- [93] Ankit Goyal, Jie Xu, Yijie Guo, Valts Blukis, Yu-Wei Chao, and Dieter Fox. Rvt: Robotic view transformer for 3d object manipulation. In *Conference on Robot Learning*, pages 694–710. PMLR, 2023.
- [94] Mark S Graham, Walter HL Pinaya, Petru-Daniel Tudosiu, Parashkev Nachev, Sebastien Ourselin, and Jorge Cardoso. Denoising diffusion models for out-of-distribution detection. In *Proceedings of the IEEE/CVF Conference on Computer Vision and Pattern Recognition*, pages 2947–2956, 2023.
- [95] Evan Greensmith, Peter L Bartlett, and Jonathan Baxter. Variance reduction techniques for gradient estimates in reinforcement learning. *Journal of Machine Learning Research*, 5(Nov): 1471–1530, 2004.
- [96] Arthur Gretton, Ralf Herbrich, Alexander Smola, Olivier Bousquet, Bernhard Schölkopf, et al. Kernel methods for measuring independence. *Journal of Machine Learning Research*, 6(70): 2075–2129, 2005. URL <http://jmlr.org/papers/v6/gretton05a.html>.
- [97] Roger Grosse, Juhan Bae, Cem Anil, Nelson Elhage, Alex Tamkin, Amirhossein Tajdini, Benoit Steiner, Dustin Li, Esin Durmus, Ethan Perez, et al. Studying large language model generalization with influence functions. *arXiv preprint arXiv:2308.03296*, 2023.

- [98] Qiao Gu, Yuanliang Ju, Shengxiang Sun, Igor Gilitschenski, Haruki Nishimura, Masha Itkina, and Florian Shkurti. Safe: Multitask failure detection for vision-language-action models. *arXiv preprint arXiv:2506.09937*, 2025.
- [99] Tuomas Haarnoja, Aurick Zhou, Pieter Abbeel, and Sergey Levine. Soft actor-critic: Off-policy maximum entropy deep reinforcement learning with a stochastic actor. In Jennifer Dy and Andreas Krause, editors, *Proceedings of the 35th International Conference on Machine Learning*, volume 80 of *Proceedings of Machine Learning Research*, pages 1861–1870. PMLR, 10–15 Jul 2018. URL <https://proceedings.mlr.press/v80/haarnoja18b.html>.
- [100] Tuomas Haarnoja, Aurick Zhou, Kristian Hartikainen, George Tucker, Sehoon Ha, Jie Tan, Vikash Kumar, Henry Zhu, Abhishek Gupta, Pieter Abbeel, et al. Soft actor-critic algorithms and applications. *International Conference on Machine Learning*, 2018.
- [101] Danijar Hafner, Timothy Lillicrap, Ian Fischer, Ruben Villegas, David Ha, Honglak Lee, and James Davidson. Learning latent dynamics for planning from pixels. In *International conference on machine learning*, pages 2555–2565. PMLR, 2019.
- [102] Danijar Hafner, Timothy Lillicrap, Jimmy Ba, and Mohammad Norouzi. Dream to control: Learning behaviors by latent imagination. *International Conference on Learning Representations (ICLR)*, 2020.
- [103] Zayd Hammoudeh and Daniel Lowd. Training data influence analysis and estimation: A survey. *Machine Learning*, 113(5):2351–2403, 2024.
- [104] Asher J Hancock, Allen Z Ren, and Anirudha Majumdar. Run-time observation interventions make vision-language-action models more visually robust. In *2025 IEEE International Conference on Robotics and Automation (ICRA)*, pages 9499–9506. IEEE, 2025.
- [105] Bear Häon, Kaylene Caswell Stocking, Ian Chuang, and Claire Tomlin. Mechanistic interpretability for steering vision-language-action models. In *Conference on Robot Learning*, pages 2743–2762. PMLR, 2025.
- [106] Kaiming He, Xiangyu Zhang, Shaoqing Ren, and Jian Sun. Deep residual learning for image recognition. In *Proceedings of the IEEE conference on computer vision and pattern recognition*, pages 770–778, 2016.
- [107] Patrick Hegemann, Tim Zechmeister, Markus Grotz, Kevin Hitzler, and Tamim Asfour. Learning symbolic failure detection for grasping and mobile manipulation tasks. In *2022 IEEE/RSJ International Conference on Intelligent Robots and Systems (IROS)*, pages 4302–4309. IEEE, 2022.

- [108] Joey Hejna, Chethan Anand Bhateja, Yichen Jiang, Karl Pertsch, and Dorsa Sadigh. Remix: Optimizing data mixtures for large scale imitation learning. In Pulkit Agrawal, Oliver Kroemer, and Wolfram Burgard, editors, *Proceedings of The 8th Conference on Robot Learning*, volume 270 of *Proceedings of Machine Learning Research*, pages 145–164. PMLR, 06–09 Nov 2025.
- [109] Joey Hejna, Suvir Mirchandani, Ashwin Balakrishna, Annie Xie, Ayzaan Wahid, Jonathan Tompson, Pannag Sanketi, Dhruv Shah, Coline Devin, and Dorsa Sadigh. Robot data curation with mutual information estimators. *arXiv preprint arXiv:2502.08623*, 2025.
- [110] Malte Helmert. The fast downward planning system. *Journal of Artificial Intelligence Research*, 26:191–246, 2006.
- [111] Jonathan Ho, Ajay Jain, and Pieter Abbeel. Denoising diffusion probabilistic models. *Advances in neural information processing systems*, 33:6840–6851, 2020.
- [112] Jörg Hoffmann. Ff: The fast-forward planning system. *AI magazine*, 22(3):57–57, 2001.
- [113] Ryan Hoque, Ashwin Balakrishna, Ellen Novoseller, Albert Wilcox, Daniel S. Brown, and Ken Goldberg. Thriftydagger: Budget-aware novelty and risk gating for interactive imitation learning. In Aleksandra Faust, David Hsu, and Gerhard Neumann, editors, *Proceedings of the 5th Conference on Robot Learning*, volume 164 of *Proceedings of Machine Learning Research*, pages 598–608. PMLR, 08–11 Nov 2022. URL <https://proceedings.mlr.press/v164/hoque22a.html>.
- [114] Edward J Hu, Yelong Shen, Phillip Wallis, Zeyuan Allen-Zhu, Yuanzhi Li, Shean Wang, Lu Wang, Weizhu Chen, et al. Lora: Low-rank adaptation of large language models. *ICLR*, 1(2):3, 2022.
- [115] De-An Huang, Suraj Nair, Danfei Xu, Yuke Zhu, Animesh Garg, Li Fei-Fei, Silvio Savarese, and Juan Carlos Niebles. Neural task graphs: Generalizing to unseen tasks from a single video demonstration. In *Proceedings of the IEEE/CVF conference on computer vision and pattern recognition*, pages 8565–8574, 2019.
- [116] De-An Huang, Danfei Xu, Yuke Zhu, Animesh Garg, Silvio Savarese, Li Fei-Fei, and Juan Carlos Niebles. Continuous relaxation of symbolic planner for one-shot imitation learning. In *2019 IEEE/RSJ International Conference on Intelligent Robots and Systems (IROS)*, pages 2635–2642. IEEE, 2019.
- [117] Wenlong Huang, Pieter Abbeel, Deepak Pathak, and Igor Mordatch. Language models as zero-shot planners: Extracting actionable knowledge for embodied agents. *arXiv preprint arXiv:2201.07207*, 2022.

- [118] Wenlong Huang, Fei Xia, Ted Xiao, Harris Chan, Jacky Liang, Pete Florence, Andy Zeng, Jonathan Tompson, Igor Mordatch, Yevgen Chebotar, Pierre Sermanet, Tomas Jackson, Noah Brown, Linda Luu, Sergey Levine, Karol Hausman, and brian ichter. Inner monologue: Embodied reasoning through planning with language models. In Karen Liu, Dana Kulic, and Jeff Ichnowski, editors, *Proceedings of The 6th Conference on Robot Learning*, volume 205 of *Proceedings of Machine Learning Research*, pages 1769–1782. PMLR, 14–18 Dec 2023. URL <https://proceedings.mlr.press/v205/huang23c.html>.
- [119] Auke Jan Ijspeert, Jun Nakanishi, and Stefan Schaal. Movement imitation with nonlinear dynamical systems in humanoid robots. In *Proceedings 2002 IEEE International Conference on Robotics and Automation (Cat. No. 02CH37292)*, volume 2, pages 1398–1403. IEEE, 2002.
- [120] Andrew Ilyas and Logan Engstrom. Magic: Near-optimal data attribution for deep learning. *arXiv preprint arXiv:2504.16430*, 2025.
- [121] Andrew Ilyas, Sung Min Park, Logan Engstrom, Guillaume Leclerc, and Aleksander Madry. Datamodels: Understanding predictions with data and data with predictions. In Kamalika Chaudhuri, Stefanie Jegelka, Le Song, Csaba Szepesvari, Gang Niu, and Sivan Sabato, editors, *Proceedings of the 39th International Conference on Machine Learning*, volume 162 of *Proceedings of Machine Learning Research*, pages 9525–9587. PMLR, 17–23 Jul 2022.
- [122] Arda Inceoglu, Eren Erdal Aksoy, Abdullah Cihan Ak, and Sanem Sariel. Fino-net: A deep multimodal sensor fusion framework for manipulation failure detection. In *2021 IEEE/RSJ International Conference on Intelligent Robots and Systems (IROS)*, pages 6841–6847, 2021. doi: 10.1109/IROS51168.2021.9636455.
- [123] Physical Intelligence, Ali Amin, Raichelle Aniceto, Ashwin Balakrishna, Kevin Black, Ken Conley, Grace Connors, James Darpinian, Karan Dhabalia, Jared DiCarlo, et al. $\pi_{0.6}^*$: A v1a that learns from experience. *arXiv preprint arXiv:2511.14759*, 2025.
- [124] Physical Intelligence, Kevin Black, Noah Brown, James Darpinian, Karan Dhabalia, Danny Driess, Adnan Esmail, Michael Equi, Chelsea Finn, Niccolo Fusai, et al. $\pi_{0.5}$: A vision-language-action model with open-world generalization. *arXiv preprint arXiv:2504.16054*, 2025.
- [125] Eric Jang, Alex Irpan, Mohi Khansari, Daniel Kappler, Frederik Ebert, Corey Lynch, Sergey Levine, and Chelsea Finn. BC-z: Zero-shot task generalization with robotic imitation learning. In *5th Annual Conference on Robot Learning*, 2021. URL <https://openreview.net/forum?id=8kbp23tSGYv>.
- [126] Michael Janner, Justin Fu, Marvin Zhang, and Sergey Levine. When to trust your model: Model-based policy optimization. *Advances in Neural Information Processing Systems*, 32, 2019.

- [127] Krishna Murthy Jatavallabhula, Alihusein Kuwajerwala, Qiao Gu, Mohd Omama, Tao Chen, Shuang Li, Ganesh Iyer, Soroush Saryazdi, Nikhil Keetha, Ayush Tewari, Joshua B. Tenenbaum, Celso Miguel de Melo, Madhava Krishna, Liam Paull, Florian Shkurti, and Antonio Torralba. Conceptfusion: Open-set multimodal 3d mapping. In *RSS*, 2023.
- [128] Yunfan Jiang, Agrim Gupta, Zichen Zhang, Guanzhi Wang, Yongqiang Dou, Yanjun Chen, Li Fei-Fei, Anima Anandkumar, Yuke Zhu, and Linxi Fan. Vima: General robot manipulation with multimodal prompts. *arXiv preprint arXiv:2210.03094*, 2022.
- [129] William B Johnson, Joram Lindenstrauss, et al. Extensions of lipschitz mappings into a hilbert space. *Contemporary mathematics*, 26(189-206):1, 1984.
- [130] L. Kaelbling, M. Littman, and A. Moore. Reinforcement learning: A survey. *Journal of Artificial Intelligence Research*, 4:237–285, 1996.
- [131] Leslie P Kaelbling and Tomás Lozano-Pérez. Integrated robot task and motion planning in the now. Technical report, MASSACHUSETTS INST OF TECH CAMBRIDGE COMPUTER SCIENCE AND ARTIFICIAL . . . , 2012.
- [132] Leslie Pack Kaelbling and Tomás Lozano-Pérez. Hierarchical task and motion planning in the now. In *2011 IEEE International Conference on Robotics and Automation*, pages 1470–1477. IEEE, 2011. doi: 10.1109/ICRA.2011.5980391.
- [133] Leslie Pack Kaelbling and Tomás Lozano-Pérez. Learning composable models of parameterized skills. In *2017 IEEE International Conference on Robotics and Automation (ICRA)*, pages 886–893. IEEE, 2017.
- [134] Dmitry Kalashnikov, Alex Irpan, Peter Pastor, Julian Ibarz, Alexander Herzog, Eric Jang, Deirdre Quillen, Ethan Holly, Mrinal Kalakrishnan, Vincent Vanhoucke, et al. Scalable deep reinforcement learning for vision-based robotic manipulation. In *Conference on Robot Learning*, pages 651–673. PMLR, 2018.
- [135] Dmitry Kalashnikov, Jacob Varley, Yevgen Chebotar, Benjamin Swanson, Rico Jonschkowski, Chelsea Finn, Sergey Levine, and Karol Hausman. Mt-opt: Continuous multi-task robotic reinforcement learning at scale. *arXiv preprint arXiv:2104.08212*, 2021.
- [136] Dmitry Kalashnikov, Jake Varley, Yevgen Chebotar, Ben Swanson, Rico Jonschkowski, Chelsea Finn, Sergey Levine, and Karol Hausman. Mt-opt: Continuous multi-task robotic reinforcement learning at scale. *arXiv*, 2021.
- [137] Daniel Kappler, Peter Pastor, Mrinal Kalakrishnan, Manuel Wüthrich, and Stefan Schaal. Data-driven online decision making for autonomous manipulation. In *Robotics: science and systems*, volume 11, 2015.

- [138] Siddharth Karamcheti, Suraj Nair, Annie S Chen, Thomas Kollar, Chelsea Finn, Dorsa Sadigh, and Percy Liang. Language-driven representation learning for robotics. *arXiv preprint arXiv:2302.12766*, 2023.
- [139] Peter Karkus, Boris Ivanovic, Shie Mannor, and Marco Pavone. Diffstack: A differentiable and modular control stack for autonomous vehicles. In *Conference on robot learning*, pages 2170–2180. PMLR, 2023.
- [140] Michael Kelly, Chelsea Sidrane, Katherine Driggs-Campbell, and Mykel J Kochenderfer. Hg-dagger: Interactive imitation learning with human experts. In *2019 International Conference on Robotics and Automation (ICRA)*, pages 8077–8083. IEEE, 2019.
- [141] S Mohammad Khansari-Zadeh and Aude Billard. Learning stable nonlinear dynamical systems with gaussian mixture models. *IEEE Transactions on Robotics*, 27(5):943–957, 2011.
- [142] Oussama Khatib. A unified approach for motion and force control of robot manipulators: The operational space formulation. *IEEE Journal on Robotics and Automation*, 3(1):43–53, 1987.
- [143] Alexander Khazatsky, Karl Pertsch, Suraj Nair, Ashwin Balakrishna, Sudeep Dasari, Siddharth Karamcheti, Soroush Nasiriany, Mohan Kumar Srirama, Lawrence Yunliang Chen, Kirsty Ellis, Peter David Fagan, Joey Hejna, Masha Itkina, Marion Lepert, Yecheng Jason Ma, Patrick Tree Miller, Jimmy Wu, Suneel Belkhale, Shivin Dass, Huy Ha, Arhan Jain, Abraham Lee, Youngwoon Lee, Marius Memmel, Sungjae Park, Ilija Radosavovic, Kaiyuan Wang, Albert Zhan, Kevin Black, Cheng Chi, Kyle Beltran Hatch, Shan Lin, Jingpei Lu, Jean Mercat, Abdul Rehman, Pannag R Sanketi, Archit Sharma, Cody Simpson, Quan Vuong, Homer Rich Walke, Blake Wulfe, Ted Xiao, Jonathan Heewon Yang, Arefeh Yavary, Tony Z. Zhao, Christopher Agia, Rohan Baijal, Mateo Guaman Castro, Daphne Chen, Qiuyu Chen, Trinity Chung, Jaimyn Drake, Ethan Paul Foster, Jensen Gao, David Antonio Herrera, Minh Ho, Kyle Hsu, Jiaheng Hu, Donovan Jackson, Charlotte Le, Yunshuang Li, Roy Lin, Zehan Ma, Abhiram Maddukuri, Suvir Mirchandani, Daniel Morton, Tony Nguyen, Abigail O’Neill, Rosario Scalise, Derick Seale, Victor Son, Stephen Tian, Emi Tran, Andrew E. Wang, Yilin Wu, Annie Xie, Jingyun Yang, Patrick Yin, Yunchu Zhang, Osbert Bastani, Glen Berseth, Jeannette Bohg, Ken Goldberg, Abhinav Gupta, Abhishek Gupta, Dinesh Jayaraman, Joseph J Lim, Jitendra Malik, Roberto Martín-Martín, Subramanian Ramamoorthy, Dorsa Sadigh, Shuran Song, Jiajun Wu, Michael C. Yip, Yuke Zhu, Thomas Kollar, Sergey Levine, and Chelsea Finn. DROID: A Large-Scale In-The-Wild Robot Manipulation Dataset. In *Proceedings of Robotics: Science and Systems*, Delft, Netherlands, July 2024. doi: 10.15607/RSS.2024.XX.120.
- [144] Beomjoon Kim, Leslie Pack Kaelbling, and Tomás Lozano-Pérez. Adversarial actor-critic method for task and motion planning problems using planning experience. In *Proceedings of the AAAI Conference on Artificial Intelligence*, volume 33, pages 8017–8024, 2019.

- [145] Beomjoon Kim, Luke Shimanuki, Leslie Pack Kaelbling, and Tomás Lozano-Pérez. Representation, learning, and planning algorithms for geometric task and motion planning. *The International Journal of Robotics Research*, 41(2):210–231, 2022.
- [146] Moo Jin Kim, Karl Pertsch, Siddharth Karamcheti, Ted Xiao, Ashwin Balakrishna, Suraj Nair, Rafael Rafailov, Ethan P Foster, Pannag R Sanketi, Quan Vuong, Thomas Kollar, Benjamin Burchfiel, Russ Tedrake, Dorsa Sadigh, Sergey Levine, Percy Liang, and Chelsea Finn. Openvla: An open-source vision-language-action model. In Pulkit Agrawal, Oliver Kroemer, and Wolfram Burgard, editors, *Proceedings of The 8th Conference on Robot Learning*, volume 270 of *Proceedings of Machine Learning Research*, pages 2679–2713. PMLR, 06–09 Nov 2025.
- [147] Pang Wei Koh and Percy Liang. Understanding black-box predictions via influence functions. In *International conference on machine learning*, pages 1885–1894. PMLR, 2017.
- [148] Pang Wei W Koh, Kai-Siang Ang, Hubert Teo, and Percy S Liang. On the accuracy of influence functions for measuring group effects. *Advances in neural information processing systems*, 32, 2019.
- [149] George Konidaris, Leslie Pack Kaelbling, and Tomas Lozano-Perez. From skills to symbols: Learning symbolic representations for abstract high-level planning. *Journal of Artificial Intelligence Research*, 61:215–289, 2018.
- [150] Oliver Kroemer and Gaurav S Sukhatme. Learning spatial preconditions of manipulation skills using random forests. In *2016 IEEE-RAS 16th International Conference on Humanoid Robots (Humanoids)*, pages 676–683. IEEE, 2016.
- [151] Sachit Kumar, Shuo Cheng, Shivang Chopra, Matthew Bronars, and Danfei Xu. Learning to discern: Imitating heterogeneous human demonstrations with preference and representation learning. In Jie Tan, Marc Toussaint, and Kourosh Darvish, editors, *Proceedings of The 7th Conference on Robot Learning*, volume 229 of *Proceedings of Machine Learning Research*, pages 1437–1449. PMLR, 06–09 Nov 2023.
- [152] Tomas Kulvicius, KeJun Ning, Miniya Tamosiunaite, and Florentin Worgötter. Joining movement sequences: Modified dynamic movement primitives for robotics applications exemplified on handwriting. *IEEE Transactions on Robotics*, 28(1):145–157, 2011.
- [153] Fabien Lagriffoul, Dimitar Dimitrov, Julien Bidot, Alessandro Saffiotti, and Lars Karlsson. Efficiently combining task and motion planning using geometric constraints. *The International Journal of Robotics Research*, 33(14):1726–1747, 2014.

- [154] Balaji Lakshminarayanan, Alexander Pritzel, and Charles Blundell. Simple and scalable predictive uncertainty estimation using deep ensembles. In I. Guyon, U. Von Luxburg, S. Bengio, H. Wallach, R. Fergus, S. Vishwanathan, and R. Garnett, editors, *Advances in Neural Information Processing Systems*, volume 30. Curran Associates, Inc., 2017. URL <https://proceedings.neurips.cc/paper/2017/file/9ef2ed4b7fd2c810847ffa5fa85bce38-Paper.pdf>.
- [155] Steven M. Lavalle. *Planning Algorithms*. Cambridge University Press, 2006. ISBN 0521862051.
- [156] Yann LeCun, Sumit Chopra, Raia Hadsell, M Ranzato, and Fufei Huang. A tutorial on energy-based learning. *Predicting structured data*, 1(0), 2006.
- [157] Katherine Lee, Daphne Ippolito, Andrew Nystrom, Chiyuan Zhang, Douglas Eck, Chris Callison-Burch, and Nicholas Carlini. Deduplicating training data makes language models better. In Smaranda Muresan, Preslav Nakov, and Aline Villavicencio, editors, *Proceedings of the 60th Annual Meeting of the Association for Computational Linguistics (Volume 1: Long Papers)*, pages 8424–8445, Dublin, Ireland, May 2022. Association for Computational Linguistics. doi: 10.18653/v1/2022.acl-long.577. URL <https://aclanthology.org/2022.acl-long.577/>.
- [158] Kimin Lee, Kibok Lee, Honglak Lee, and Jinwoo Shin. A simple unified framework for detecting out-of-distribution samples and adversarial attacks. In S. Bengio, H. Wallach, H. Larochelle, K. Grauman, N. Cesa-Bianchi, and R. Garnett, editors, *Advances in Neural Information Processing Systems*, volume 31. Curran Associates, Inc., 2018. URL https://proceedings.neurips.cc/paper_files/paper/2018/file/abdeb6f575ac5c6676b747bca8d09cc2-Paper.pdf.
- [159] Michelle A Lee, Matthew Tan, Yuke Zhu, and Jeannette Bohg. Detect, reject, correct: Crossmodal compensation of corrupted sensors. In *2021 IEEE international conference on robotics and automation (ICRA)*, pages 909–916. IEEE, 2021.
- [160] Marion Lepert, Jiaying Fang, and Jeannette Bohg. Masquerade: Learning from in-the-wild human videos using data-editing. *arXiv preprint arXiv:2508.09976*, 2025.
- [161] Xiang Lisa Li, Ari Holtzman, Daniel Fried, Percy Liang, Jason Eisner, Tatsunori Hashimoto, Luke Zettlemoyer, and Mike Lewis. Contrastive decoding: Open-ended text generation as optimization. *arXiv preprint arXiv:2210.15097*, 2022.
- [162] Xinghang Li, Minghuan Liu, Hanbo Zhang, Cunjun Yu, Jie Xu, Hongtao Wu, Chilam Cheang, Ya Jing, Weinan Zhang, Huaping Liu, Hang Li, and Tao Kong. Vision-language foundation models as effective robot imitators. In *The Twelfth International Conference on Learning Representations*, 2024. URL <https://openreview.net/forum?id=1FYj0oibGR>.
- [163] Jacky Liang, Wenlong Huang, Fei Xia, Peng Xu, Karol Hausman, Brian Ichter, Pete Florence, and Andy Zeng. Code as policies: Language model programs for embodied control. *arXiv preprint arXiv:2209.07753*, 2022.

- [164] Ruofan Liang, Zan Gojcic, Huan Ling, Jacob Munkberg, Jon Hasselgren, Zhi-Hao Lin, Jun Gao, Alexander Keller, Nandita Vijaykumar, Sanja Fidler, and Zian Wang. Diffusionrenderer: Neural inverse and forward rendering with video diffusion models. In *The IEEE Conference on Computer Vision and Pattern Recognition (CVPR)*, June 2025.
- [165] Timothy P Lillicrap, Jonathan J Hunt, Alexander Pritzel, Nicolas Heess, Tom Erez, Yuval Tassa, David Silver, and Daan Wierstra. Continuous control with deep reinforcement learning. *CoRR*, 2015.
- [166] Jinxu Lin, Linwei Tao, Minjing Dong, and Chang Xu. Diffusion attribution score: Evaluating training data influence in diffusion model. In *The Thirteenth International Conference on Learning Representations*, 2025. URL <https://openreview.net/forum?id=kuutidLf6R>.
- [167] Zijun Lin, Jiafei Duan, Haoquan Fang, Dieter Fox, Ranjay Krishna, Cheston Tan, and Bihan Wen. Failsafe: Reasoning and recovery from failures in vision-language-action models. *arXiv preprint arXiv:2510.01642*, 2025.
- [168] Bo Liu, Yuqian Jiang, Xiaohan Zhang, Qiang Liu, Shiqi Zhang, Joydeep Biswas, and Peter Stone. Llm+ p: Empowering large language models with optimal planning proficiency. *arXiv preprint arXiv:2304.11477*, 2023.
- [169] Huihan Liu, Shivin Dass, Roberto Martín-Martín, and Yuke Zhu. Model-based runtime monitoring with interactive imitation learning. In *IEEE International Conference on Robotics and Automation (ICRA)*, 2024.
- [170] Jeremiah Zhe Liu, Zi Lin, Shreyas Padhy, Dustin Tran, Tania Bedrax-Weiss, and Balaji Lakshminarayanan. Simple and principled uncertainty estimation with deterministic deep learning via distance awareness, 2020.
- [171] Zeyi Liu, Arpit Bahety, and Shuran Song. Reflect: Summarizing robot experiences for failure explanation and correction. In Jie Tan, Marc Toussaint, and Kouros Darvish, editors, *Proceedings of The 7th Conference on Robot Learning*, volume 229 of *Proceedings of Machine Learning Research*, pages 3468–3484. PMLR, 06–09 Nov 2023. URL <https://proceedings.mlr.press/v229/liu23g.html>.
- [172] Zifan Liu, Amin Karbasi, and Theodoros Rekatsinas. Tsds: Data selection for task-specific model finetuning. *Advances in Neural Information Processing Systems*, 37, 2024.
- [173] Ilya Loshchilov and Frank Hutter. SGDR: Stochastic gradient descent with warm restarts. In *International Conference on Learning Representations*, 2017. URL <https://openreview.net/forum?id=Skq89Scxx>.

- [174] Yao Lu, Karol Hausman, Yevgen Chebotar, Mengyuan Yan, Eric Jang, Alexander Herzog, Ted Xiao, Alex Irpan, Mohi Khansari, Dmitry Kalashnikov, et al. Aw-opt: Learning robotic skills with imitation and reinforcement at scale. In *Conference on Robot Learning*, pages 1078–1088. PMLR, 2022.
- [175] Yifan Lu, Xuanchi Ren, Jiawei Yang, Tianchang Shen, Zhangjie Wu, Jun Gao, Yue Wang, Siheng Chen, Mike Chen, Sanja Fidler, et al. Infinicube: Unbounded and controllable dynamic 3d driving scene generation with world-guided video models. In *Proceedings of the IEEE/CVF International Conference on Computer Vision*, pages 27272–27283, 2025.
- [176] Rachel Luo, Shengjia Zhao, Jonathan Kuck, Boris Ivanovic, Silvio Savarese, Edward Schmerling, and Marco Pavone. Sample-efficient safety assurances using conformal prediction. In Steven M. LaValle, Jason M. O’Kane, Michael Otte, Dorsa Sadigh, and Pratap Tokekar, editors, *Algorithmic Foundations of Robotics XV*, pages 149–169, Cham, 2023. Springer International Publishing. ISBN 978-3-031-21090-7.
- [177] Rachel Luo, Rohan Sinha, Yixiao Sun, Ali Hindy, Shengjia Zhao, Silvio Savarese, Edward Schmerling, and Marco Pavone. Online distribution shift detection via recency prediction. In *Proceedings of the 2024 IEEE International Conference on Robotics and Automation (ICRA)*, Yokohama, Japan, 2024. IEEE.
- [178] Yecheng Jason Ma, Shagun Sodhani, Dinesh Jayaraman, Osbert Bastani, Vikash Kumar, and Amy Zhang. VIP: Towards universal visual reward and representation via value-implicit pre-training. In *The Eleventh International Conference on Learning Representations*, 2023. URL <https://openreview.net/forum?id=YJ7o2wetJ2>.
- [179] Aleksander Madry, Andrew Ilyas, Logan Engstrom, Sung Min Park, and Kristian Georgiev. Data attribution at scale. <https://ml-data-tutorial.org/>, 2024. Tutorial at ICML 2024.
- [180] Anirudha Majumdar, Mohit Sharma, Dmitry Kalashnikov, Sumeet Singh, Pierre Sermanet, and Vikas Sindhwani. Predictive red teaming: Breaking policies without breaking robots. *arXiv preprint arXiv:2502.06575*, 2025.
- [181] Zhao Mandi, Homanga Bharadhwaj, Vincent Moens, Shuran Song, Aravind Rajeswaran, and Vikash Kumar. Cacti: A framework for scalable multi-task multi-scene visual imitation learning. *arXiv preprint arXiv:2212.05711*, 2022.
- [182] Ajay Mandlekar, Danfei Xu, Roberto Martín-Martín, Yuke Zhu, Li Fei-Fei, and Silvio Savarese. Human-in-the-loop imitation learning using remote teleoperation. *CoRR*, abs/2012.06733, 2020. URL <https://arxiv.org/abs/2012.06733>.

- [183] Ajay Mandlekar, Danfei Xu, Josiah Wong, Soroush Nasiriany, Chen Wang, Rohun Kulkarni, Li Fei-Fei, Silvio Savarese, Yuke Zhu, and Roberto Martín-Martín. What matters in learning from offline human demonstrations for robot manipulation. In Aleksandra Faust, David Hsu, and Gerhard Neumann, editors, *Proceedings of the 5th Conference on Robot Learning*, volume 164 of *Proceedings of Machine Learning Research*, pages 1678–1690. PMLR, 08–11 Nov 2022.
- [184] Ajay Mandlekar, Soroush Nasiriany, Bowen Wen, Ireteayo Akinola, Yashraj Narang, Linxi Fan, Yuke Zhu, and Dieter Fox. Mimicgen: A data generation system for scalable robot learning using human demonstrations. In Jie Tan, Marc Toussaint, and Kouros Darvish, editors, *Proceedings of The 7th Conference on Robot Learning*, volume 229 of *Proceedings of Machine Learning Research*, pages 1820–1864. PMLR, 06–09 Nov 2023.
- [185] Jiageng Mao, Boyi Li, Boris Ivanovic, Yuxiao Chen, Yan Wang, Yurong You, Chaowei Xiao, Danfei Xu, Marco Pavone, and Yue Wang. Dreamdrive: Generative 4d scene modeling from street view images. In *2025 IEEE International Conference on Robotics and Automation (ICRA)*, pages 367–374. IEEE, 2025.
- [186] Alonso Marco, Elias Morley, and Claire J. Tomlin. Out of distribution detection via domain-informed gaussian process state space models. In *2023 62nd IEEE Conference on Decision and Control (CDC)*, pages 5487–5493, 2023. doi: 10.1109/CDC49753.2023.10383566.
- [187] James Martens. New insights and perspectives on the natural gradient method. *Journal of Machine Learning Research*, 21(146):1–76, 2020. URL <http://jmlr.org/papers/v21/17-678.html>.
- [188] Warwick Masson, Pravesh Ranchod, and George Konidaris. Reinforcement learning with parameterized actions. In *Thirtieth AAAI Conference on Artificial Intelligence*, 2016.
- [189] Takamitsu Matsubara, Sang-Ho Hyon, and Jun Morimoto. Learning stylistic dynamic movement primitives from multiple demonstrations. In *2010 IEEE/RSJ International Conference on Intelligent Robots and Systems*, pages 1277–1283. IEEE, 2010.
- [190] Drew McDermott, Malik Ghallab, Adele Howe, Craig Knoblock, Ashwin Ram, Manuela Veloso, Daniel Weld, and David Wilkins. *PDDL—The Planning Domain Definition Language Version 1.2*, 1998.
- [191] Oier Mees, Lukas Hermann, Erick Rosete-Beas, and Wolfram Burgard. Calvin: A benchmark for language-conditioned policy learning for long-horizon robot manipulation tasks. *IEEE Robotics and Automation Letters (RA-L)*, 7(3):7327–7334, 2022.
- [192] Takatoki Migimatsu. *Long Horizon Planning in the Real World*. Ph.d. dissertation, Stanford University, 2023. URL <https://pur1.stanford.edu/gg626sc8638>.

- [193] Toki Migimatsu, Wenzhao Lian, Jeannette Bohg, and Stefan Schaal. Symbolic state estimation with predicates for contact-rich manipulation tasks. In *2022 International Conference on Robotics and Automation (ICRA)*, pages 1702–1709. IEEE, 2022.
- [194] Bruno Kacper Mlodozieniec, Runa Eschenhagen, Juhan Bae, Alexander Immer, David Krueger, and Richard E. Turner. Influence functions for scalable data attribution in diffusion models. In *The Thirteenth International Conference on Learning Representations*, 2025. URL <https://openreview.net/forum?id=esYrEndGsr>.
- [195] Krikamol Muandet, Kenji Fukumizu, Bharath Sriperumbudur, Bernhard Schölkopf, et al. Kernel mean embedding of distributions: A review and beyond. *Foundations and Trends® in Machine Learning*, 10(1-2):1–141, 2017.
- [196] Ofir Nachum, Shixiang Shane Gu, Honglak Lee, and Sergey Levine. Data-efficient hierarchical reinforcement learning. *Advances in neural information processing systems*, 31, 2018.
- [197] Ashvin Nair, Abhishek Gupta, Murtaza Dalal, and Sergey Levine. Awac: Accelerating online reinforcement learning with offline datasets. *arXiv preprint arXiv:2006.09359*, 2020.
- [198] Suraj Nair, Aravind Rajeswaran, Vikash Kumar, Chelsea Finn, and Abhinav Gupta. R3m: A universal visual representation for robot manipulation. *arXiv preprint arXiv:2203.12601*, 2022.
- [199] Soroush Nasiriany, Huihan Liu, and Yuke Zhu. Augmenting reinforcement learning with behavior primitives for diverse manipulation tasks. In *2022 International Conference on Robotics and Automation (ICRA)*, pages 7477–7484. IEEE, 2022.
- [200] Soroush Nasiriany, Fei Xia, Wenhao Yu, Ted Xiao, Jacky Liang, Ishita Dasgupta, Annie Xie, Danny Driess, Ayzaan Wahid, Zhuo Xu, et al. Pivot: Iterative visual prompting elicits actionable knowledge for vlms. *arXiv preprint arXiv:2402.07872*, 2024.
- [201] Octo Model Team, Dibya Ghosh, Homer Walke, Karl Pertsch, Kevin Black, Oier Mees, Sudeep Dasari, Joey Hejna, Charles Xu, Jianlan Luo, Tobias Kreiman, You Liang Tan, Lawrence Yunliang Chen, Pannag Sanketi, Quan Vuong, Ted Xiao, Dorsa Sadigh, Chelsea Finn, and Sergey Levine. Octo: An open-source generalist robot policy. In *Proceedings of Robotics: Science and Systems*, Delft, Netherlands, 2024.
- [202] OpenAI. Gpt-4 technical report, 2023.
- [203] Maxime Oquab, Timothée Darcet, Théo Moutakanni, Huy Vo, Marc Szafraniec, Vasil Khalidov, Pierre Fernandez, Daniel Haziza, Francisco Massa, Alaaeldin El-Nouby, et al. Dinov2: Learning robust visual features without supervision. *arXiv preprint arXiv:2304.07193*, 2023.

- [204] Long Ouyang, Jeff Wu, Xu Jiang, Diogo Almeida, Carroll L Wainwright, Pamela Mishkin, Chong Zhang, Sandhini Agarwal, Katarina Slama, Alex Ray, et al. Training language models to follow instructions with human feedback. *arXiv preprint arXiv:2203.02155*, 2022.
- [205] Sung Min Park, Kristian Georgiev, Andrew Ilyas, Guillaume Leclerc, and Aleksander Madry. Trak: Attributing model behavior at scale. In *International Conference on Machine Learning*, pages 27074–27113. PMLR, 2023.
- [206] Peter Pastor, Heiko Hoffmann, Tamim Asfour, and Stefan Schaal. Learning and generalization of motor skills by learning from demonstration. In *2009 IEEE International Conference on Robotics and Automation*, pages 763–768. IEEE, 2009.
- [207] Georgios Pavlakos, Dandan Shan, Ilija Radosavovic, Angjoo Kanazawa, David Fouhey, and Jitendra Malik. Reconstructing hands in 3d with transformers. In *Proceedings of the IEEE/CVF Conference on Computer Vision and Pattern Recognition*, pages 9826–9836, 2024.
- [208] Karl Pertsch, Youngwoon Lee, and Joseph J Lim. Accelerating reinforcement learning with learned skill priors. *Conference on Robot Learning (CoRL)*, 2020.
- [209] Silviu Pitis, Michael R Zhang, Andrew Wang, and Jimmy Ba. Boosted prompt ensembles for large language models. *arXiv preprint arXiv:2304.05970*, 2023.
- [210] Charles Ruizhongtai Qi, Li Yi, Hao Su, and Leonidas J Guibas. Pointnet++: Deep hierarchical feature learning on point sets in a metric space. *Advances in neural information processing systems*, 30, 2017.
- [211] Julian Quevedo, Percy Liang, and Sherry Yang. Evaluating robot policies in a world model. *arXiv preprint arXiv:2506.00613*, 2025.
- [212] Sadegh Rabiee and Joydeep Biswas. Ivoa: Introspective vision for obstacle avoidance. *2019 IEEE/RSJ International Conference on Intelligent Robots and Systems (IROS)*, pages 1230–1235, 2019. URL <https://api.semanticscholar.org/CorpusID:67855498>.
- [213] Alec Radford, Jong Wook Kim, Chris Hallacy, Aditya Ramesh, Gabriel Goh, Sandhini Agarwal, Girish Sastry, Amanda Askell, Pamela Mishkin, Jack Clark, et al. Learning transferable visual models from natural language supervision. In *International conference on machine learning*, pages 8748–8763. PMLR, 2021.
- [214] Rouhollah Rahmatizadeh, Pooya Abolghasemi, Ladislau Bölöni, and Sergey Levine. Vision-based multi-task manipulation for inexpensive robots using end-to-end learning from demonstration. In *2018 IEEE international conference on robotics and automation (ICRA)*, pages 3758–3765. IEEE, 2018.

- [215] Aravind Rajeswaran, Vikash Kumar, Abhishek Gupta, Giulia Vezzani, John Schulman, Emanuel Todorov, and Sergey Levine. Learning Complex Dexterous Manipulation with Deep Reinforcement Learning and Demonstrations. In *Proceedings of Robotics: Science and Systems (RSS)*, 2018.
- [216] Machel Reid, Nikolay Savinov, Denis Teplyashin, Dmitry Lepikhin, Timothy Lillicrap, Jean-baptiste Alayrac, Radu Soricut, Angeliki Lazaridou, Orhan Firat, Julian Schrittwieser, et al. Gemini 1.5: Unlocking multimodal understanding across millions of tokens of context. *arXiv preprint arXiv:2403.05530*, 2024.
- [217] Davis Rempe, Jonah Philion, Leonidas J Guibas, Sanja Fidler, and Or Litany. Generating useful accident-prone driving scenarios via a learned traffic prior. In *Proceedings of the IEEE/CVF Conference on Computer Vision and Pattern Recognition*, pages 17305–17315, 2022.
- [218] Allen Z. Ren, Anushri Dixit, Alexandra Bodrova, Sumeet Singh, Stephen Tu, Noah Brown, Peng Xu, Leila Takayama, Fei Xia, Jake Varley, Zhenjia Xu, Dorsa Sadigh, Andy Zeng, and Anirudha Majumdar. Robots that ask for help: Uncertainty alignment for large language model planners. In *Proceedings of the Conference on Robot Learning (CoRL)*, 2023.
- [219] Tianhe Ren, Shilong Liu, Ailing Zeng, Jing Lin, Kunchang Li, He Cao, Jiayu Chen, Xinyu Huang, Yukang Chen, Feng Yan, et al. Grounded sam: Assembling open-world models for diverse visual tasks. *arXiv preprint arXiv:2401.14159*, 2024.
- [220] Charles Richter and Nicholas Roy. Safe visual navigation via deep learning and novelty detection. In *Proceedings of Robotics: Science and Systems*, Cambridge, Massachusetts, July 2017. doi: 10.15607/RSS.2017.XIII.064.
- [221] Stéphane Ross and Drew Bagnell. Efficient reductions for imitation learning. In *Proceedings of the thirteenth international conference on artificial intelligence and statistics*, pages 661–668. JMLR Workshop and Conference Proceedings, 2010.
- [222] Stéphane Ross, Geoffrey Gordon, and Drew Bagnell. A reduction of imitation learning and structured prediction to no-regret online learning. In *Proceedings of the fourteenth international conference on artificial intelligence and statistics*, pages 627–635. JMLR Workshop and Conference Proceedings, 2011.
- [223] Reuven Rubinfeld. The cross-entropy method for combinatorial and continuous optimization. *Methodology and computing in applied probability*, 1(2):127–190, 1999.
- [224] Lukas Ruff, Robert Vandermeulen, Nico Goernitz, Lucas Deecke, Shoaib Ahmed Siddiqui, Alexander Binder, Emmanuel Müller, and Marius Kloft. Deep one-class classification. In Jennifer Dy and Andreas Krause, editors, *Proceedings of the 35th International Conference on*

- Machine Learning*, volume 80 of *Proceedings of Machine Learning Research*, pages 4393–4402. PMLR, 10–15 Jul 2018. URL <https://proceedings.mlr.press/v80/ruff18a.html>.
- [225] Lukas Ruff, Jacob R. Kauffmann, Robert A. Vandermeulen, Grégoire Montavon, Wojciech Samek, Marius Kloft, Thomas G. Dietterich, and Klaus-Robert Müller. A unifying review of deep and shallow anomaly detection. *Proceedings of the IEEE*, 109(5):756–795, 2021. doi: 10.1109/JPROC.2021.3052449.
- [226] Fabio Ruggiero, Vincenzo Lippiello, and Bruno Siciliano. Nonprehensile dynamic manipulation: A survey. *IEEE Robotics and Automation Letters*, 3(3):1711–1718, 2018.
- [227] Som Sagar, Jiafei Duan, Sreevishakh Vasudevan, Yifan Zhou, Heni Ben Amor, Dieter Fox, and Ransalu Senanayake. From mystery to mastery: Failure diagnosis for improving manipulation policies. *arXiv preprint arXiv:2412.02818*, 2024.
- [228] Som Sagar, Aditya Taparia, Harsh Mankodiya, Pranav Bidare, Yifan Zhou, and Ransalu Senanayake. Batcave: Trustworthy explanations for robot behaviors. In *2025 IEEE/RSJ International Conference on Intelligent Robots and Systems (IROS)*, pages 13867–13874. IEEE, 2025.
- [229] Stefan Schaal. Is imitation learning the route to humanoid robots? *Trends in Cognitive Sciences*, 3(6):233–242, 1999. doi: 10.1016/s1364-6613(99)01327-3.
- [230] Stefan Schaal. Dynamic movement primitives—a framework for motor control in humans and humanoid robotics. In *Adaptive motion of animals and machines*, pages 261–280. Springer, 2006.
- [231] Ramanan Sekar, Oleh Rybkin, Kostas Daniilidis, Pieter Abbeel, Danijar Hafner, and Deepak Pathak. Planning to explore via self-supervised world models. In *International Conference on Machine Learning*, pages 8583–8592. PMLR, 2020.
- [232] Junwon Seo, Kensuke Nakamura, and Andrea Bajcsy. Uncertainty-aware latent safety filters for avoiding out-of-distribution failures. In Joseph Lim, Shuran Song, and Hae-Won Park, editors, *Proceedings of The 9th Conference on Robot Learning*, volume 305 of *Proceedings of Machine Learning Research*, pages 4442–4472. PMLR, 27–30 Sep 2025. URL <https://proceedings.mlr.press/v305/seo25a.html>.
- [233] Burr Settles. *Active Learning*. Morgan & Claypool Publishers, 2012.
- [234] Dhruv Shah, Peng Xu, Yao Lu, Ted Xiao, Alexander Toshev, Sergey Levine, and Brian Ichter. Value function spaces: Skill-centric state abstractions for long-horizon reasoning. *International Conference on Learning Representations (ICLR)*, 2022.

- [235] Harshay Shah, Sung Min Park, Andrew Ilyas, and Aleksander Madry. Modeldiff: A framework for comparing learning algorithms. In *International Conference on Machine Learning*, pages 30646–30688. PMLR, 2023.
- [236] Tanmay Shankar and Abhinav Gupta. Learning robot skills with temporal variational inference. In *International Conference on Machine Learning*, pages 8624–8633. PMLR, 2020.
- [237] Tanmay Shankar, Shubham Tulsiani, Lerrel Pinto, and Abhinav Gupta. Discovering motor programs by recomposing demonstrations. In *International Conference on Learning Representations*, 2019.
- [238] Lin Shao, Toki Migimatsu, Qiang Zhang, Karen Yang, and Jeannette Bohg. Concept2robot: Learning manipulation concepts from instructions and human demonstrations. *The International Journal of Robotics Research*, 40(12-14):1419–1434, 2021.
- [239] Apoorva Sharma, Navid Azizan, and Marco Pavone. Sketching curvature for efficient out-of-distribution detection for deep neural networks. In Cassio de Campos and Marloes H. Maathuis, editors, *Proceedings of the Thirty-Seventh Conference on Uncertainty in Artificial Intelligence*, volume 161 of *Proceedings of Machine Learning Research*, pages 1958–1967. PMLR, 27–30 Jul 2021. URL <https://proceedings.mlr.press/v161/sharma21a.html>.
- [240] Archit Sharma, Shixiang Gu, Sergey Levine, Vikash Kumar, and Karol Hausman. Dynamics-aware unsupervised discovery of skills. *International Conference on Learning Representations (ICLR)*, 2020.
- [241] Mohit Shridhar, Lucas Manuelli, and Dieter Fox. Cliport: What and where pathways for robotic manipulation. In *Conference on Robot Learning*, pages 894–906. PMLR, 2022.
- [242] Mohit Shridhar, Lucas Manuelli, and Dieter Fox. Perceiver-actor: A multi-task transformer for robotic manipulation. *arXiv preprint arXiv:2209.05451*, 2022.
- [243] Tom Silver, Rohan Chitnis, Aidan Curtis, Joshua B Tenenbaum, Tomas Lozano-Perez, and Leslie Pack Kaelbling. Planning with learned object importance in large problem instances using graph neural networks. In *Proceedings of the AAAI conference on artificial intelligence*, volume 35, pages 11962–11971, 2021.
- [244] Tom Silver, Rohan Chitnis, Joshua Tenenbaum, Leslie Pack Kaelbling, and Tomás Lozano-Pérez. Learning symbolic operators for task and motion planning. In *2021 IEEE/RSJ International Conference on Intelligent Robots and Systems (IROS)*, pages 3182–3189. IEEE, 2021.
- [245] Tom Silver, Ashay Athalye, Joshua B. Tenenbaum, Tomás Lozano-Pérez, and Leslie Pack Kaelbling. Learning neuro-symbolic skills for bilevel planning. In *6th Annual Conference on Robot Learning*, 2022. URL <https://openreview.net/forum?id=0IaJRu05UXy>.

- [246] Tom Silver, Varun Hariprasad, Reece S Shuttleworth, Nishanth Kumar, Tomás Lozano-Pérez, and Leslie Pack Kaelbling. Pddl planning with pretrained large language models. In *NeurIPS 2022 Foundation Models for Decision Making Workshop*, 2022.
- [247] Anthony Simeonov, Yilun Du, Beomjoon Kim, Francois R Hogan, Joshua Tenenbaum, Pulkit Agrawal, and Alberto Rodriguez. A long horizon planning framework for manipulating rigid pointcloud objects. *Conference on Robot Learning (CoRL)*, 2020.
- [248] Avi Singh, Huihan Liu, Gaoyue Zhou, Albert Yu, Nicholas Rhinehart, and Sergey Levine. Parrot: Data-driven behavioral priors for reinforcement learning. *International Conference on Learning Representations (ICLR)*, 2021.
- [249] Ishika Singh, Valts Blukis, Arsalan Mousavian, Ankit Goyal, Danfei Xu, Jonathan Tremblay, Dieter Fox, Jesse Thomason, and Animesh Garg. Progprompt: Generating situated robot task plans using large language models. *arXiv preprint arXiv:2209.11302*, 2022.
- [250] Rohan Sinha, Apoorva Sharma, Somrita Banerjee, Thomas Lew, Rachel Luo, Spencer M Richards, Yixiao Sun, Edward Schmerling, and Marco Pavone. A system-level view on out-of-distribution data in robotics. *arXiv preprint arXiv:2212.14020*, 2022. Available at <https://arxiv.org/abs/2212.14020>.
- [251] Rohan Sinha, Amine Elhafsi, Christopher Agia, Matt Foutter, Edward Schmerling, and Marco Pavone. Real-Time Anomaly Detection and Reactive Planning with Large Language Models. In *Proceedings of Robotics: Science and Systems*, Delft, Netherlands, July 2024. doi: 10.15607/RSS.2024.XX.114.
- [252] Marta Skreta, Naruki Yoshikawa, Sebastian Arellano-Rubach, Zhi Ji, Lasse Bjørn Kristensen, Kourosh Darvish, Alán Aspuru-Guzik, Florian Shkurti, and Animesh Garg. Errors are useful prompts: Instruction guided task programming with verifier-assisted iterative prompting. *arXiv preprint arXiv:2303.14100*, 2023.
- [253] Marta Skreta, Zihan Zhou, Jia Lin Yuan, Kourosh Darvish, Alán Aspuru-Guzik, and Animesh Garg. Replan: Robotic replanning with perception and language models. *arXiv preprint arXiv:2401.04157*, 2024.
- [254] Laura Smith, Alex Irpan, Montserrat Gonzalez Arenas, Sean Kirmani, Dmitry Kalashnikov, Dhruv Shah, and Ted Xiao. Steer: Flexible robotic manipulation via dense language grounding. *arXiv preprint arXiv:2411.03409*, 2024.
- [255] Jascha Sohl-Dickstein, Eric Weiss, Niru Maheswaranathan, and Surya Ganguli. Deep unsupervised learning using nonequilibrium thermodynamics. In *International conference on machine learning*, pages 2256–2265. PMLR, 2015.

- [256] Yang Song, Jascha Sohl-Dickstein, Diederik P Kingma, Abhishek Kumar, Stefano Ermon, and Ben Poole. Score-based generative modeling through stochastic differential equations. In *International Conference on Learning Representations*, 2021. URL <https://openreview.net/forum?id=PXTIG12RRHS>.
- [257] Simon Stepputtis, Joseph Campbell, Mariano Phielipp, Stefan Lee, Chitta Baral, and Heni Ben Amor. Language-conditioned imitation learning for robot manipulation tasks. *Advances in Neural Information Processing Systems*, 33:13139–13150, 2020.
- [258] Richard S Sutton, David McAllester, Satinder Singh, and Yishay Mansour. Policy gradient methods for reinforcement learning with function approximation. *Advances in neural information processing systems*, 12, 1999.
- [259] Richard S Sutton, Doina Precup, and Satinder Singh. Between mdps and semi-mdps: A framework for temporal abstraction in reinforcement learning. *Artificial intelligence*, 112(1-2): 181–211, 1999.
- [260] Shuhan Tan, Boris Ivanovic, Yuxiao Chen, Boyi Li, Xinshuo Weng, Yulong Cao, Philipp Kraehenbuehl, and Marco Pavone. Promptable closed-loop traffic simulation. In *Conference on Robot Learning*, pages 5087–5105. PMLR, 2025.
- [261] Gemini Robotics Team, Abbas Abdolmaleki, Saminda Abeyruwan, Joshua Ainslie, Jean-Baptiste Alayrac, Montserrat Gonzalez Arenas, Ashwin Balakrishna, Nathan Batchelor, Alex Bewley, Jeff Bingham, et al. Gemini robotics 1.5: Pushing the frontier of generalist robots with advanced embodied reasoning, thinking, and motion transfer. *arXiv preprint arXiv:2510.03342*, 2025.
- [262] Gemini Robotics Team, Saminda Abeyruwan, Joshua Ainslie, Jean-Baptiste Alayrac, Montserrat Gonzalez Arenas, Travis Armstrong, Ashwin Balakrishna, Robert Baruch, Maria Bauza, Michiel Blokzijl, et al. Gemini robotics: Bringing ai into the physical world. *arXiv preprint arXiv:2503.20020*, 2025.
- [263] Gemini Robotics Team, Krzysztof Choromanski, Coline Devin, Yilun Du, Debidatta Dwivedi, Ruiqi Gao, Abhishek Jindal, Thomas Kipf, Sean Kirmani, Isabel Leal, Fangchen Liu, Anirudha Majumdar, Andrew Marmon, Carolina Parada, Yulia Rubanova, Dhruv Shah, Vikas Sindhwani, Jie Tan, Fei Xia, Ted Xiao, Sherry Yang, Wenhao Yu, and Allan Zhou. Evaluating gemini robotics policies in a veo world simulator, 2025. URL <https://arxiv.org/abs/2512.10675>.
- [264] Kushal Tirumala, Daniel Simig, Armen Aghajanyan, and Ari Morcos. D4: Improving llm pretraining via document de-duplication and diversification. *Advances in Neural Information Processing Systems*, 36:53983–53995, 2023.

- [265] Marc Toussaint. Logic-geometric programming: An optimization-based approach to combined task and motion planning. In *Twenty-Fourth International Joint Conference on Artificial Intelligence*, 2015.
- [266] Marc Toussaint, Kelsey Allen, Kevin Smith, and Joshua B Tenenbaum. Differentiable physics and stable modes for tool-use and manipulation planning. In *Proceedings of Robotics: Science and Systems*, Pittsburgh, Pennsylvania, June 2018. doi: 10.15607/RSS.2018.XIV.044.
- [267] Hugo Touvron, Thibaut Lavril, Gautier Izacard, Xavier Martinet, Marie-Anne Lachaux, Timothée Lacroix, Baptiste Rozière, Naman Goyal, Eric Hambro, Faisal Azhar, et al. Llama: Open and efficient foundation language models. *arXiv preprint arXiv:2302.13971*, 2023.
- [268] Aleš Ude, Andrej Gams, Tamim Asfour, and Jun Morimoto. Task-specific generalization of discrete and periodic dynamic movement primitives. *IEEE Transactions on Robotics*, 26(5): 800–815, 2010.
- [269] Karthik Valmeekam, Alberto Olmo, Sarath Sreedharan, and Subbarao Kambhampati. Large language models still can’t plan (a benchmark for llms on planning and reasoning about change). *arXiv preprint arXiv:2206.10498*, 2022.
- [270] Ashish Vaswani, Noam Shazeer, Niki Parmar, Jakob Uszkoreit, Llion Jones, Aidan N Gomez, Łukasz Kaiser, and Illia Polosukhin. Attention is all you need. *Advances in neural information processing systems*, 30, 2017.
- [271] Sai Vemprala, Rogerio Bonatti, Arthur Buckner, and Ashish Kapoor. Chatgpt for robotics: Design principles and model abilities. Technical Report MSR-TR-2023-8, Microsoft, February 2023.
- [272] Joseph A Vincent, Haruki Nishimura, Masha Itkina, Paarth Shah, Mac Schwager, and Thomas Kollar. How generalizable is my behavior cloning policy? a statistical approach to trustworthy performance evaluation. *IEEE Robotics and Automation Letters*, 2024.
- [273] Nghia Vuong, Hung Pham, and Quang-Cuong Pham. Learning sequences of manipulation primitives for robotic assembly. In *2021 IEEE International Conference on Robotics and Automation (ICRA)*, pages 4086–4092. IEEE, 2021.
- [274] Homer Walke, Kevin Black, Abraham Lee, Moo Jin Kim, Max Du, Chongyi Zheng, Tony Zhao, Philippe Hansen-Estruch, Quan Vuong, Andre He, Vivek Myers, Kuan Fang, Chelsea Finn, and Sergey Levine. Bridgedata v2: A dataset for robot learning at scale. In *Conference on Robot Learning (CoRL)*, 2023.
- [275] Chen Wang, Danfei Xu, and Li Fei-Fei. Generalizable task planning through representation pretraining. *IEEE Robotics and Automation Letters*, 7(3), 2022.

- [276] Yan Wang, Wenjie Luo, Junjie Bai, Yulong Cao, Tong Che, Ke Chen, Yuxiao Chen, Jenna Diamond, Yifan Ding, Wenhao Ding, et al. Alpamayo-r1: Bridging reasoning and action prediction for generalizable autonomous driving in the long tail. *arXiv preprint arXiv:2511.00088*, 2025.
- [277] Zi Wang, Caelan Reed Garrett, Leslie Pack Kaelbling, and Tomás Lozano-Pérez. Active model learning and diverse action sampling for task and motion planning. In *2018 IEEE/RSJ International Conference on Intelligent Robots and Systems (IROS)*, pages 4107–4114. IEEE, 2018.
- [278] Zi Wang, Caelan Reed Garrett, Leslie Pack Kaelbling, and Tomás Lozano-Pérez. Learning compositional models of robot skills for task and motion planning. *The International Journal of Robotics Research*, 40(6-7):866–894, 2021.
- [279] Zihao Wang, Shaofei Cai, Anji Liu, Xiaojian Ma, and Yitao Liang. Describe, explain, plan and select: Interactive planning with large language models enables open-world multi-task agents. *arXiv preprint arXiv:2302.01560*, 2023.
- [280] Nick Webb, Dan Smith, Christopher Ludwick, Trent Victor, Qi Hommes, Francesca Favaro, George Ivanov, and Tom Daniel. Waymo’s safety methodologies and safety readiness determinations. *arXiv preprint arXiv:2011.00054*, 2020.
- [281] Jason Wei, Xuezhi Wang, Dale Schuurmans, Maarten Bosma, brian ichter, Fei Xia, Ed H. Chi, Quoc V Le, and Denny Zhou. Chain of thought prompting elicits reasoning in large language models. In Alice H. Oh, Alekh Agarwal, Danielle Belgrave, and Kyunghyun Cho, editors, *Advances in Neural Information Processing Systems*, 2022. URL https://openreview.net/forum?id=_VjQlMeSB_J.
- [282] Grady Williams, Andrew Aldrich, and Evangelos Theodorou. Model predictive path integral control using covariance variable importance sampling. *arXiv preprint arXiv:1509.01149*, 2015.
- [283] Ronald J Williams. Simple statistical gradient-following algorithms for connectionist reinforcement learning. *Machine learning*, 8:229–256, 1992.
- [284] Bohan Wu, Suraj Nair, Li Fei-Fei, and Chelsea Finn. Example-driven model-based reinforcement learning for solving long-horizon visuomotor tasks. *5th Conference on Robot Learning (CoRL)*, 2021.
- [285] Bohan Wu, Suraj Nair, Roberto Martin-Martin, Li Fei-Fei, and Chelsea Finn. Greedy hierarchical variational autoencoders for large-scale video prediction. In *Proceedings of the IEEE/CVF Conference on Computer Vision and Pattern Recognition*, pages 2318–2328, 2021.
- [286] Jimmy Wu, Rika Antonova, Adam Kan, Marion Lepert, Andy Zeng, Shuran Song, Jeannette Bohg, Szymon Rusinkiewicz, and Thomas Funkhouser. Tidybot: Personalized robot assistance with large language models. *arXiv preprint arXiv:2305.05658*, 2023.

- [287] Yilin Wu, Thomas Tian, Gokul Swamy, and Andrea Bajcsy. From foresight to forethought: Vlm-in-the-loop policy steering via latent alignment. In *Proceedings of Robotics: Science and Systems*, Los Angeles, CA, USA, June 2025. doi: 10.15607/RSS.2025.XXI.076.
- [288] Mengzhou Xia, Sadhika Malladi, Suchin Gururangan, Sanjeev Arora, and Danqi Chen. Less: Selecting influential data for targeted instruction tuning. In *International Conference on Machine Learning*, pages 54104–54132. PMLR, 2024.
- [289] Kevin Xie, Homanga Bharadhwaj, Danijar Hafner, Animesh Garg, and Florian Shkurti. Skill transfer via partially amortized hierarchical planning. In *International Conference on Learning Representations (ICLR)*, 2021.
- [290] Tong Xie, Haoyu Li, Andrew Bai, and Cho-Jui Hsieh. Data attribution for diffusion models: Timestep-induced bias in influence estimation. *Transactions on Machine Learning Research*, 2024. ISSN 2835-8856. URL <https://openreview.net/forum?id=P3Lyun7CZs>.
- [291] Danfei Xu, Suraj Nair, Yuke Zhu, Julian Gao, Animesh Garg, Li Fei-Fei, and Silvio Savarese. Neural task programming: Learning to generalize across hierarchical tasks. In *2018 IEEE International Conference on Robotics and Automation (ICRA)*, pages 3795–3802. IEEE, 2018.
- [292] Danfei Xu, Ajay Mandlekar, Roberto Martín-Martín, Yuke Zhu, Silvio Savarese, and Li Fei-Fei. Deep affordance foresight: Planning through what can be done in the future. In *2021 IEEE International Conference on Robotics and Automation (ICRA)*, pages 6206–6213. IEEE, 2021.
- [293] Jun Xu, Tao Mei, Ting Yao, and Yong Rui. Msr-vtt: A large video description dataset for bridging video and language. In *Proceedings of the IEEE conference on computer vision and pattern recognition*, pages 5288–5296, 2016.
- [294] Jingkang Yang, Kaiyang Zhou, Yixuan Li, and Ziwei Liu. Generalized out-of-distribution detection: A survey. *CoRR*, abs/2110.11334, 2021. URL <https://arxiv.org/abs/2110.11334>.
- [295] Jingyun Yang, Max Sobol Mark, Brandon Vu, Archit Sharma, Jeannette Bohg, and Chelsea Finn. Robot fine-tuning made easy: Pre-training rewards and policies for autonomous real-world reinforcement learning, 2023.
- [296] Jingyun Yang, Zi ang Cao, Congyue Deng, Rika Antonova, Shuran Song, and Jeannette Bohg. Equibot: Sim(3)-equivariant diffusion policy for generalizable and data efficient learning, 2024.
- [297] Jingyun Yang, Congyue Deng, Jimmy Wu, Rika Antonova, Leonidas Guibas, and Jeannette Bohg. Equivact: Sim(3)-equivariant visuomotor policies beyond rigid object manipulation. In *2024 IEEE International Conference on Robotics and Automation (ICRA)*, 2024.

- [298] Jingyun Yang, Isabella Huang, Brandon Vu, Max Bajracharya, Rika Antonova, and Jeannette Bohg. Mobi- π : Mobilizing your robot learning policy. In Joseph Lim, Shuran Song, and Hae-Won Park, editors, *Proceedings of The 9th Conference on Robot Learning*, volume 305 of *Proceedings of Machine Learning Research*, pages 3516–3536. PMLR, 27–30 Sep 2025. URL <https://proceedings.mlr.press/v305/yang25b.html>.
- [299] Tianhe Yu, Ted Xiao, Jonathan Tompson, Austin Stone, Su Wang, Anthony Brohan, Jaspiar Singh, Clayton Tan, Dee M, Jodilyn Peralta, Karol Hausman, Brian Ichter, and Fei Xia. Scaling Robot Learning with Semantically Imagined Experience. In *Proceedings of Robotics: Science and Systems*, Daegu, Republic of Korea, July 2023. doi: 10.15607/RSS.2023.XIX.027.
- [300] Michał Zawalski, William Chen, Karl Pertsch, Oier Mees, Chelsea Finn, and Sergey Levine. Robotic control via embodied chain-of-thought reasoning. In Pulkit Agrawal, Oliver Kroemer, and Wolfram Burgard, editors, *Proceedings of The 8th Conference on Robot Learning*, volume 270 of *Proceedings of Machine Learning Research*, pages 3157–3181. PMLR, 06–09 Nov 2025.
- [301] Eric Zelikman, Qian Huang, Gabriel Poesia, Noah D Goodman, and Nick Haber. Parsel: A unified natural language framework for algorithmic reasoning. *arXiv preprint arXiv:2212.10561*, 2022.
- [302] Andy Zeng, Adrian Wong, Stefan Welker, Krzysztof Choromanski, Federico Tombari, Aavek Purohit, Michael Ryoo, Vikas Sindhwani, Johnny Lee, Vincent Vanhoucke, et al. Socratic models: Composing zero-shot multimodal reasoning with language. *arXiv preprint arXiv:2204.00598*, 2022.
- [303] Lihan Zha, Apurva Badithela, Michael Zhang, Justin Lidard, Jeremy Bao, Emily Zhou, David Snyder, Allen Z Ren, Dhruv Shah, and Anirudha Majumdar. Guiding data collection via factored scaling curves. *arXiv preprint arXiv:2505.07728*, 2025.
- [304] Tianhao Zhang, Zoe McCarthy, Owen Jow, Dennis Lee, Xi Chen, Ken Goldberg, and Pieter Abbeel. Deep imitation learning for complex manipulation tasks from virtual reality teleoperation. In *2018 IEEE international conference on robotics and automation (ICRA)*, pages 5628–5635. IEEE, 2018.
- [305] Tony Z. Zhao, Vikash Kumar, Sergey Levine, and Chelsea Finn. Learning Fine-Grained Bimanual Manipulation with Low-Cost Hardware. In *Proceedings of Robotics: Science and Systems*, Daegu, Republic of Korea, July 2023. doi: 10.15607/RSS.2023.XIX.016.
- [306] Zihao Zhao, Eric Wallace, Shi Feng, Dan Klein, and Sameer Singh. Calibrate before use: Improving few-shot performance of language models. In *International conference on machine learning*, pages 12697–12706. PMLR, 2021.

- [307] Xiaosen Zheng, Tianyu Pang, Chao Du, Jing Jiang, and Min Lin. Intriguing properties of data attribution on diffusion models. In *The Twelfth International Conference on Learning Representations*, 2024. URL <https://openreview.net/forum?id=vKViCoKgCB>.
- [308] Luowei Zhou, Hamid Palangi, Lei Zhang, Houdong Hu, Jason Corso, and Jianfeng Gao. Unified vision-language pre-training for image captioning and vqa. In *Proceedings of the AAAI conference on artificial intelligence*, volume 34, pages 13041–13049, 2020.
- [309] Brianna Zitkovich, Tianhe Yu, Sichun Xu, Peng Xu, Ted Xiao, Fei Xia, Jialin Wu, Paul Wohlhart, Stefan Welker, Ayzaan Wahid, Quan Vuong, Vincent Vanhoucke, Huong Tran, Radu Soricut, Anikait Singh, Jaspiar Singh, Pierre Sermanet, Pannag R. Sanketi, Grecia Salazar, Michael S. Ryoo, Krista Reymann, Kanishka Rao, Karl Pertsch, Igor Mordatch, Henryk Michalewski, Yao Lu, Sergey Levine, Lisa Lee, Tsang-Wei Edward Lee, Isabel Leal, Yuheng Kuang, Dmitry Kalashnikov, Ryan Julian, Nikhil J. Joshi, Alex Irpan, Brian Ichter, Jasmine Hsu, Alexander Herzog, Karol Hausman, Keerthana Gopalakrishnan, Chuyuan Fu, Pete Florence, Chelsea Finn, Kumar Avinava Dubey, Danny Driess, Tianli Ding, Krzysztof Marcin Choromanski, Xi Chen, Yevgen Chebotar, Justice Carbajal, Noah Brown, Anthony Brohan, Montserrat Gonzalez Arenas, and Kehang Han. Rt-2: Vision-language-action models transfer web knowledge to robotic control. In Jie Tan, Marc Toussaint, and Kouros Darvish, editors, *Proceedings of The 7th Conference on Robot Learning*, volume 229 of *Proceedings of Machine Learning Research*, pages 2165–2183. PMLR, 06–09 Nov 2023. URL <https://proceedings.mlr.press/v229/zitkovich23a.html>.